THE STRESS-CORROSION CRACKING OF CARBON STEEL IN CO-CO_2-H_2O

by

Josias van der Merwe

Submitted in partial fulfilment of the requirements for the degree

Philosophiae Doctor

in the Faculty of Engineering, the Built Environment and Information Technology
University of Pretoria

July 2013

Abstract

Stress-corrosion cracking of steel occurs in the CO-CO_2-H_2O system when these three environmental components are present together. The dissolved carbon monoxide in the water forms an inhibitive layer on the surface of the steel. Rupture of the adsorbed layer by slip steps on the surface of the steel causes the exposure of uninhibited steel if plastic deformation occurs. Dissolved carbon dioxide accelerates the corrosion rate at this location. A crack forms when the corrosion is concentrated to form a crack tip, while corrosion of the crack flanks is inhibited. Due to the conservation of charge, crack growth relies on cathodic processes on the external surfaces. Cathodic reactions need not be confined to the crack tip and crack flanks, but may also occur on the external surfaces. To handle cracking in a practical context, critical stress intensities and corresponding growth rates are necessary for design purposes. The critical stress intensity for stress-corrosion cracking – K_{ISCC} – was determined by measuring the current flow from an external cathode, with comparisons with the crack growth rate. Crack propagation was measured with the potential drop method. The double cantilever beam specimens were coated with silicone rubber to limit corrosion to a small region around the crack. This allowed measuring of the current flow between the crack tip and two steel cathodes at the sides of the specimen. The current responses were correlated with the actual crack propagation. Experiments were conducted by testing C-Mn steel in distilled water with a 50% CO – 50% CO_2 gas mixture at 45°C and 800 kPa. It was found that K_{ISCC} can be predicted by using the current measurements. It appears that with such "electrochemical noise measurements" important factors that influence the cracking process can be investigated. The required inhibitor addition was evaluated and between 200 and 1000 ppm potassium bichromate was required to mitigate stress-corrosion cracks significantly. Constant deflection tests confirmed the low stress threshold of C-Mn steel exposed to industrial environments with carbon monoxide and carbon dioxide. Therefore, the ineffectiveness of stress relieving post-weld heat treatments to inhibit cracking is clear.

Acknowledgements

I would like to express my appreciation to my supervisors, Professors M. du Toit and R.F. Sandenbergh, as well as the initial inputs and instrumentation from Professors G.T. van Rooyen and P.C. Pistorius.

My colleague, Professor L. Cornish, for advice and encouragement.

All my family and friends for their support.

The Lord Jesus Christ for his love and saving grace.

Table of Contents

Table of Figures

List of Symbols and Abbreviations

A ..... area, cm^2

Ag/AgCl ..... silver – silver chloride

ASTM ..... American Society for Testing and Materials

B ..... specimen thickness

c .....concentration, mol cm^{-3}

C ..... carbon

CE ..... counter electrode

CO_2..... carbon dioxide

CO.....carbon monoxide

CV ..... crack velocity

D ..... diffusion coefficient, cm^2s^{-1}

d_0 ..... original diameter

d ..... final diameter in the necked region

$d\varepsilon/dt$ ..... creep rate (strain rate)

e^- ..... an electron

E_B ..... anodic breakdown potential, V

E_{corr} ..... corrosion potential, V

EDS, EDX, EDXS... energy dispersive X-ray spectroscopy

EIS ..... electrochemical impedance spectroscopy

ϵ ..... strain

ε_f ..... strain to rupture the film

$\dot{\varepsilon}_{ct}$ ..... crack-tip strain rate

F ..... Faraday's constant

Fe ..... iron

GR ..... crack growth rate per cycle

H^+ ..... hydrogen ion

H_2 ..... hydrogen gas

H_2O ..... water

H_2SO_4 ..... sulphuric acid

H_2CO_3..... carbonic acid

HCl ..... hydrochloric acid

HCN..... hydrogen cyanide

hcp ..... hexagonal close packed

i ..... current at over voltage

i_a ..... anodic current density

i_{corr} ..... corrosion current density, A/cm^2

i_{crit} ..... critical current density, A/cm^2

i_{pass} ..... passivation current density, A/cm^2

i_{pp} ..... primary passivation current, A/cm^2

K_{ISCC}..... stress intensity threshold

log ..... logarithm

LSV ..... linear sweep voltammetry

l_0 ..... original gauge length

l ..... final gauge length

M ..... metal

m^{n+} ..... metal ion

n ..... number of electrons

N ..... number of cycles

n_c ..... crack nucleation rate

N_2 ..... nitrogen

Na_2SO_4 ..... sodium sulphate

NaCl ..... sodium chloride

NF..... no failure

Ni ..... nickel

n_L ..... number of large cracks coalescing

O_2 ..... oxygen gas

OCP ..... open circuit potential

pH ..... $-\log_{10}[H^+]$

Q_f..... charge density passed

RA ..... reduction of area

R_p ..... polarisation resistance

σ ..... stress

SEM ..... scanning electron microscopy

SCE ..... standard calomel electrode

SSC ..... silver/silver chloride

t ..... Time

W ..... specimen width

YS..... yield strength

z ..... valency of the solvated species

Z ..... reduction in area

1 CHAPTER I

1.1 Introduction

Coal gasification is a process used for the production of petrochemical products and in South Africa this is an important process for fuel production. It forms a major part of the country's fuel supplies. During this process, coal is burned and some of the gaseous products that are formed are carbon monoxide and carbon dioxide; these gases are then converted to synthetic oils and further refined. However, along the way, a considerable amount of contaminated water is formed as a by-product and this black, smelly water is used in various places and has to be transported through pipelines and is exposed to various types of components such as pipes, pumps, valves and heat exchangers. In some instances, this water is used as a cooling water and it is treated to ensure a low corrosivity. This water by-product contains dissolved concentrations of carbon monoxide and carbon dioxide at varying amounts and in some cases, this water by-product induces stress-corrosion cracking of the low carbon steel components in contact with it.

1.2 Problem statement

The effect of the dissolved gas composition on the crack initiation and propagation rates in the steel is not clear, especially at very low concentrations of either carbon monoxide or carbon dioxide possibly over longer periods of time. The crack propagation rates with the applied stress intensity give an indication of stress threshold below which stress corrosion is no longer supported. This is an important value since the relieving of stress can then lead to the stress corrosion inhibition and mitigation. These thresholds have not been determined and will therefore contribute to the knowledge base and will help to alleviate, or at least to plan around the situation. With these values, it can then be possible to lower stress-corrosion sensitivity by decreasing the stress to a level close to or below the threshold. In actual concentrations, it is then possible to do this by introducing a post weld heat treatment which lowers the residual stresses in the vicinity of the welds. The effectiveness of the treatment and the level of the stress threshold for stress-corrosion cracking will dictate whether this is a feasible operation to inhibit cracking altogether.

1.3 Research questions

A number of issues have been raised that needs to be addressed; firstly, the value of a stress threshold below which cracking will be inhibited. This then leads to the role of dissolved gas composition and its influence on this stress threshold. Secondly, the crack propagation rate values are important for plant design and have to be addressed. Again this has to be done with relation to the gas composition, especially for the low carbon monoxide concentrations, as well as other environmental parameters. Thirdly, it is important to understand the corrosion characteristics and the basic environmental conditions that would lead to stress-corrosion of steel. Traditionally it is known that the presence of stress-corrosion is dependent upon the co-existence of three spheres of reference, namely: stress, specific environment and susceptible material. For this current investigation, however, the focus was on the environment and stress, and their interaction. Once the threshold stress is established it becomes important to determine the possibility of corrosion monitoring and current response measurements for the initiation and propagation of cracks. In addition the characteristics of cracking have to be correlated with the industrial applications. The following questions summarises the direction of the research:

1. What is the minimum stress intensity that would sustain stress-corrosion cracking of steel in this system?
2. What is the dependence of the stress-corrosion stress intensity threshold on the dissolved gas composition, and in particular considering the carbon monoxide lower limit?
3. How does stress and strain rate interact in this environment and how would these parameters influence the crack propagation rate?
4. What is the role of corrosion kinetics in the cracking process?
5. How is crack propagation rate affected during the normal plant operation?

1.4 Scope

The work was presented and divided into chapters that were based on the experimental techniques that were employed, the reason for treating it in this fashion was the focus of each technique could be used to evaluate a certain aspect of the

corrosion/cracking process. The progression was from the more broadly environmental issues to a focus on the crack propagation and stress related issues, and then finally using an industrial application to evaluate the findings. Therefore, the work was initiated around the slow strain-rate technique evaluating various environmental and material parameters in Chapter 3, followed by characterising the corrosion reactions through polarisation techniques in Chapter 4. This lead to the realisation of the time dependency of corrosion reaction and therefore the influence of stress fluctuations was investigated in Chapter 5. Understanding these foundational aspects then lead to the evaluation of cracking at a fracture mechanics approach to answer the first issue mentioned above about the stress intensity threshold in Chapter 6. Chapter 7 is an investigation into the possibility of using current response measurements in evaluating the cracking of a system. Then the extent of passivation that will be required to inhibit cracking completely was looked at in Chapter 8 and finally in Chapter 9 two industrial applications are investigated with C-ring specimens stressed to varying levels.

This study aims to develop a better understanding of cracking, which can be used to predict the cracking behaviour of the steel under certain environmental and stress conditions. Although stress-corrosion is so environment-material-stress interdependent it still makes sense to analyse these interactions independently and to define the characteristics clearly. Therefore, with an understanding of the cracking process it should include an understanding of the stress threshold for cracking in these environments as well as once cracking has initiated the crack propagation rates have to be predicted so that proper design and remaining life decisions can be made.

Parts of this work were presented at two international conferences, namely:

- EuroCorr2010, Stockholm Sweden, September, 2011, (conference proceedings CD) and
- The 18th International Corrosion Congress, Perth Australia (November 2011). *18th International Corrosion Congress 2011*, v 2, p 1519-1528, 2011, ISBN-13: 9781618393630

Two journal articles have been published:

- J. W. van der Merwe, "Environmental and Material Influences on the Stress-Corrosion Cracking of Steel in H_2O-CO-CO_2 Solutions," International Journal of Corrosion, vol. 2012, Article ID 414156, 13 pages, 2012. doi:10.1155/2012/414156: http://www.hindawi.com/journals/ijc/2012/414156/

- J.W. van der Merwe and M du Toit, "Mitigation of stress corrosion cracking of carbon steel exposed to CO-CO_2-H_2O environments through inhibitor addition", Anti-Corrosion Methods and Materials, 2013.

This study also contributed to the understanding of stress-corrosion cracking of components in the Sasol Secunda environments, and assisted in post-weld heat treatment procedures that have been prescribed.

CHAPTER 2

BACKGROUND TO THE STRESS CORROSION CRACKING OF STEEL IN CO-CO_2-H_2O ENVIRONMENTS

2.1 Introductory comments

Generally and historically, it has been accepted that stress corrosion cracking occurs only if a material sensitive to cracking is attacked by a specific corrosive medium in the presence of a sufficiently high mechanical stress[1]. However, these three requirements should be regarded as interdependent parameters. "Material plus medium" should be considered a "corrosion system". There are critical influencing factors for any system that are interconnected, e.g. temperature, solution concentration, and electrochemical potential. Similarly, in relation to mechanics, not only is the absolute value of stress level important, but also how the stress in the structure reacts with the corrosion system and influences the localised corrosion by the emergence of slip steps and thereby influencing the effective strain rate. In the light of this interactive relationship, the main factors that cause cracking to take place will be considered here from a more compartmentalised view.

2.1.1 CO-CO_2-H_2O – steel system

The stress-corrosion cracking of steel in CO-CO_2-H_2O occurs over a range of circumstances and environments and stress conditions. This review will attempt to address this variety of conditions and what has been documented for each, so that an ordered analysis can be performed on the known knowledge base. The stress-corrosion system has been studied by a variety of researchers over a number of years.

Firstly, the area of interest that will be addressed will be the influence of the environment on cracking. As it is known, stress-corrosion cracking is dependent upon three main parts and these are the following: the environment, the material and the

stress condition[2]. When one of these parts is removed the stress-corrosion will be eliminated.

The environment is very dependent upon the material and the way the material reacts to the environment under a certain stress condition. In the subject addressed, the environment will consist of a number of variables and all of these have to be considered if possible, obviously according to the research that has been performed. Environmental variables would be the gas composition, partial pressures of carbon monoxide and carbon dioxide as well as other contaminant gasses. But the primary concern will be the presence of carbon monoxide and carbon dioxide.

Secondly, is the role of the material, or the corrosivity of the material during the cracking process. In the instance of steel, the material condition cannot be significantly different in terms of corrosion properties without the addition of other alloying elements. Therefore, the material/steel interaction with the environment is important and how it reacts during corrosion and these can be influenced by surface finish and the time of exposure to the environment, therefore, how fast the corrosion reaction occurs. In this study the effect of the stress, the third component, becomes important because the stress intensity threshold, K_{ISCC}, for cracking leads to the development of a condition where cracking does not occur below the threshold. Significant contributions can be made by understanding the stress and the interaction it has with the rest of the environment, therefore, the strain rate and how it interacts with the crack propagation rate. Strain rate has to be seen in two ways, firstly as the strain rate as applied to the length of the sample and secondly, the strain rate that is seen at the crack tip. This is especially significant for the crack propagation rate, whereas the strain rate over the gauge length would influence the crack initiation. From here it would then be important to determine how the crack tip strain rate is altered by the application of an external load, and of course in the same instance the effect of the applied load on the global strain rate. It could be that the strain rate at the crack tip will change with increasing crack lengths and this has to be evaluated. Strain rate and the corrosion reaction rate, as well as the passivation rate caused by the carbon monoxide adsorption, all play a role and contribute to the crack propagation. Therefore, the balance between these has to be established and predicted accurately. In addition, the effect of stress intensity has to be investigated in order to correlate the crack propagation rate with changing stress intensity.

Therefore, this review will consider the independent parameters that would fall into the three broad categories of: stress, environment and material, yet considering the interactive processes of each of these parameters. This will form a foundational understanding for the experimental work. Firstly, the environmental influences will be considered, including: gas composition, dissolved oxygen concentration or the oxygen pressure in the gas, hydrogen and methane, and then the main parameters, carbon dioxide and carbon monoxide concentrations, and finally temperature. Secondly, the electrochemical characteristics, which of course are dependent on both environment and material properties, will be considered. Thirdly, the influence of passivity and the characteristics of corrosion inhibition will be looked at. Then, the influence of the metallurgy will be considered, which will include: alloy additions, heat treatment and the surface finish. Lastly then to complete the consideration of the three main areas influencing stress corrosion, the effect of stress will be studied. Mechanistically this type of stress corrosion will be addressed by looking at: crack growth kinetics, crack propagation process, specifically the constant load double cantilever beam specimens, and lastly the mechanism of cracking. To conclude the various significant test methods that will be employed will be considered in the last section of the literature review.

2.2 Historical overview

Only in the 1960s the problem of transgranular stress corrosion cracking in plain carbon steels started to receive more serious attention as a problem in industry. Earlier research was done on the intergranular stress corrosion cracking with some work on transgranular cracking[3,4]. The environments that had mostly been involved with the ferritic steels were those containing hydroxides or nitrates. Problems occurred in the gas-water systems for chemical process plants and for similar conditions in town gas (a gaseous fuel produced from coal firing) manufacture and storage[5]. In the late 1960s cracking of plain carbon steel vessels used as containers for moist gases, consisting of CO_2 and CO, occurred on a wide scale[6].

Kowaka and Nagata[7] reported severe cracking in the region of weld seams and in separator and a heat exchanger tubing. The material used was mild steel and the temperature range of observed failures occurred was 20°C to 60°C. The main

components of the flowing gases were CO, CO_2, H_2 and some hydrocarbon gases at a pressure of 20 kg/cm^2. No HCN was detected in the environment, which also contributes to the passivation process and can be an important component in the cracking process.

Incidents of transgranular stress corrosion cracking of low strength steels have occurred in the handling of reformed and coal gas and in an inert gas miscible flood in Ventura, a California oil field[8]. The gas used had significant concentrations of CO (3.5% mole) and traces of O_2 (0.03%) in the presence of CO_2. Carbon-manganese steels of minimum yield strengths 379 MPa and 552 MPa, failed after cracking originated on the exterior surfaces. For these systems, failures occurred with temperature ranging from ambient temperatures to approximately 66°C.

2.3 Environmental influences

2.3.1 Gas composition

The general gas composition, as well as traces of gases, as impurities, can play a significant role in the susceptibility to stress corrosion cracking of mild steel in the CO-CO_2-H_2O environments.

Brown et al.[9] found that transgranular cracking only occurred in wet, and not dry, environments and therefore appeared to be related to a corrosion-driven process rather than a dry embrittling gas. They found the presence of CO to be essential for cracking to occur and stated that CO_2 and O_2 accelerate cracking but do not directly cause cracks to form. However, this was disputed by the results of Hannah et al.[10], they concluded:

"1. At atmospheric pressure, cracking of C-Mn steels in CO-CO_2-H_2O environments occurs by a hydrogen embrittlement mechanism. The presence of CO_2 in the environment is necessary and sufficient for cracking. The source for hydrogen is undissociated carbonic acid."

And for elevated pressure:

"... cracking of C-Mn steels in CO-CO_2-H_2O environments can occur by hydrogen embrittlement, under cathodic polarisation and by stress corrosion cracking at the free corrosion potential and under anodic polarisation."

Parkins et al.[11] who found cracking to occur in the presence of carbon dioxide with no carbon monoxide. Kowaka[12] gave an integrated perspective of these two gasses as shown in Figure 2-1. Note that cracking occurs in carbon dioxide with small quantities of carbon monoxide of around 2 kg/cm^2 and 6 kg/cm^2 carbon dioxide. When both, carbon monoxide and carbon dioxide, were at concentrations below 4 kg/cm^2 it appears that cracking did not occur after 1 000 hours of exposure.

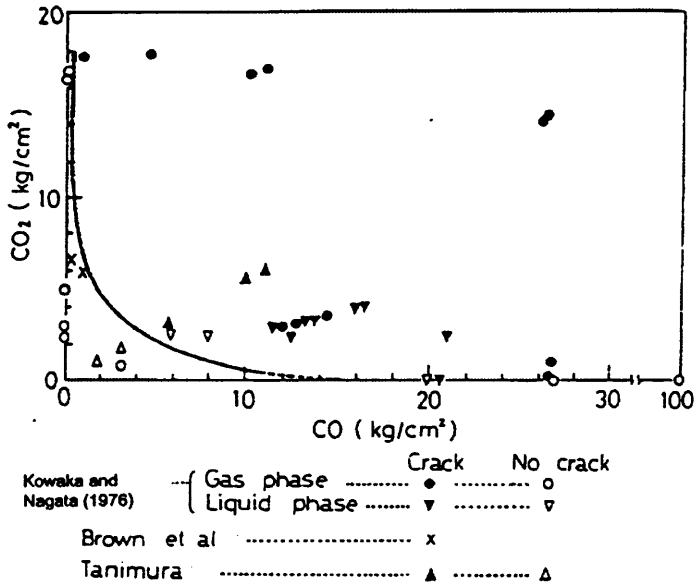

Figure 2-1. Effect of partial pressure of CO and CO_2 on stress corrosion cracking of carbon and Mn-steels between 18 and 70°C for 168 - 1000 hours (Kowaka and Nagata, 1976[7]).

The sensitivity to cracking was dependent on both gasses being present simultaneously, with evidence of cracking even when either CO or CO_2 was only present in low concentrations. In the absence of CO_2, the curve moves toward the CO-axis and seems to cross it between 10 and 20 kg/cm^2 (1 and 2 MPa). Spahn et al.[13] also reported the failure of gas cylinders containing pure carbon monoxide with possible traces of CO_2 but did not clarify the conditions precisely.

Where the CO partial pressure was below 12 kg/cm^2 (136 kPa), cracking promoted by binary gas mixtures of CO_2 and CO was either slowed down or non-existent, unless external anodic polarisation was applied[5]. However, addition of oxygen to these systems did promote cracking in freely corroding conditions and crack growth was more rapid and obvious in freely corroding conditions when the CO pressure exceeded 690 kPa[5]. The incidence and rate of cracking increased with higher stress levels, increased CO pressures, increasing anodic polarisation within a narrow potential band of approximately 100 mV, and with O_2 additions[5]. Brown et al.[5] also found that cracking occurred under freely corroding conditions at applied stresses as low as 25% of the tensile strength.

2.3.2 Oxygen

As mentioned above, the presence of oxygen is not the cause of cracking as oxygen in the presence of carbon dioxide and carbon monoxide did not alter the form of cracking but rather changed the rate and conditions of cracking. However, it seems that the effect of dissolved oxygen cannot be described in a singular simplistic relationship when the divergent results are considered. Brown et al.[5] evaluated the SCC of steel in a binary gas mixture of CO-CO_2 at 136 kPa and 655 kPa respectively, and an applied potential of -550 mV. They found that the cracking rate increased from $6x10^{-7}$ mm/s to $1.3x10^{-6}$ mm/s with the addition of oxygen at a partial pressure of 21 kPa and an applied stress of 448 MPa. At a lower stress, 269 MPa, the effect of the oxygen addition to the same environment was lower. Without the addition of oxygen, the crack propagation rate was measured at about $2x10^{-7}$ mm/s and although an increase in the crack propagation rate was seen with the addition of oxygen, it was only from $2x10^{-7}$ mm/s to $3x10^{-7}$ mm/s. This is a clear demonstration of the interdependent nature of influencing factors on the stress corrosion cracking, and in this instance, the influence of the stress level on the crack enhancement was by increasing oxygen concentration.

Oxygen addition moves the free corrosion potential to more noble potentials and the polarisation resistance decreases, i.e. increasing the free corrosion rate (Brown et al.[5]). However, these changes are small and do not change the character of the reactions. The effect of the oxygen is more noted in CO inhibited systems. Brown et

al.[5] concluded that oxygen additions shift the free corrosion potential into the susceptible range of cracking, without applying external polarisation. They did not give any explanation for the higher propagation rates, but if the cracking process was by anodic dissolution at the crack tip and there was inhibition of the crack sides, the decreased polarisation resistance might explain the higher cracking rate in the presence of oxygen additions. The passivation reaction by carbon monoxide is necessary to limit the increased free corrosion currents.

From electrochemical studies, Dunlop and Olson[14] found that the addition of 20 kPa O_2 at 22°C with CO and CO_2 partial pressures of 69 and 165 kPa, caused the potential where cracking occurs to be negative and moved the free corrosion potential slightly anodic, thus causing stress corrosion cracking both above and below the free corrosion potential. In the absence of oxygen and with the addition of 100 ppm NaCl stress corrosion cracking occurred at a lower potential, closer to the corrosion potential, which was also lowered and when a small amount of oxygen was added with sodium chloride, cracking increased. They mentioned that the rigorous exclusion of contaminant traces of oxygen produced more, rather than less, cracking. However, this was not consistent with some of their results, considering the influence of small O_2 additions.

Berry and Payer[15] found that oxygen had a major influence on the behaviour of X52 steel, a C-Mn steel used for gas-transmission pipe, in CO-CO_2-H_2 aqueous solutions by significantly increasing the severity of stress corrosion cracking or general corrosion. They found no stress corrosion cracking in the absence of oxygen. When carbon monoxide and carbon dioxide were both present, the addition of oxygen promoted severe stress corrosion cracking and caused failure after approximately 100 hours. In the presence of only carbon dioxide and hydrogen (with partial pressures of 276 kPa and 69 kPa respectively), the addition of 69 kPa oxygen greatly enhanced general corrosion, but confirmed the findings of Brown et al.[5] in that no stress corrosion cracking was observed in the absence of carbon monoxide. The addition of oxygen resulted in more positive free corrosion potentials in all aqueous solutions that were tested, in accordance with the aforementioned results[15]. Cracking was the most severe in CO-CO_2-H_2 gases where corrosion potentials were shifted anodically by approximately 100 mV. Berry and Payer[15] concluded that stress-corrosion cracking

increased with increasing oxygen for conditions that promote little or no corrosion; otherwise general corrosion increased[5].

These results indicate that oxygen increased the severity of cracking, but the extent of this influence is dependent upon the prevalent environmental conditions. This includes the carbon monoxide and carbon dioxide partial pressures and the applied stress. The reason for enhanced cracking by the rigorous exclusion of oxygen is unclear. Therefore, the influence of oxygen is dependent upon the corrosion characteristics and stress condition of the steel. However, it seems that although oxygen does not change the free corrosion current significantly, it does alter the free corrosion potential to cause cracking. It is therefore likely that a better understanding of the electrochemistry involved in stress-corrosion cracking of this system could help explain the role of oxygen on cracking.

2.3.3 Hydrogen and methane

In the quaternary (or pentamorous) aqueous gas mixture, $CO\text{-}CO_2\text{-}O_2\text{-}H_2\text{-}(CH_4)$, the inhibiting effect of higher pressures of methane and hydrogen increase the time to failure, or resistance to cracking, as seen in Table 2-1[15]. High pressures of methane increased time to failure by an order of magnitude in $CO\text{-}CO_2\text{-}H_2O$ mixtures, although these methane partial pressures were very high and high compared to the partial pressures of the more crack inducing gasses. The methane partial pressure was nearly 90% of the total gas pressure for all the tests, when it was present. As the hydrogen partial pressure was increased its inhibition effect on cracking is apparent. With an increase of 69 to 827 kPa of the hydrogen partial pressure it resulted in no failure of the steel samples after 1500 hours, whereas failures occurred between 112 and 170 hours at the lower hydrogen partial pressures.

Berry and Payer[15] also investigated the partial pressure of methane with the slow strain rate test with the CO_2 and CO partial pressures at 69 and 6.9 kPa respectively. However, no clear pattern emerged but severe stress-corrosion cracking occurred at the highest partial pressure of methane, 4.72 MPa. At 28 kPa, the lowest pressure tested, stress corrosion cracking was observed (sharp cracks), but at slightly higher partial pressures of methane, 241 and 1,280 kPa, no cracking occurred. With the addition of oxygen in the gas (69 kPa CO_2 and 6.9 kPa CO), severe cracking occurred;

methane had a strong inhibiting effect under these conditions which was observed in constant stress tests. Methane added to the inhibition of the corrosion reaction together with carbon monoxide, leading to a greater sensitivity to cracking as it does not passivate the steel enough to inhibit cracking completely.

Table 2-1 Effect of hydrogen and methane on stress corrosion cracking of X-52 steel (after Berry and Payer[15]).

Gas composition [kPa]					**Time to failure** [hours]
CO	CO_2	O_2	H_2	CH_4	
69	414	69	69		112;170
69	414	69	827		NF*;(1 500)
345	414	69	69		60;102
345	414	69	69	6100	985
69	414	69	69	6380	1 365
69	414	69	827	5620	NF;(4 200)

* *No failure in the number of hours indicated.*

An embrittling factor in CO-CO_2 stress corrosion cracking can be the absorption of hydrogen into the metal as suggested by Hannah, Newman and Procter[10], however due to the low strength of C-Mn steels this is unlikely, but will be discussed. Carbon dioxide adsorption at the cathode increased hydrogen entry into the metal by inhibiting the hydrogen recombination reaction in much the same way as hydrogen sulphide does in sour systems, but much less efficiently[16]. Carbon monoxide increased the rate of hydrogen entry by between 4 and 10 times over that caused by carbon dioxide,

therefore supporting a hydrogen embrittlement mechanism[17]. This will be further considered when the mechanism of cracking is discussed.

2.3.4 Carbon dioxide

The discussion of the influence of carbon dioxide covers the electrochemical corrosion in oxygen-free CO_2 environments. Since cracking is dependent on the passivation as well as increased corrosion rate of the steel produced by the presence of carbon dioxide it is important to consider this mechanism. Although corrosion is not the only factor, it is an important element that will enhance the cracking process, either by localised corrosion or by the production of adsorbed hydrogen atoms which could contribute to the cracking process. If indeed the presence of hydrogen will contribute to the cracking of this low strength material.

Carbonic acid, which forms as carbon dioxide dissolves in water, is known to be a weak acid, but the uniform corrosion of steel by aqueous solutions of carbon dioxide at a given pH is more severe than by hydrochloric acid[18] at the same pH. The corrosion rate of steel at ambient temperature in oxygen-free carbon dioxide solution is controlled by the kinetics of hydrogen evolution, and hydrogen evolution from carbon dioxide solutions can occur by two fundamentally different mechanisms[19,20,21].

Schmitt[17] proposed two reaction sequences with the presence of carbon dioxide. Firstly, hydrogen evolves by electrochemical reduction of hydrogen ions (Equation 2-a) which originates from the bulk solution from the dissociation of carbonic acid (Equation 2-b) and then diffused to the metal surface (Equation 2-c). In this respect carbon dioxide is not different from dilute mineral acids.

$$H_3O^+_* + e^- \Leftrightarrow H_{ad} + H_2O_* \quad \text{.....2-1}$$

$$H_2CO_{3_{sol}} + H_2O \Leftrightarrow H_3O^+_{sol} + HCO^-_{3_{sol}} \quad \text{.....2-2}$$

$$H_3O^+_{sol} \Leftrightarrow H_3O^+_* \quad \text{.....2-3}$$

$$CO_{2_{sol}} + H_2O \Leftrightarrow H_2CO_{3_{sol}} \quad \text{.....2-4}$$

Secondly, hydrogen formation may proceed according to the reaction sequence (1): 2-e → 2-f → 2-g → 2-i; or sequence (2) 2-e → 2-f → 2-h → 2-i. The important difference to the reaction sequence 2-a to 2-d, is that in the second sequence, the hydration of carbon dioxide to carbonic acid occurs in a heterogeneous reaction on the metal surface (Equation 2-d). This is where it differs from mineral acids and it is also an important difference for cracking to take place since the cracking process is also a heterogeneous reaction. The adsorbed carbonic acid may be reduced directly (Equation 2-f) or can dissociate while still adsorbed (Equation 2-g) to give hydrogen ions, which are then reduced (Equation 2-i).

$$CO_{2_{sol}} \Leftrightarrow CO_{2_{ad}} \quad \text{.....2-5(2a)}$$

$$CO_{2_{ad}} + H_2O \Leftrightarrow H_2CO_{3_{ad}} \quad \text{.....2-6(2b)}$$

$$H_2CO_{3_{ad}} + e^- \Leftrightarrow H_{ad} + HCO^-_{3\ ad} \quad \text{.....2-7(2c)}$$

$$H_2CO_{3_{ad}} + H_2O_* \Leftrightarrow H_3O^+_* + HCO^-_{3_*} \quad \text{.....2-8(2d)}$$

$$H_3O^+_* + e^- \Leftrightarrow H_{ad} + H_2O_* \quad \text{.....2-9(2e)}$$

$$HCO^-_{3_{ad}} + H_3O^+ \Leftrightarrow H_2CO_{3_{ad}} + H_2O \quad \text{.....2-10(2f)}$$

As in mineral acids, hydrogen ions are reduced on the iron surface, (Equation 2-i) as ions that were transported from the bulk solution to the metal surface and electron transfer yields adsorbed hydrogen atoms. Chemical recombination according to the Tafel reaction or electrochemical recombination according to the Heyrowski reaction

gives adsorbed molecular hydrogen which can desorb from the surface to allow subsequent adsorption and reduction of other hydrogen ions. Instead of recombining, the adsorbed hydrogen atoms can also be absorbed by the metal lattice to induce brittleness. Hydrogen is not the only adsorbed species and the adsorption of carbon dioxide also plays a role.

Molecules of CO_2 adsorb on the metal surface (Equation 2-e) and analogous to the adsorption of CO_2 on platinum in acid solutions[22], it can also be assumed that the adsorption of CO_2 on the iron surface is accompanied by an interaction with Fe-H bonds, resulting in an adsorbed formate radical (COOH) on the metal surface. This reaction Subsequent hydration of the formate radical yields chemisorbed carbonic acid (Equation 2-f). This species can either be reduced directly to give an adsorbed hydrogen atom and adsorbed bicarbonate (Equation 2-g) or it can dissociate to produce hydrogen ions near the phase boundary which are reduced (Equation 2-h).

These reactions can take place as part of a catalytic cycle. Adsorbed bicarbonate is neutralised by a hydrogen ion to re-form adsorbed carbonic acid from which hydrogen can again be produced. From their experimental results, De Waard and Milliams[23,24] concluded that the cathodic hydrogen evolution in carbon dioxide corrosion proceeds in a catalytic way by the direct reduction of carbonic acid (Equations: 2-g $\rightarrow$ 2-j $\rightarrow$ 2-g$\rightarrow$etc.). They assumed that the charge transfer reaction (Equation 2-g) was the rate determining step. The transport reactions were not rate determining, but from the experimental data obtained with rotating disc electrodes, it was shown that the rate determining step is the heterogeneous hydration of adsorbed carbon dioxide (Equation 2-f). This is a very important factor for the stress corrosion cracking in this system, because again it is a heterogeneous reaction on the steel surface that is influenced by the inhibition of the steel by the carbon monoxide.

The De Waard work was mostly concerned with corrosion in CO_2-H_2O systems. They showed that the direct reduction of the carbonic acid increased the corrosion rate above that of simple acid systems. The adsorbed CO might displace the adsorbed H_2CO_3 and so passivate the steel. If the kinetics of H_2CO_3 adsorption is faster than that of CO, a transient active period will be created where high reaction rates are possible at the crack tip and this will favour SCC.

2.3.4.1 Influence of alloying additions on uniform corrosion in CO_2 solutions

Considering the influence of alloy elements on the resistance to uniform attack, it is known that chromium decreases the corrosion rate in iron alloys[25,26]. Chromium alloys with 9% Cr, with or without 1% Mo, gave good performances in sweet gas (typically natural gas without significant amounts of hydrogen sulphide) condensate wells. Nickel generally improved the corrosion resistance; although the effect was not very distinct, even with additions of 9%. Steels with 9% Ni have been used in corrosive, high CO_2 partial pressure environments with acceptable results[27,28], but occasionally suffered from cracking and pitting. The susceptibility to cracking increased with increasing strength, which indicates the possibility of hydrogen embrittlement. The manganese and nickel low alloy steels were comparable in their corrosion resistance, altough manganese grades seemed to be more susceptible to pitting corrosion. Chromium-nickel steels with more than 12% Cr are very resistant to corrosion by wet CO_2 even at high CO_2 partial pressures[29]. However, in the presence of chlorides pitting and crevice corrosion occur.

2.3.4.2 Stress corrosion cracking in the CO_2-H_2O-system

Brown et al[5] found that the CO_2-H_2O system has generally not been considered to cause stress-corrosion cracking of steels. Kowaka and Nagata[7] in their investigations on the possibility of stress-corrosion cracking in the CO-CO_2-H_2O system, found all experimental attempts to produce corrosion cracking in an environment containing only CO_2 and water were unsuccessful. However, experimentally, cracking was observed only under severe conditions, with highly stressed, high strength carbon steels under high CO_2 partial pressures[30]. An example is that no cracking occurred at 100 kPa CO_2 in 5% NaCl solution within 695 days, even with 130% deformation with a hardness of 38 R_C, but the same specimens failed with 110% deformation at 2.0 MPa CO_2. Other examples of cracking and bursting of high strength low alloy steel vessels demonstrated that the CO_2-H_2O system can cause corrosion cracking. However, the cracking mechanism of the failures remained uncertain because classical stress-corrosion cracking, as well as hydrogen induced stress corrosion cracking or embrittlement, were given as explanations. Further testing of low alloy steels in the system CO_2-H_2O tested under constant load with CO_2 pressures of up to 6,0 MPa

showed cracking under the appropriate conditions. The susceptibility to cracking was a function of the strength of the steel, the load, the CO_2 pressure and the temperature. However, cracking also occurred below the yield strength at high CO_2 pressures. The data shown in Figure 2-2[17] indicate that the susceptibility to cracking increased with increasing strength of the steel, load and temperature. At 25°C, no cracking occurred under constant loads less than 75% of the yield strength (Figure 2-2b). Classical stress-corrosion cracking is apparently not a reasonable explanation for the steel-carbon dioxide system, as the cracking occurs without inhibition of the steel by carbon monoxide.

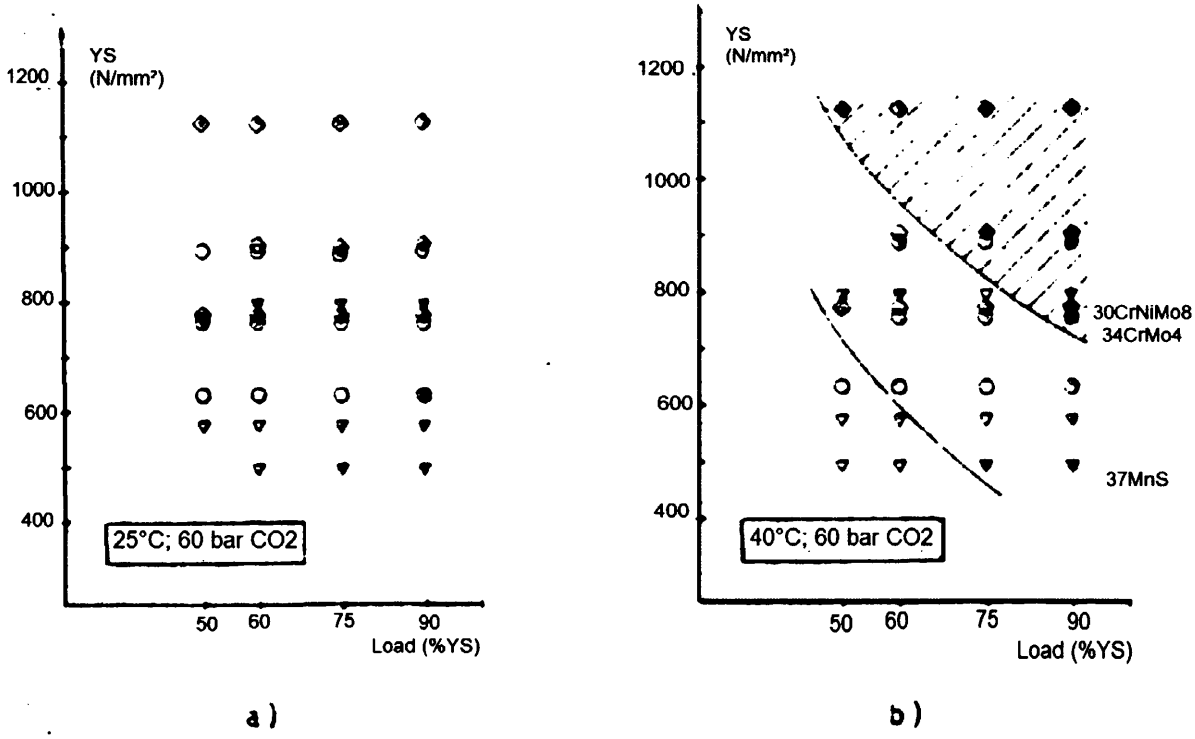

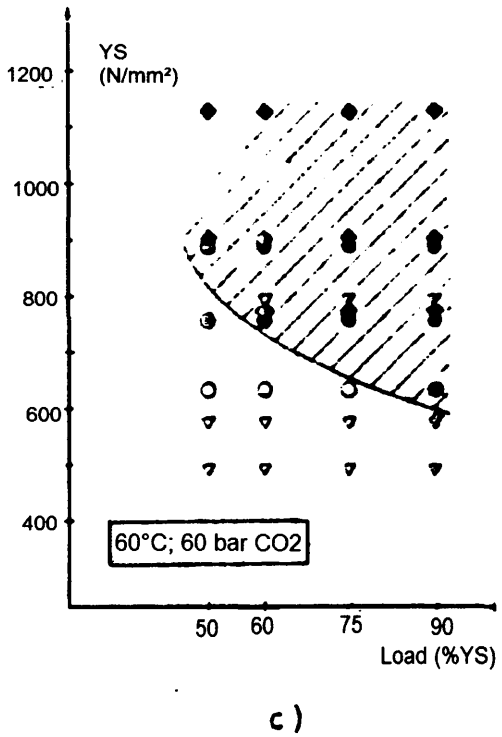

Figure 2-2. Influence of temperature on the cracking susceptibility of low alloy steels in the system CO_2-H_2O at 6 MPa CO_2 as a function of yield strength (YS) and the level of load related to the yield strength, Schmitt[17]. (◊ 30CrNiMo8; O 34CrMo4; ▽ 37MnS; open symbols: no cracks, half-filled symbols: start of cracks, filled symbols: cracks)

2.3.4.3 Mechanism of cracking in the CO_2-H_2O-system

Schmitt[17] used the classical anodic stress corrosion cracking approach to explain the mechanism of cracking. He supported it by findings that cracking susceptibility increased with increasing temperature. In the case of hydrogen embrittlement, the greater susceptibility to stress corrosion cracking would be expected at ambient temperature. Using scanning electron microscopy did not reveal typical indications of of hydrogen participation in the cracking, by the lack of characteristic features such intergranular cracking or blistering on the fracture surface.

Schmitt[3131] also found that the hydrogen permeation rate increased sharply if the CO_2 pressure increased from 100 to 500 kPa. Further increase of the CO_2 pressure at

25°C lead to a decrease, and at 40°C, to an increase in the permeation rate, but with diffusion slopes much less than for the range of 100 to 500 kPa CO_2.

In the CO-CO_2-H_2O system at 60°C in the presence of 100 kPa carbon monoxide, there was no discernable influence of the CO_2 pressure up to 60 bar, indicating the strong inhibiting effect of carbon monoxide and enforcing that cracking would occur by the slip-step dissolution model.

2.3.5 Carbon monoxide

Carbon monoxide falls in the category of an adsorption inhibitor (Heusler[32]) and therefore inhibits the corrosion process of the steel by strong chemisorbtion[24,25]. This was confirmed for iron, on which it reacts slowly to form carbonyl, which is not stable in acid solutions[32], making carbon monoxide not a very effective inhibitor, but one that could be disrupted by slip steps.

Cotton and Wilkinson[33] indicated that carbon monoxide possessed an electronic structure similar to cyanide, in that it is a reproducing complexing ligand that bonds with the metal atom via the carbon atom. Here the weak electron donor properties of the molecule and the vacant orbitals of the metal are involved, as suggested by Trabanelli[34].

Durrant[35] proposed that the carbon monoxide bond on the surface is through the incomplete d-orbitals, by the structure:

$$M{:}C\overset{\pi}{\underset{\pi}{=}}O \qquad \text{2-11}$$

where M is the metal.

The carbon monoxide molecule has a pair of electrons strongly directed away from the carbon-oxygen bond[22], which facilitate adsorption on a metal with unfilled electron levels. Carbon monxide is not adsorbed on zinc, and does not inhibit zinc dissolution as found by King and Rau[36]. They found that carbon monoxide was not completely effective as an inhibitor, since during weight loss experiments, there was some weight

loss, even for short exposure times, which is usually not true for pure adsorption inhibitors. The reason for this ineffectiveness might be the slow adsorption of carbon monoxide to protect certain regions, as found by Heusler[26]. Carbon monoxide adsorbs reversibly on iron in sulphuric acid. The adsorption causes a slight shift in potential, but the overall effect is seen on the anodic polarisation curve, with a considerable diminution of the corrosion rate.

Heusler[32] monitored the corrosion potential of iron while a stream of pure carbon monoxide was passed through the solution, and it became more noble and reached a maximum after about 10 minutes. The corrosion potential ennobled slowly and approached a steady state after 50-75 hours. Similar behaviour was observed after iodide was added to the solution, but the whole process occurred about 100 times faster. If the carbon monoxide was replaced by helium, the corrosion potential ennobled in the first 30 minutes, and moved back afterwards toward the corrosion potential in the pure sulphate solution, which was reached within 2-3 hours.

Trabanelli, Zucchi, and Zucchini[34] worked on the inhibition of iron and nickel by carbon monoxide in hydrochloric acid and sulphuric acid. They produced polarisation curves of the cathodic and anodic behaviour of iron in hydrochloric acid and studied the influence of time on the inhibition process. The corrosion potential of the iron moved to more noble potentials as the time of inhibition increased, but after 240 minutes, the corrosion potential moved back to the uninhibited corrosion potential. This shift in the potential was in the order of 50mV. However, in sulphuric acid, the corrosion potential increased with nearly 50 mV after 15 minutes, and it remained at a potential of -450 mV. With the change in the corrosion potential, the current density also lowered and in hydrochloric acid after 240 minutes, the region of passivity increased considerably compared to the shorter times. Therefore, the kinetics of the carbon monoxide adsorption reaction plays an important role in the passivation of the steel.

Malik and Nawaz[37] did find that cracking occurred with only carbon monoxide present.

2.3.6 Effect of temperature

Kowaka and Nagata[7] observed that cracking occurred in the liquid phase at 40°C and 70°C but not in the gas phase at 100°C and 150°C, although in the gas phase,

microcracking was still found at 100 and 150°C. Cracking decreased with increasing temperature, both in the liquid and the gas phases. They also found that above 100°C, severe general corrosion occurred on the specimens and at lower temperatures little corrosion product was formed[7].

On the effect of temperature, Gräffen and Schlecker[38] reported on steel grade STE 355 in a mixture of CO_2 (2.0 MPa)-CO (1.0 MPa)-H_2O at 60°C, 80° and 105°C. In the case of anodic polarisation, the reduction of area at 60°C was considerably lower than that at room temperature at the same potential. With rising temperature and anodic polarisation, general corrosion increased. While stress corrosion cracking was still found to increase at 80°C, it no longer occurred at 105°C.

Schmitt, Schlerkmann and Aachen[31] also investigated the influence of temperature on stress-corrosion cracking of two high strength low alloy steels, 34CrMo4 and 30CrNiMo8 (0.3% C, 0.25% Si, 0.41% Mn, 1.90% Cr, 1.97% Ni and 0.34% Mo), at 6 and 1 MPa with varying between 0 and 60°C. These were tested with constant load tests, as shown in *Figure 2-3*.

At a CO_2 pressure of 10 MPa, only a slight susceptibility to cracking, indicated by a slight reduction in the reduction in area, was noted at all temperatures. This is in contrast to the results obtained at 6 MPa CO_2 where severe stress-corrosion cracking was observed at the higher temperatures.

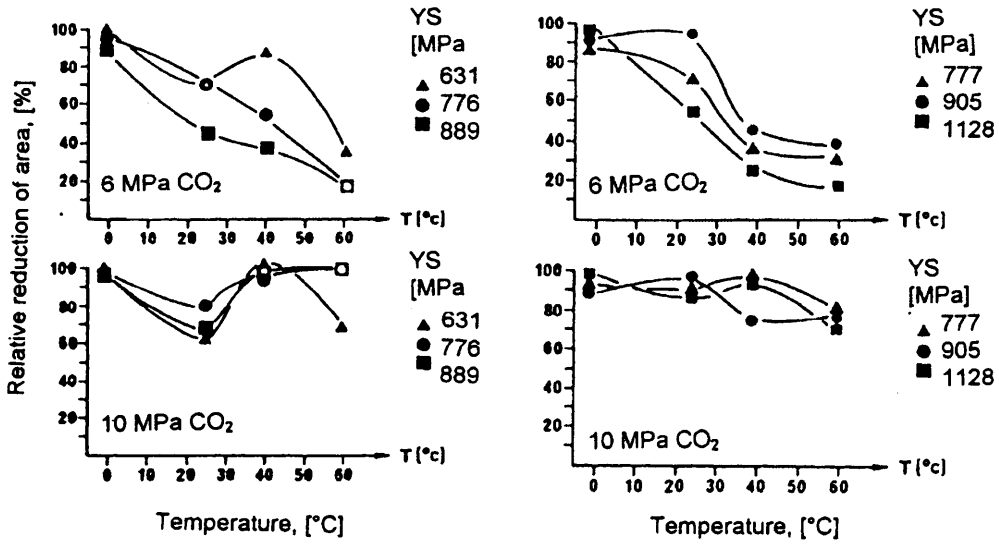

Figure 2-3. Temperarure dependence of the relative reduction of area at 34CrMo4 and 30CrNiMo8 grades loaded with 90% of yield strength at 1 and 6 MPa CO_2, Schmitt et al.[31]

The overall gas pressure plays a significant role in the sensitivity to temperature as seen from the work of Malik and Nawaz[37] as they pointed out that sensitivity to stress corrosion was not severe.

2.4 Electrochemical characteristics

2.4.1 General findings

Brown et al.[5] found that the potential applied to the specimen exerted strong effects both upon the rate of crack growth and overall behaviour, as illustrated in Figure 2-4.

They also found that at potentials more negative than -575mV SCE, cracking was not observed and cracking ceased when the control potential was moved into this range. Between -575 mV and -475 mV SCE, cracking occurred with an increasing rate as the potential was made more positive up to a peak value at -475mV, beyond which cracking was replaced by severe general corrosion. However, the rates of cracking were low in comparison with typical stress corrosion cracking systems. Brown et al.[5] also measured polarisation data for steel exposed to water equilibrated with carbon dioxide at 790 kPa and 260 kPa as shown in Figure 2-5. The influence of CO_2 on the polarisation characteristics was small, with slightly higher current densities at higher CO_2 partial pressures.

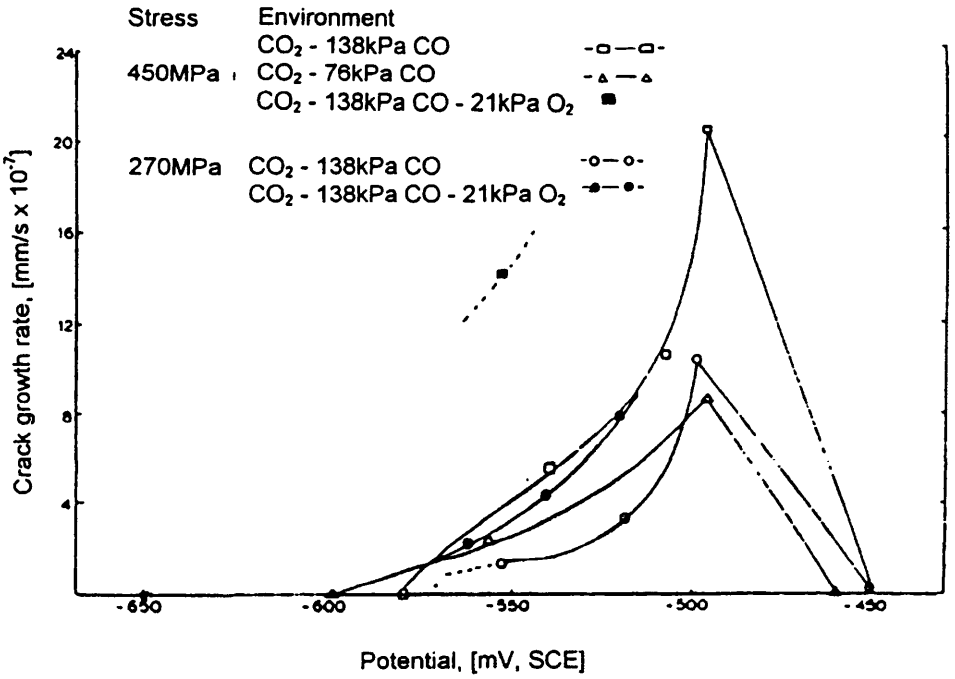

Figure 2-4. *Average crack growth rates as a function of potential for various environments based upon H_2O-CO_2-CO-O_2 mixtures, after Brown et al.*[9].

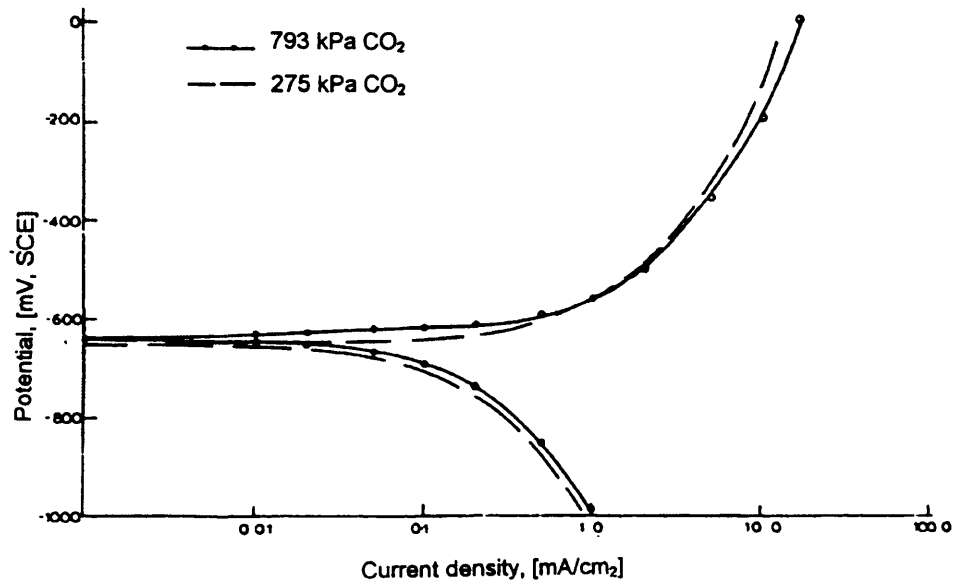

Figure 2-5. Effect of CO_2 pressure on the polarisation curve for plain carbon steel H_2O-CO_2 from Brown et al.[9].

The low conductivity of the solution introduced a resistance error to the polarisation data which creates an increased curvature and masked the detailed kinetic data. However, it is evident that, within the potential range relevant to stress corrosion cracking, this system did not promote passivation of the steel surface.

However, since only ferrous ions could be detected in solution, and hydrogen was detected in the gas phase, the overall corrosion process is most likely to be:

$Fe \rightarrow Fe^{2+} + 2e^-$, *and* 2-12

$2H_3O^+ + 2e^- \rightarrow H_2 + 2H_2O$ 2-13

for low pH levels.

Brown et al.[5] also investigated the influence of CO on the polarization behaviour of a C-Mn steel in CO_2-H_2O environments. Their results, shown in Figure 2-6, indicate that CO significantly reduced both the anodic and cathodic activities.

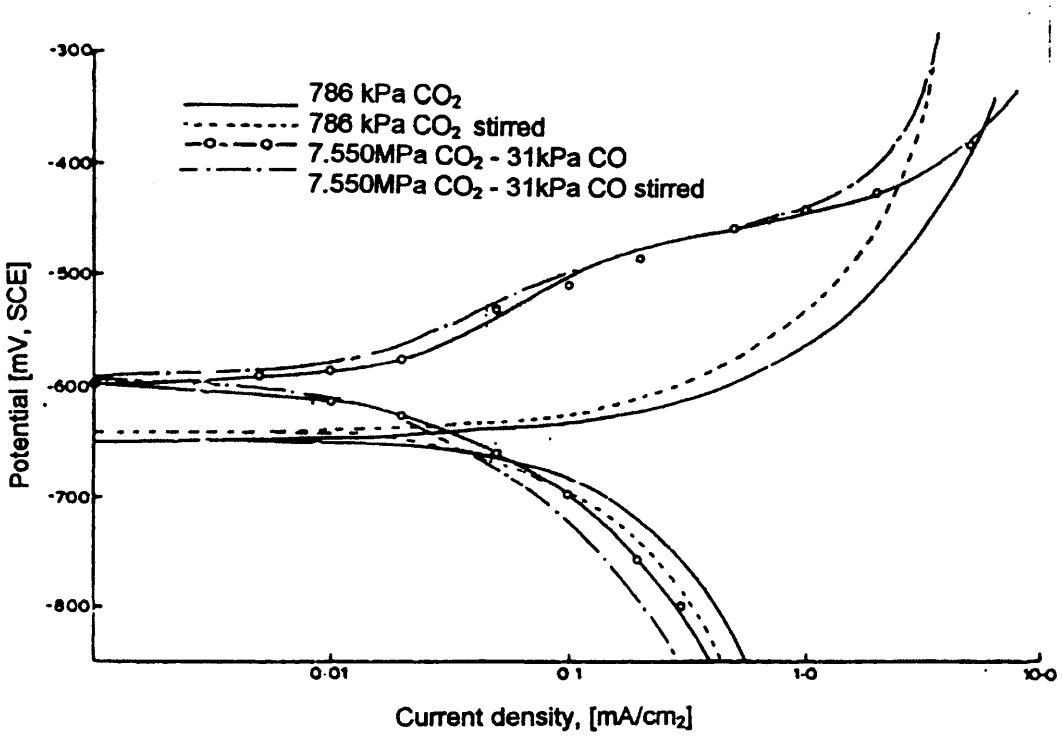

Figure 2-6. Effect on polarisation curve of CO in the gas phase.(Brown et al.[5])

As a general trend, increase of CO pressure caused more positive free corrosion potentials and decreasing rates of anodic and cathodic reactions. The effect of the variation in the carbon monoxide partial pressure on the polarisation characteristics is shown in *Figure 2-7*. Brown et al.[5] suggested that the effect of stirring can possibly be explained by the removal of species that increase the conductivity of the solution from the surface. This will increase the solution resistance and hence the measured overpotential at a certain current density.

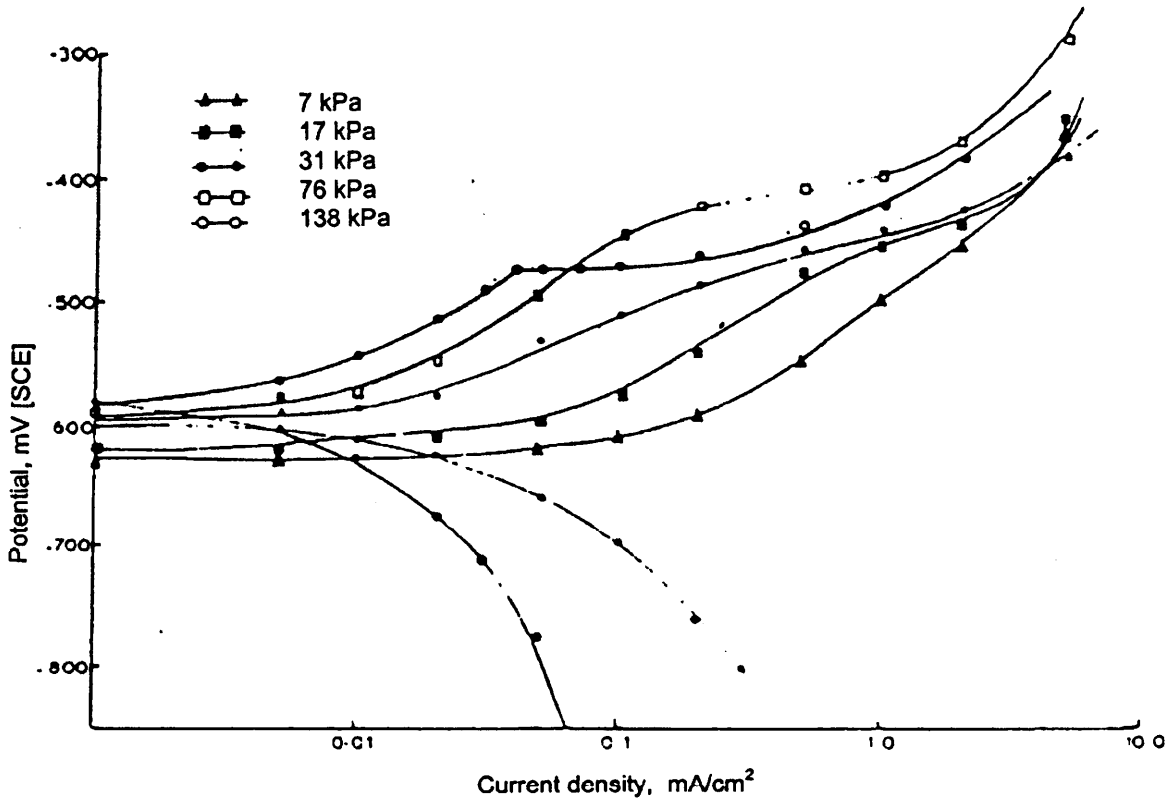

Figure 2-7. Polarisation curves for plain carbon steel in H_2O-CO_2-CO at 793 kPa pressure for various CO partial pressures. (Brown et al.[5])

Polarisation characteristics are mainly influenced by increased carbon monoxide presence and independent of carbon dioxide partial pressure. Increasing the partial CO pressure generally caused a positive shift in the free corrosion potential.

Brown et al.[5] found that carbon monoxide modified the polarisation characteristics in three obvious ways:

a) It produces a positive shift in the free corrosion potential,

b) causes the cathodic reaction to be retarded at all potentials up to -1000 mV SCE, standard calomel electrode, and,

c) reduces the anodic reaction rate at potentials from the free corrosion potential to -350mV SCE.

The ability of oxygen additions to change the polarisation behaviour in the gas-water system was found to be small. However, the interpretation is complicated by the additional cathodic reaction. *Figure 2-8* compares the behaviour in the presence of CO_2 as well as CO-CO_2, both in the presence and absence of O_2.

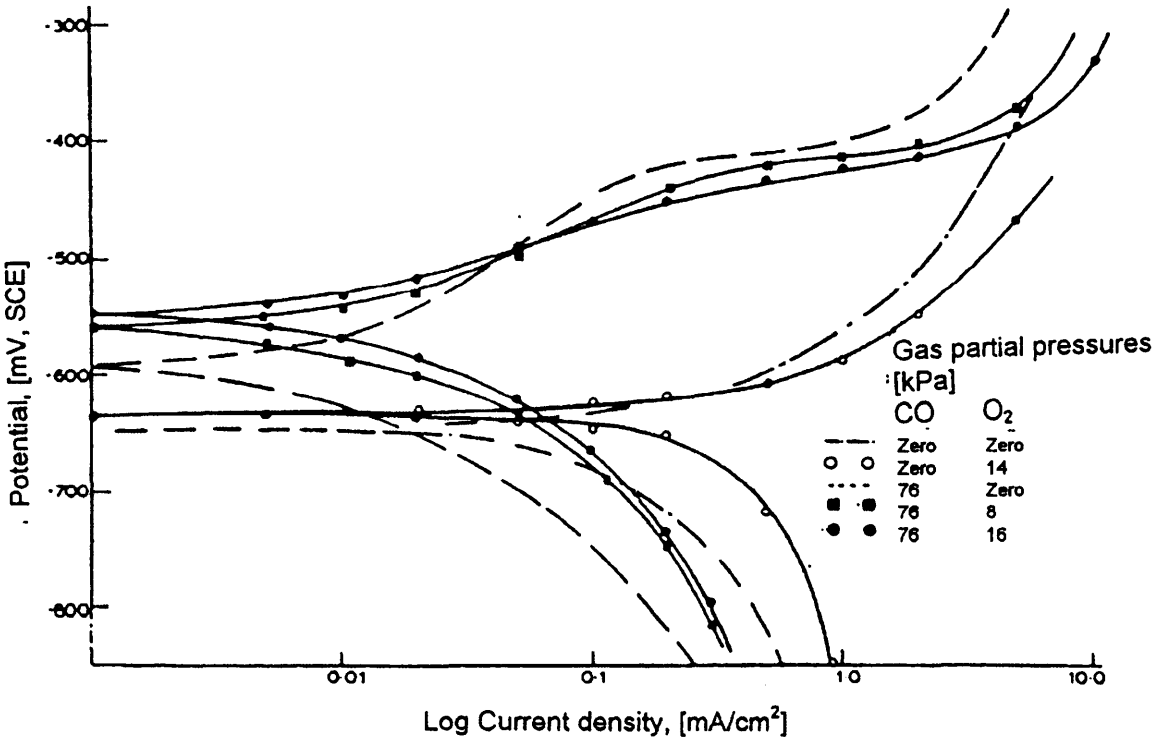

Figure 2-8. Polarisation curves for plain carbon steel in water saturated with oxygen containing mixtures of CO2 and CO. (Brown et al.[5])

From these results, O_2 cause an increase in free corrosion potentials and small general increases in reaction rates. Within the partial pressure range of 6.9 to 34 kPa, O_2 did not affect the characteristics significantly.

The H_2O-CO_2–O_2 system was most strikingly affected where CO was additionally present; both anodic and cathodic reaction rates were reduced at potentials close to

the free corrosion potential. Although this was true at all cathodic potentials tested[5], a region of lower activity appeared in the anodic curve at potentials approximately 150 mV positive of the free corrosion potential, which was measured as -450 mV SCE. At more anodic potentials, the reaction rates moved to those measured in the absence of CO. The extent of the decrease in reaction rates was a function of the CO partial pressure.

2.4.2 Potential dependence of cracking

The observed instances of stress corrosion cracking have all occurred at potentials within the range -575mV to -475mV SCE[5]. This range is largely unaffected by either the stress level for testing, or the CO content of the environment. Brown et al.[5] found that the cracking band corresponded exactly with the range of potentials for maximum corrosion inhibition as affected by CO. A combination of the potential dependence of cracking, with the appropriate polarisation curve, on a common potential axis shows this relation clearly (*Figure 2-9*).

It is also apparent that the elimination of stress corrosion cracking by excessive anodic polarisation, +150mV, coincides with potentials at which inhibition has broken down, and the rates of reaction becoming those for a CO_2-water environment which is a generally corrosive system. Therefore, quite plainly stress-corrosion cracking is associated with the conditions in which corrosion is inhibited and it is absent in conditions where uninhibited general corrosion occurs. However, the cracking band does not span the entire potential range within which dissolution inhibition arises. Cracking rates diminish as the extent of polarisation is reduced, which might be expected since the dissolution aspect of stress-corrosion cracking diminishes. It is possible that the dissolution rates appropriate to the freely corroding situation are so low that insufficient exposure periods were allowed for stress corrosion cracking to be exhibited under these conditions.

The effect of polarisation on stress corrosion cracking of mild steel in water with CO-CO_2 mixtures was studied. Severe cracking occurred during the anodic polarisation, but not during cathodic polarisation. At higher temperatures, stress corrosion cracking of mild steel did not occur, although the steel was anodically polarised. These tests

suggest that the phenomenon is stress-corrosion cracking rather than hydrogen embrittlement.

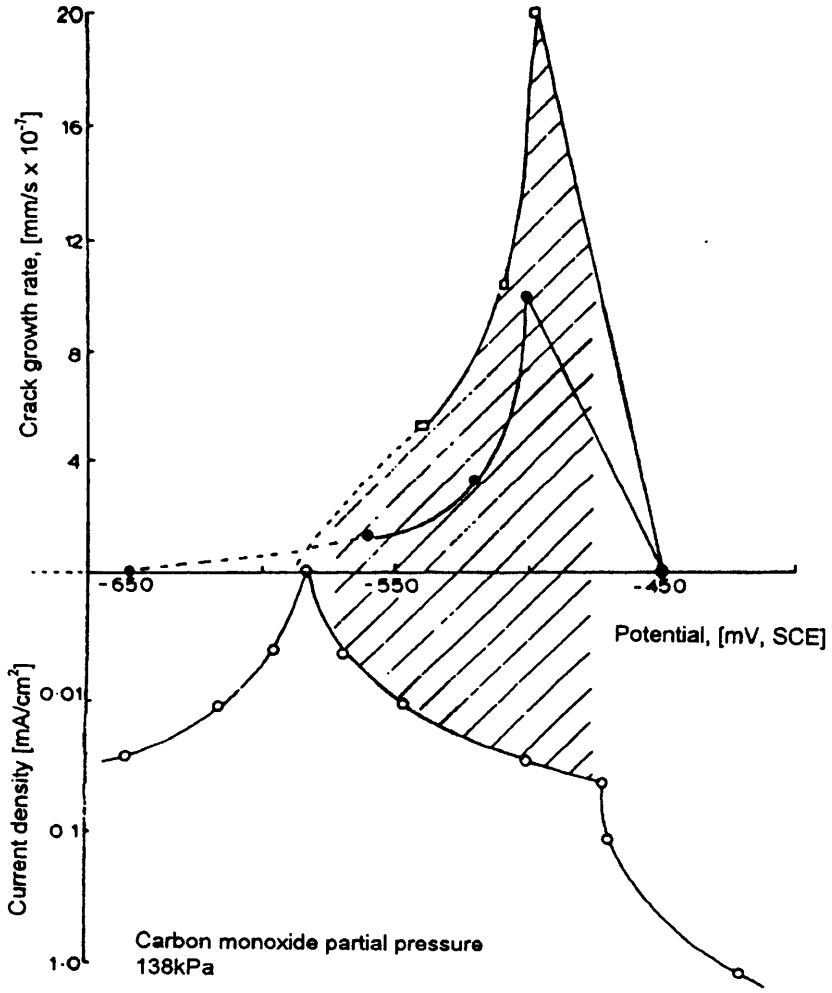

Figure 2-9. Relation between rate of crack growth and extent of CO inhibition as a function of electrochemical potential. (Brown et al.[5])

2.4.3 Electrochemical characteristics at room temperature and atmospheric pressure

Traversa and Calderon[39] investigated the electrochemical characteristics at room temperature and atmospheric pressure. The polarisation curves were obtained for carbon steel in an aqueous environment saturated with the gas mixture that was

bubbled through. The gas mixture as shown in Table 2-2 was used, as well as carbon dioxide with no carbon monoxide.

In the absence of carbon monoxide, the conditions were very stable and reproducible, especially as far as the free corrosion potential is concerned, while in the presence of the gas mixture, marked fluctuations were noticed for the same kind of tests[39]. Polarisation characteristics at both a low scanning rate of 0,01 mV/s and a higher scanning rate of 2 mV/s did not exhibit the critical potential range for stress corrosion cracking. However, the free corrosion potential shifted to a more positive value at the

Table 2-2. Gas mixture composition used for the tests[39].

Component	% used in the gas mixture
CO	68
CO_2	17
O_2	0,5
N_2	14,4

lower scanning rate. Traversa and Calderon[39] performed tests at several different imposed potentials, both for the carbon dioxide and the carbon monoxide-carbon dioxide-water environments. They measured the current densities after 24 hours at the different potentials and found the critical range for stress corrosion cracking as shown in *Figure 2-10*.

The current density increased up to -530 mV SCE and then decreased to -500 mV SCE, with a later increase with increasing potential[39]. These results indicated an active-passive transition, corresponding to the critical potential range in which the steel is susceptible to stress-corrosion cracking, which is approximately -540 to -460 mV SCE. They found the upper limit of this range was more difficult to define, because at the higher potentials, the current density increase was slower. However, in Figure 2-10 the potentiostatic measurements are compared to the 2 mV/s scanning rate, but when this is compared to the 0,01 mV/s scanning rate the current densities of

the potentiostatic measurements were higher than at a scanning rate of 0,01 mV/s. This is unexpected as they claimed at 24 hours 'stationary conditions' were reached, and at the slow scan rate the situation is further away from equilibrium. There is therefore some discrepancy in the results, or a reactivation of the anodic current density after a certain period, or an enhancing of passivity at slow potential scanning rates.

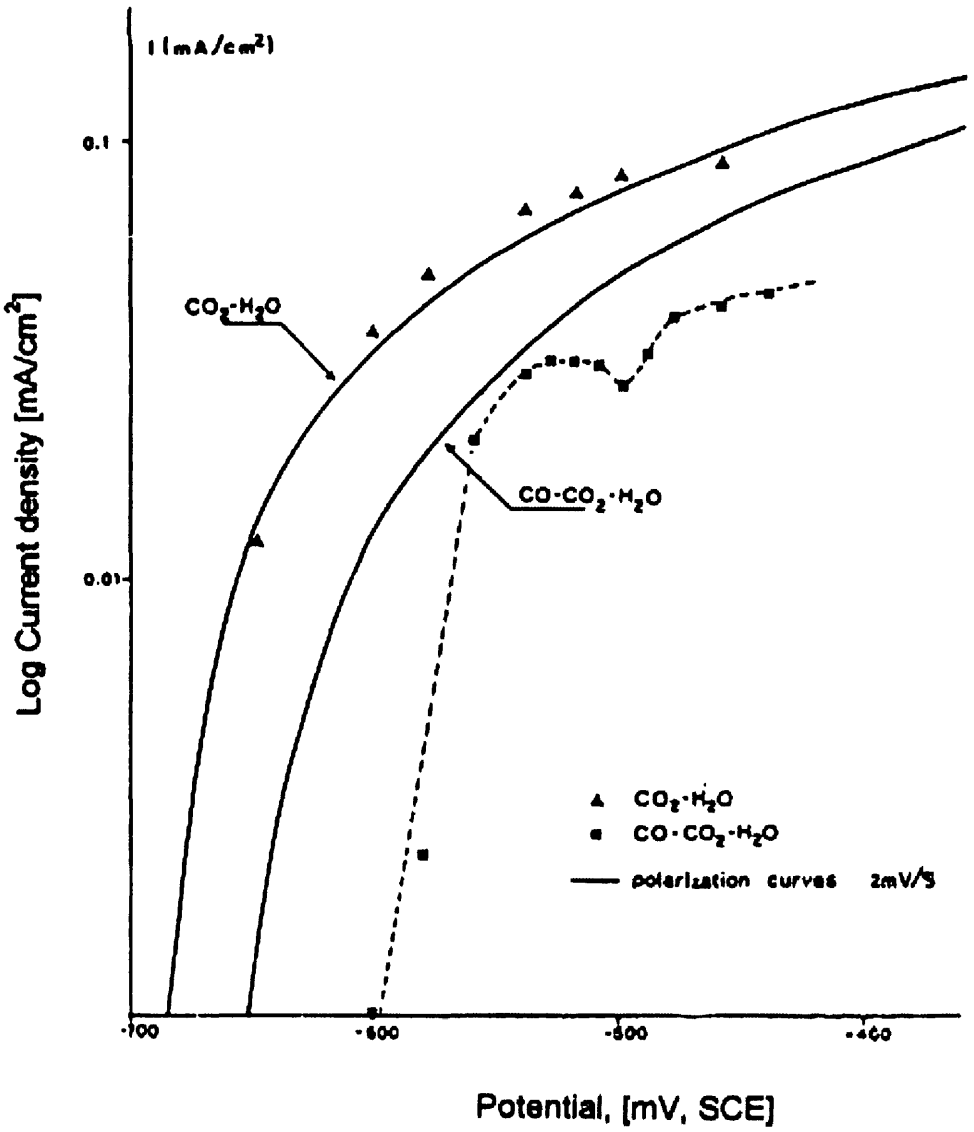

Figure 2-10. Chronopotentiostatic tests of carbon steel in CO_2-H_2O and CO- CO_2-H_2O environments, in comparison with the anodic polarisation curves obtained at a scanning rate of 2mV/s. *(Traversa and Calderon[39])*

Heaver[40] obtained polarisation curves in condensate, from a process line saturated with carbon dioxide and carbon monoxide gas, and found that the system was 'virtually independent of carbon monoxide partial pressure', or more realistically that for the 2,6% and 10% carbon monoxide, he tested, the polarisation characteristics were similar. However, even this statement needs qualification, since this is only true after sufficient time is given for the curves to settle to the same shape, regardless of the two partial pressures. At the low carbon monoxide partial pressure, this process is quite slow and there is a greater tendency towards free corrosion, as expected. Anodic and

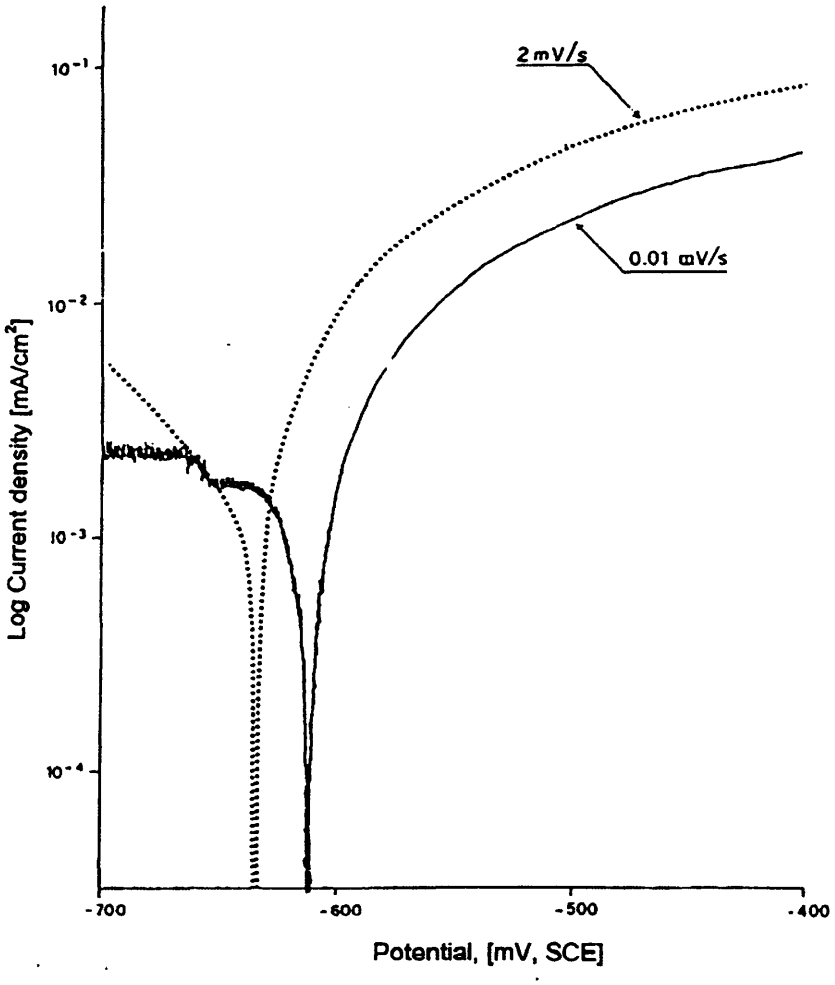

Figure 2-11. Polarisation curves for carbon steel in CO-CO_2-H_2O environment at two different scanning rates. . (Traversa and Calderon[39])

cathodic polarisation in the CO-CO_2-H_2O system showed a marked time dependence and was characterised by significantly early cathodic inhibition that shifted the cathodic to lower current densities. This was accompanied by a movement of the free corrosion potential to more negative values. The time dependency is further seen in the slower inhibition of the anodic reaction, and the free corrosion potential moves to more positive potentials, although when anodic and cathodic passivation occurred simultaneously, there was little change in the corrosion potential. The anodic passivation was typified by a breakdown potential, which is time dependent and moves to more positive values after longer exposure times. Above the breakdown potential, small changes in potential gave rise to high current densities.

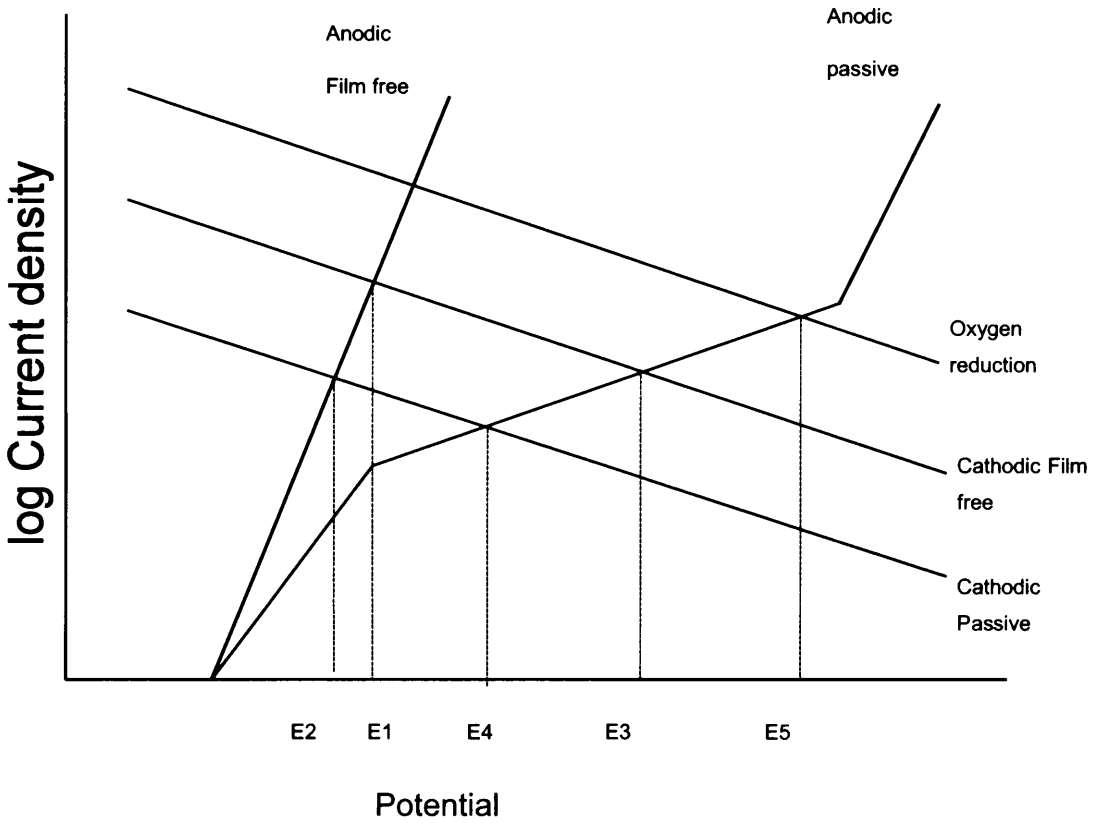

Figure 2-12. Evans diagram showing the effect of anodic and cathodic inhibition on E_{corr} after Heaver[40].

In the presence of oxygen the corrosion potential is located at significantly higher potentials than when oxygen was absent. This is explained in the Evans diagram as proposed by Heaver[34], shown in Figure 2-12. Inhibition of the cathodic reaction will result in a slightly lower corrosion potential from E_1 to E_2 if the anode remains film free. By the same token, anodic passivation will shift the corrosion potential from E_1 to more positive values at E_3, should the cathode stay flim free. However, if the cathode is simultaneously passivated the corrosion potential will eventually settle at E_4. With the addition of the oxygen reduction reaction to the Evans diagram, the corrosion potential was moved to significantly higher potentials at E_5 after anodic passivation. However, from the results of Brown et al.[5], the effect of increased oxygen was not observed.

2.5 Mitigation of cracking by changing the passivity of the steel

As explained already, the incomplete inhibition by the adsorbed carbon monoxide is the apparent cause of the localised attack of cracking, for either stress corrosion cracking or hydrogen embrittlement. As this localisation becomes more general, the cracking is mitigated. If the inhibition of the steel is promoted and passivation occurs sufficiently and at a high rate, cracking can be mitigated as will be described.

2.5.1 Inhibition

Dunlop and Olson[14] worked on the inhibition of stress corrosion cracking in CO-CO_2-H_2O environments after incidents of transgranular cracking of low strength steels occurred in the handling of reformed and coal gas. In the gas, there has been significant concentrations of carbon monoxide (ca 3,5% mole) and traces of dissolved oxygen (0,03%) at pressures and temperatures that cause cracking. According to the mechanism of cracking proposed by Brown et al.[5] and Kowaka and Nagata[7], cracking can be mitigated by addition of either salts to destroy the passivity or inhibitors effective enough to protect the entire surface. Dunlop and Olson[14] studied both scenarios for mitigating stress-corrosion cracking, using U-bend specimens to evaluate the environments. They tested nine salt and mixed salt additions and found that 0.5wt% NaCl and 0.2wt% mixed salt (simulated oil field brine) additions inhibited cracking. The lowest concentration for “effective” inhibition of cracking was

0.1wt% potassium iodide. Sodium benzoate and sodium sulphate at concentrations of 0.5wt% and 5wt% respectively inhibited cracking. These solutions, except for sodium benzoate, caused considerable pitting and are not a viable solution. They also tested inhibitors and biocides. Amido amine was ineffective at the level of 0.12vol% but proved effective at 0.5vol%. The biocide, dicoco quaternary ammonium chloride, was effective at 0,12vol% with and without the inhibitor amido amine present. Olel propylenediamine, a difunctional inhibitor, was effective down to 0.015vol% in distilled water. A proprietary polycyclic amidine was also effective in distilled water and brine but no concentration was given.

Dunlop and Olson[14] further showed that interaction between inhibitor, biocides and brines also necessitated that higher concentrations were required for effective inhibition of cracking. In simulated field brine, the inhibitor amido amine prevented cracking, not influencing the effect of the brine, but with the addition of the biocide quaternary ammonium chloride cracking results. Cracking was only prevented when the biocide concentration is at 0.015vol%. The strong adsorption of the quaternary ammonium chloride had an antagonistic effect on inhibition. For the other quaternary biocide dicoco quaternary, ammonium chloride which is more bulky and disubstituted, and is expected to adsorb weaker than quaternary ammonium chloride the effect was less, as expected.

Dunlop and Olson[14] tested a neutralising amine, ethylene diamine. It did prevent cracking, but was unreliable up to a pH of 9. They tested a mixed inhibitor containing an oil soluble filming amine and morpholine (a neutralising amine), which prevented cracking in distilled water and condensate (225 ppm total salts), and 0,3wt% inhibitor prevented cracking. They found that polyfunctional molecules (oleyl diamine) showed stronger adsorption are more effective. Therefore, these inhibitors were only effective at relatively high concentrations which limit their use considerably.

Heaver[40] tested inhibitors that were mostly film forming inhibitors, which enhance the passivity. He used the slow strain-rate test to evaluate these inhibitors. The repeatability of these tests was not particularly good, because reported reductions in area varied over a 15% range which was nearly 50% of the measured value[40]. In a rich gas with partial pressures for carbon monoxide and carbon dioxide, at 210 kPa and 230 kPa respectively and a test temperature of 50°C, the only inhibitor that

showed a significant increase in reduction was Petrotec 1420, and only at 5000 ppm. Petrotec is a water dispersible inhibitor-neutraliser, which contains a mixture of thiophosphates (30-60), fatty amine quaternaty salts and an acid phosphate ester, in aromatic hydrocarbons. Unfortunately, this significant inhibition only occurred at 5000 ppm and not 1000 ppm as for the other inhibitors. The improved percentage reduction in area was due to its neutralising ability as the amine component neutralised the dissolved carbon dioxide. The only other inhibitor that showed improved behaviour was Reomet 42 (or Ranomet 42 - it is not stated clearly in the text). Already at 100 ppm, an improvement was noted, but at 1000 ppm two tests were performed, of which one was lower than the lowest uninhibited test. Reomet is a multimetal inhibitor and the active chemical ingredient is a triazole derivative. Tests done in a lean gas (partial pressures of carbon monoxide and carbon dioxide were 34kPa and 266kPa respectively) showed KXO-63 to give the best result, which was still within the scatter of the 25°C uninhibited test results. KXO-63 is a formulation of acid phosphate esters (30-60) phosphoric acid and thiophosphates (10-30) in water. These results of Heaver[34] and Dunlop and Olson[10] are difficult to compare, because of the test methods that were used. The slow strain-rate test is a severe test and good for screening, whereas the constant load test is not as severe.

Kowaka and Nagata[3] tested H_2S as an impurity. The inhibitive effect of H_2S was observed, and cracking did not occur in the CO-CO_2 mixture with water containing 395 ppm H_2S.

Heaver[40] based the choice of inhibitors on the work done by Parkins[41] where the inhibitors were classified for stress-corrosion cracking into two categories: firstly, those which moved the potential out of the zone of susceptibility, thereby preventing stress-corrosion cracking, or secondly, by inhibiting the attack while the potential remains in the susceptible range. The former is considered unsafe due to the possibiity that the potential might drift back to the susceptible range. From the work that was done, it seemed clear that effective inhibition is not a viable option practically. It is known that cracking does occur in a very narrow potential range, and therefore might the former type of inhibitor work better.

2.6 Metallurgy

2.6.1 Alloy additions

Kowaka and Nagata[3] worked on various commercial alloys and found that the mild steel, Mn-V steel and the 3,5 Ni steel all showed cracking in these environments. However, a 18Cr-8Ni stainless steel did not show cracking. No stress corrosion cracking occurred for alloys with a chromium content higher than 9%. A 5Cr-0.5Mo steel cracked in the liquid phase, but not in the gas phase.

Tanimura et al. [42] investigated steels with increasing chromium content in the wet-gaseous phase at 20°C and total pressure of 4,1 MPa. The gas composition was 24,7% CO, 13.7% CO_2 and 61.6% N_2. Carbon steel, 2.25Cr – 0.5Mo steel and 7Cr - 0,5Mo steel failed by stress corrosion cracking, while 9Cr - 1Mo steel, 10Cr - 1Mo steel, 13 Cr steel and 17 Cr steel did not exhibit stress corrosion cracking.

All of the work indicates that stress-corrosion cracking in CO-CO_2-H_2O can occur in low alloy steels, irrespective of strength level over a range of CO and CO_2 partial pressures.

2.6.2 Heat treatment

Tanimura et al.[42] investigated the effects of pipe grade and heat treatment in 65% CO - 35 % CO_2 at 1,6 MPa total pressure. Normalised C-Mn steel was less susceptible to stress corrosion cracking than quenched and tempered C-Mn steel with tensile stengths of 772 and 793 MPa, respectively. A C-Cr-Mo steel, quenched and tempered to 873 MPa tensile strength, was comparable in stress-corrosion cracking sensitivity to the quenched and tempered C-Mn steel, whereas more severe stress corrosion cracking was observed for the C-Cr-Mo steel quenched and tempered to 1029 MPa tensile strength. From these results, it seemed that more severe cracking occurs at higher tensile strengths.

However, from the work of Schmitt, Schlerkmann and Aachen[23] on the influence of temperature and total pressure on the high strength-low alloy steels with a different yield strength, no pattern is seen from the results (*Figure 2-13*) except that at 1 and 6 MPa total pressure and 0°C, the highest yield strength steel gave a relative reduction in area that was about 80% lower than the other yield strength steels tested. This

might be an indication of another mechanism at work, such as hydrogen embrittlement, since at low temperatures hydrogen embrittlement is not necessarily inhibited. At the other temperatures considerable scatter was found on all the heat treatments. The higher pressure showed a more significant pattern with a definite maximum susceptibility at the intermediate temperatures, except for the high yield strength steel that showed significant embrittlement up to 40°C. The lowest yield strength steel showed maximum susceptibility at lower temperatures, around 25°C.

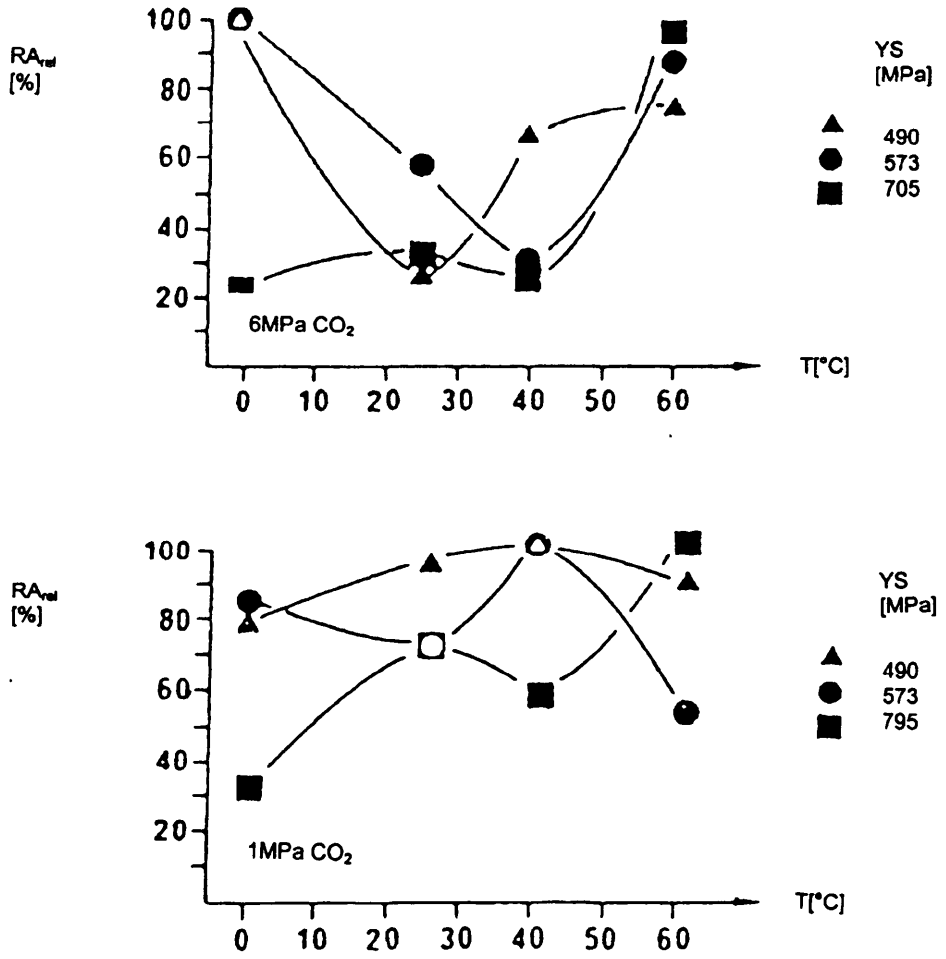

Figure 2-13. Temperature dependence of the relative reduction of area at 37Mn5 grades loaded with 90% of the yield strength at 1and 6MPa. (Schmitt et al.[31])

2.6.3 Surface finish

Kowaka and Nagata[7] found that four-point beam tests on specimens with different surface finishes showed that an acid pickling finish gave the best results, followed closely by an emery finish for the C-Mn steel they evaluatated. Cracking was more severe with mill scale present, than when it was removed. Specimens with scale still showed cracking at 0.3 x yield strength, while the emery finish did not show cracking at 0.5 x yield strength.

2.7 Stress related issues

2.7.1 Strain rate

Berry and Payer[15] performed slow strain-rate tests with decreasing strain rates, and found that the percentage reduction in area decreased with the strain rate. The minimum strain rate tested was at $2x10^{-7}$ with a reduction in area of 10%, as shown in Figure 2-14. Therefore, what occurred at lower strain rates was not revealed by their results, and if a point of maximum susceptibility to stress-corrosion cracking does exist, it would give some indication of the cracking mechanism.

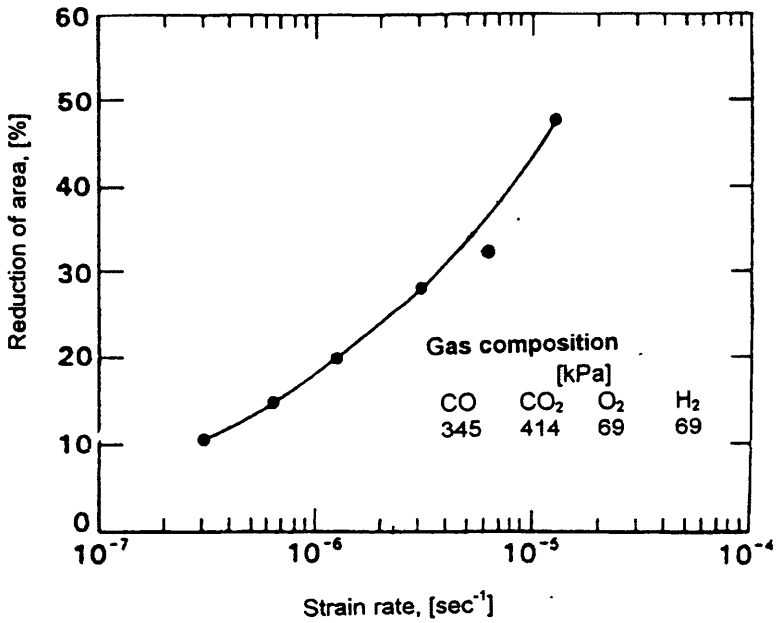

Figure 2-14. Effect of strain rate on severity of stress corrosion cracking of X52 steel[15].

Parkins[43] studied the strain rate effects on stress-corrosion cracking which although, not directly related to the stress-corrosion system studied is similar. This is because pipeline steels in carbonate-bicarbonate solutions exhibit external cracking, and this might enhance the understanding of the current system. Since engineering design is mostly based upon stressing considerations, and creep - or the time dependence of strain - is usually regarded as a high temperature phenomenon, there is sometimes reluctance to contemplate the implications of strain rates in the context of environment sensitive cracking. However, Parkins[43] showed that crack growth kinetics provided a more rigorous approach, through the concepts of surface or crack-tip strain rates, to model environment sensitive cracking, than do stress or stress intensity factor considerations. Although microplastic deformation is induced by the application of stress to a structure, the synergistic effects of the time dependency of corrosion-related reactions and microplastic deformation provided a framework for understanding and modelling environment-sensitive cracking, which cannot be adequately described by simple stress relations. In the system that was studied the single factor that influence corrosion inhibition the most in the presence of carbon monoxide is the time dependency, which again depends on other factors.

Many systems sensitive to the effects of strain rate involve dissolution and film rupture in the crack growth mechanism, but even hydrogen-related cracking, involves the disruption of films to allow hydrogen entry to the metal and the transportation of hydrogen once it is absorbed into the metal lattice, indicating the importance of strain rate for both kinds of cracking systems. Parkins[43] considered intergranular stress corrosion cracking of high-pressure pipelines fabricated from ferritic steels with the stress-corrosion induced by a carbonate-bicarbonate solution derived from the ground water. A beam deflection test showed that when the electrochemical potential was changed to a value that promoted cracking after the creep rate had diminished below a value that initiates or sustains cracking, crack propagation was not discerned. However, with the potential initially outside the critical range for crack propagation, but adjusting the potential to a cracking sensitive range before the creep rate fell below a value that sustained cracking, it induced a stress-corrosion crack to propagate. Therefore, creep rate is essential for the continued crack propagation and even when conditions for cracking is ideal, and the creep rate was too low, cracking terminated.

The effect of stress, σ, upon creep rate, $d\varepsilon/dt$, is frequently expressed in the form of a power law or in logarithmic form, as

$$\log d\varepsilon / dt = \log a + b \log \sigma \quad \text{.....2-14}$$

where a and b are constants.

Analysis of the creep curves for a range of pipeline steels showed that while the creep responses varied between the steels, as reflected in the constants a and b, they all conformed to Equation 2-o.

The creep response of pipeline steels can be varied by subjection to different strain aging treatments. Figure 2-15 allows a comparison of the calculated and experimentally determined threshold stresses for a pipeline steel subjected to various aging treatments. The calculated values were determined from the creep response of the steel as a function of stress and the limiting beam deflection rate of 5×10^{-7}mm/s. There is reasonable agreement between the calculated and observed values, supporting the argument that it is strain rate that is the controlling parameter in stress corrosion cracking growth.

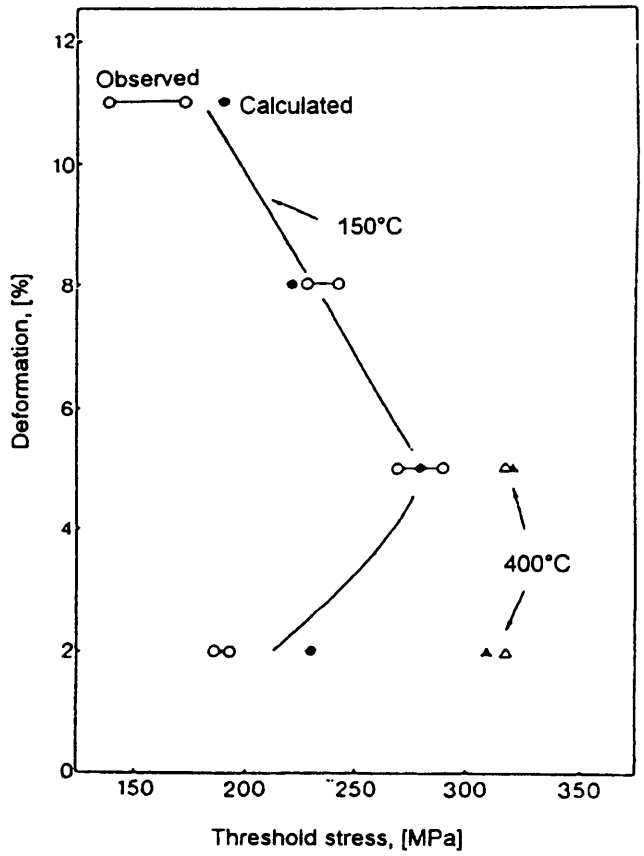

Figure 2-15. Observed and calculated values of the threshold net section stresses for cracking of a pipeline steel in carbonate-bicarbonate solutions at 75°C and -0.65V (SCE) after various deformations and aging treatments involving 1 hour at 150°C and 72 hours at 400°C, Parkins[43].

Constant load tests on plain steel specimens yields a creep rate that will diminish as work hardening occurs with the application of load, but initiating cracks will enhance creep in their associated plastic zones. Which of these two opposing effects dominates will determine whether or not crack propagation is sustained. If cracking maintains the creep rate above the limiting value, cracking continues and total failure will ensue, as is true for all tests performed above the threshold stress. But if the rate of crack growth is not sufficient to maintain the creep rate above the limiting value, then crack growth ceases, which happens at stresses below the threshold. This threshold stress is not the stress above which cracks form, but rather is the stress above which they continue to propagate. However, this crack propagation above the threshold is not always continuous. Nevertheless, specimens tested below the threshold stress revealed cracks and the depths of these cracks varied with the initial applied stress as shown in *Figure 2-16*[43].

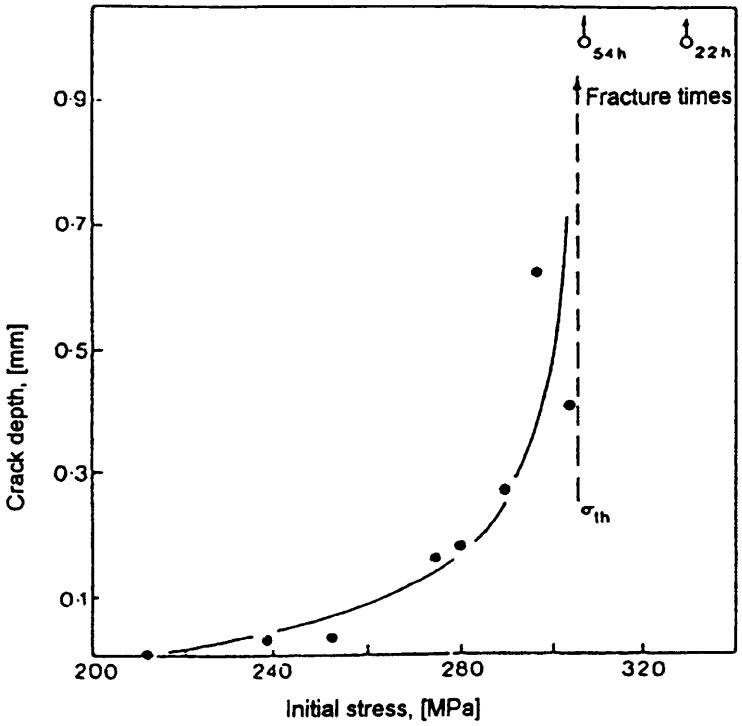

Figure 2-16. Maximum intergranular crack depths for different applied stresses below the threshold stress (σ_{th}) for a C-Mn steel in carbonate-bicarbonate solution at 90°C and -0.65V (SCE), Parkins[43].

The depth of the terminated cracks diminished as the initial stress was reduced until no cracks were formed. The data for these results were obtained from constant load tests, but if appropriate strain rates were to be applied to specimens, as opposed to allowing them to creep under constant load, crack growth would be sustained if the applied strain rate produced appropriate crack-tip strain rates. However, to apply these findings, in relating the creep or strain rate effects indicated above for laboratory tests to practical situations is difficult, since operating pressures are appreciably below hydrostatic test pressures, and the chance of achieving a strain rate that will promote stress corrosion cracking appears very remote, at least on the basis of design criteria. However, Parkins[43] proposed cyclic loading to which pipelines are subjected at varying degrees will sustain creep. This creep rate will be greater than that induced under static loading conditions for the same maximum stress.

2.7.2 Cyclic loading effects that induces critical strain rates

At temperatures of the order involved with pipelines, creep is limited by work hardening, reflected in the time dependence of creep indicated by Equation 2-p. At relatively low temperatures, the time dependence of creep is usually found to be logarithmic with the total plastic strain, ε, and time, t:

$$\varepsilon = \alpha \ln t + \beta \quad \text{.....2-15}$$

where α and β are constants.

Loading each increment of strain results in dislocations, and storage of dislocations therefore leads to a continuous reduction in the rate of plastic strain. However, if the load is wholly or partly removed, the structure developed in work hardening may be unstable, and on reloading, additional transient creep may occur until the strain rate is again reduced by work hardening.

Parkins[43] found that load cycling produced stress corrosion cracking at significantly lower stresses than those with static loading. A pipeline steel exposed to a carbonate-bicarbonate solution cracked intergranularly under static and cyclic loading conditions at various frequencies. In the absence of cyclic loading, the K_{ISCC} value was observed at about 22MPa.m^{½} (Figure 2-17).

However, with cyclic loading at 0.19 Hz, the intergranular cracking region extended to an amplitude of nearly 20 MPa.m^{½} and the stress corrosion cracking threshold mean stress intensity factor was lowered to 10 MPa.m^{½}. This occurred at a low stress intensity factor amplitude of 2 to 3 MPa.m^{½}, and the cracking region extended to a stress intensity amplitude of nearly 20 MPa.m^{½}. However, when the frequency was increased to 11 Hz, the mean stress intensity threshold factor for stress corrosion cracking was not lowered, and the amplitude stress intensity factor was 5 MPa.m^{½} when there was a transition in the mode of fracture to transgranular cracking.

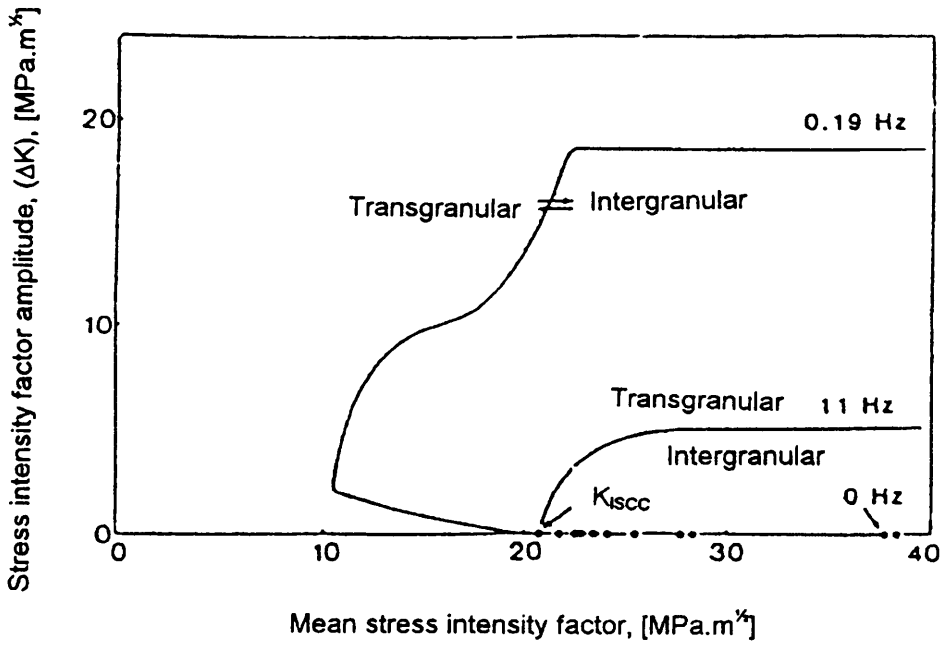

Figure 2-17. Modified Goodman diagram indicating loading parameters for which intergranular and transgranular cracking were observed in a pipeline steel exposed to carbonate-bicarbonate solution at 75°C and -0.65V (SCE), Parkins[43].

Parkins[43] found that load changes in pipeline steel tested had a dramatic effect. Under static loading, creep was virtually exhausted after a certain time and with simple loading and unloading creep was dramatically revived. The creep strain or cumulative cyclic strain was dependent on the amplitude of the load reversals, the frequency with which the load changes were made, the proportion of load removed, and the temperature. These factors originate from the extensive re-arrangement, or annihilation, of dislocations necessary for a sustained creep rate during load cycling. The maximum stress applied to the specimen also had a strong influence on the accumulated creep strain rate, and at a certain maximum stress, the threshold mean stress responded differently to the stress amplitude of different steels. As the stress amplitude was raised, the threshold mean stress was lowered, but the decrease depended on the particular steel that was tested. This was likely to be due to differing microplastic deformation responses to cyclic loading. The microplastic deformation response was supported by measurements of the plastic deformation of an X-70 pipeline steel loaded at a frequency of $1{,}5 \times 10^{-4}$ Hz. The plastic strain increased approximately linearly to the logarithm of time, and the total plastic strain (after 100

cycles) shown in Figure 2-18, increased markedly with the mean stress close to the threshold stress for stress corrosion cracking.

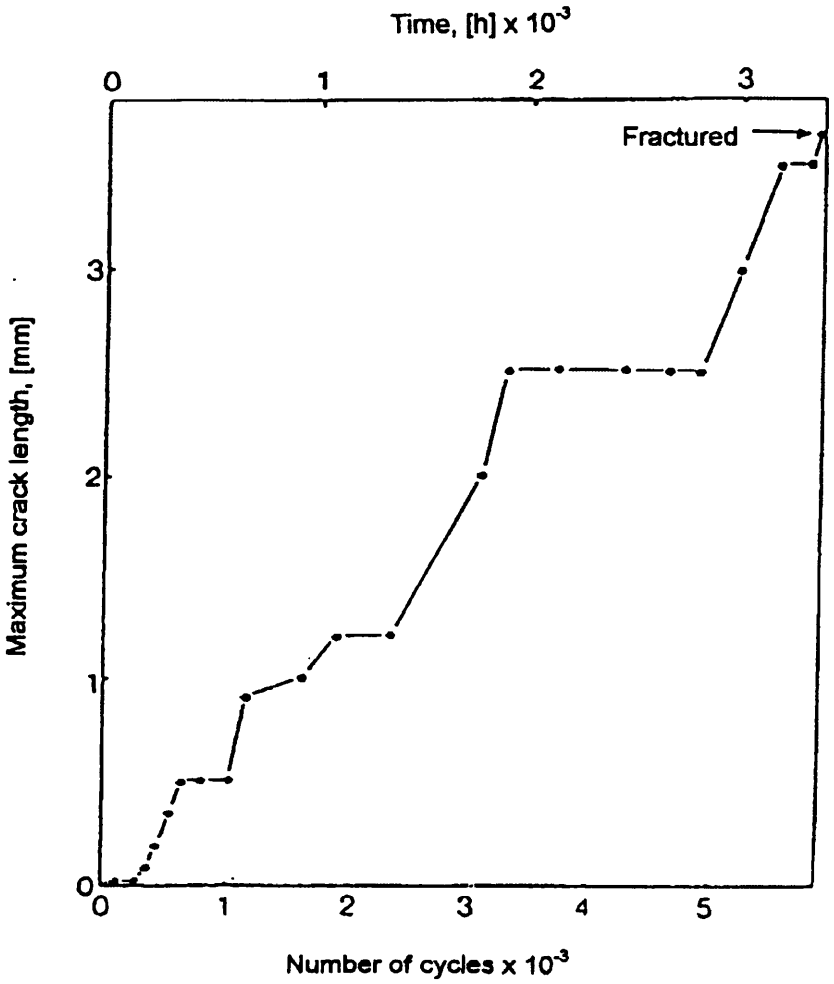

Figure 2-18. Microplastic strain after 100 cycles as a function of the mean stress for two levels of fluctuating stress, together with the threshold mean stress for stress corrosion cracking at those fluctuating stresses, Parkins[43].

The influence of plastic strain is further underlined by the increase of the threshold maximum stress for cracking as the limit of proportionality increases for different pipeline steels.

2.8 Crack growth kinetics

Microplastic strain and its time dependence are important in relation to crack growth rates. Many authors have shown that where stress corrosion cracking growth is by a dissolution process, the crack velocity, CV, is reasonably represented by writing Faraday's second law as a penetration rate,

$$CV = i_a \cdot \frac{M}{zFd} \quad \text{.....2-16}$$

where i_a=anodic current density;

M=atomic weight of the metal,

d = of density;

z = valency of the solvated species; and

F = Faraday's constant.

However, the stressing conditions necessary to yield such crack velocities as calculated in Equation 2-q are unrealistically high for operating conditions of structures, and are only likely to be achieved in the later stages of growth, when the stress corrosion cracks have resulted in considerable stress intensification. This discrepancy of only predicting correct crack velocities at high stresses has a number of probable explanations, but one is that Equation 2-q represents an upper-bound velocity that is only observed so long as the crack tip remains unfilmed. If filming occurs to the extent that dissolutions ceases, the local crack growth rate will remain at zero until the rupture of such films reactivates dissolution. Thus, the processes of metal dissolution, film formation and film rupture collectively determine the average crack growth rate, which can be anywhere between the upper bound given by Equation 2-q and zero, depending upon the relative contributions of the three processes mentioned. The crack-tip strain rate becomes an important parameter because it determines the time interval between film rupture events, in the extreme, creating bare metal at a rate that exceeds the film growth rate to permit the upper-bound growth rate to be achieved. This possible bare metal scenario requires the anodic current density in Equation 2-q to be replaced by the appropriately integrated

current transients that are obtained between film rupture events, so that Equation 2-q becomes:

$$CV = \frac{Q_f}{\varepsilon_f}.\dot{\varepsilon}_{ct}.\frac{M}{zFd} \quad \text{.....2-17}$$

where Q_f = the charge density passed,

ε_f = strain to rupture the film, and

$\dot{\varepsilon}_{ct}$ = crack-tip strain rate.

The initiation of stress corrosion cracking requires the disruption of surface films, just as does their continued growth. The time dependence of plastic strain therefore implies that crack nucleation will be time dependent. Moreover, while data such as those shown in *Figure 2-19*, or expressed in the form of Equation 2-q, refer to the strain averaged over some effective gauge length, the strain is not uniformly dispersed.

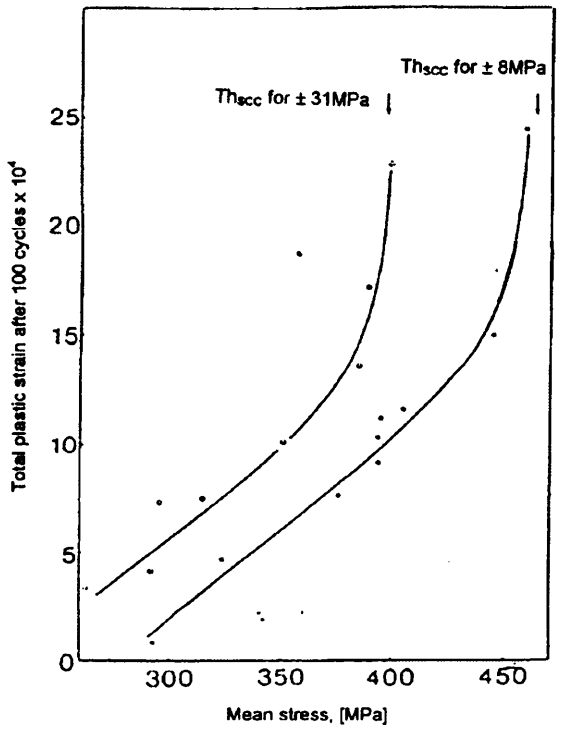

Figure 2-19. Maximum crack length as a function of test time for an X70 pipeline steel subjected to a maximum stress of 390 MPa and a fluctuating stress of 39 MPa at a frequency of 4.8 x 10^{-4} Hz while immersed in carbonate-bicarbonate.[43]

Instead the strain is locally concentrated at slip lines, persistent slip bands or at grain boundaries, due to grain rotation. Consequently, when the average strain rate is very small, the localized strain may be relatively high, so that the initiation of cracks may still occur when the average strain rate has undergone considerable decay. It is to be expected therefore that cracks will continue to be nucleated, even with a diminishing rate, with increasing time. While the average crack growth rate diminishes with time, the number of cracks shows the reverse trend. This is consistent with the fact that pipelines, like many other structures, develop colonies of cracks and that once a stress corrosion crack is initiated, it alone does not propagate to produce failure. Therefore, equations that describe the propagation of a single crack are not helpful in the context of failure. Parkins[43] suggested that longer cracks virtually cease to propagate, whereas the smaller cracks continued to grow. In *Figure 2-20* this is illustrated for a cyclic load test on an X-70 steel in which the maximum crack length at the surface of the specimen was measured at various intervals[44]. Obviously, there are extended periods during which there is no growth of the longest cracks, and these periods appeared to be more extensive the longer the crack.

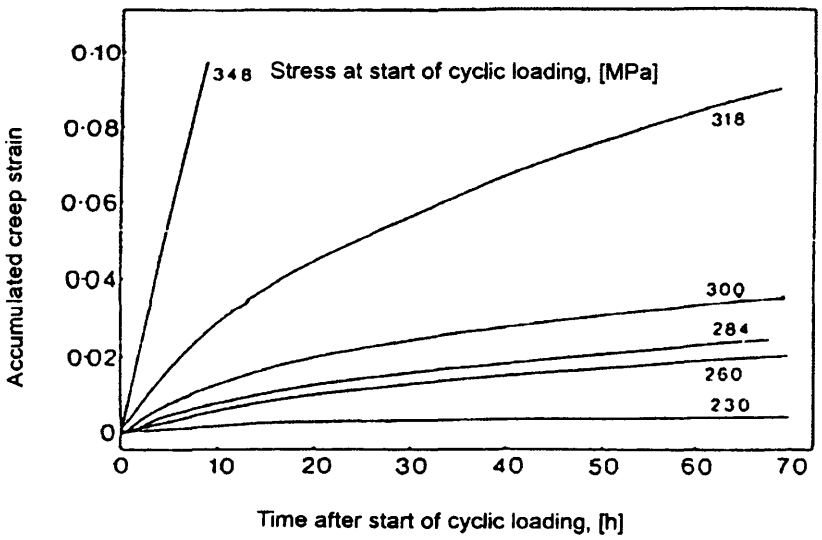

Figure 2-20. Envelope of creep curves produced by cyclic loading a pipeline steel at 20°C showing the effects of different applied maximum stresses, Parkins[43].

Parkins[43] cited two reasons why a crack should stop propagating. Firstly, work hardening at the crack tip region reduces the strain rate below that necessary for cracking, or secondly, the collection of corrosion products within the crack prevents crack closure and so reduces the effective strain range with cyclic loading. However, in the system he investigated, this explanation is not realistic since crack tip blunting to reduce the stress intensity factor was unlikely in a system which cracks very readily at a free surface or from a notch. Therefore, work hardening seems to be the best explanation for the interruption of crack growth of larger cracks. However, these cracks began to grow again, and Parkins[43] showed this to be due to cracks that coalesce.

2.8.1 Crack coalescence

Parkins[43] showed that stress-corrosion cracks in a joint of a high pressure gas pipeline coalesced from separately nucleated cracks. This was evident from the crack front that formed clearly from separately nucleated cracks. He further showed a form of crack coalescence observed at external surfaces: two, or more, slightly misaligned cracks on the external surface initially propagated beyond one another, and then their closest tips moved toward one another and joined. Corrosion fatigue cracks in a high-strength steel exposed to a sodium chloride solution were observed by Kitagawa et al.[45] to coalesce in the same manner. They considered the interactions between cracks in terms of the stress intensity factors and showed that because of decreasing K_I and increasing K_{II} when two appropriately spaced cracks passed one another, the tips curved and approached to achieve coalescence.

For cracks to coalesce in this manner, the lateral distance between the cracks would be expected to be important, since if the separation is too large for given sized cracks, the stress fields associated with the two cracks would not interact. Parkins[43] showed that for an X70 pipeline steel subjected to a maximum stress of 390 MPa and a fluctuating stress of 39 MPa at a frequency of 4.8×10^{-4} Hz while immersed in carbonate-bicarbonate solution, with lateral separations of greater than 0.75 of half of the crack length, merging was not likely. Instead coalescence was more likely after the nearest tips had passed one another, rather than before. Therefore, it seemed that while most, if not all, cracks did not grow continuously, some dormant cracks may be

reactivated because of the nucleation of new cracks in close enough proximity of the dormant crack, and then subsequently they coalesced. The enhanced microplasticity associated with the enlarged crack would facilitate growth until work hardening again caused the crack-tip strain rate to fall below the value needed to sustain growth, and then the process would be repeated when the crack is activated again. Parkins[43] found that the nucleation of new cracks, while virtually randomly spaced when the total crack number and maximum size were both relatively small, would be restricted as more cracks form and larger cracks were created. Thus, new cracks tended to nucleate preferentially in some areas, and not to nucleate in other regions, relative to existing cracks. This may explain why he found that cracks appeared to arrest more readily or for longer periods than shorter cracks, since the density of cracks in regions where only relatively small cracks exist appeared greater than in the vicinity of larger cracks.

2.9 Crack propagation process

Parkins[46] described four stages in the time before failure of a pipeline steel in carbonate-bicarbonate solution, as shown in Figure 2-21. In Stage 1, the conditions for stress-corrosion cracking do not exist and the time to the end of Stage 1 can be best predicted by a probalistic approach. Once the environmental requirements for cracking are met with a susceptible steel and appropriate stressing conditions, Stage 2 is entered and cracks are intitiated, but their growth rate diminishes with time. New cracks continue to nucleate and they coalesce with small dormant cracks, to eventually sustain the average growth rate at a level (Stage 3) that is some two orders of magnitude or more below the upper bound given by Equation 2-p. Coalescence will eventually produce cracks that result in K_{ISCC} being exceeded, so that the crack velocity increases to the upper bound values. If single cracks grow under those conditions, a leak will eventually occur, but if a number of such larger cracks coalesce, K_{IC} is reached and fast fracture results.

For laboratory tests in which Stage1 is excluded, it is possible to quantify the events in Figure 2-21. Parkins[43] did this, and for repetitive cyclic loading, the time dependence was reflected in the number of load cycles, N, and for the crack growth (mm) per cycle:

$$GR = 0{,}026N^{-0{,}822} \quad \text{.....2-18}$$

while the crack nucleation rate,

n_c, (no./cm/cycle), is represented by:

$$n_c = 98{,}4N^{-0{,}803} \quad \text{.....2-19}$$

The conditions for crack coalescence are represented by the expression:

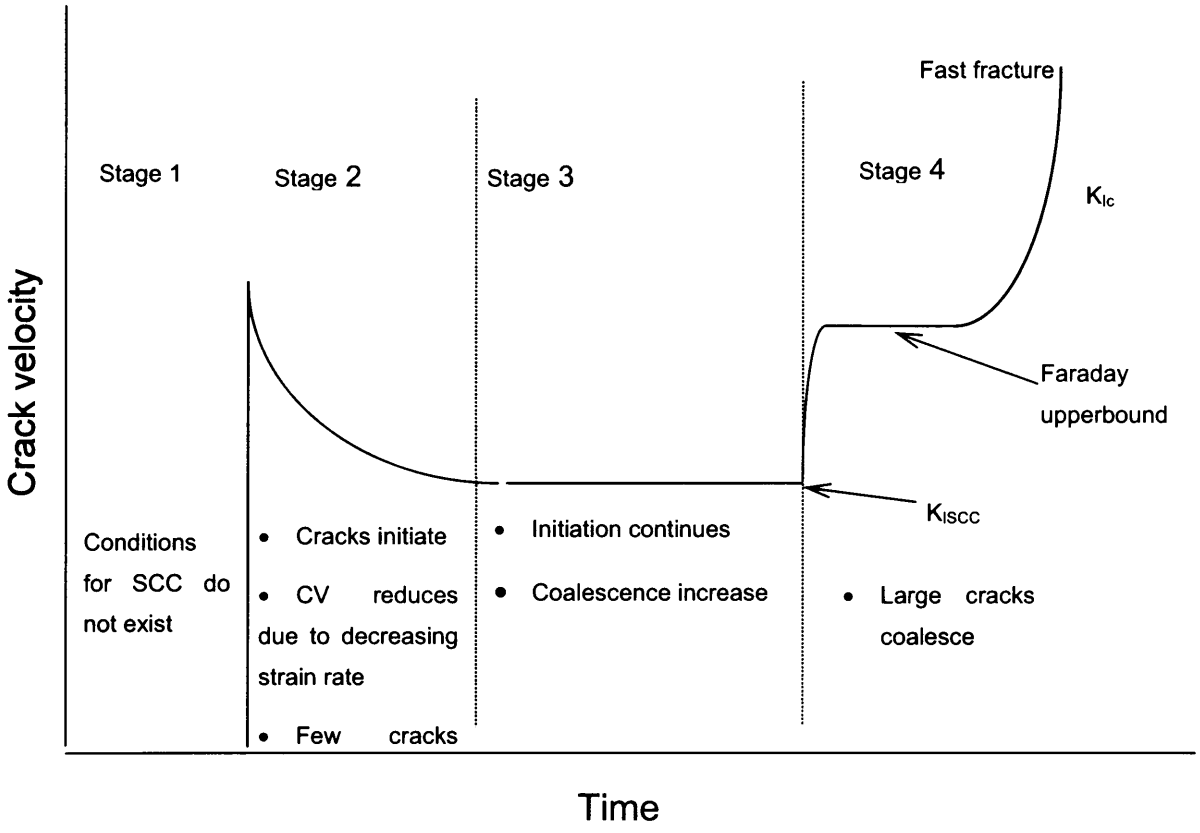

Figure 2-21. Schematic illustration of the effect of time upon stress corrosion cracking velocity of pipeline steel exposed to carbonate-bicarbonate solution (after Parkins[43]).

$$I_z = 0{,}025 + 0{,}14(2a) \quad \text{2-20}$$

where I_z is the size of the interaction zone for coalescing cracks, and

$2a$ represents the average length of the two coalescing cracks.

2.9.1 Life prediction

It is possible to make some progress in relation to life prediction by using the time dependence of crack velocity which is consistent with strain rate effects. In addition, the evidence relating to crack coalescence indicated the necessity of incorporating it into any life prediction calculations. It appears likely that Stage 2 will be dominated by work hardening with relatively few crack coalescences, since the average spacing of the cracks will be too great for the crack sizes involved to achieve the conditions for coalescence.

In Stage 3, cracks grow until they reach the size whereby K_{ISCC} is exceeded and the time in that stage will be determined by the number of crack coalescences (n_s) and the average lengthwise crack velocity (CV_3), as well as the crack length required to achieve K_{ISCC} ($l_{K_{ISCC}}$). Assuming that each crack just before coalescence is 0.46 mm long and that each crack grows from both of its ends at the surface, then

$$t_3 = \frac{l_{K_{ISCC}} - (0{,}46 n_s)}{n_s \cdot 2 \cdot CV_3} \quad \text{2-21}$$

where t_3 is the time in Stage 3.

When K_{ISCC} is achieved the crack velocity will increase (Stage 4) to the upper bound given by Equation 2-w, because the crack-tip strain rate increases to the point where the crack tip is maintained bare and dissolution can occur continuously.

$$CV = i_a \cdot \frac{M}{zFd} \quad \text{2-22}$$

where i_a is the anodic current density

M the atomic weight

Z the valency of the solvated species

d density

F Faraday's constant

Growth in Stage 4 will occur until the pipe wall is penetrated and a leak occurs, or, if macroscopic crack coalescence occurs until the critical crack size corresponding to K_{Ic} is reached and fast fracture results. The time written in Stage 4, t_4 can be written as:

$$t_4 = \frac{l_{K_{Ic}} - 6 \cdot n_L}{n_L \cdot 2CV_4} \quad \text{.....2-23}$$

where n_L is the number of large cracks coalescing,

$l_{K_{Ic}}$ is the crack length for fast fracture and

CV_4 is the crack velocity in Stage 4.

These simple approaches to defining the times spent in the various stages of stress-corrosion cracking growth in a pipeline, according to the work of Parkins[43], which can be summarised in a quantitative form of the schematic illustration of Figure 2-21.

2.10 Constant load DCB specimen testing

Heaver[40] evaluated the crack propagation rate in the CO-CO_2-H_2O environment for double cantilever beam (DCB) specimens. Unexpectedly, Heaver[40] reported that after numerous exposures both in laboratory and plant conditions, no crack extension was recorded, even though smooth C-ring specimens exposed for the same time cracked due to stress-corrosion. He explained this phenomenon through the possible drift in potential in the DCB specimens, while the electrochemical potential of the smooth specimens might have remained in the stress corrosion cracking susceptible range. Therefore, with the potential of the DCB specimens out of the range, no cracking occurred. This agreed with Parkins[43], where in carbonate-bicarbonate systems, cracks

grew from the tip of the pre-fatigue crack, indicating a stronger dependence on the local potential than on the stress intensity. Heaver[40] measured the electrochemical potential of the specimens with the stainless steel autoclave as the reference electrode, and found that the rest potential changed from about -480 mV to -160 mV during the first two weeks but afterwards stayed around -120 mV, even after re-pressurisation. However, this did not give an adequate idea of what happened at the crack tip regarding the electrochemical potential.

The crack growth rates that Parkins[43] measured for the C-ring specimens were in the order of 1 to 5 mm/year for the two gas mixtures that he used, and the ringweld specimen showed the same crack growth rate. The slow strain-rate test and tests done by Brown and Beacham[47] yielded plateau crack growth rates for DCB specimens of nearly an order of magnitude higher, bearing in mind the results of Parkins[43] on the effect of the strain rate, a decaying strain rate might have decreased crack propagation and even the crack initiation process. The reason for the crack growth in the C-ring specimens and not in the DCB specimens might have been the rigidity of the DCB specimen compared to the C-ring specimen, as crack growth enhances a variation in the stress level of the specimen, whereas the DCB specimen was not influenced, and the load application was also very constant, without any fluctuation. On the other hand, the slow strain-rate test induced a continuous strain rate compared to the rate of creep under constant loading, which meant that the crack tip had the opportunity to stay in the unfilmed condition for the duration of the test.

2.11 Mechanism of cracking

The mechanism of stress-corrosion cracking for the CO-CO_2-H_2O system has been described by most as the slip step dissolution model. Plain carbon steels have a body centred cubic structure giving fine slip steps when strained. According to the slip step dissolution model, the susceptibility to stress corrosion cracking increases with a dislocation array and ability to produce course slip steps when strained. Therefore, transgranular cracking in plain carbon steels is more unlikely to occur than, for example, in stainless steels. However, Kowaka and Nagata[48], Brown et al.[5], and Kowaka[8] contributed cracking in this system to the slip step dissolution model. Kowaka[8] did a test to verify the possibility for stress-corrosion cracking or hydrogen

embrittlement by polarising specimens cathodically and anodically with CO and CO_2 partial pressures at 210 and 25kPa respectively. For three tests at two test temperatures, the cathodically polarised specimen did not show cracking after one week, although the anodically polarised specimen showed severe cracking. However, Kowaka[8] also contrasted tests by Nakagawa et al.[49] showing that stress-corrosion cracking of high strength steels, HT60, HT80 and SM41B, tested at a slow strain rate in a low partial pressure aqueous binary gas mixture of CO-CO_2 occurred by a hydrogen embrittlement mechanism. The difference between these two instances of cracking might be due to the two major differences of the tests, namely: the total pressure of the gas mixture and the test technique, which was the U-bend test for Kowaka's[8] tests, whereas Nakagawa et al.[33] used the slow strain rate technique. However, the steels tested by Nakagawa et al.[33] were also high strength steels. These results indicated the possibility for both these mechanisms (stress-corrosion and hydrogen embrittlement) to occur, and the occurrence might be affected by the strength of the steel, pressure of the gas mixture and the strain rate. Therefore both of these mechanisms need to be discussed.

2.11.1 Slip step dissolution model in the H_2O-CO_2-CO environment

With the slip step dissolution model, localised corrosion is enhanced by the formation of some passivating film and the contribution of stresses in the structure that causes the effective strain. Therefore, the initial stage is the inhibition of general corrosion by adsorption of CO onto the metal surface. Crack initiation then occurs at flaws in the adsorbed layer, whatever the cause might be, and this causes attack at those flaws by the corrosive CO_2-H_2O environment. As the crack is initiated, it then propagates by anodic dissolution at the crack tip, while the crack sides are inhibited.

2.11.2 Hydrogen embrittlement as an additional model for crack propagation

In 1976 Kowaka and Nagata[7] mentioned for crack propagation that stress-environmental interaction appeared probable as a cause, yet hydrogen embrittlement seemed inappropriate in view of the low strength of the steel.

Hannah, Newman and Procter[10] studied the mechanism of cracking and proposed a mechanism. Their study showed that it was more complex and it was no longer clear that the transgranular cracking was solely due to anodic dissolution. Instead, it now seemed likely that two different mechanisms could operate, depending on the overall pressure of the system: hydrogen embrittlement is thought to occur at atmospheric pressure, and stress-corrosion cracking by slip step dissolution at elevated pressures. Slow strain-rate tests at atmospheric pressure with 10%, 90% and 100% carbon monoxide concentrations, showed cracking for all the environments that contained carbon dioxide, and no cracking at 100% carbon monoxide.

Cracking at atmospheric pressure was inhibited by anodic polarisation and enhanced by cathodic polarisation, and it seemed that cracking was produced by hydrogen embrittlement[10]. At the low carbon monoxide concentrations, the cracking was also more severe, which reinforced the possibility of hydrogen embrittlement, since the higher carbon dioxide concentration enhanced the reaction for the evolution of hydrogen, which can then be adsorbed into the matrix. When the test with the low carbon monoxide concentration was cathodically polarised, the cracking increased dramatically, but when polarised anodically, the cracking did not change significantly from cracking seen at the free corrosion potential condition. They[10] unfortunately did not indicate the repeatability of these results, which makes their work difficult to interpret. The results are shown in Table 2-3 for atmospheric pressure and at 900 kPa.

Table 2-3. Results of slow strain rate data at atmospheric and elevated pressures (Hannah, Newman and Procter[10]).

Atmospheric pressure			
Test conditions			**Cracking severity**
Gas mixture	**Polarisation**	**% Reduction in area**	**Cracked?**
Laboratory air		63	No cracking
H_2O + 100% CO_2	None	48	Cracking
H_2O + 90% CO_2 + 10% CO	None	32	Cracking
H_2O + 10% CO_2 + 90% CO	None	50	Cracking
H_2O + 100% CO	None	61	No cracking
0,1M Na_2SO_4 10% CO_2 + 90% CO	None	38	Cracking
0,1M Na_2SO_4 10% CO_2 + 90% CO	-700mV SCE - Cathodic	29	Severe cracking
0,1M Na_2SO_4 10% CO_2 + 90% CO	-580mV SCE - Anodic	57	Slight cracking
Elevated pressure – 897 kPa			
Laboratory air		81	No cracking
H_2O + 414 kPa CO_2 + 483 kPa CO	None	26	Slight cracking
H_2O + 414 kPa CO_2 + 483 kPa CO	-780mV SCE - Cathodic	20	Cracking
H_2O + 414 kPa CO_2 + 483 kPa CO	-495mV SCE - Anodic	22	Severe cracking
H_2O + 758 kPa CO_2 + 138 kPa CO	-495mV SCE - Anodic	29	Cracking
H_2O + 414 kPa CO_2 + 483 kPa Ar	-495mV SCE - Anodic	48	Slight cracking

At 897 kPa, cracking was promoted by both anodic and cathodic polarisation, so that the applied potential did not indicate a mechanism that enhanced the cracking. However, examination of the failed specimens showed that under cathodic polarisation, the cracking was similar to that at amospheric pressure, in that cracks were again confined to the necked region. Hinton and Procter[50] showed that when cracking was due to hydrogen embrittlement, it was confined to the necked area of the slow strain rate specimen, because the triaxial stress was higher, since the cross section was reduced. This might be necessary for propagation of hydrogen induced cracks. Hannah, Newman and Procter[10] concluded that, because cracks were confined to the necked region, cracking had to be hydrogen induced. This might not be conclusive evidence to exclude stress-corrosion cracking by slip step dissolution, as cracking might be induced in the necked region only and if the strain rate during necking favoured crack propagation by the slip step model then this mechanism is possible.

The elevated pressure (897 kPa) caused significant cracking, compared to the results at ambient pressure. For two tests done at the same applied potential, the results differed completely when the carbon monoxide was absent from the environment. This is an obvious example of the influence of the carbon monoxide on the anodic polarisation characteristics that are inhibited in the presence of carbon monoxide. Therefore, when the inhibition from the carbon monoxide is not present, neither is the cracking that is induced by it, according to the original proposed mechanism. As the CO partial pressure was reduced from 483 kPa to 0, the reduction in area increased from 22 to 48%. Furthermore, the characteristics of the cracking changed from stress-corrosion in the presence of CO, to hydrogen embrittlement in the absence of CO, because of the inhibiting effect that is important in the slip step dissolution mechanism. Therefore, cracking was accelerated when the potential shifted anodically away from the free corrosion potential, and in practice this could be achieved either by the presence of oxygen, or by the galvanic effect of surface films, including carbonaceous deposits. They supported their findings by detailed fractography of the specimens tested at atmospheric and elevated pressures. Both fractures showed flat, cleavage-like transgranular facets, with river markings in the cracking direction. In addition, both showed striations that were perpendicular to the direction of local crack growth. However, an important difference under anodic polarisation at elevated pressure was

distinct thumb-nail cracks around their edges; these are typical of surface-initiated stress-corrosion cracking. In contrast, specimens tested at atmospheric pressure, or at elevated pressure without anodic polarization, exhibited considerable internal cracking, which is characteristic of hydrogen embrittlement. Therefore, in this system, one can expect to find that hydrogen embrittlement plays a role, but it is not the major cause of cracking. However, these results of Hannah et al.[10] were in contrast to the findings of Kowaka[7] who did not find cathodic polarization to sustain cracking.

2.11.3 *Strain rate and the interaction with hydrogen embrittlement*

Hinton and Procter[50] studied the effect of strain-rate and cathodic potential on the tensile ductility of X-65 pipeline steel. During cathodic protection of pipelines, significant hydrogen evolution can occur, but the influence of the hydrogen on the tensile ductility of these steels had not been adequately investigated, because these steels with yield strengths below 500 MPa show immunity to environmentally induced cracking under constant load conditions. However, when held at cathodic potentials and cyclically loaded at low frequencies, low strength pipeline steels were susceptible to environmentally induced cracking.[51,52] Hinton and Procter showed that specimens exposed to slow, monotonic tensile loading had the same susceptibility to cracking than cyclically loaded specimens. They further showed that, even when cathodically polarised, the steel was only susceptible to hydrogen embrittlement under conditions of continuous slow straining. Therefore, one of the major roles of the continuous straining in producing embrittlement is its involvement in the entry or absorption of hydrogen into the specimen. They suggested that the role of straining in producing the level of hydrogen necessary for embrittlement involved the creation of fresh surfaces by the cathodic reduction and discharge of hydrogen ions. Under static conditions, the discharged hydrogen ions (i.e. adsorbed hydrogen atoms) would have to compete for absorption and entry sites with dissolved oxygen, which is known to adsorb more strongly on clean surfaces than hydrogen and adsorbed water molecules

From these results of Hinton and Procter[50], it seems that hydrogen embrittlement definitely occurred for the tests performed at the atmospheric pressures. However, the occurrence of hydrogen embrittlement at higher pressures is debatable, and the evidence is not overwhelmingly in favour when the different authors are considered.

The dependence of the hydrogen embrittlement on the strain rate might indicate a possibility of interaction in the basic aqueous gas mixture, since it depends on the availability of the adsorbed hydrogen from the carbonic acid and carbonate that produces atomic hydrogen. Furthermore, all of these reactions were dependent on the rupture of a passive layer, which forms a barrier to the other reactions, such as dissolution or production of adsorbed hydrogen atoms for embrittling. Stress-corrosion and hydrogen embrittlement as two models for cracking might both be operative to cause cracking as was seen in the above-mentioned results, when cracking occurred in both anodic and cathodic polarisations. However, when polarised away from the cracking sensitive region, embrittlement of the steel decreased.

2.12 Test methods

Stress-corrosion tests are used to give an understanding of the cracking process or simply just to be used as a ranking procedure. The ranking can be either to evaluate a specific material, material condition, or environmental parameters. A very effective and widely used ranking method is the slow strain-rate test technique, and this was used in this current study as a starting point to develop an indication of mostly the environmental parameters. Since the environment-material interaction is a very important part of the understanding of stress-corrosion, secondly, the potentiodynamic characteristics of the steel exposed to several environmental variants were investigated in order to establish electrochemical characteristics. Thirdly, from the emphasis of Parkins on the influence of stress fluctuations, cyclic stresses on smooth samples were performed. Fourthly, the study of fracture mechanics gives significant insight into the crack propagation rates at various stress intensities and added to this was the measurement of electrochemical noise during crack initiation and propagation. Lastly, the stress-corrosion susceptibility was analysed in the industrial conditions by the use of the constant deformation test. These test methods will be described here in more detail.

2.12.1 Slow strain-rate test

The constant strain-rate or slow strain-rate test was developed as a test procedure where the straining induces more severe conditions for stress-corrosion. Hoar and West[53] originally performed straining electrode experiments, but these were done at a much higher strain rate. Parkins[54] developed the constant strain-rate technique at lower strain-rates of 10^{-6} s^{-1}. Although this technique is known as a 'slow strain-rate' or 'constant strain-rate' it would be more correct to refer to it as a 'constant deflection rate'. This is especially true once the necked region has formed and the deflection rate stays constant, but the localised strain rate of the necked region becomes significantly higher. Normally stress-corrosion occurs over an extended period and this technique gives an accelerated test procedure enhancing the screening of various parameters. The test would normally be performed over a period of two to three days, after which the specimen failed as a result of ductile fracture or stress-corrosion cracking, according to the susceptibility towards the latter[54]. This is in contrast to the constant loading type techniques, where failure of the specimens might not occur leaving inconclusive results. With this definitive type results and over a short period of time, it becomes an attractive technique.

Parkins[54] found that the constant strain-rate test constitute a more severe type of test, promoting stress-corrosion, where other stressing techniques of plain specimens do not promote cracking. He found that the strain-rate is important as the most severe strain-rate is not the same for all the stress-corrosion systems, and has to be determined for a particular material-environment combination. The deflection rate is achieved by a geared drive or hydraulic valve control.

Especially two parameters can be used to evaluate the ductility of a sample after it has undergone slow strain-rate testing, namely: Elongation and Reduction in area. These parameters are measured as follows:

$$\% \text{ Elongation} = \%A = (l - l_0)/l_0 \times 100 \quad \text{.....2-24}$$

$$\% \text{ Reduction in area} = \%Z = (A_0 - A)/A_0 \times 100 = (d_0^2 - d^2)/d_0^2 \times 100 \quad \text{.....2-25}$$

Where:

l_0 = original gauge length

l = final gauge length

d_0 = original diameter

d = final diameter in the necked region.

When these values are calculated and compared with value of a specimen tested in air where no stress-corrosion is expected, an embrittling index can be calculated by dividing the embrittled value by the value of the non-embrittled sample.

2.12.2 *Potentio-dynamic test*

The potentio-dynamic test provides a technique that gives a relatively rapid analysis of the electrochemical characteristics of the material exposed to the particular environment. This type of test is in particular helpful when considering systems involving active-path corrosion. From the anodic characteristics of the potential scan it is possible to deduct potential ranges where stress-corrosion sensitivity is high. Parkins[55] showed this with the use of fast and slow potential scan rates, . Slow scan rates give the characteristics of the surface with the passive film and the fast scan rates film-free conditions. Since stress-corrosion in the current system is dependent upon the presence of the film, this is a very helpful technique to establish the nature, potential range and inhibition of the passivation reaction. The use of anodic polarisation curves and related measurements is discussed in ASTM G 5[56]

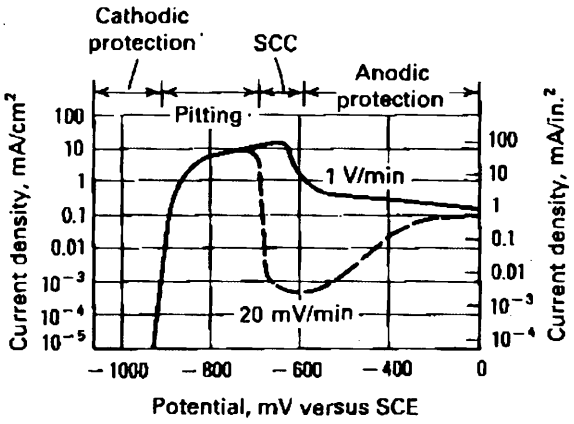

Figure 2-22. Potentiodynamic polarization curves for carbon-manganese steel in 1 N sodium carbonate plus 1 N sodium bicarbonate at 90°C showing the domains of behaviour predicted from the curves[55].

2.12.3 *Cyclic smooth specimen test*

This test method was based in part on the technique described in section 2.8 based on the work of Parkins.

2.12.4 *Fracture mechanics test*

For the design of plants and structures exposed to environments that would induce cracking, such as current investigation, it is important to determine crack propagation rates and stress intensity threshold values in order to ensure safe operation. The use of mechanically pre-cracked specimens can be used to establish these parameters and their relation to varying conditions.

2.12.4.1 Test specimens

Plane-strain fracture toughness test specimens can be used for stress-corrosion testing, and standard configurations should be used to ensure valid fracture analyses. Examples of such specimens are shown in Figure 2-23[57], where they are classified according to loading and crack morphology. ASTM E 399[58] gives clear guidelines on the more commonly used specimens. Sprowls[59] mentioned that minor modifications can be made to these configurations to accommodate different loading arrangements and precracking without invalidating the plane-strain constraints on the specimen.

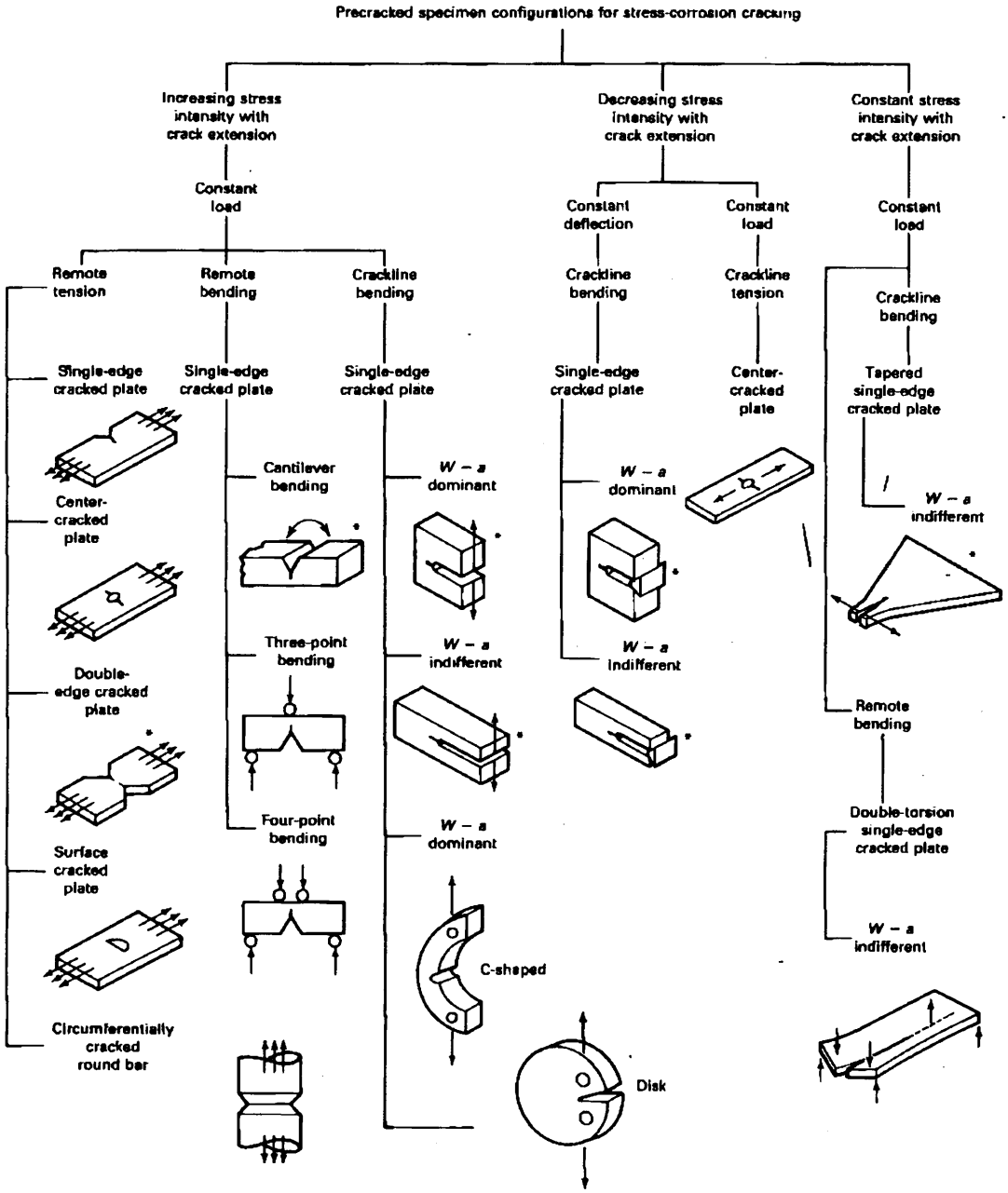

Figure 2-23. Classification of precracked specimens for stress-corrosion cracking testing. Asterisks denote commonly used configurations[57].

2.12.4.2 Double Cantilever Beam Specimens

For the evaluation of the stress intensity, double cantilever beam specimens were used according to ASTM E399 – 83. The specimen configuration and measurements are shown in Figure 2-24.

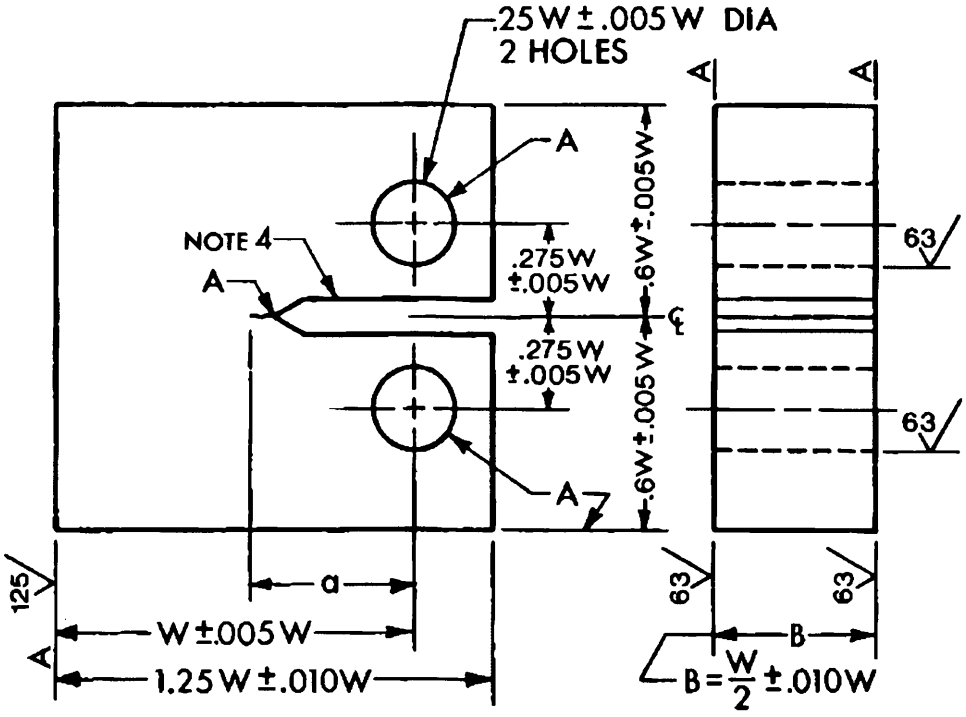

Figure 2-24. Compact specimen C(T) with standard proportions and tolerances.

K_Q for the compact specimen was calculated from the following shown here in Equations 2-x and 2-y:

$$K_Q = \left(\frac{P_Q}{B\sqrt{W}}\right).f\left(\frac{a}{W}\right) \quad \text{.....2-26}$$

Where:

$$f\left(\frac{a}{W}\right) = \frac{\left(2+\frac{a}{W}\right)\left(0.866+4.64\frac{a}{W}-13.32\frac{a^2}{W^2}+14.72\frac{a^3}{W^3}-5.6\frac{a^4}{W^4}\right)}{\left(1-\frac{a}{W}\right)^{\frac{3}{2}}} \quad \text{.....2-27}$$

Where:

P_Q = load

B = Specimen thickness

W = specimen width

a = crack length

For the setup that was used in this current study the dimensions were:

W = 50 mm

B = 12 mm

2.12.5 *Current response measurements*

The current response to crack propagation as measured from an external electrode was investigated by Manahan et al.[60] on 304 stainless steel in pure water. They determined the stress intensity threshold for stress-corrosion cracking as the current response measurements gave an indication of cracking.

The current response concept would be viable based on the following possibilities. Consider a crack existing as illustrated in Figure 2-25 (D D Macdonald and M Urquidi-Macdonald[61]), for a situation in which crack propagation occurs by film rupture/slip dissolution at the crack tip. Three possibilities exist:

a) Either the cathodic processes take place within the confines of the crack and no current emanates from the crack mouth, or,

b) the cathodic reactions occur entirely on the external surface, or,

c) fractional up take of the current in the crack occurs.

A current in proportion to the rate of crack advance should be detected flowing from the crack mouth to the external surfaces if the latter option is true. However, even if the former is correct then charge conservation must still be obeyed.

Manahan et al.[60] have shown the response of current measurements to the change in the stress intensity. They investigated the fate of the current that is generated during crack growth in engineering alloys in power plant environments. On loading (beyond

the stress corrosion cracking stress intensity threshold), the zero resistance ammeter current shifted rapidly in the positive direction, corresponding to a reversal in polarity due to activation of the crack and to a flow of positive current through the environment

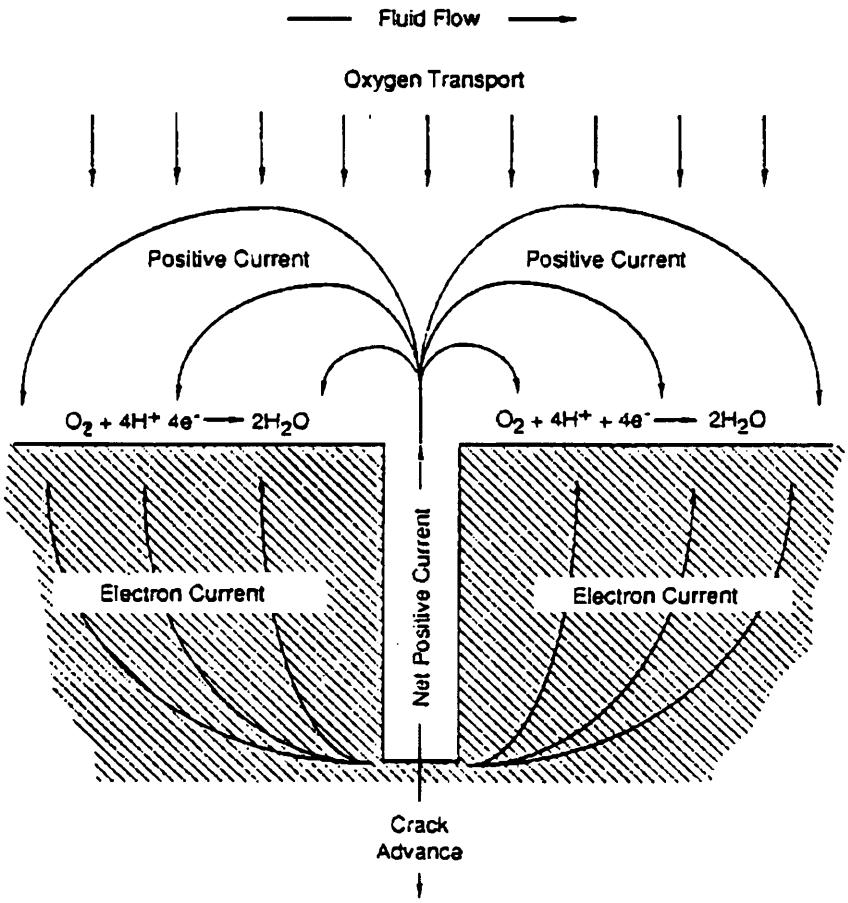

Figure 2-25. Coupling of the internal and external environments by oxygen reduction on the external steel surfaces. (MacDonald et al.[61])

from the crack to the external cathode. They saw the current reaching a plateau approximately 10 minutes after load application, which they speculated to be due to the crack growth through the intensely plastically deformed region in front of the fatigue pre-crack. Once the crack grew through this region, the zero resistance

ammeter (ZRA) current increased again corresponding to a rise in the crack growth rate. Greater oscillations were also seen after the crack propagated through the region that was highly strained. This same phenomenon was detected for crack growth in sensitized Type 304 stainless steel in thiosulphate solutions at ambient temperature[62]. On unloading, the ZRA current returned immediately to the crack-inactive state.

Manahan et al.[60] clearly demonstrated that current flows from a crack to an external cathode during stress-corrosion cracking of sensitized Type 304 stainless steel in pure water at the elevated temperatures that are typical of light water reactors (LWRs). The cathodic reaction was not restricted to the crack flanks or crack mouth, but occurred predominantly on the external surfaces. This demonstrated that the model of the electrochemical cell which includes the internal crack environment, as well as the external steel surfaces, and which imposes charge conservation, is a physically correct model and is clearly superior to semi-empirical treatments.

2.12.6 *Constant deformation C-ring test*

This testing technique is described in ASTM G 39[63] and is a very functional and economical technique. This is typically a constant-strain specimen which is tensioned with the tightening of a bolt centred on the diameter of the ring, inducing a tensile stress on the exterior in between the bolt holes. Figure 2-26 shows the various C-ring configurations with various outcomes, namely: constant strain, constant load and a notched version.

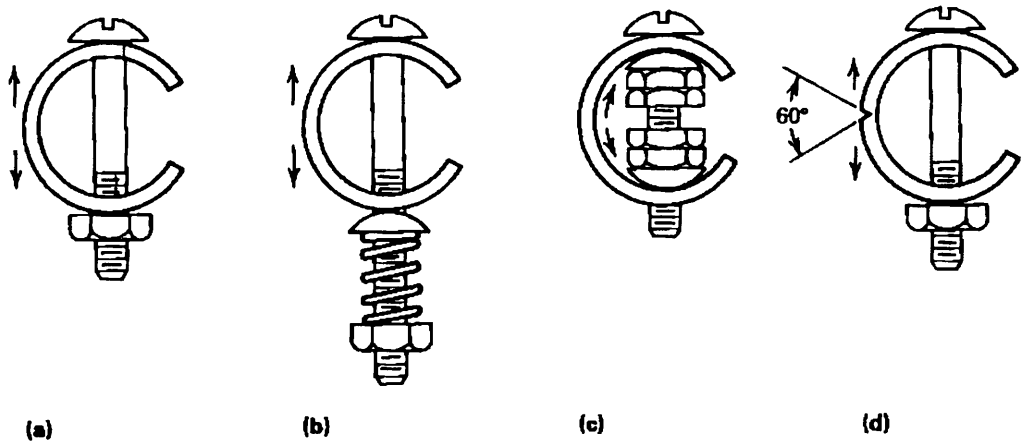

Figure 2-26. Methods of stressing C-rings. (a) Constant strain. (b) Constant load. (c) Constant strain. (d) Notched C-ring; a similar notch could be used on the side of (a), (b), or (c)[63].

2.13 Summary

2.13.1 General

Cracking occurred only in the presence of carbon monoxide, carbon dioxide and water and not when any of these are absent according to a number of investigators, although the concentrations of carbon monoxide and carbon dioxide were very low for cracking. Oxygen also played a role in the cracking process, even in the trace form, and it was difficult to describe its behaviour accurately. However, the way in which oxygen influenced the electrochemical potential of the system determined the influence on the cracking process. Hydrogen and methane caused an inhibition in cracking at high pressures, but at lower pressures, the influence on cracking was uncertain.

Carbon dioxide as a corrodent shows aggressive attack of the steel and the factor that enhanced the corrosion process compared to the mineral acids, was the adsorption on the steel surface and the reaction takes place on the surface of the steel, which means that the reaction can be inhibited by the adsorption of other species. This also allows for the absorption of hydrogen atoms into the steel matrix to cause hydrogen embrittlement. This whole corrosion process is therefore important in the contribution to stress corrosion cracking as well. It was shown that the alloy additions to the steel influenced the corrosion properties in aqueous carbon dioxide solutions, and 9% chromium alloying additions gave good resistance, and above 12% chromium, these

steels were very resistant to corrosion. Stress-corrosion cracking occurred in the H_2O-CO_2 system under severe circumstances with high strength steel. Carbon monoxide inhibited the steel by adsorbing on the water-steel matrix interface by a strong chemisorbtion. This adsorption of the CO causes the corrosion potential to be moved in a positive direction.

It is not very clear what happens with the susceptibility to stress-corrosion cracking from room temperature up to the point where cracking diminishes. The total gas pressure plays a more distinct role than the temperature.

2.13.2 *Electrochemical characteristics and the potential dependence of the cracking process*

The effect of the strain rate and, more specifically, the crack tip strain rate played a major role in the crack propagation rate as indicated by the work of Parkins[43], and without the prevailing critical crack tip strain rate, crack propagation terminated, or the crack propagated in a suitable environment, until the crack tip strain rate is lowered out of the critical range. The lack of crack extension in the results of the DCB specimens in the work of Heaver[40] indicated further the likely importance of strain rate. However, no evidence existed that indicated a similar relationship, as for the work of Parkins[43] and in the current system being investigated, and this has to be addressed. The role of crack coalescence in the system currently under study seems to be a source for continued crack growth, when the work of Parkins[43] is considered.

Inhibiting the stress corrosion cracking of steel in the CO-CO_2-H_2O system was not satisfactory, and from the slow strain-rate test results, it seemed that repeatability of these tests was problematic, especially when inhibitors were tested. Thus, strain rate played a crucial role in the crack propagation.

CHAPTER 3

3 THE EVALUATION OF SCC USING SLOW STRAIN-RATE TESTS

3.1 Introduction

The slow strain-rate test consists of subjecting a specimen to an increasing strain, while exposing it to the embrittling environment. It is a simple test to discriminate between environments to reveal sensitivity to cracking. With the appropriate strain-rate, it is possible to induce stress-corrosion cracking. The most important characteristic of the test is the relatively slow strain rate generated at the region of crack initiation and growth. A principle advantage of the test is the rapidity with which the stress-corrosion susceptibility may be assessed. For many systems, a tensile strain rate of 10^{-5} to 10^{-6} s^{-1} promotes cracking, but the absence of embrittling at these rates would not be indicative of immunity to cracking if other strain rates have not been investigated. The strain-rate is constant for most of the test, but as soon as the neck starts to form, the localised strain-rate increases dramatically, and the sensitivity to cracking also diminishes. However, at this stage, the cracks have formed already, and the ductile failure induced by the higher strain-rates is reduced, because of the existing cracks that formed during the uniform strain-rate application. The effective strain-rate once cracks have initiated cannot be measured. With the slow strain-rate test it is possible to control the rate determining step which is the strain-rate of the deforming specimen.

Comparison between identical specimens exposed to the embrittling environment and inert conditions can be used to assess the susceptibility to cracking. In this study the parameters used were the percentage elongation, as well as the percentage reduction in area, as these are easily measured. Another method would be to determine the percentage of the brittle cracks present on the fracture surface of the failed tensile specimens. However, this is a very timeous procedure and is more difficult to perform

accurately with the transitions from brittle to ductile fractures not being clear. Turnbull[64] recommended using not only reduction in area, because if failure occurred before the ultimate tensile strength was reached, the change in reduction in area would be small.

In this chapter, the slow strain-rate test was used to evaluate the susceptibility of A516 pressure vessel steel in terms of a variety of parameters that influence the cracking of steel in carbon monoxide-carbon dioxide-water environments. The slow strain-rate test served as a relatively rapid (several days per test), evaluation technique to establish a foundation for the rest of the testing to be performed.

The stress-corrosion cracking characteristics of A516 pressure vessel steel were investigated in terms of the influence of the gas composition, rolling direction, temperature, total gas pressure, applied electrochemical potential, time of exposure before testing, surface finish and strain-rate. The interrelationship of these factors was investigated to determine conditions of maximum susceptibility to cracking.

3.2 Experimental procedure

3.2.1 Material

The steel used throughout the study was A516 pressure vessel steel, with the composition shown in Table 3-1. The composition was determined by using: Leco Carbon/Sulphur Analysers, 3460 Emission Spectrometer and 8680 + 72RET XRF Spectrometers.

Table 3-1. The A516 pressure vessel steel composition.

Element	Al	B	C	Co	Cr	Cu	V	Mn
wt%	0.0090	0.0019	0.2170	0.0100	0.0100	0.0100	0.0100	1.0300
Element	Mo	N_2	Nb	Ni	P	S	Ti	Si
wt%	0.0100	0.0074	0.0040	0.0200	0.0090	0.0030	0.0010	0.2900

Stress-corrosion cracking was evaluated by using the slow strain-rate method according to ISO 7539-7 (ASTM E8), with the initial slow strain-rate being 10^{-6} s^{-1}. A schematic drawing of the test rig used is shown in Figure 3-1.

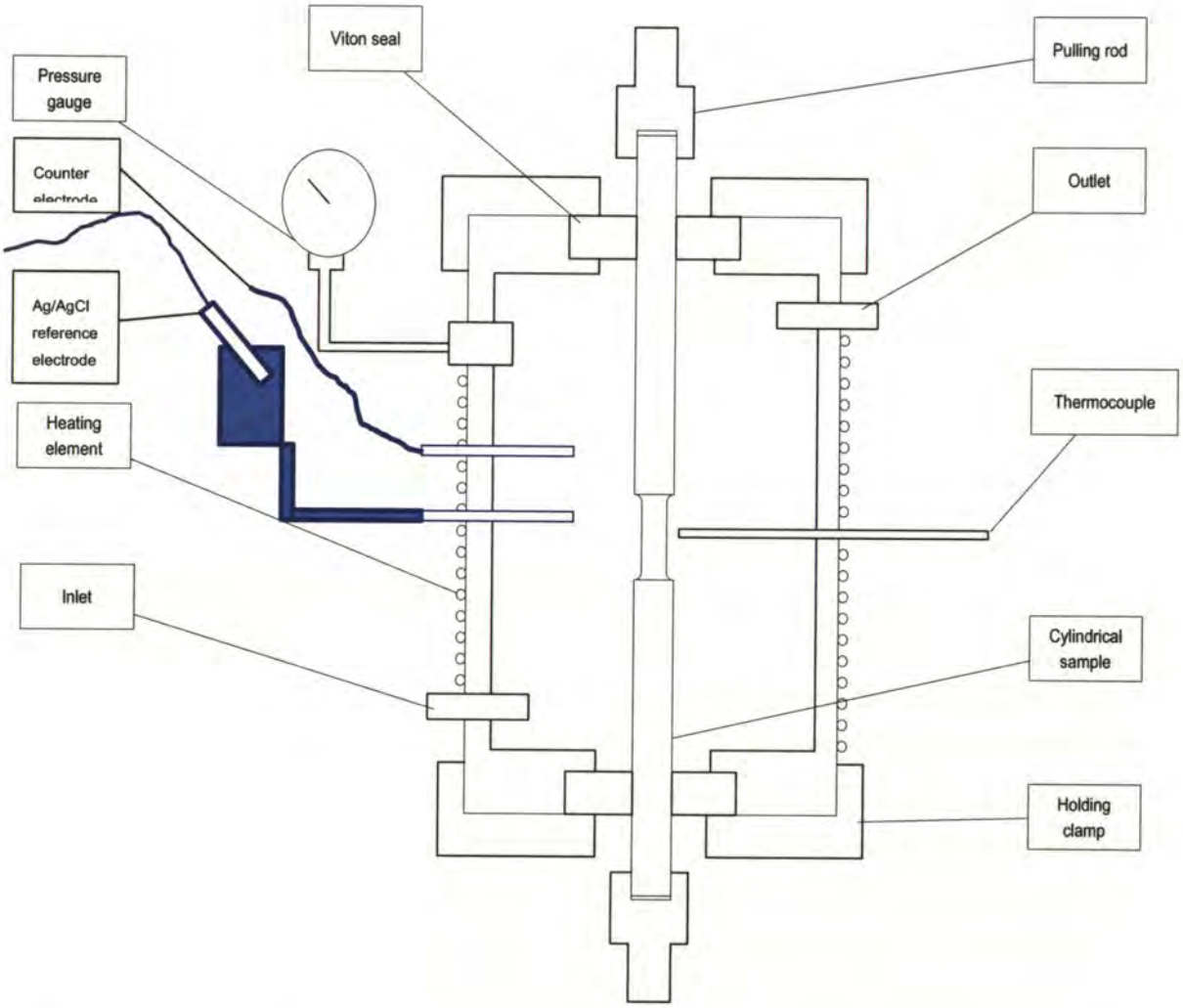

Figure 3-1. A schematic presentation of the tensile specimen in the autoclave that was used for the slow strain-rate test.

The environment consisted of water saturated with a CO/CO_2 gas mixture of 25% CO pressure. Small sized specimens proportional to the standard specimen according to ASTM Standard E8 for cylindrical tensile test specimens were used, with a diameter of 4.0 mm and a reduced section length of 22.5 mm, slightly longer than the standard which is at 19.0 mm, a schematic drawing of the tensile specimen is shown in Figure 3-2.

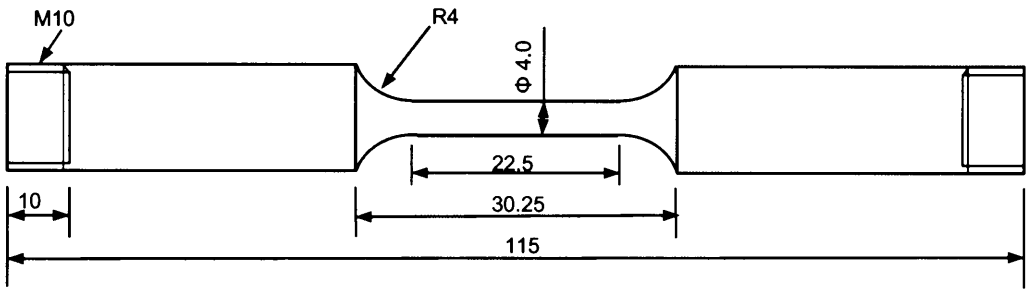

Figure 3-2. The configuration of the tensile specimen used.

3.2.2 Detailed experimental procedure

The water-gas mixture was prepared in a stainless steel pressure vessel of approximately 160 litres. This set up was also used for the other laboratory tests performed during this study. The pressure vessel was filled with distilled water and purged with nitrogen for long enough to ensure that the dissolved oxygen concentration was below 0.1 ppm. Following the nitrogen purge, was a purge with the appropriate gas mixture for approximately 20 minutes and thereafter the vessel was sealed and pressurised to a specific level. Most of the experiments for the slow strain-rate tests were performed at a pressure of 800 kPa and a gas composition of 25% carbon monoxide and 75% carbon dioxide. The gas mixture was prepared beforehand by Afrox Gas according to the required concentrations.

The prepared solution was then transferred to the cell with the slow strain-rate tensile specimen as shown in Figure 3-1. The solution was allowed to flow through this unit to ensure that the same conditions were achieved in the environment of the tensile

specimen. The temperature was measured with a K-type thermocouple that was introduced into the autoclave with a Swagelock© fitting and the temperature was controlled by a temperature controller that regulated a heating element which was wrapped around the autoclave. The pressure in the slow strain-rate autoclave was measured with a pressure gauge that was also introduced into the autoclave with a 1/8" stainless steel tube and Swagelock© fitting. Two Viton© seals were used to seal and insulate tensile specimen from the autoclave. The autoclave was manufactured from stainless steel which would have shown insignificant corrosion with very little contamination. Each tensile specimen was further insulated from the testing rig at the pulling rod ends, to ensure that no galvanic cell was formed between the stainless steel autoclave and the carbon steel specimen.

With most of the tests, unless otherwise noted, the specimen was installed in the autoclave, after which the autoclave was filled with the solution and the test was started shortly afterwards. The tensile specimen was also slightly pre-stressed to ensure that no time was wasted during the tensioning of the frame and pulling rods, since the strain-rate was low and this would have increased the duration of the test considerably.

The specimen was measured beforehand with a vernier calliper in terms of its gauge length and original diameter. The accuracy of these measurements was to the nearest 0.1 mm, according to the accuracy of the vernier calliper. The gauge length measurements were made from shoulder to shoulder on the tensile specimen, which included the radii where no elongation would be expected, but these positions were the best defined and consistent on all the specimens. The original and final diameters were measured, and the final diameter, after the test, was measured by carefully re - joining the two fractured pieces. This measurement was difficult and the accuracy disputable with a definite higher margin of error.

The electrochemical potential was measured with a Ag/AgCl reference electrode that was introduced into the autoclave through a Luggin probe with porous plug. A platinum wire was introduced to serve as a counter electrode. The test solution was released through the smaller autoclaves sporadically to ensure a fresh solution.

The slow strain-rate tests were performed over a temperature range of 25° to 75°C.

3.3 Results

The results from the slow strain-rate tests for samples machined parallel to the rolling direction are shown in Table 3-2. Here the lengths of the two fractured sections were given as l_1 and l_2, therefore l_f, the final length of the specimen was:

$l_{final} = l_1 + l_2$ .....*Equation 3-1*

The elongation of the specimen was calculated as follows:

$$Elongation = \frac{l_{final} - l_0}{l_0} \; x \; 100 \text{.....} \textit{Equation 3-2}$$

Where l_0 was the original length of the specimen, measured from shoulder to shoulder. The reduction in area was given by:

$$Reduction\ in\ area = \frac{d_0^2 - d_{final}^2}{d_0^2} \; x \; 100 \text{ .....} \textit{Equation 3-3}$$

Where d_0 was the original diameter, and d_{final} the final diameter of the gauge length of the sample.

Table 3-3 gives the results of the samples tested perpendicular to the rolling direction. The results are further presented in Figure 3-3 to Figure 3-7. Figure 3-3 and Figure 3-4 show the influence of the orientation of the specimen to the rolling direction of the plate, as well as the environment temperature in terms of the reduction in area. The stress-corrosion cracking susceptibility was demonstrated by the loss in the reduction in area. The errors were calculated by considering the accuracy of the measuring equipment, and especially on the reduction in area the error was significant. These results did not show considerable repeatability and this will be clarified towards the end of this section. The influence of rolling direction on the susceptibility to cracking is not significant and the environmental parameters rather influence cracking characteristics.

Table 3-2. Temperature dependent results of samples machined parallel to the rolling direction

Sample	Temperature	Total pressure	l_1	l_2	l_{total}	Elongation	d_{final}	Reduction in area
	(°C)	(kPa)	(mm)	(mm)	(mm)	(%)	(mm)	(%)
L1	20	350	10.3	23.7	34.0	17.8	3.05	41.8
L3	20	500	23.8	10.35	34.15	18.4	3.20	36.0
L15	20	800	14.1	20.3	34.4	19.6	3.30	31.9
L13	20	1000	23.6	10.1	33.7	16.4	3.55	21.2
L10	20	Air	11.0	25.5	36.5	28.9	2.20	69.8
L16	30	800	11.2	22.8	34.0	17.8	3.35	30.3
L7	35	800	10.2	22.1	32.3	10.2	3.68	15.6
L4	35	800	12.5	21.4	33.9	17.3	3.30	31.9
L9	40	200	23.2	11.7	34.9	21.8	3.00	43.8
L6	40	800	11.1	22.15	33.25	14.4	3.45	25.6
L8	45	800	23.2	10.2	33.4	15.1	3.55	21.2
L14	50	800	20.5	12.5	32.0	13.5	3.45	25.6
L17	60	800	24.7	8.5	33.2	14.4	3.35	29.4

* *This total length includes the shoulders of the specimen and does not refer to the gauge length*

Figure 3-5 illustrates the influence of the total pressure of the medium in terms of the elongation, reduction in area and a correlation of both, expressed as a sensitivity to cracking factor with temperature. These results were all done for samples machined parallel to the rolling direction and at a temperature of 45°C.

Table 3-3. Temperature dependent results of samples machined perpendicular to the rolling direction.

Sample	Temperature	Total pressure	l_1	l_2	l_{total}	Elongation	d_{final}	Reduction in area
	(°C)	(kPa)	(mm)	(mm)	(mm)	(%)	(mm)	(%)
K7	20	800	24.55	10.50	35.05	22.4	3.12	39.2
K4	20	1000	15.10	20.00	35.10	22.7	3.1	39.9
K9	30	800	23.15	10.40	33.55	15.8	3.17	37.2
K2	35	800	17.20	17.50	34.70	20.8	3.15	38.0
K6	35	1000	15.50	18.25	33.75	16.7	3.42	26.9
K1	45	1000	20.55	12.45	33.0	13.3	3.55	21.2
K5	45	800	15.70	17.50	33.20	14.2	3.7	14.4
K8	50	800	24.95	7.80	32.75	12.2	3.65	16.7
K11	60	1000	24.40	9.20	33.6	16.0	3.34	30.3

The influence of the temperature on transverse samples exposed to 50% carbon monoxide and 50% carbon dioxide, was investigated and the detailed results are shown in Table 3-4. The tests were performed at 800 kPa. These tests show similar results as compared to the tests performed in 25% CO and 75% CO_2, where there exists a range of greater stress-corrosion susceptibility for the intermediate temperatures, such as from 40°C to 60°C.

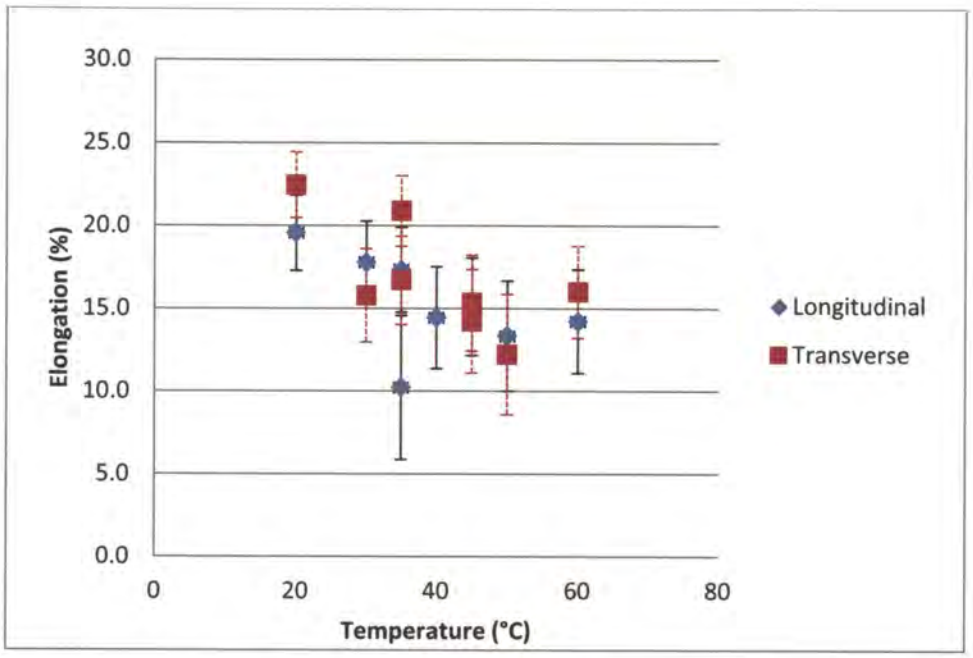

Figure 3-3. Elongation as a function of temperature for specimens machined longitudinal and transverse to the rolling direction, at 800 kPa with a gas mixture of 25% CO and 75% CO_2.

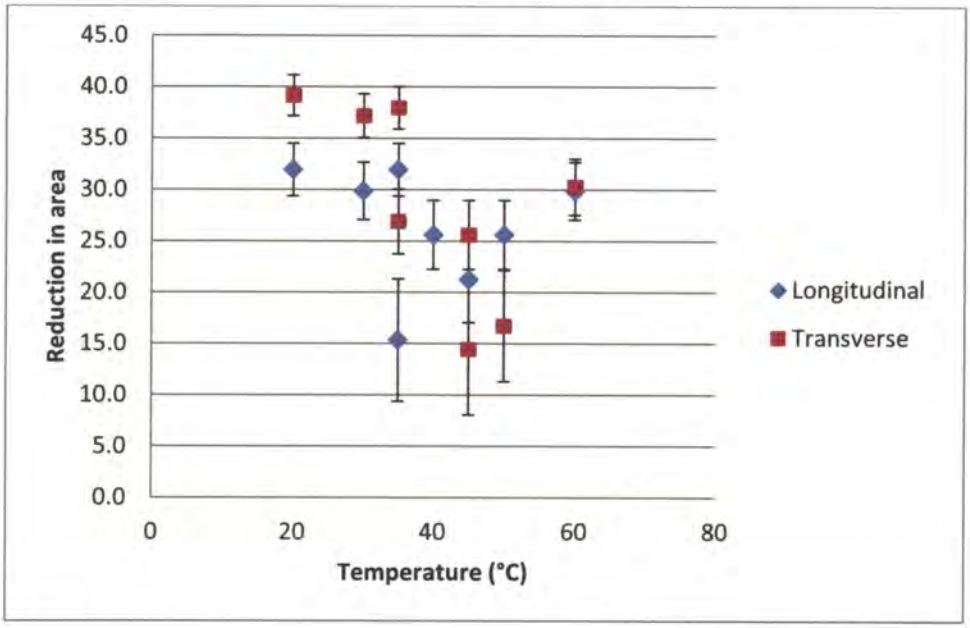

Figure 3-4. Reduction in area as a function of temperature for specimens machined longitudinal and transverse to the rolling direction, at 800 kPa with a gas mixture of 25% CO and 75% CO_2.

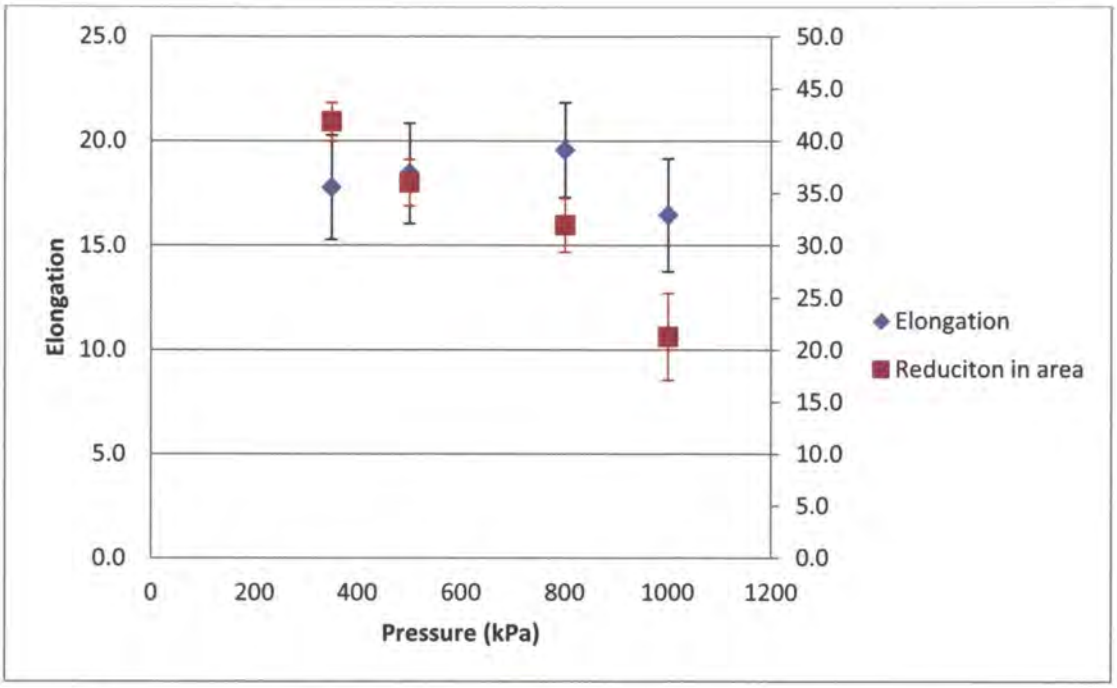

Figure 3-5. Reduction in area and elongation as a function of pressure of slow strain-rate tests performed at 20°C with a gas mixture of 25% CO and 75% CO_2.

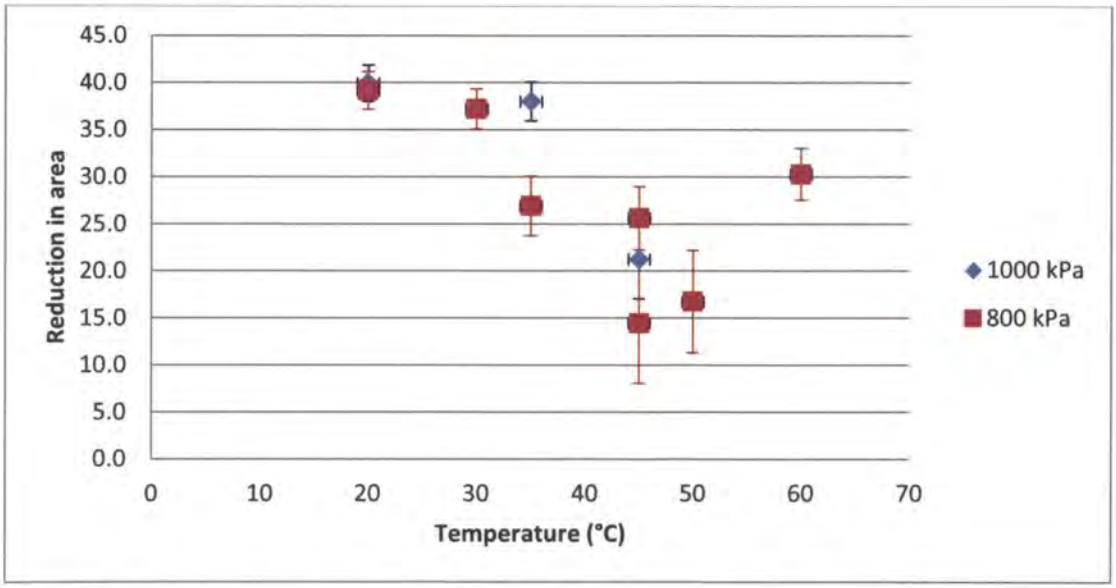

Figure 3-6. Comparison of two pressures over a temperature range with regard to reduction in area for a 25% CO and 75% CO_2 gas mixture.

Table 3-4. Temperature dependent results of samples machined perpendicular to the rolling direction and tested in 50% CO – 50% CO_2.

Temperature (°C)	l_1 (mm)	l_2 (mm)	l_{total} (mm)	Elongation (%)	d_{final} (mm)	Reduction in area (%)
25	8.18	25.24	33.42	15	3.06	41
30	10.90	23.26	34.16	18	3.22	35
35	7.84	26.00	33.84	17	3.38	29
40	14.82	18.52	33.34	15	3.50	23
45	13.80	20.92	34.72	21	3.40	28
48	12.42	21.90	34.32	19	3.60	19
50	20.92	12.18	33.10	14	3.56	21
60	12.16	21.00	33.16	14	3.64	17
70	8.94	25.00	33.94	18	3.30	32
75	19.50	14.20	33.70	16	3.48	24

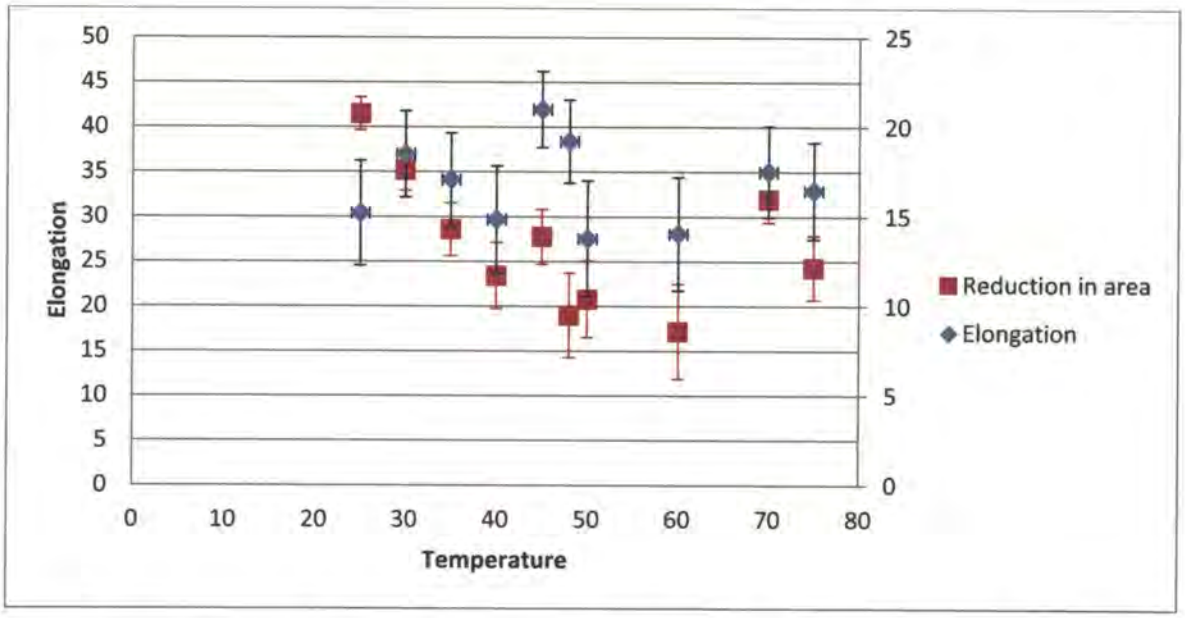

Figure 3-7. Elongation and reduction in area as a function of temperature for specimens machined transverse to the rolling direction, at 800 kPa with a gas mixture of 50% CO and 50% CO_2.

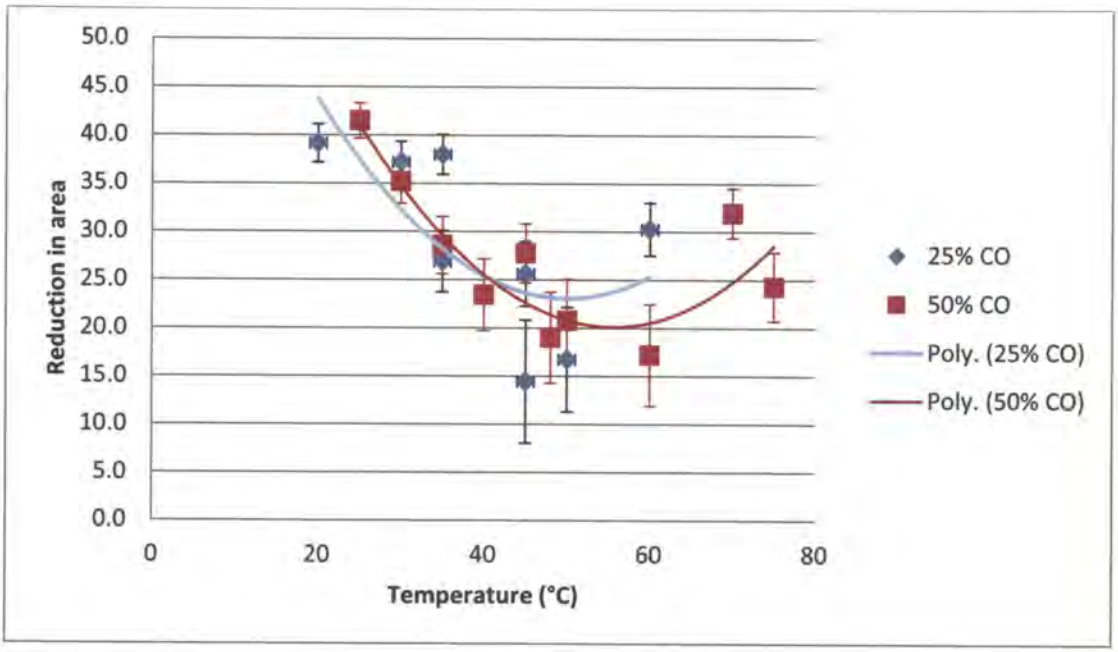

Figure 3-8. Comparison of results with two different gas mixtures, 25% CO and the other 50% CO.

The electrochemical potential dependence was investigated by using a *Voltamograph CV-27* to keep the sample at a certain potential for the whole duration of the slow strain-rate test. These tests were performed at 45°C, 800 kPa, and a carbon monoxide concentration of 25% and 75% carbon dioxide. The potential was measured with a Ag/AgCl reference electrode that was introduced into the autoclave by a Luggin probe. The results are shown in Table 3-5, where the sensitivity to cracking factor is plotted as a function of the applied electrochemical potential in terms of the Ag/AgCl reference electrode.

Table 3-5. Potential dependent results of samples tested in 25% CO – 75% CO_2 at 45°C.

Potential (mV)	l_1 (mm)	l_2 (mm)	l_{total} (mm)	Elongation (%)	d_{final} (mm)	Reduction in area (%)
-600	8.9	26.3	35.2	23.11	3.05	41.85
-585	13.2	20.9	34.1	18.1	3.34	30.27
-575	17.8	15.3	33.1	13.6	3.64	17.19
-550	15.8	17.9	33.7	16.4	3.56	21.68
-550	8.0	26.9	34.9	21.86	3.19	36.4
-525	12.9	19.45	32.35	10.4	3.45	25.6
-500	24.9	8.0	32.9	12.98	3.57	20.34
-500	26.15	8.2	34.35	19.5	3.05	41.86
-475	10.95	22.7	33.65	16.2	3.16	37.59
-450	23.8	10.8	34.6	20.8	2.9	47.43

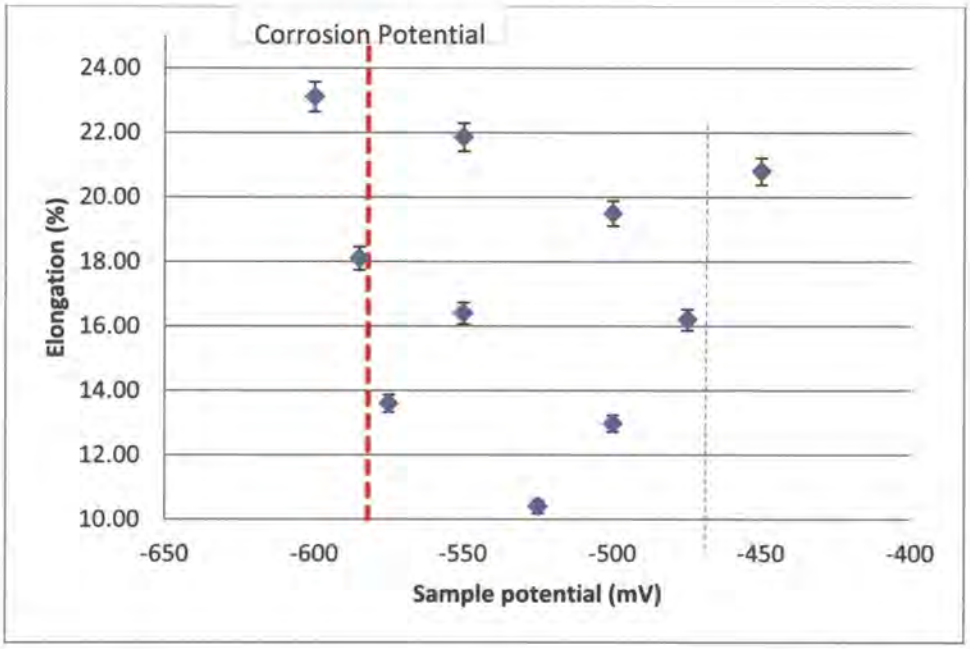

Figure 3-9. Elongation as a function of the applied electrochemical potential at 800 kPa and 45°C with a gas mixture of 25% CO and 75% CO.

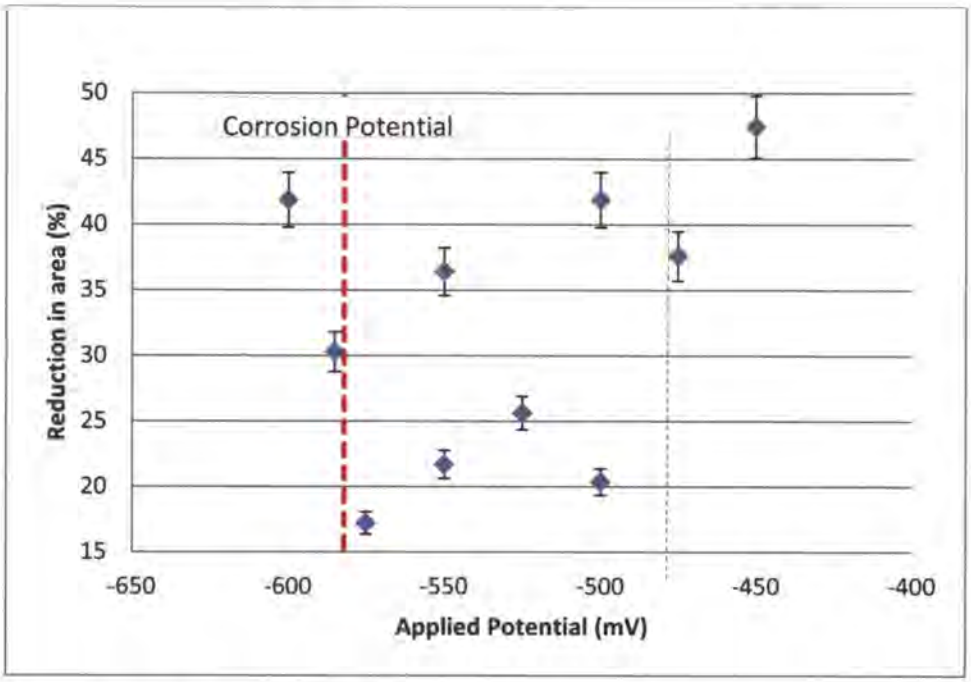

Figure 3-10. Elongation as a function of the applied electrochemical potential at 800 kPa and 45°C with a gas mixture of 25% CO and 75% CO.

The effect of surface roughness was investigated when scanning electron micrographs showed crack initiation on grinding marks as seen in Figure 3-11. Here the cracks formed on what seems to be a 45° angle, which turned out to be the grinding angle for the specific sample. Slow strain-rate tests were performed on samples with different surface finishes. Grinding papers with the following grit: 180, 200, 400, 600, 800 and 1200 were used on separate samples, where the 180 is the roughest and 1200 the smoothest paper. Figure 3-13 and Figure 3-14 show the results of the slow strain-rate tests in terms of the reduction in area and elongation, here it can be seen that elongation does not show a marked difference in the influence of the machining marks on the surface of the samples. However, the reduction in area showed a decrease, greater susceptibility, with increasing surface roughness. This trend is slightly masked by the scatter in results.

Table 3-6. Results of the slow strain-rate tests performed at 45°C, total pressure of 800 kPa and 25%CO for different surface finishes.

Sample	Grit finish	A	Z	Sensitivity to cracking factor - A	Sensitivity to cracking factor - Z
L52	1200	24	41.86	0.8307	0.6001
L70	1200	21.69	31.94	0.7508	0.4579
L68	800	22.13	38.38	0.766	0.5646
L59	600	26.13	36	0.6369	0.328
L57	400	22.8	34.39	0.7892	0.493
L67	400	16.04	26.04	0.5552	0.3733
L63	220	22.22	31.9	0.7691	0.4573
L66	180	26.22	31.9	0.9076	0.4573

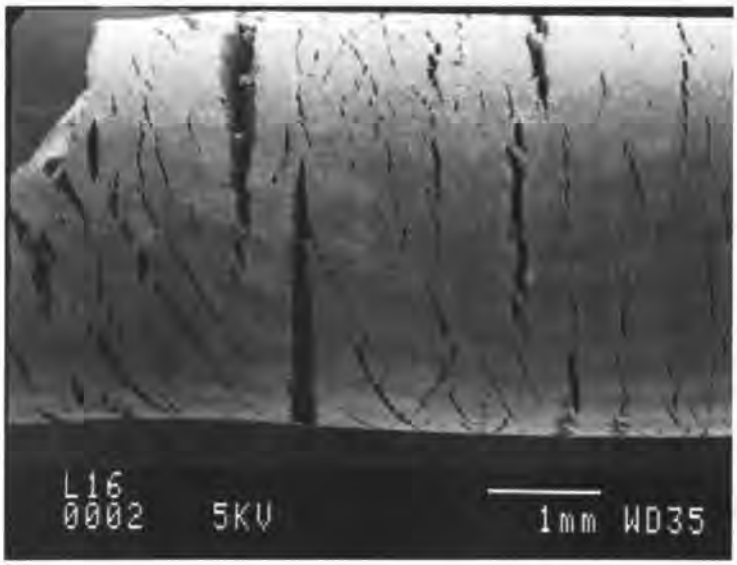

Figure 3-11. The influence of grinding marks on crack initiation for a slow strain-rate sample tested at 45°C and 800kPa 25% CO – 75% CO_2.

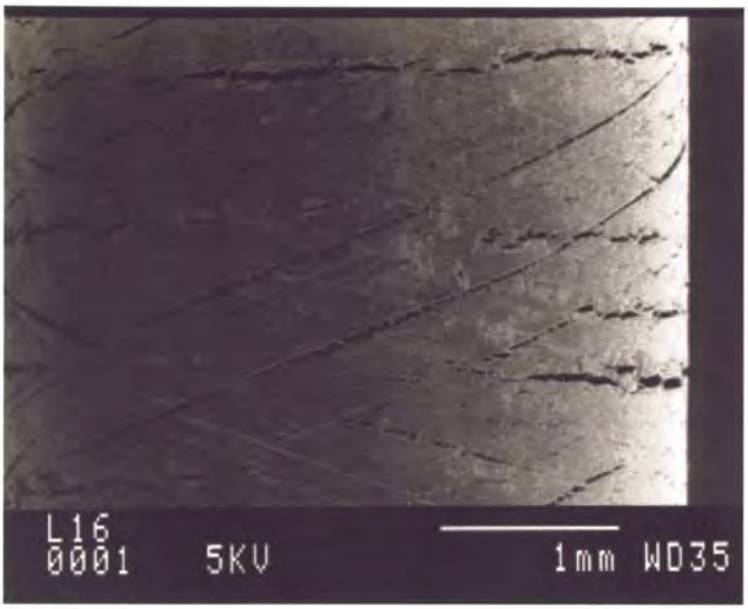

Figure 3-12. The same sample as shown above at a slightly higher magnification revealing how the cracks followed the grinding marks on the sample after a slow strain-rate test at 45°C and 800kPa 25% CO – 75% CO_2.

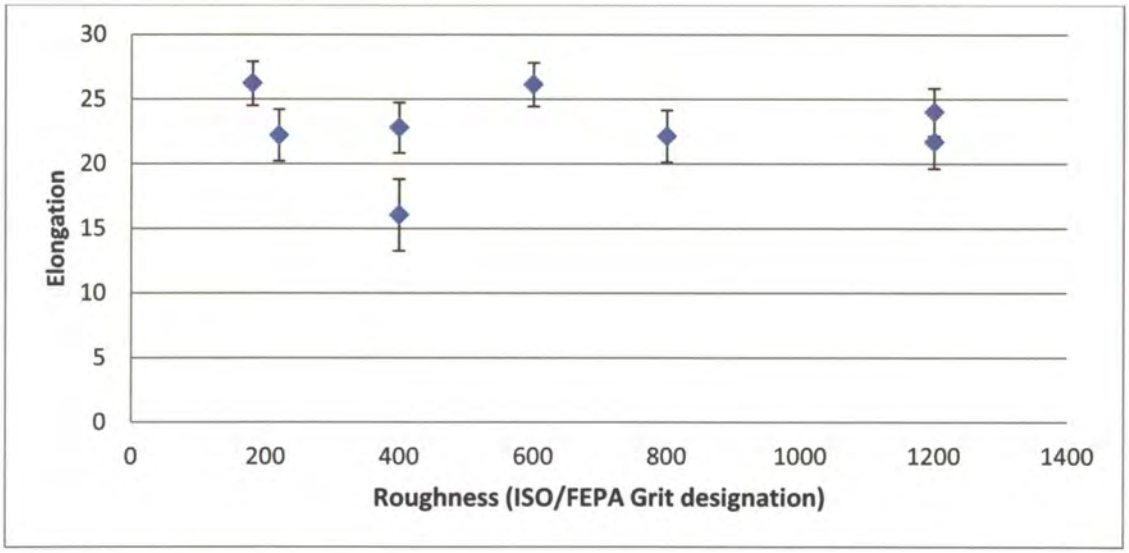

Figure 3-13. Slow strain-rate test results showing the influence of the surface roughness on the stress-corrosion resistance of steel at 45°C and 800 kPa.

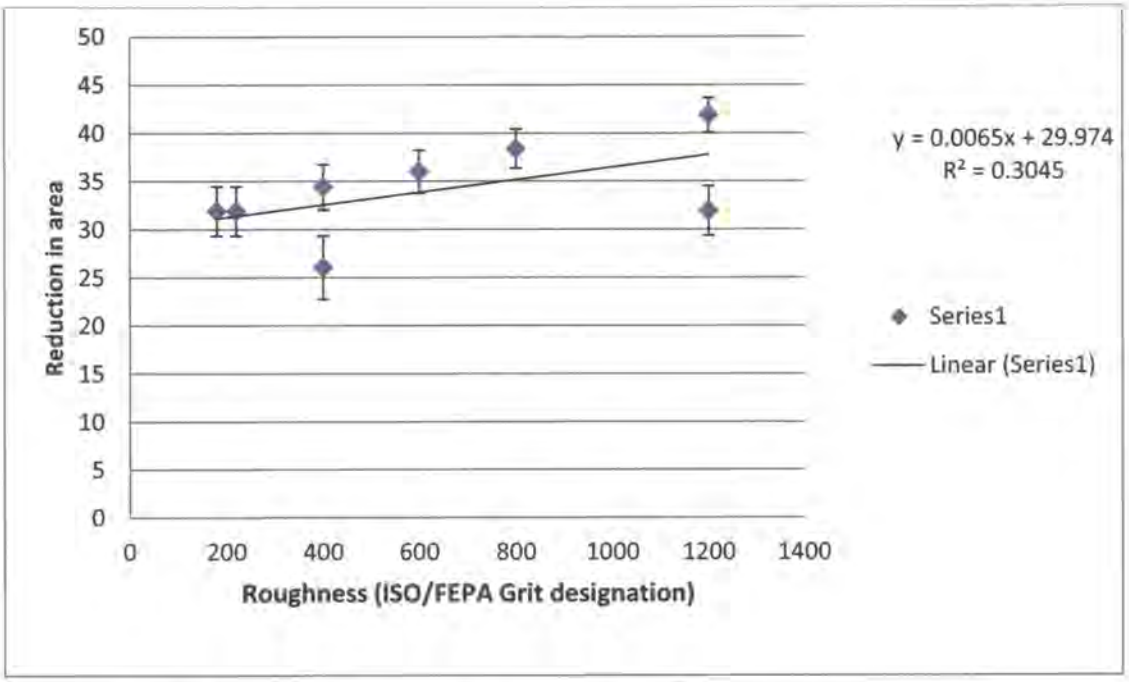

Figure 3-14. Slow strain-rate test results showing the influence of the surface roughness on the stress-corrosion resistance of steel at 45°C and 800 kPa.

The time of exposure of the specimen to the solution before test was started was investigated when it accidently became evident that a specimen showed increased brittleness when the test was not performed immediately. In Figure 3-15 the sensitivity to cracking factor index is plotted against the time of exposure prior to testing. For these exposure tests the experimental parameters were: a total gas pressure of 800 kPa, a temperature of 45°C, and a strain rate of 10^{-6} s^{-1}. Here the time of exposure before the test had a significant effect on the sensitivity to cracking of the sample, which is unexpected, especially considering the degree of cracking that was found. The sensitivity to cracking indices for reduction in area and elongation both dropped in the order of 50% when the samples were not exposed to the environment before the test, and when the samples were exposed for 48 hours before testing. This trend was confirmed by the intermediate sample that was only exposed for 24 hours.

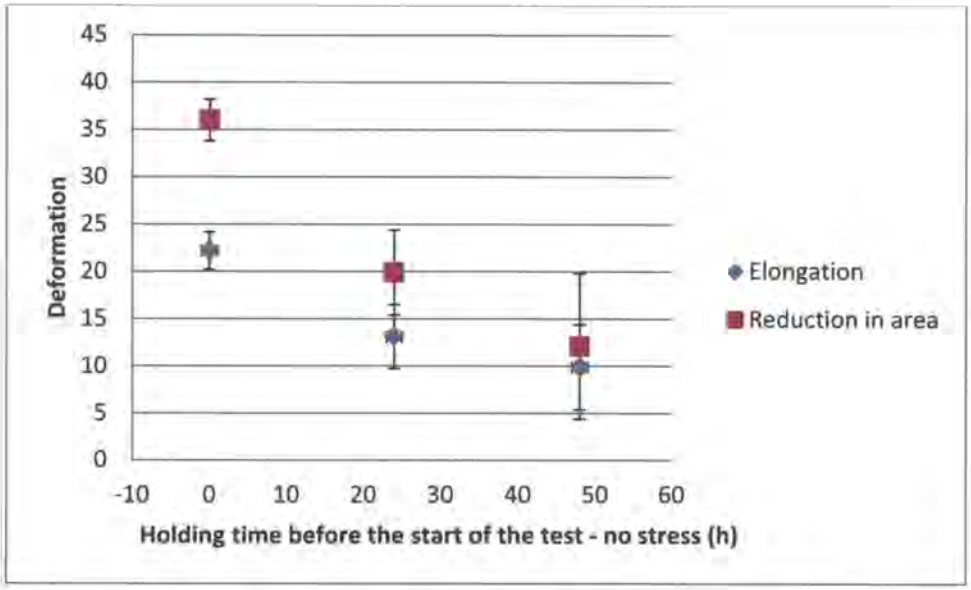

Figure 3-15. The sensitivity to cracking of the steel as a function of the time of exposure prior to testing at 45°C and 800 kPa.

The influence of the strain-rate was investigated and in Figure 3-16 the sensitivity to cracking factor index is plotted as a function of the strain-rate. These tests were also performed at 45°C, 800 kPa, and 25% CO - 75% CO_2. The strain-rate varied from 10^{-5} s^{-1} down to 10^{-8} s^{-1}, unfortunately only one test was performed at 10^{-8} s^{-1}. The reduction in area index for cracking increased from 0.2% to 0.4% when the strain-rate decreased from 10^{-7} s^{-1} to 10^{-8} s^{-1}, and the same trend was seen on the elongation of the samples, it went from slightly above 0.2 to 0.7 when the strain-rate was decreased.

In Figure 3-17 the fracture surface of a specimen tested at 45°C and 800 kPa indicated the typical transgranular cleavage cracking for these tests. Some pearlite colonies are seen as the crack propagated through the colony and was possibly etched by the environment. A cross section was also made to show the transgranular nature.

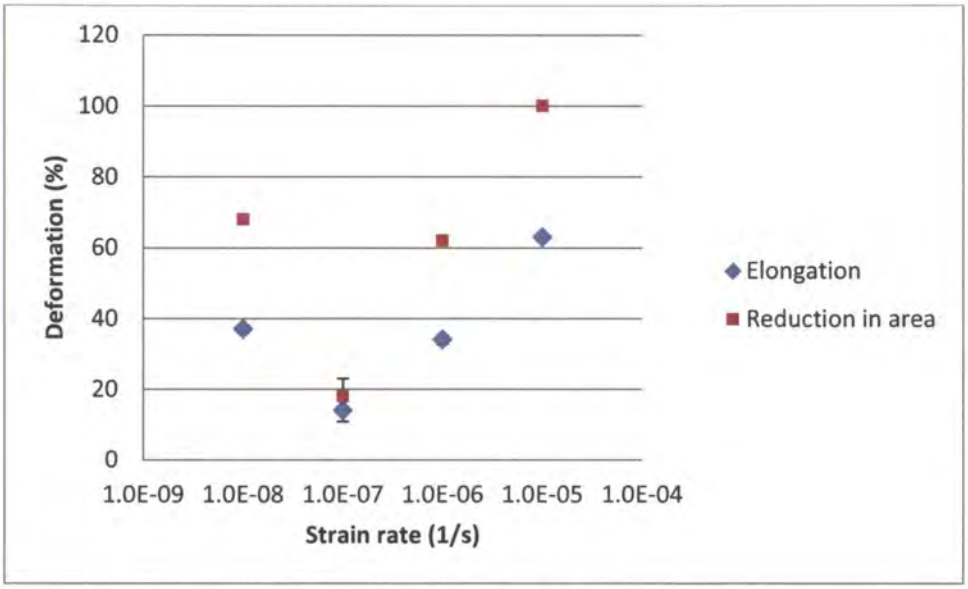

Figure 3-16. The embrittling factor index as a function of the strain rate of the slow strain-rate test at 45°C and 800 kPa.

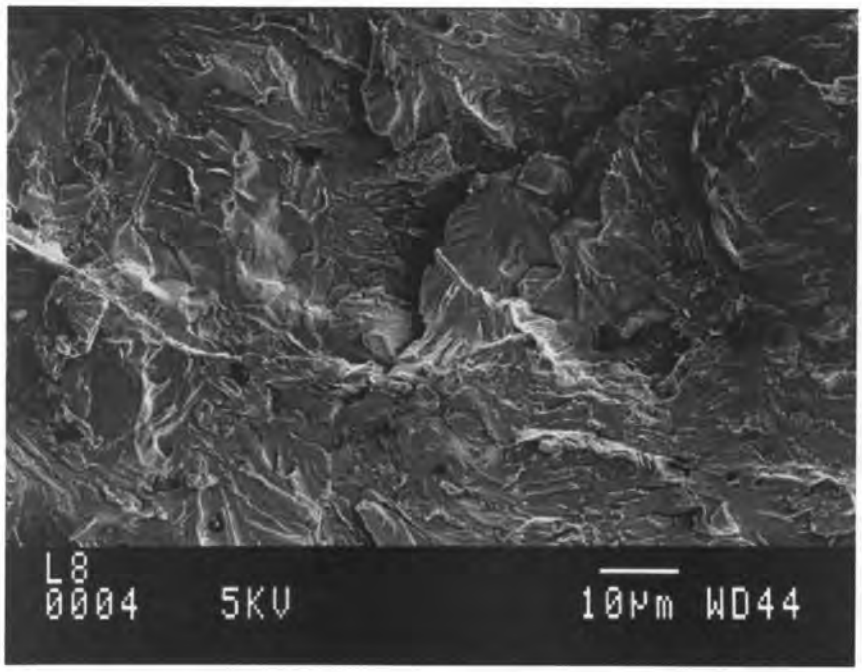

Figure 3-17. A scanning electron micrograph of the fractured surface of a slow strain-rate specimen tested in 25% CO at 45°C and 800 kPa total pressure.

A test was performed in 100% CO, 800 kPa, at a strain rate of 10^{-7} s^{-1} and 45°C. These specimens did show cracking with the elongation at 21.8%.

3.4 Discussion

Although the results determined do not all reveal new trends that were not known before, they do lay a foundation for the work that will be discussed in the following chapters in terms of the specific environments that were used for this study and the sensitivity to cracking behaviour of the A516 pressure vessel steel.

3.4.1 Rolling direction

The results in Figure 3-4 do not give a clear indication of any major difference between the two situations of testing specimens being aligned parallel or perpendicular to the rolling direction, since there was much scatter, thus the fitted lines are only an indication. From the elongation and reduction in area, the same tendency was found. The microstructures of the two orientations to the rolling direction are shown below:

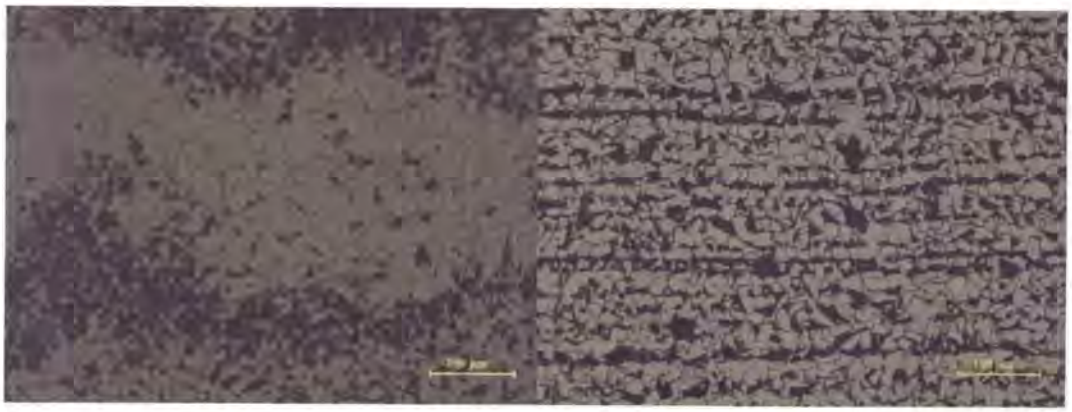

Figure 3-18. The microstructures of the steel seen from the two different orientations.

The ferrite-pearlite microstructure although different did not affect the sensitivity to cracking significantly.

3.4.2 Total pressure

The results in Figure 3-6 show that according to the % reduction in area, higher pressures increase the susceptibility to stress-corrosion cracking. However, this is in

the range of 200 to 1000 kPa. According to the % elongation a similar trend is followed with a slight increase at 800 kPa. It is also seen (Figure 4 and 5) that with an increase in the temperature, the effect of the total pressure is even greater, although this was based on two samples, and more information is needed for statistical certainty. These results are similar to those of Hannah et al.[10] where the reduction in area of the samples decreased with increasing pressures.

3.4.3 Gas composition

It is clear that at higher carbon monoxide concentrations the susceptibility to cracking increases dramatically.

3.4.4 Temperature

The influence of temperature was examined for two situations, samples parallel and perpendicular to the rolling direction.

3.4.4.1 Samples perpendicular to the rolling direction

When looking at the reduction in area, these samples show a minimum in the order of 45°C to 55°C. This means that there is an increase to both sides - the region close to room temperature as well as higher temperatures. The increase in the resistance to stress-corrosion cracking at higher temperatures (60°C), is given by one data point and further examination is necessary to be able to give a better estimation.

3.4.4.2 Samples parallel to the rolling direction

The results show that same tendency in sensitivity to temperature for both the samples machined perpendicularly and parallel to the rolling direction. The normalised reduction in area decreased in the temperature range 40°C to 50°C, this seems to be in agreement with the work of Kowaka and Ngata[7] as well as Itoh[65], on the general trend of the effect of temperature. The normalised elongations for these samples gave the same region of greater embrittlement. This behaviour is expected due to the

influence of the temperature upon the kinetics of the corrosion reaction and the passivity of the steel. Here decreased sensitivity to cracking is an indirect effect, due to the decreasing solubility of the carbon monoxide in water at increasing temperatures. Schmitt[17] also showed a decrease in ductility of various carbon steel with the increase in temperature, from 25°C to 50°C. Although Schmitt et al.[31] found a maximum susceptibility around 40°C for 37Mn5 steel grades loaded to 90% of yield strength at 10 bar CO_2.

3.4.5 Applied electrochemical potential

In Figure 3-9 the region where the testing was performed the cracking resistance increased towards the higher and lower limits. Sensitivity to cracking was prevalent from around -575 mV to -475 mV, which is very similar to results obtained by Brown et al.[5]. The fractured specimens at the more noble potentials were characterised by general corrosion and little cracking. Towards the more active limit, hydrogen formation could have induced cracking, but here the resistance to cracking also increased, thus, indicating that cracking is not enhanced by an excess of hydrogen. It could be argued that cracking could still be promoted by the presence of a small amount of hydrogen, but if this was the case, higher concentrations would have decreased the resistance to cracking. The situation is convoluted by the shifting of the corrosion potential with time, but this is evaluated in the next section.

3.4.6 Time of exposure

The results in Figure 3-15 indicate the importance of the adsorbed CO species on the surface of the specimen and the effectiveness of this layer before the sample is stressed. Although only three samples were tested the trend is very clearly a greater sensitivity towards cracking. Because of this trend the polarisation characteristics will be evaluated as a function of time with an emphasis on the effect of the holding time. It is expected that passivation of the steel would be one of the most significantly effected reactions.

3.4.7 Surface finish

The effect of the surface finish was first noted when one of the specimens was studied with the scanning electron microscope, and it was found that cracking occurred along most of the scratches left from the machining and grinding process (Figure 3-11 and Figure 3-12). The grinding marks served as crack initiation points. This indicated the sensitivity of the cracking process to crack initiation. Although the influence of grinding grooves was not severe, there was a tendency towards a greater resistance to cracking when the surfaces had finer grinding grooves. Therefore, it would seem that the crack initiation was more probable with the larger grooves and might be one of the reasons why cracking would occur in one area and not another. The grooving is expected to be similar on the surface, although, it is possible that larger grooves remained from previously applied, coarser grinding papers.

3.4.8 Strain rate

Strain-rate is a very important variable and this was evaluated to a greater extent with other test methods. However, as shown by Kim and Wilde[66], with slow strain-rate testing, it is possible to differentiate between the hydrogen induced cracking and stress-corrosion cracking. This is because of the repassivation reaction of the steel that prevents the corrosion reaction of the bare steel, since the repassivation occurs at a faster rate than the exposure of the steel due to the slip step emergence. From the results, it is clear that the minimum resistance to cracking is in the order of 10^{-7} s^{-1}. The resistance to cracking increased at 10^{-8} s^{-1}, which means that the passivation rate at the crack tip could keep up with the bare surface that was formed due to the crack tip strain-rate. This is an important result that also indicates that the cracking is dependent upon the passivation of the steel, and again not the hydrogen embrittlement. Therefore, if the passivation of the steel can be influenced, either by enhancing or breaking it down, the stress-corrosion cracking can be mitigated. Unfortunately, the test at 10^{-8} s^{-1} strain rate was performed over a very long period and only one of these tests was performed; therefore, this is not completely conclusive evidence, but suggests that strain rate is a very important component in the cracking process.

3.5 Conclusions

1. An increase in the total pressure of the gas increases the susceptibility of the steel to stress-corrosion cracking.
2. Samples machined longitudinal to the rolling direction showed a slightly increased sensitivity to stress-corrosion as compared to those machined transverse to the rolling direction.
3. Maximum susceptibility to stress-corrosion cracking is between 40°C to 50°C.
4. Cracking is dependent on the electrochemical potential and cracking decreases on the cathodic side of the polarisation diagram.
5. A waiting time before the test is started reduces the resistance to cracking.
6. The surface finish does not have a large effect on the cracking resistance, although with a finer finish, the cracking is less.
7. Strain-rate dependence shows a maximum susceptibility at around 10^{-7} s^{-1}.

CHAPTER 4

4 ELECTROCHEMICAL CHARACTERISTICS OF THE STEEL IN CO-CO_2-H_2O ENVIRONMENTS

4.1 Introduction

Both applied stress and the environmental interaction contribute to cause environment induced cracking. It has been noted that cracking is most likely to occur close to electrochemical regions of passive-transpassive transitions where the passivation and the slip step emergence interaction would cause crack initiation and propagation. Therefore, if this passivity can be described adequately a better understanding of the cracking process can be formulated. In the CO-CO_2-H_2O system the passivity induced by carbon monoxide has been described and it is clear that this contributes to the cracking process. However, the rate of the carbon monoxide inhibition (adsorption) reaction is not clear for this specific system.

The stress-corrosion process needed to be understood from the electrochemical side to gain a better understanding of the corrosion processes that takes place as cracking occurs. The work done by Staehle et al.[67] has shown that stress-corrosion cracking can be closely related to the polarisation characteristics. They showed that when cracking occurs by the film rupture model, where a film forming on the surface of the steel was necessary to induce cracking, cracking was related to the electrochemical regions where passivation of the substrate was indicated by polarisation characteristics. It was shown that cracking occurred on the passive to actve transitions found for various systems, e.g. stainless steel in chloride solutions at higher temperatures. At a specific potential, the corrosion rate of a bare metal surface (with no passivating film) and a passivated surface was determined by using a fast and a slow scan rate respectively. With this technique, the corrosion rates at the crack tip, as well as the passivated crack walls and outer surface were described.

The possibility of pitting, cracking and general corrosion depends on the electrochemical characteristics. A broad range of corrosion behaviour exists as a function of gas composition and oxidizing potential of the environment.

In this study, the influence of the gas mixture on the extent of passivation, as well as the rate of passivation was determined. Therefore, the holding time was an important parameter. The change of the corrosion potential also gave an indication of the degree of passivation.

4.2 Experimental setup

4.2.1 Equipment

A Solartron 1286 was used to undertake the potentiodynamic tests on the steel specimens, the same steel was used as described in Table 3-1. A three electrode system was used: working, auxiliary and reference electrodes. A silver/silver chloride reference electrode with a Luggin probe was used with a Na_2SO_4 solution as the conducting medium. *Figure 4-1* is a schematic diagram of the entire setup. The working electrode (WE) consisted of a specimen mounted in an epoxy resin, the auxiliary electrode (AE) was in the form of a platinum wire and all of the electrodes introduced into the autoclave through the top lid were properly insulated. The tests were performed inside a Parr© autoclave, which was manufacture from 316L stainless steel, and the solution was contained in a full length glass beaker contained inside the stainless steel autoclave. This beaker almost reached the lid of the autoclave. Temperature was measured with a thermocouple that was positioned close to the working electrode, and the temperature was controlled by immersing the autoclave into a constant temperature, water bath. The connections to the autoclave were all Swagelok© fittings, or similar, and the autoclave itself had a Teflon O-ring, this ensured that no leakages was possible.

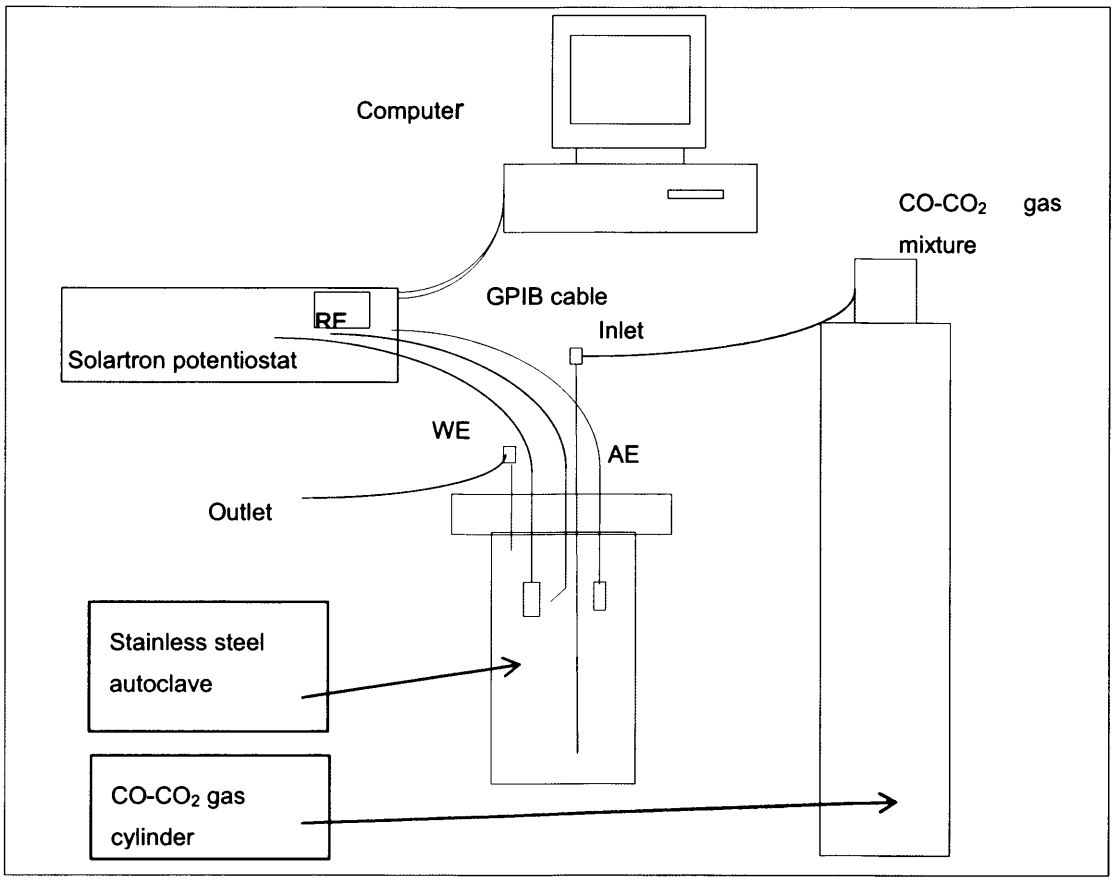

Figure 4-1. The experimental set up for the polarisation tests.

4.2.2 Experimental procedure

A 0,7 M $KClO_4$ solution was used as an electrolyte to ensure better conductivity than the distilled water only, Dunlop and Olson[14] used this and reported that their results correlated with that of Brown et al.[9]. The electrolyte was de-aerated before it was used to eliminate the influence of dissolved oxygen, therefore simplifying the corrosion reactions. The appropriate gas mixture was bubbled through the electrolyte for 30 minutes and then it was pressurised in an autoclave to establish equilibrium. A steel specimen with an area of 1 cm^2 was used and for every test the specimen was ground with a 600 grit paper and dried afterwards. The tests were performed at

0,1 mV/s except where it is differently stated. The gas composition used comprised carbon monoxide and carbon dioxide. the concentration carbon monoxide is given in the tables below and the remainder consisted of carbon dioxide. The autoclave was pressurised to 800 kPa and this was maintained for 30 minutes before testing was ensued. The experiments were performed according to the conditions given in the Tables 4-1 to 4-9 for the various gas mixtures.

Table 4-1. Test conditions for 75 %CO.

Name	Temperature	Pressure	Scan rate	CO	Exposure time
	(°C)	(kPa)	(mV/s)	(%)	(min)
Coco88	25	800	0.1	75	5
Coco94	25	800	0.1	75	10
Coco89	25	800	0.1	75	15
Coco90	25	800	0.1	75	30
Coco92	25	800	0.1	75	45
Coco91	25	800	0.1	75	60
Coco93	25	800	0.1	75	120
Coco96	25	800	0.1	75	120
Coco97	25	800	5	75	120
Coco87	25	800	0.1	75	600
Coco95	25	800	0.1	75	1800

Table 4-2. Test conditions for 50% CO

Name	Temperature	Pressure	Scan rate	CO	Exposure time
	(°C)	(kPa)	(mV/s)	(%)	(min)
Coco68	25	800	0.1	50	5 min
Coco73	25	800	0.1	50	5 min
Coco70	25	800	0.1	50	12 min
Coco67	25	800	0.1	50	15 min
Coco71	25	800	0.1	50	20 min
Coco84	25	800	0.1	50	45 min
Coco69	25	800	0.1	50	2 hours
Coco100	25	800	0.1	50	30 hours

Table 4-3. Test conditions for 25% CO

Name	Temperature	Pressure	Scan rate	CO	Exposure time
	(°C)	(kPa)	(mV/s)	(%)	(min)
Coco42	25	800	0.1	25	0
Coco57	25	800	0.1	25	1
Coco54	25	800	0.1	25	5
Coco52	25	800	0.1	25	10
Coco31	25	800	0.1	25	20
Coco53	25	800	0.1	25	20
Coco39	25	800	0.1	25	25

Name	Temperature	Pressure	Scan rate	CO	Exposure time
Coco44	25	800	0.1	25	25
Coco43	25	800	0.1	25	30
Coco65	25	800	0.1	25	30
Coco60	25	800	0.1	25	45
Coco55	25	800	0.1	25	60
Coco29	25	800	0.1	25	75
Coco64	25	800	0.1	25	300
Coco40	25	800	0.1	25	690
Coco41	25	800	0.1	25	900
Coco101	25	800	0.1	25	1800
Coco33	25	800	0.1	25	2520
Coco49	25	800	0.1	25	3000

Table 4-4. Test conditions for 9% CO

Name	Temperature	Pressure	Scan rate	CO	Exposure time
	(°C)	(kPa)	(mV/s)	(%)	(min)
Coco77	25	800	0.1	9	5
Coco105	25	800	0.1	9	12
Coco72	25	800	0.1	9	20
Coco103	25	800	0.1	9	30
Coco104	25	800	0.1	9	45

Name	Temperature	Pressure	Scan rate	CO	Exposure time
Coco76	25	800	0.1	9	120
Coco78	25	800	0.1	9	300
Coco83	25	800	0.1	9	720
Coco102	25	800	0.1	9	1800

Table 4-5. Test conditions for 1% CO

Name	Temperature	Pressure	Scan rate	CO	Exposure time
	(°C)	(kPa)	(mV/s)	(%)	(min)
Coco116	25	800	0.1	1	10
Coco108	25	800	0.1	1	30
Coco106	25	800	0.1	1	60
Coco117	25	800	0.1	1	120
Coco118	25	800	0.1	1	300
Coco109	25	800	0.1	1	600
Coco115	25	800	0.1	1	600
Coco107	25	800	0.1	1	1800

And at 45°C the following tests were performed:

Table 4-6. Test conditions for 75%CO

Name	Temperature	Pressure	Scan rate	CO	Exposure time
	(°C)	(kPa)	(mV/s)	(%)	(min)
Coco133	45	800	0.1	75	5
Coco134	45	1400	0.1	75	5
Coco135	45	2000	0.1	75	5
Coco136	45	2000	0.1	75	5

Table 4-7, Test conditions for 50% CO

Name	Temperature	Pressure	Scan rate	CO	Exposure time
	(°C)	(kPa)	(mV/s)	(%)	(min)
Coco85	45	800	0.1	50	10
Coco86	45	800	0.1	50	45
Coco138	45	800	0.1	50	10 hours

Table 4-8. Test conditions for 25% CO

Name	Temperature	Pressure	Scan rate	CO	Exposure time
	(°C)	(kPa)	(mV/s)	(%)	(min)
Coco121	45	800	0.1	25	5
Coco130	45	1000	0.1	25	5

Name	Temperature	Pressure	Scan rate	CO	Exposure time
Coco131	45	1400	0.1	25	5
Coco132	45	1200	0.1	25	5
Coco119	45	800	0.1	25	10
Coco120	45	800	0.1	25	30
Coco128	45	800	0.1	25	60
Coco129	45	800	0.1	25	60
Coco137	45	800	0.1	25	60
Coco123	45	800	0.1	25	300
Coco124	45	800	0.1	25	600
Coco15	45	800	1	25	1200
Coco14	45	800	0.01	25	0

Table 4-9. Test conditions for 9% CO

Name	Temperature	Pressure	Scan rate	CO	Exposure time
	(°C)	(kPa)	(mV/s)	(%)	(min)
Coco20	45	800	0.01	9	0
Coco19	45	800	0.1	9	0
Coco21	45	800	1	9	0
Coco22	45	800	10	9	0

In addition to the above-mentioned tests, one test was performed at 1% CO, 45°C, 800 kPa, a scan rate of 0.01 mV/s, and with no holding time.

4.3 Results

4.3.1 Slow scan-rate tests

Tests were performed for all of the gas mixtures at the slow scan rate. The tests were also performed after a variety of exposure (holding) times at open circuit potential (OCP) to determine the passivation rate of the adsorption reaction. Figure 4-2 to Figure 4-23 show the results of the tests after various exposure times for the different gas mixtures.

Firstly, the polarisation characteristic for 1% carbon monoxide is shown in Figure 4-2. The red curve was performed after 10 min exposure at OCP and the cathodic side of the curve was measured at much higher current densities than the rest of the curves that were determined at longer exposure times. The difference in these curves is not very distinct, and only after long exposure times of more than 5 hours, the pink and grey curves, were significant passivation reactions noticed.

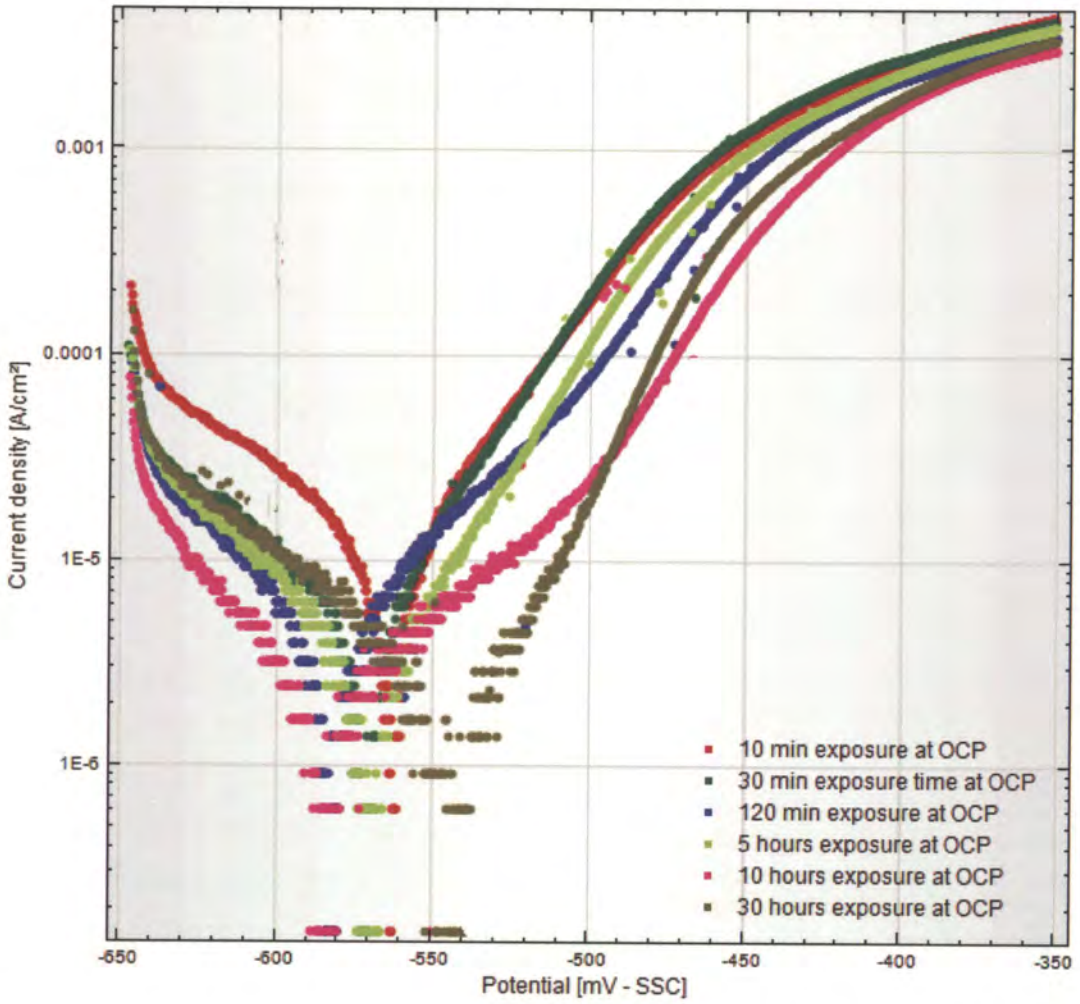

Figure 4-2. Polarisation characteristics of A516 pressure vessel steel exposed to 1% CO – 99% CO_2 at 25°C, at a scan rate of 0.1 mV/s after it was held at open circuit potential (OCP) for various times as indicated.

Showing a smaller number of these curves (Figure 4-3) improves the clarity of the trend. There was an increase of almost 50 mV, in corrosion potential, after 30 hours exposure.

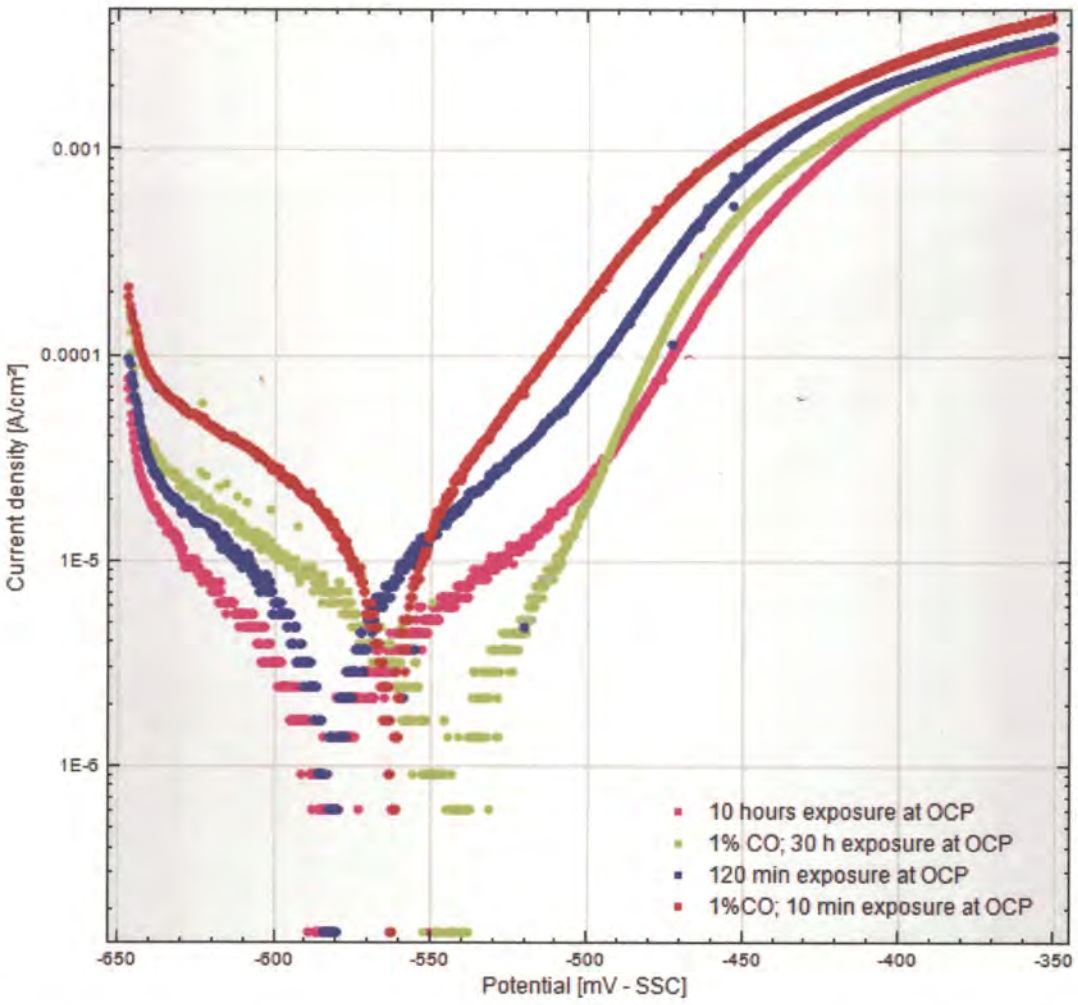

Figure 4-3. The same but fewer curves as shown in Figure 4-2, for polarisation characteristics of A516 pressure vessel steel exposed to 1% CO – 99% CO_2 at 25°C, at a scan rate of 0.1 mV/s after it was held at open circuit potential (OCP) for various times as indicated.

At 9% carbon monoxide a similar tendency was found. Figure 4-4 shows this with a significant change in passivity occurring after 45 minutes. During the first 45 minutes, the repeatability of the curves were acceptable, although the passive region after 5 minutes extended further than for all of the curves up to 45 minutes holding time, although the level of passivity was very consistent up to this point. With increasing times from 2 to 30 hours (dark purple – 2 h, blue – 5 h, pink – 12 h and light purple – 30 h), significant changes occurred on the passivity of the steel. Again after 30 hours

(light purple), the corrosion potential of the steel shifted significantly to more noble potentials.

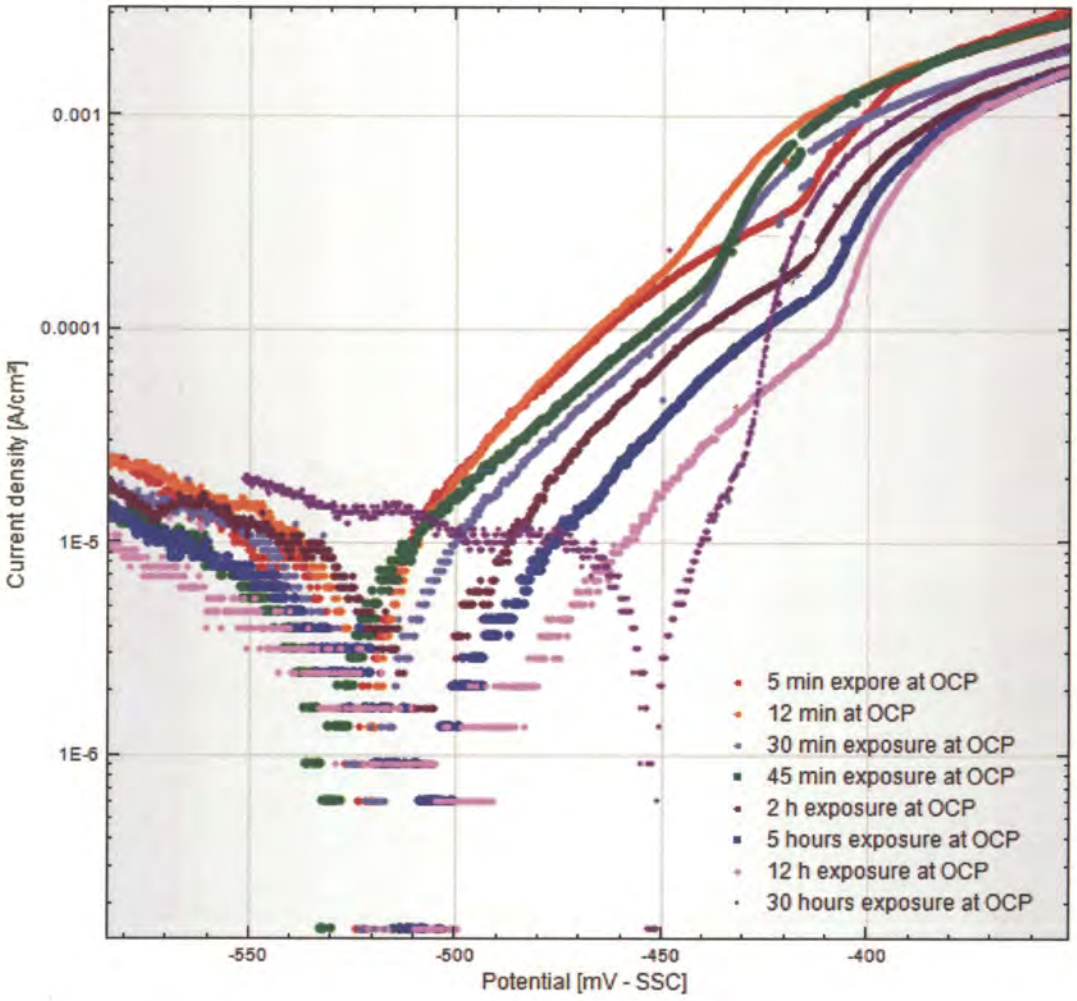

Figure 4-4. Polarisation characteristics of A516 pressure vessel steel exposed to 9% CO – 91% CO_2 at 25°C and 800 kPa, at a scan rate of 0.1 mV/s after it was held at open circuit potential (OCP) for various times from 5 minutes to 30 hours.

With fewer curves (Figure 4-5), the trend is very clear; moving from 12 min (dark yellow) to 2 hours (green), there was a significant drop in the passivation current density. Then to 5 hours exposure (blue) there was still a decrease in the current density of the passive region. And after 12 hours (pink), the current density showed a

further decrease, but from 2 to 12 hours, the position of the passive range in terms of the potential did not change significantly. It was only after 30 hours that the significant shift occurred.

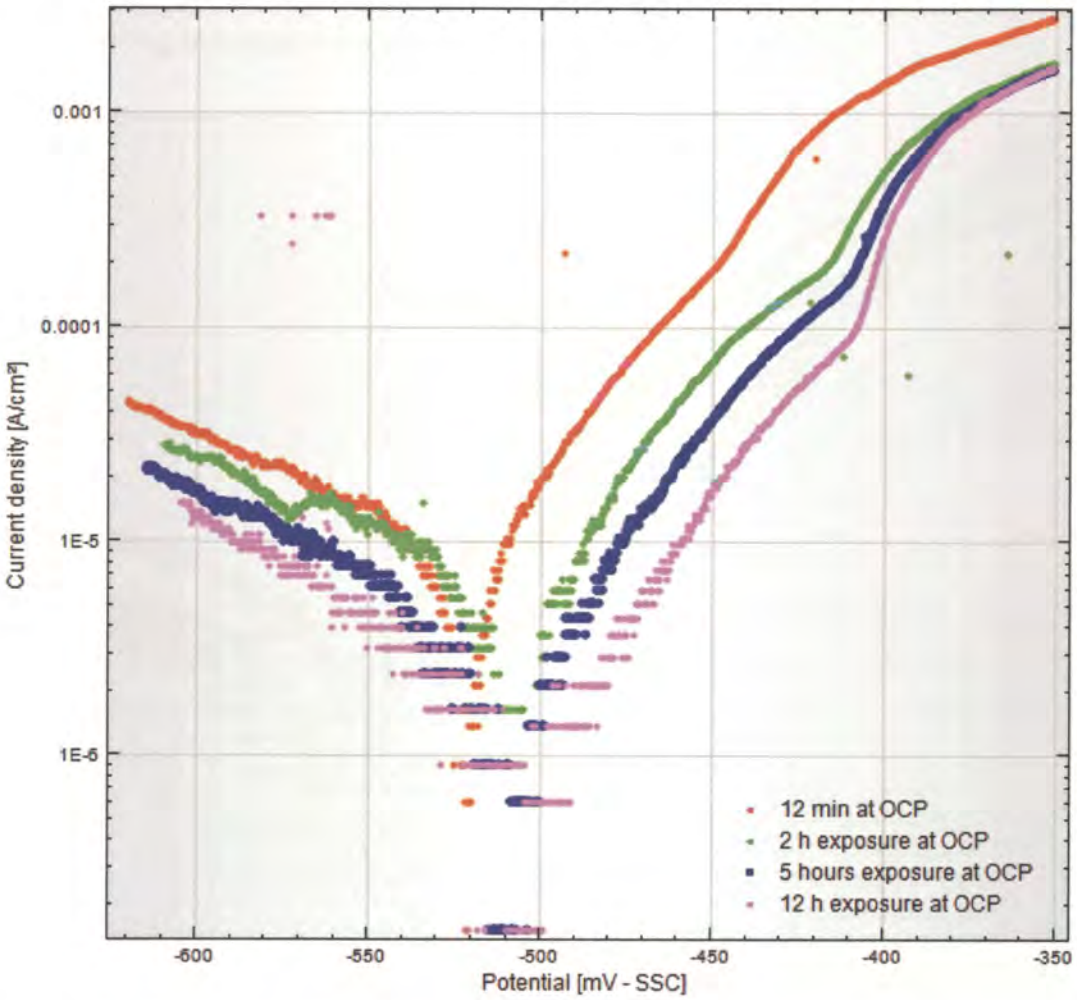

Figure 4-5. The same but fewer curves as shown in Figure 4-4, for polarisation characteristics of A516 pressure vessel steel exposed to 1% CO – 99% CO_2 at 25°C, at a scan rate of 0.1 mV/s after it was held at open circuit potential (OCP) for various times as indicated.

At 25% CO (Figure 4-6) the progression was the same with the passivation of the steel, and because this carbon monoxide concentration was evaluated extensively in Chapter 3, the polarisation characteristics were also evaluated more thoroughly with the first 30 minutes of exposure. The blue line was measured almost immediately after

exposure and there was no sign of a passive region. The dark yellow curve, 1 minute of exposure, showed a slight kink indicating the beginning of passivation. After 10 minutes up to 30 minutes, the curves were almost the same, all with a definite indication of passivation and varying in passive current density but the trans-passive region starting at almost the same potential.

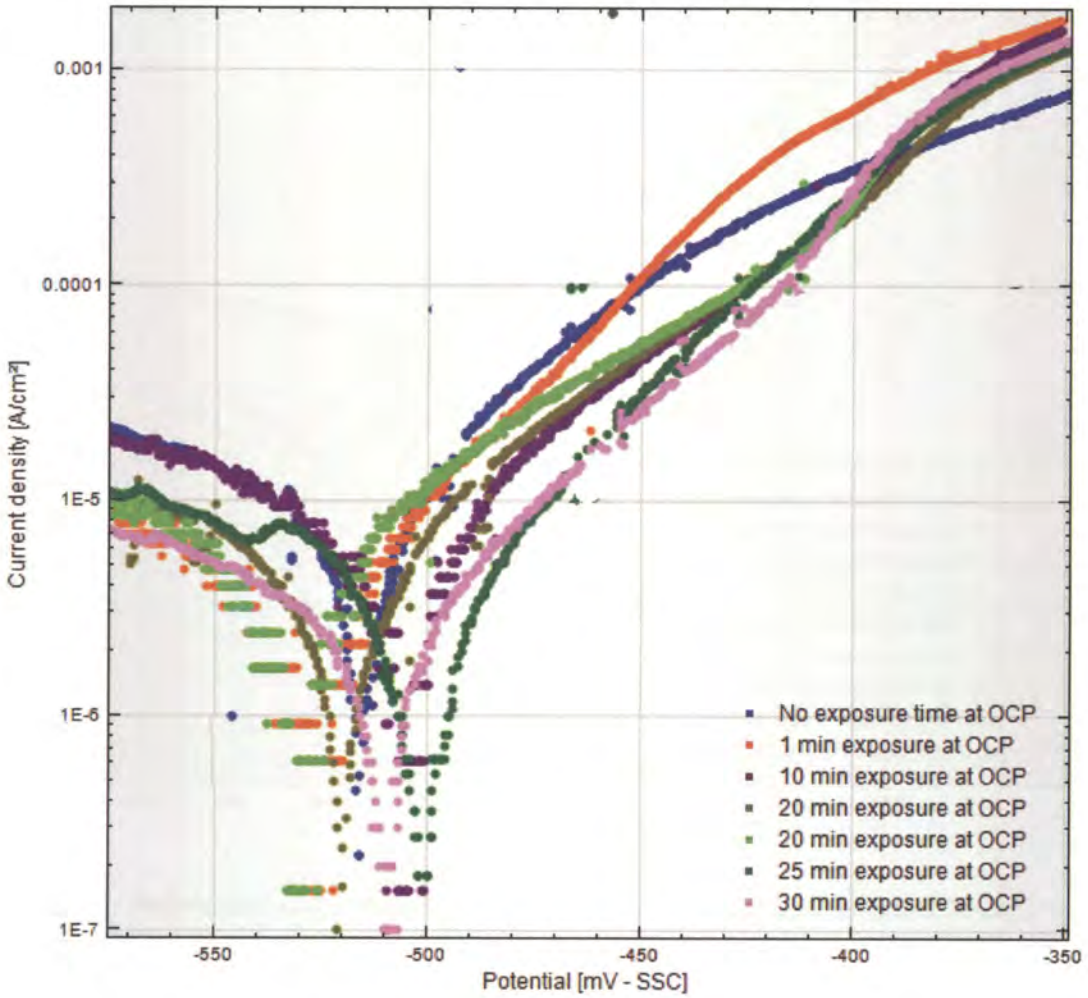

Figure 4-6. Polarisation characteristics of A516 pressure vessel steel exposed to 25% CO – 75% CO_2 at 25°C and 800 kPa, at a scan rate of 0.1 mV/s after it was held at open circuit potential (OCP) for the first 30 minutes of exposure.

The rest of the exposure times are shown in Figure 4-7 with exposure times from 30 minutes up to 50 hours.

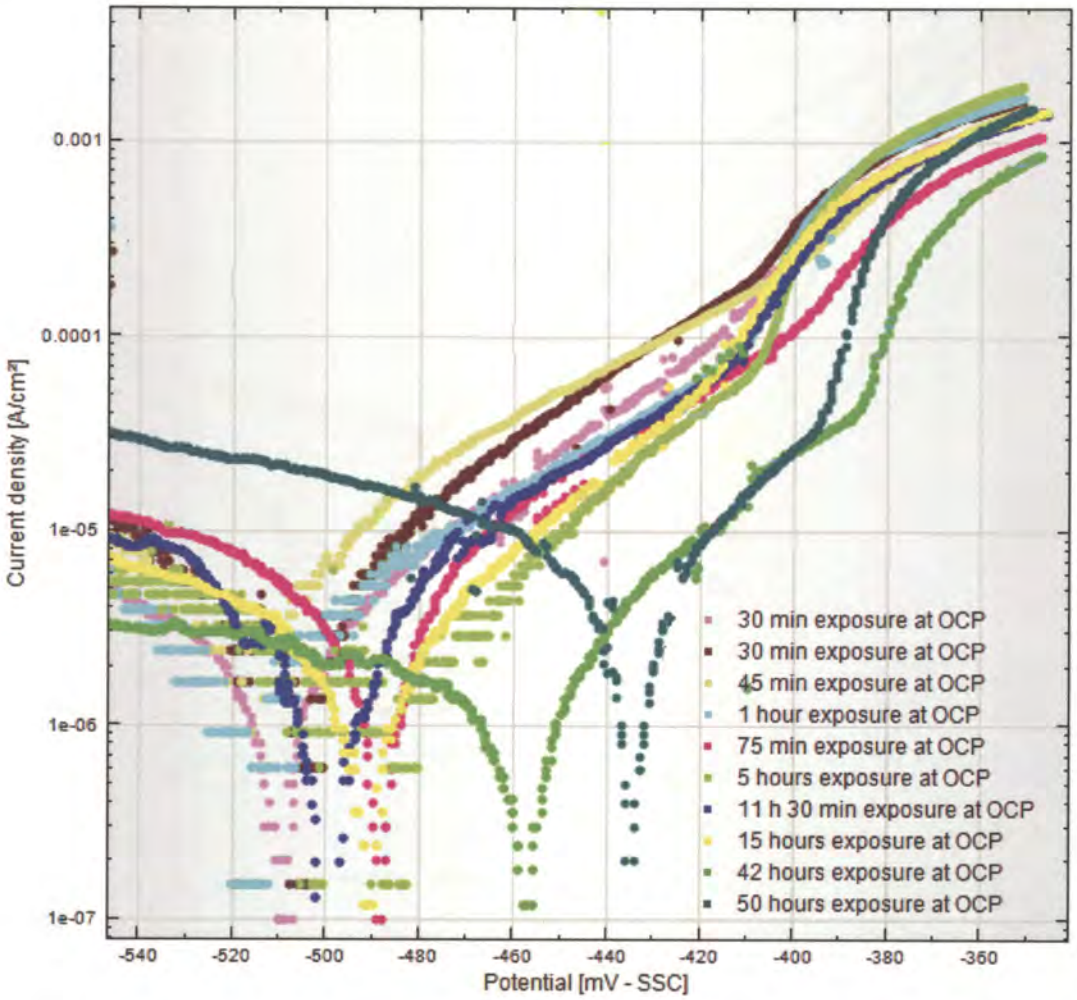

Figure 4-7. Polarisation characteristics of A516 pressure vessel steel exposed to 25% CO – 75% CO_2 at 25°C and 800 kPa, at a scan rate of 0.1 mV/s after it was held at open circuit potential (OCP) from 30 minutes up to 50 hours.

The extent of the passivation over the whole period is seen with greater clarity in Figure 4-8 with fewer curves. The difference from 1 (dark yellow) to 10 minutes (purple) exposure was considerable and the passive region quickly formed as compared to the time it took at the lower carbon monoxide concentrations, where this type of passivity only occurred after almost an hour of exposure. After 50 hours of

exposure, the corrosion potential shifted to more noble potentials, as was seen with the other carbon monoxide concentrations Figure 4-2 to 4-12.

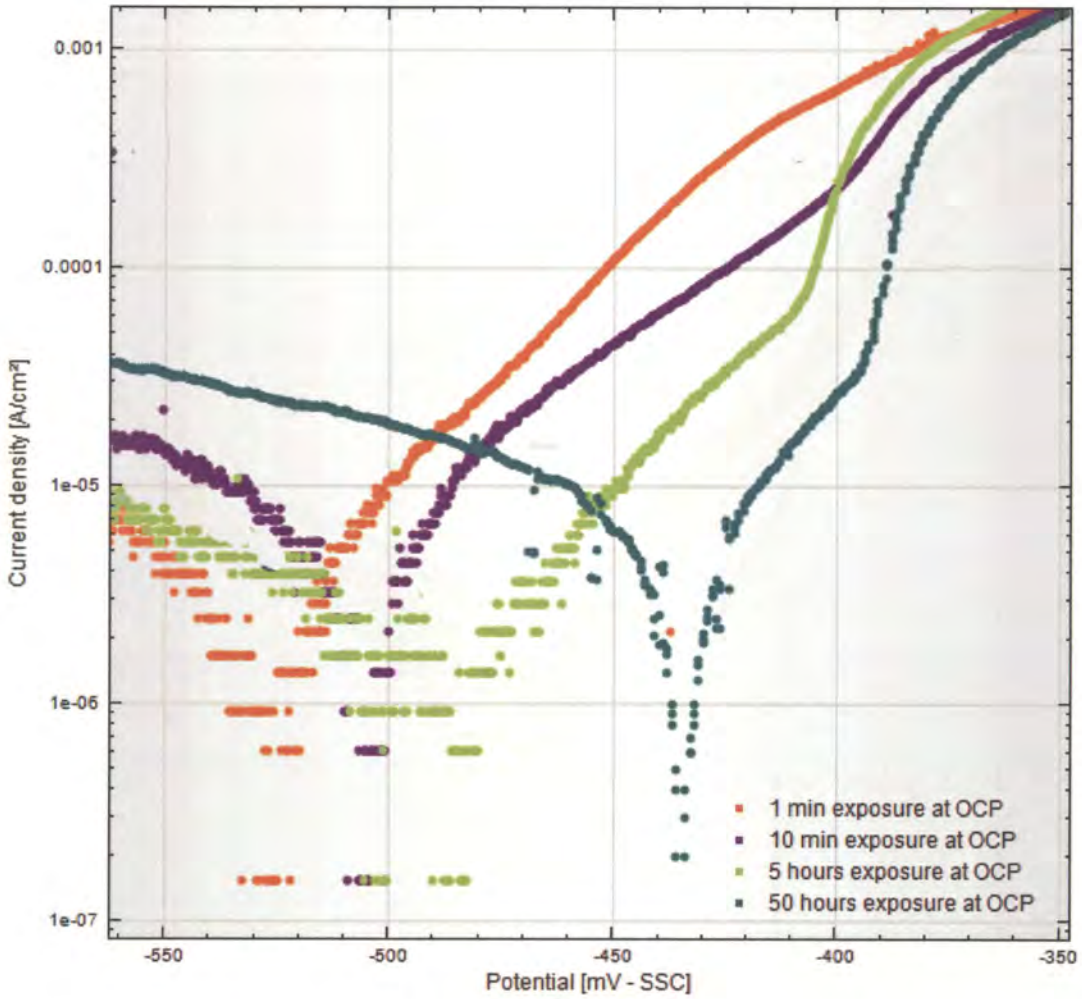

Figure 4-8. The same but fewer curves as shown in Figure 4-6 and 4-7, for polarisation characteristics of A516 pressure vessel steel exposed to 25% CO – 75% CO_2 at 25°C, at a scan rate of 0.1 mV/s after it was held at open circuit potential (OCP) for various times as indicated.

At 50% CO, the passivation reaction was more prominent and there was very little difference between the initial exposure times at OCP (5 min – blue, 12 min – purple, 15 min – dark pink, 20 min – light pink) and the exposure times of up to 2 hours (red

curve). Only after 30 hours was the extent of passivation more prominent and, as before (Figure 4-2 to 4-5), the corrosion potential moved to more noble potentials.

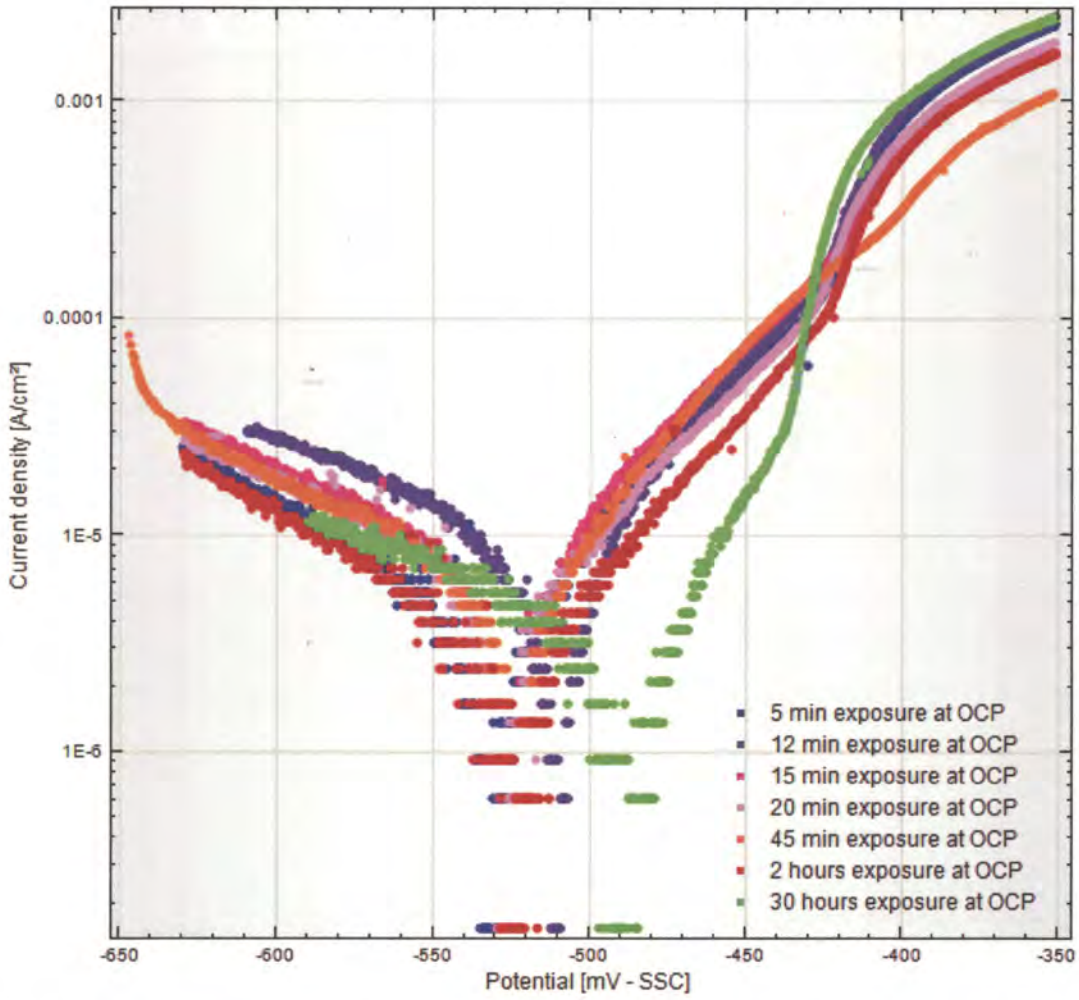

Figure 4-9. Polarisation characteristics of A516 pressure vessel steel exposed to 50% CO – 50% CO_2 at 25°C and 800 kPa, at a scan rate of 0.1 mV/s after it was held at open circuit potential (OCP) for various times from 5 minutes to 30 hours.

With a fewer curves plotted together (Figure 4-10), the passivation reaction rate is more easily followed. Again, it is clear that after 12 and 45 min exposure, there was little difference in the curves, except for the drop in the current density of the 45 min

curve after the passive region. The reason for this is not clear, as the 30 hours exposure curve goes back to follow the purple (12 min exposure) curve after the passive region.

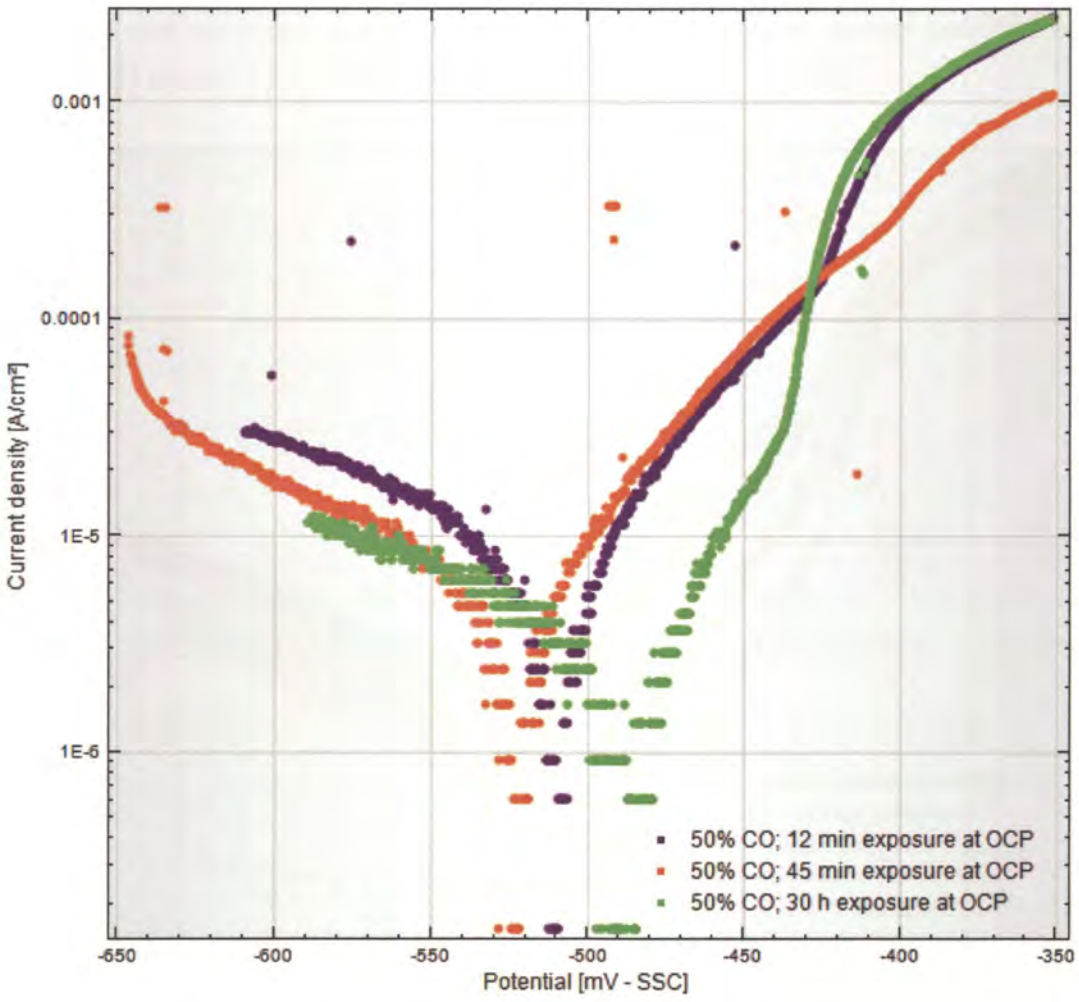

Figure 4-10. The same but fewer curves as shown in Figure 4-9, for polarisation characteristics of A516 pressure vessel steel exposed to 50% CO – 50% CO_2 at 25°C, at a scan rate of 0.1 mV/s after it was held at open circuit potential (OCP) for various times as indicated.

At 50% CO (Figure 4-9 and 4-10) and especially 75%CO (Figure 4-11), the passive region was more stable, and as seen in Figure 4-11 all the curves showed very similar

transpassive potentials. Again, the progression of increased passivation followed the exposure times: firstly the 5 min exposure (blue curve), then the 10 min (dark pink) and 15 min (pink) exposures are almost the same. Following these, are 30 min (light green) and 45 min (dark green). After 1 (light red) and 2 hours (brown) of exposure, the passivation was more significantly different, and then after 10 hours (red) the difference was not much, but after 30 hours (grey) the passive current densities were significantly lower.

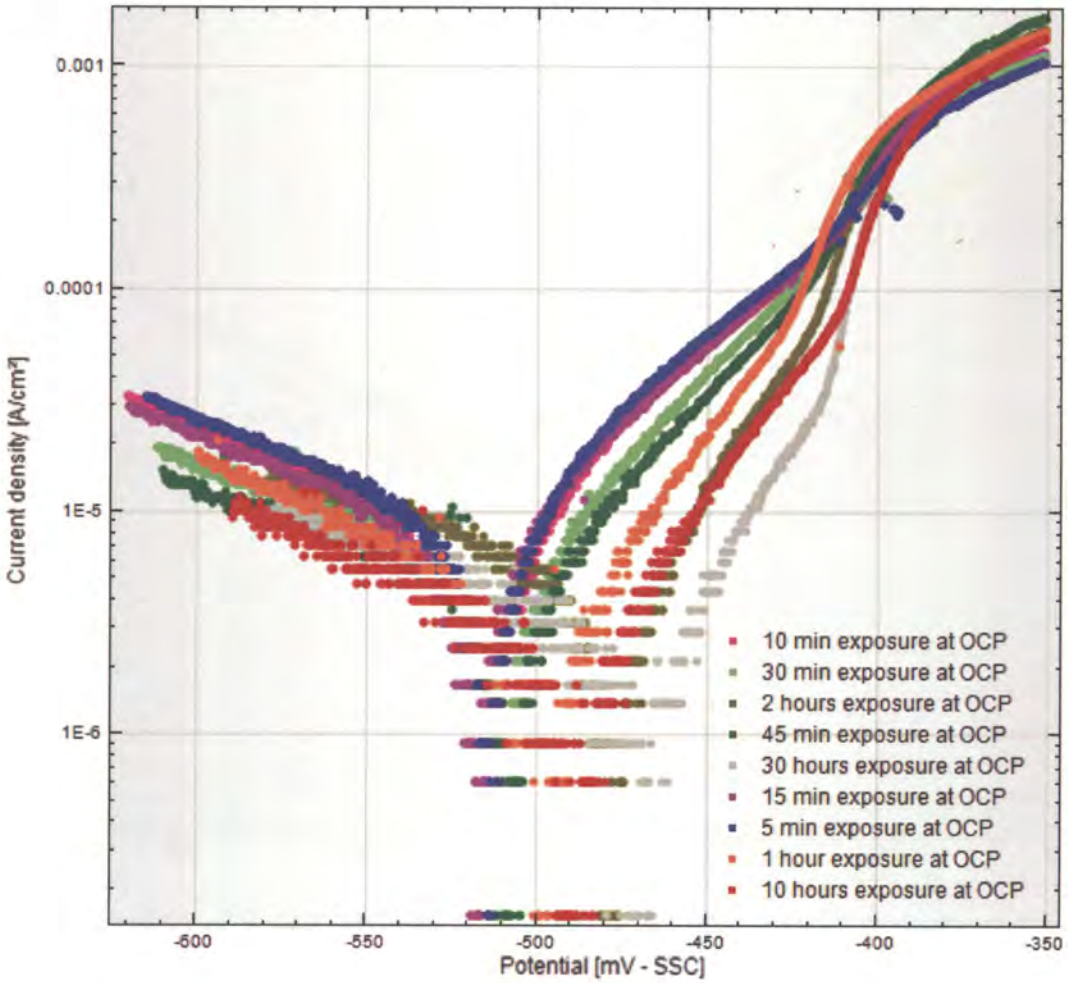

Figure 4-11. Polarisation characteristics of A516 pressure vessel steel exposed to 75% CO – 25% CO_2 at 25°C and 800 kPa, at a scan rate of 0.1 mV/s after it was held at open circuit potential (OCP) for various times from 5 minutes to 30 hours.

With only three curves (Figure 4-12), the progression and the effect of the holding time on passivation is clearer, with a steady formation of the passive region over time. Only after 2 hours the corrosion potential had moved to more noble potentials, and after 30 hours it had not moved much more. The transpassive potential was also very constant, as was seen for the 50% carbon monoxide environment (Figure 4-10).

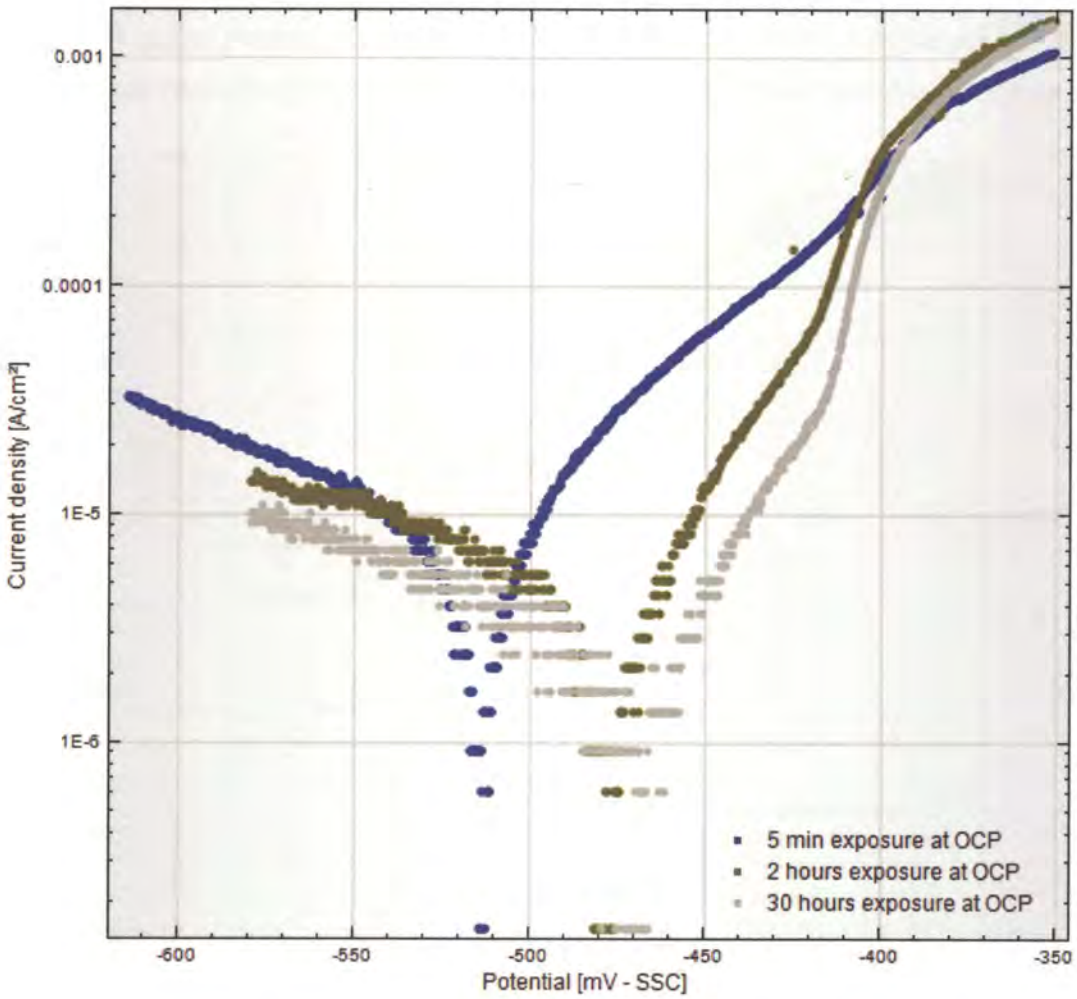

Figure 4-12. The same but fewer curves as shown in Figure 4-11, for polarisation characteristics of A516 pressure vessel steel exposed to 75% CO – 25% CO_2 at 25°C, at a scan rate of 0.1 mV/s after it was held at open circuit potential (OCP) for various times as indicated.

The slow strain-rate tests revealed that the susceptibility to stress-corrosion cracking increased around 45°C, and the curves show the effect of the holding times at OCP for

steel exposed to a 25% CO environment. Unfortunately, due to experimental difficulties, fewer tests were performed at the higher temperatures, the potentiostat control became unreliable and scatter on the curves was significantly more. When the steel was almost immediately exposed (orange curve) to the environment, no passive region was evident, but even after 10 minutes (pink curve) the passive region was pronounced. The following exposure times, 30 min (black curve) and 1 hour (red, green and purple) were close to one another, revealing an acceptable repeatability, after 5 hours (dark grey) the passive region moved to slightly more noble potentials.

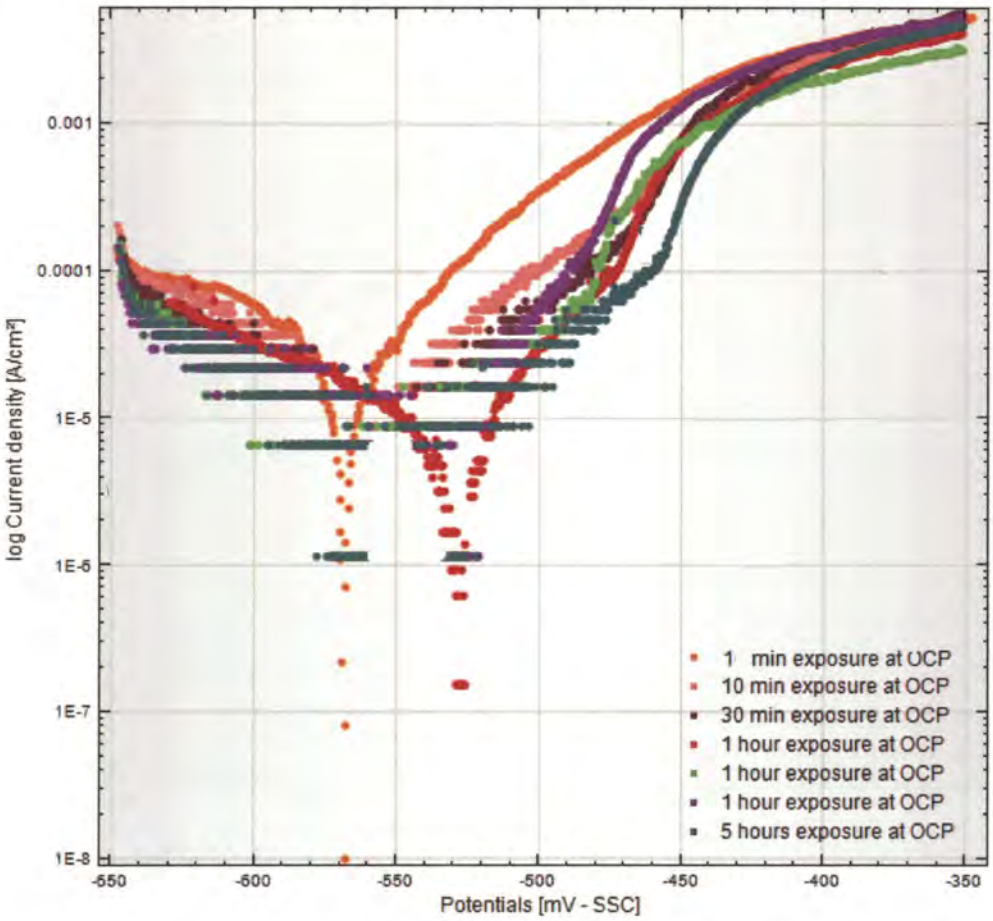

Figure 4-13. Polarisation characteristics of A516 pressure vessel steel exposed to 25% CO – 75% CO_2 at 45°C and 800 kPa, at a scan rate of 0.1 mV/s after it was held at open circuit potential (OCP) for various times from 1 minutes to 5 hours.

With fewer curves, the progression was clearer, with very little exposure (dark grey curve). The passive region was not present, and then as the time increased to 10 minutes (purple curve) and 1 hour (red curve), the passive region very clearly formed, occurring at a higher rate than at the lower temperatures, as expected.

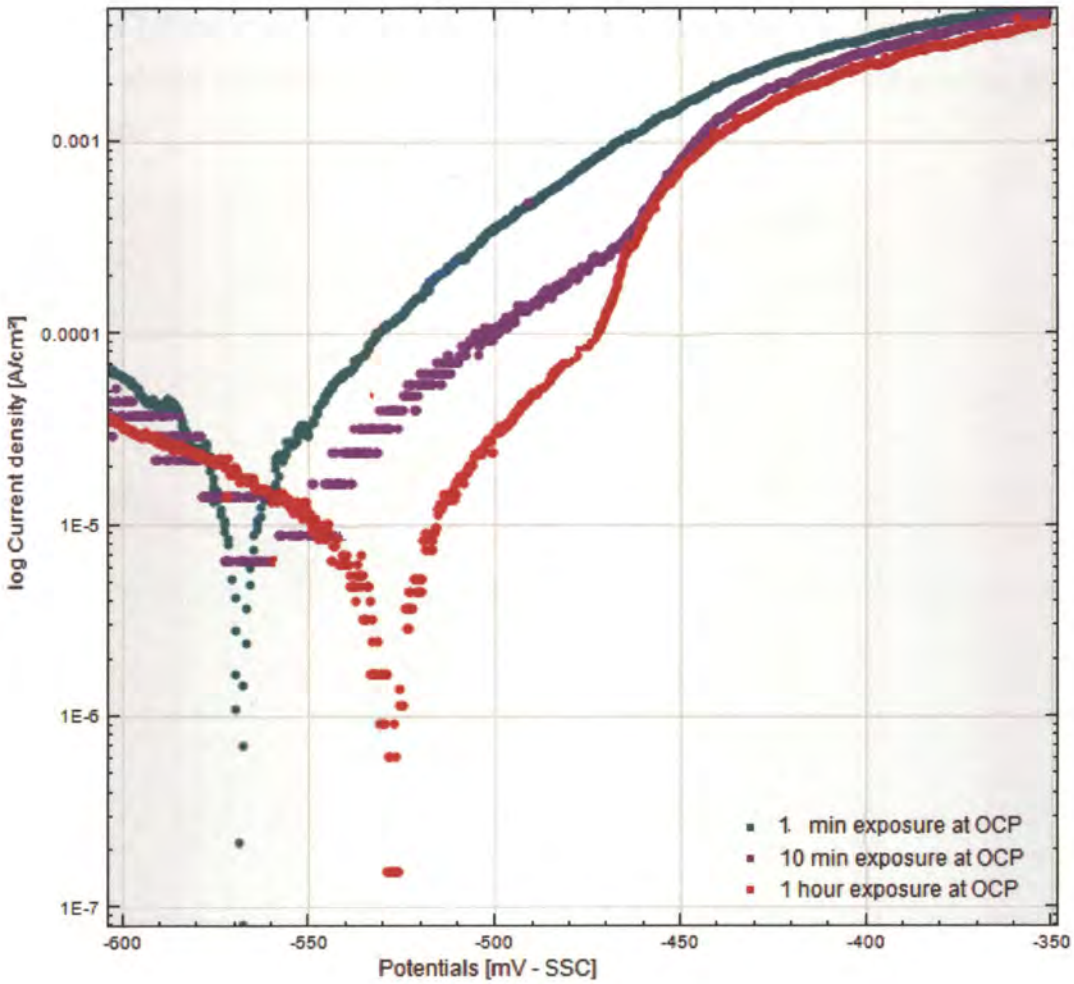

Figure 4-14. The same but fewer curves as shown in Figure 4-13, for polarisation characteristics of A516 pressure vessel steel exposed to 25% CO – 75% CO_2 at 45°C, at a scan rate of 0.1 mV/s after it was held at open circuit potential (OCP) for various times as indicated.

4.3.2 Temperature

When the effect of temperature was compared in the 25% carbon monoxide environment, the rate of the passivation reaction was clear, as well as the higher current densities at the higher temperatures, as shown in Figure 4-15. The corrosion potentials of the higher temperature curves moved to more active potentials. The passivity for the higher temperature curves extended over smaller potential ranges than those for the lower temperatures. With very little exposure of the steel at 45°C, the curve shows no passive region, but at 25°C, the curve does show some sign of passivation.

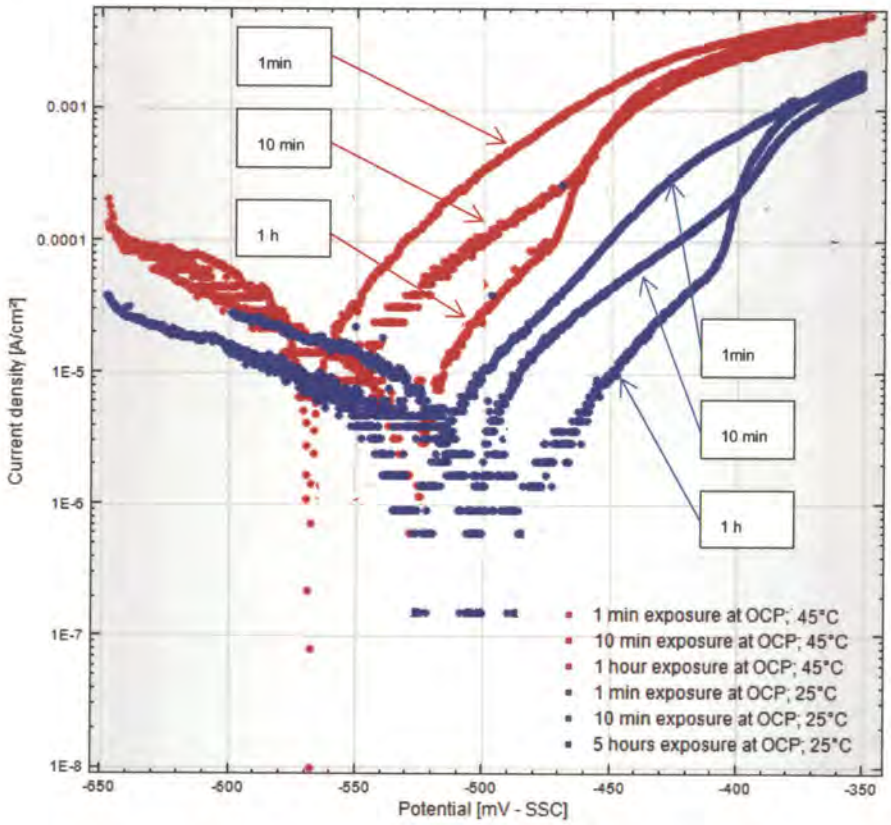

Figure 4-15. Polarisation characteristics of A516 pressure vessel steel exposed to 25% CO – 75% CO_2 at 800 kPa, at a scan rate of 0.1 mV/s after it was held at open circuit potential (OCP) for various times from 1 minutes to 5 hours. Note blue curves were performed at 25°C and the red curves at 45°C.

With a 50% carbon monoxide environment at 45°C (Figure 4-16), the results were similar: the passive region was present after 10 minutes exposure (blue curve) and dropped after 45 minutes to lower current densities. However, after 10 hours of exposure the curve shows very similar results and is in the same position as the 45 minutes exposure curve (Figure 4-16).

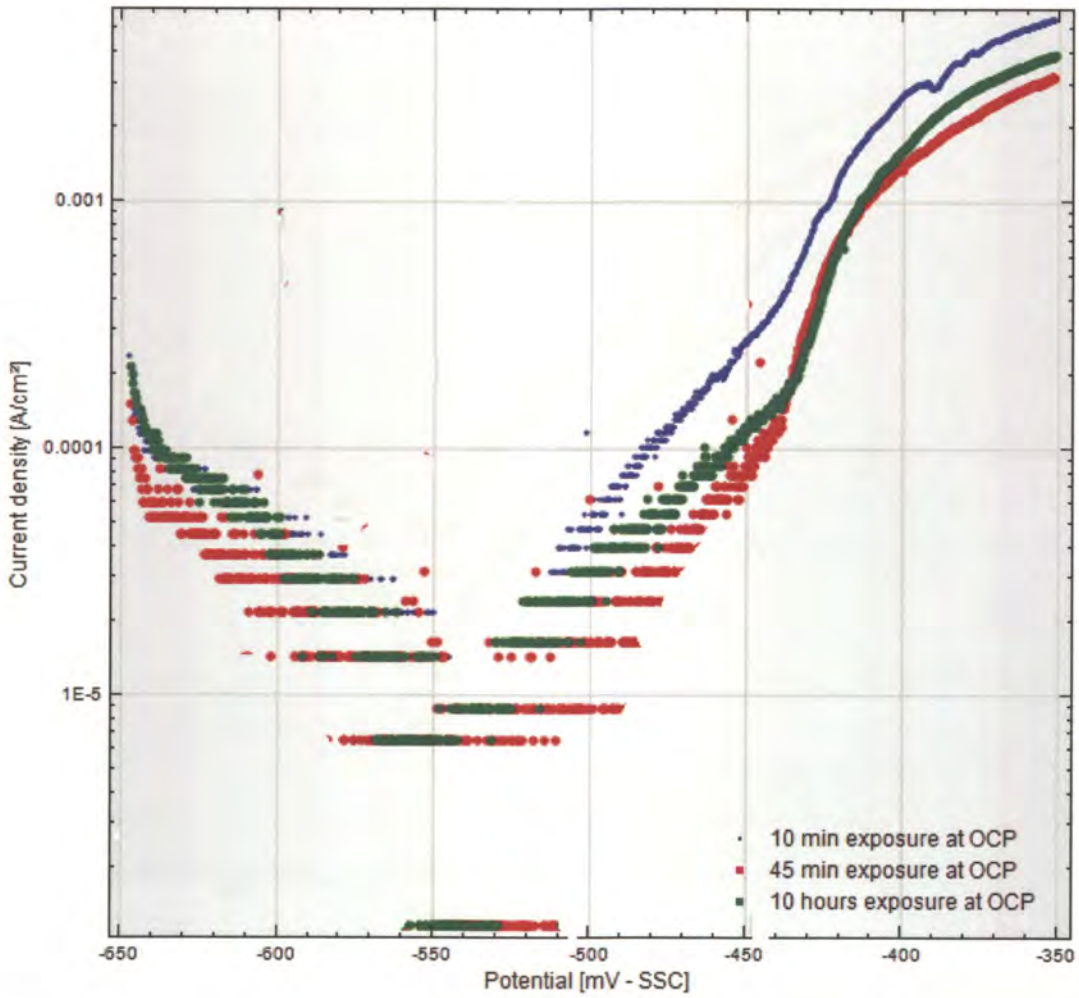

Figure 4-16. Polarisation characteristics of A516 pressure vessel steel exposed to 50% CO – 50% CO_2 at 45°C and 800 kPa, at a scan rate of 0.1 mV/s after it was held at open circuit potential (OCP) for various times from 10 minutes to 10 hours.

When these curves are compared with similar conditions at 25°C with the red curves at 45°C and the blue curves at 25°C in Figure 4-17, it can be seen that the current density of the passive region for the steel exposed to 45°C for 10 minutes is higher than for all the other curves shown. However, when the steel was exposed for 45 minutes at 45°C, the current density of the passive region was almost exactly the same as the current densities at 25°C. The corrosion potentials were almost similar, although, the potential range of the passive region is smaller at the higher temperature.

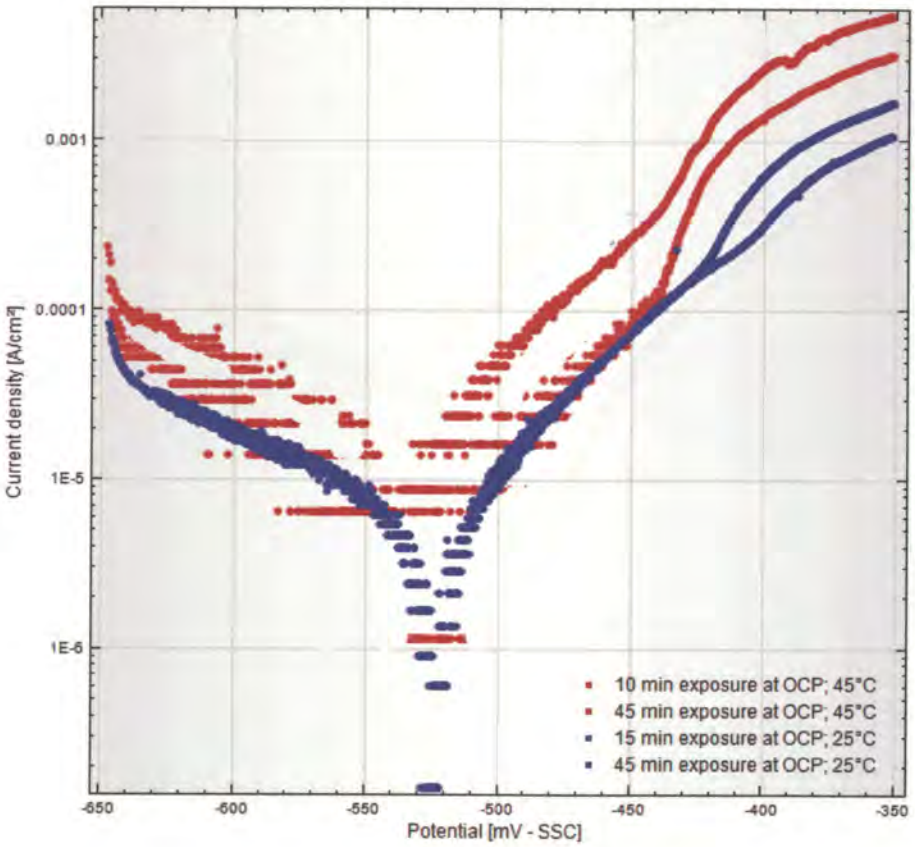

Figure 4-17. Polarisation characteristics of A516 pressure vessel steel exposed to 50% CO – 50% CO_2 at 800 kPa, at a scan rate of 0.1 mV/s after it was held at open circuit potential (OCP) for various times from 1 minutes to 5 hours. Note blue curves were performed at 25°C and the red curves at 45°C.

In the 75% carbon monoxide environment (Figure 4-18),the effect of temperature caused a similar passive current density when the steel was exposed to the environment for only 5 minutes. However, the whole curve is moved to more active potentials by approximately 60 mV.

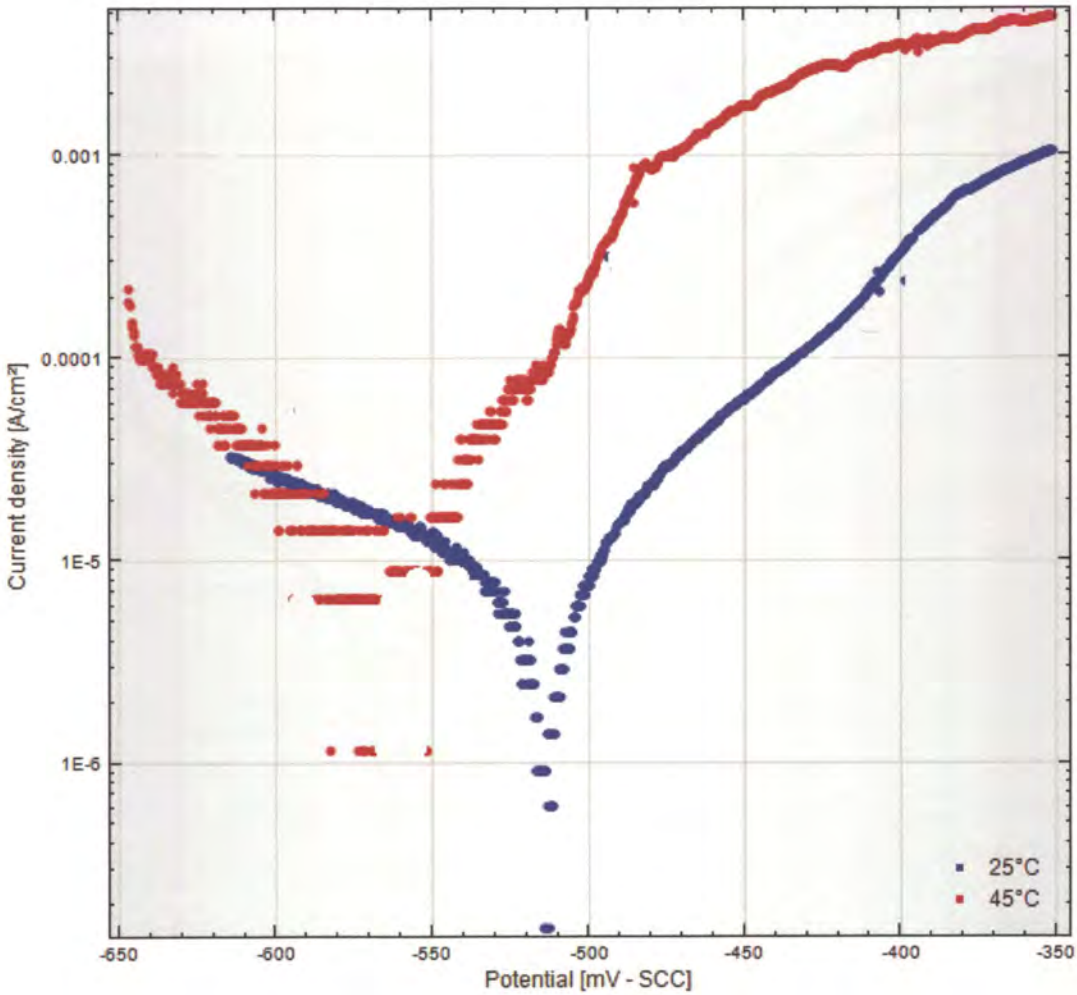

Figure 4-18. Polarisation characteristics of A516 pressure vessel steel exposed to 75% CO – 25% CO_2 at 800 kPa, at a scan rate of 0.1 mV/s after it was held at open circuit potential (OCP) for 5 minutes. Note the blue curve was performed at 25°C and the red curve at 45°C.

4.3.3 Total pressure

The slow strain-rate test showed that stress-corrosion susceptibility increased with the total pressure of the system. At a concentration of 25% carbon monoxide and a temperature of 45°C, the passive region became more pronounced at higher total pressures with a decrease in the overall current densities (Figure 4-19).

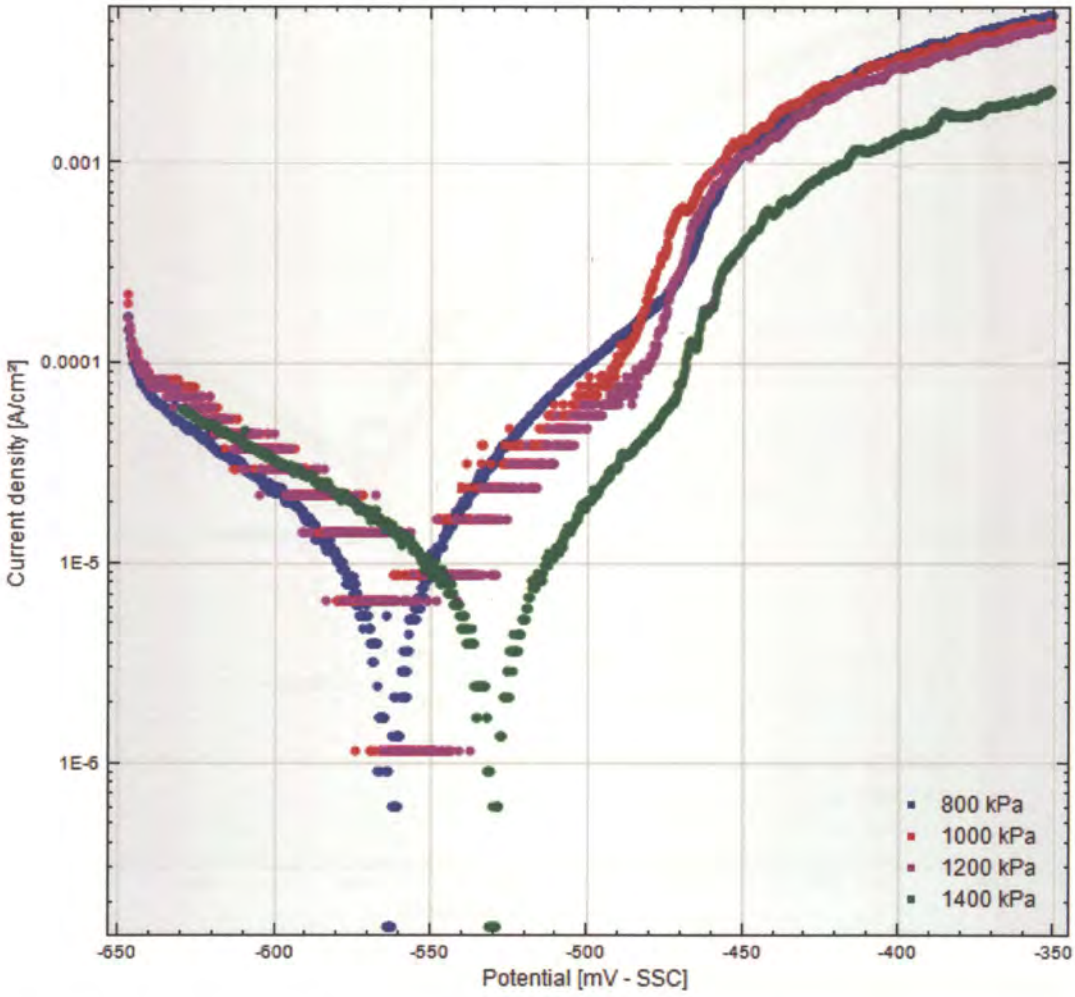

Figure 4-19. Polarisation characteristics of A516 pressure vessel steel exposed to 25% CO – 75% CO_2 at various total pressures, a temperature of 45°C, and a scan rate of 0.1 mV/s after it was held at open circuit potential (OCP) for 5 minutes.

The effect of pressure with 75% carbon monoxide at 45°C showed a similar tendency, but the effect was not as dramatic with difference between the 800 kPa and the 1400 kPa curves, smaller than it was with the 25% carbon monoxide (Figure 4-20). However, at 2000 kPa, the curve was at significantly lower current densities and the corrosion potential moved to more noble potentials.

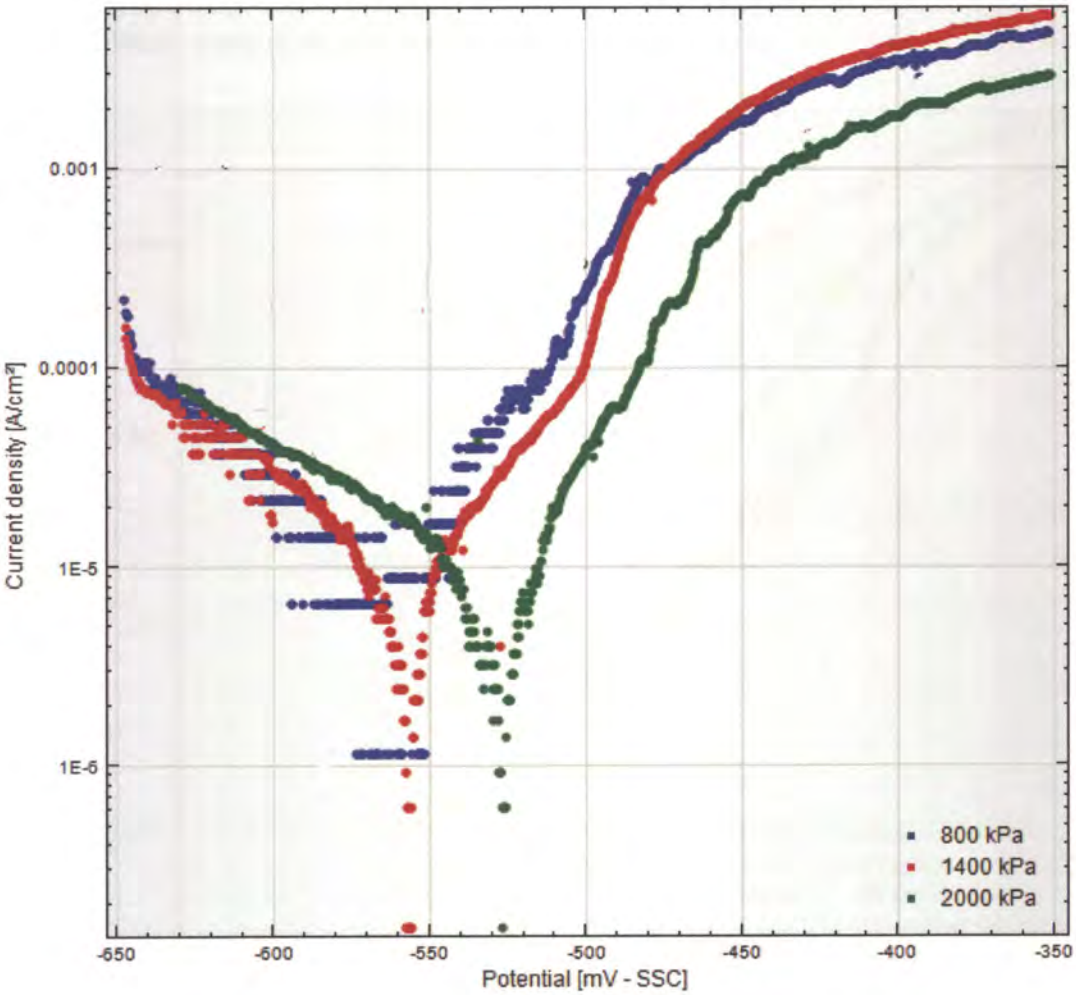

Figure 4-20. Polarisation characteristics of A516 pressure vessel steel exposed to 75% CO – 25% CO_2 at various total pressures, a temperature of 45°C, and a scan rate of 0.1 mV/s after it was held at open circuit potential (OCP) for 5 minutes.

4.3.4 Carbon monoxide content

The effect of carbon monoxide concentration was evaluated at the different exposure times, firstly at 10 min, then 45 minutes and 30 hours. At 10 minutes exposure of the steel, the response to the different carbon monoxide concentrations is shown in Figure 4-21. The 1% carbon monoxide curve (red) showed little evidence of a passive region after 10 minutes, but from 25%, the presence of the passive region was evident, even at 9% the passive region was present.

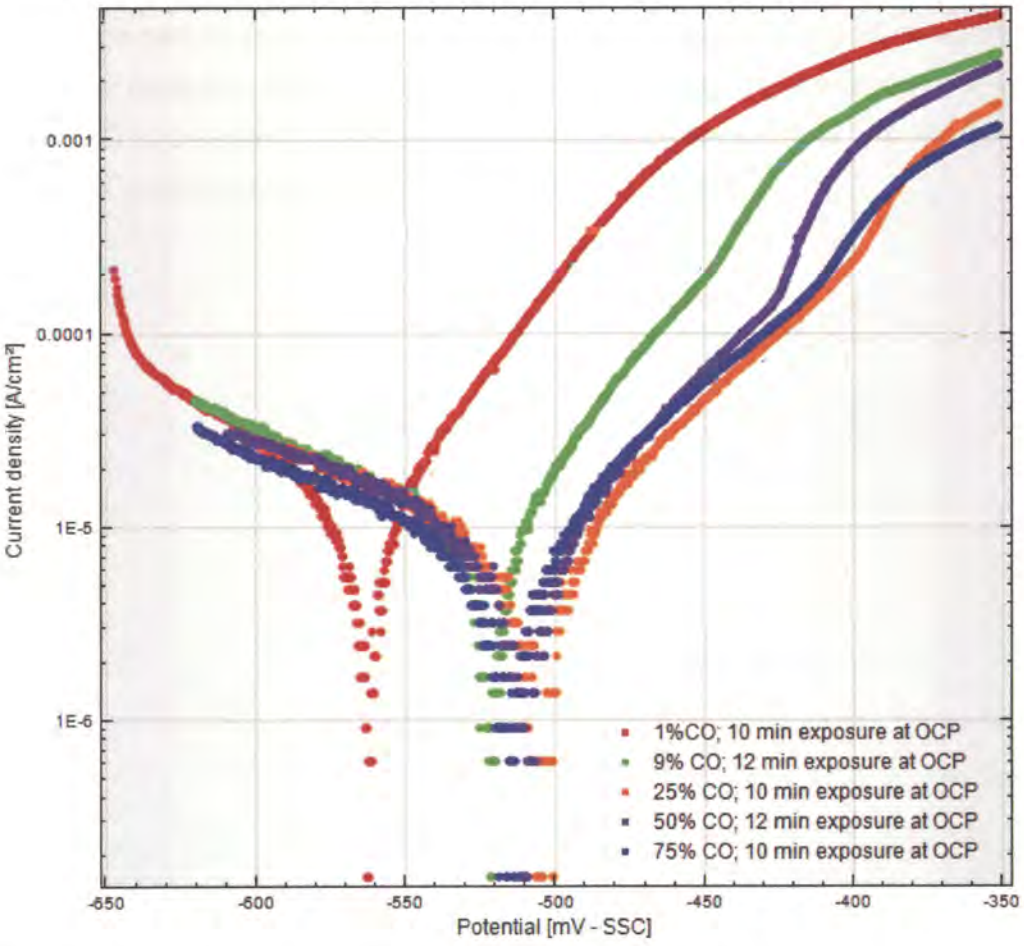

Figure 4-21. CO concentration comparison after approximately 10 minutes exposure at OCP for polarisation characteristics of A516 pressure vessel steel exposed to 800 kPa, a temperature of 25°C, and a scan rate of 0.1 mV/s after it was held at open circuit potential (OCP) for around 10 minutes..

After 30 minutes (Figure 4-22) the steel in 1% carbon monoxide still did not show a significant passive region, compared to the other carbon monoxide concentrations (however, note that the exposure time was 45 minutes for the other concentrations). At all the other concentrations, the steel showed a definite passive region and the passive region in the 9% carbon monoxide was at the highest current densities, and the lowest current density was at 75% CO. The other two curves are very close to one another, but the steel showed a higher current density in the 50% carbon monoxide. The transpassive potential also increased to more noble potentials with increased percentage carbon monoxide, but this was slightly different for the 25 and 50% carbon monoxide contents, although both curves were mostly in between the 9 and 75% curves. The corrosion potential of the steel was very similar for all the carbon monoxide concentrations, except for of 1% carbon monoxide.

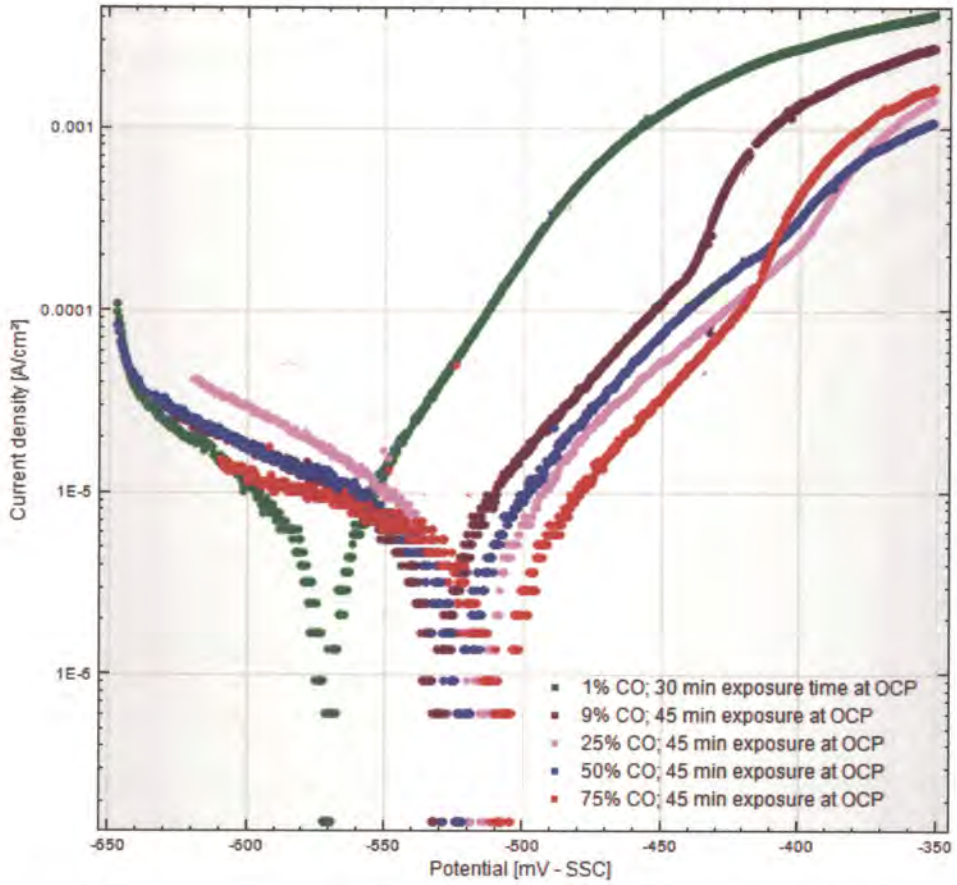

Figure 4-22. CO concentration comparison after approximately 45 minutes exposure at OCP for polarisation characteristics of A516 pressure vessel steel exposed to 800 kPa, a temperature of 25°C, and a scan rate of 0.1 mV/s. (Note that the sample exposed to 1%CO was tested after an exposure time of 30 minutes.)

After 30 hours (Figure 4-23), the steel in the 1% carbon monoxide (red curve) showed a very slight passive region compared to the other concentrations. At the other concentrations, the transpassive potentials were relatively close to each other, but the corrosion potentials were quite different. The corrosion potential of the steel tested in the 1% carbon monoxide (red curve) was the most active potential, and then, surprisingly, the 9% (green curve) was the most noble. This was followed by 75% (blue curve), being slightly more active than 50% (purple curve), and then 25%

(orange curve) was the most active next to the 1% curve. All of these are not different from what was expected.

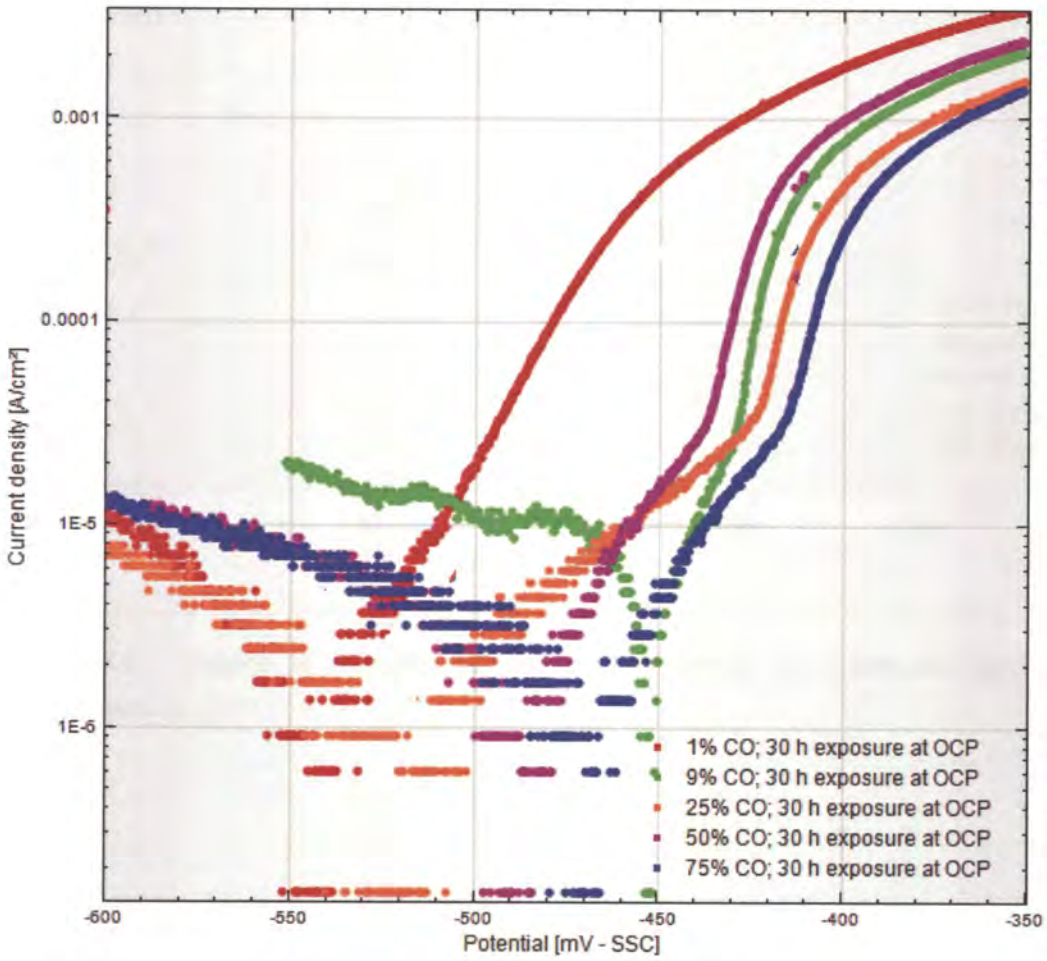

Figure 4-23. CO concentration comparison after approximately 30 hours exposure at OCP for polarisation characteristics of A516 pressure vessel steel exposed to 800 kPa, a temperature of 25°C, and a scan rate of 0.1 mV/s.

The passivation kinetics at various CO concentrations and OCP exposures are shown in Figure 4-24. Change in the "transpassive" current density over time for various CO concentrations at 25°C, here the passive current density at the point where the curve moves into a "transpassive" state is plotted over the exposure time. The fitted power

curves gave very similar values in the passivation kinetics. Note in Figure 4-25 the change in the corrosion potential for the

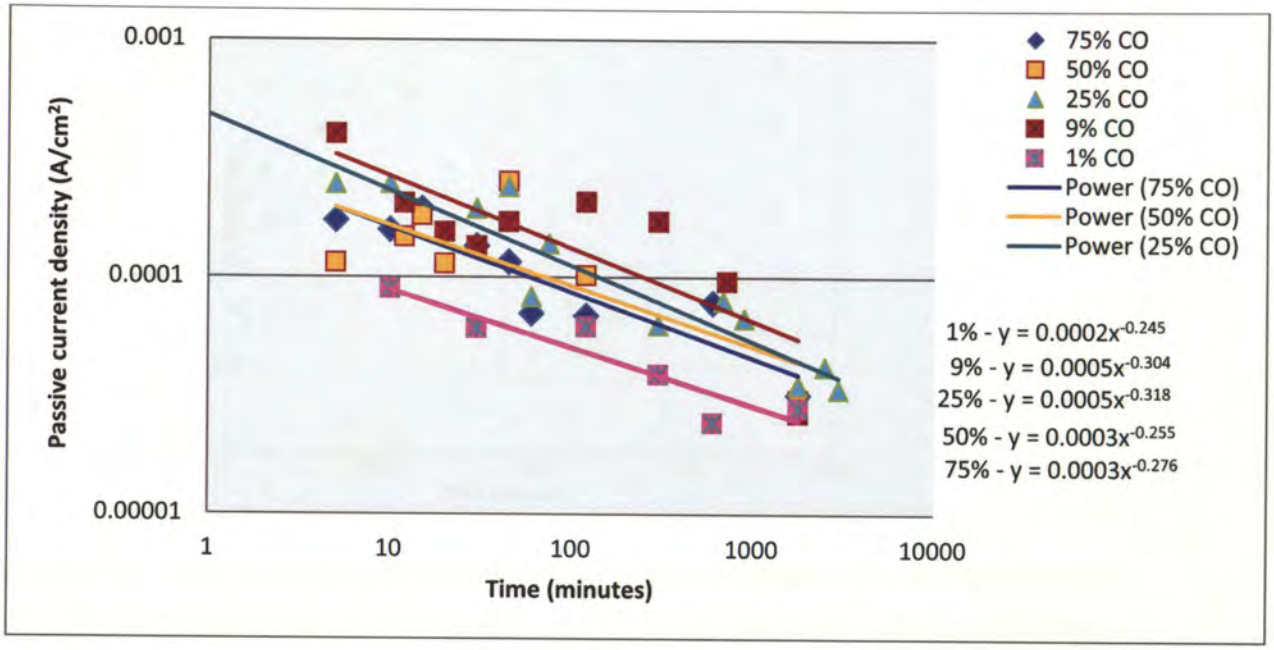

Figure 4-24. Change in the "transpassive" current density over time for various CO concentrations at 25°C.

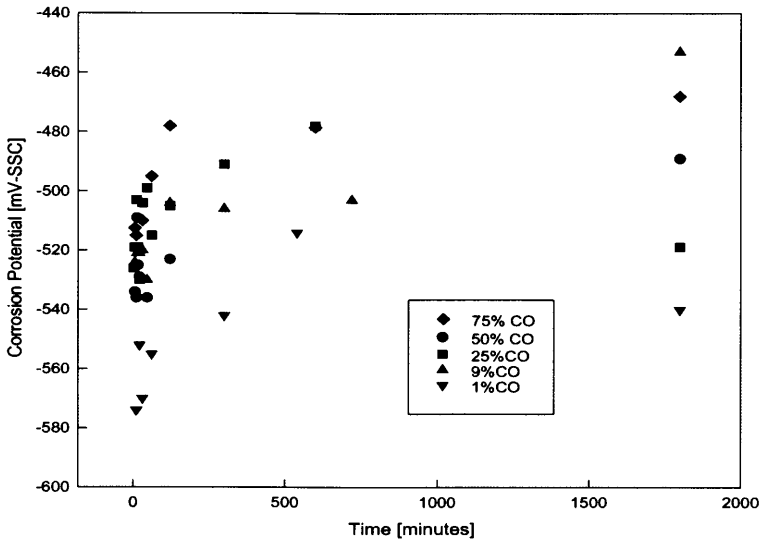

Figure 4-25. The corrosion potential measured from the polarisation curve against the holding time right before the test was started at 25°C and 0.1mV/s, for the various CO concentrations.

different CO concentrations, in most cases the corrosion potential first increased and then decreased slightly after very long exposures. One exception to this is 9% CO, where the corrosion potential increased even at long exposure times.

4.4 Discussion

The experimental procedure showed that the polarisation scan started in the cathodic region after an open circuit potential exposure of varying times. In some instances this cathodic potential was quite negative with regards to the corrosion potential and generally one would expect a stripping of the surface by such a procedure. However, in this instance this did not occur since the pseudo passivity was still seen in spite of this cathodic exposure on the samples. This is indicative of the tenacity of the passivated surface and nature of the adsorbed carbon monoxide.

It is known that cracking occurs readily, and only a small amount of CO gas is needed to induce cracking[15]. The reason for this phenomenon is explained in the form of the

polarisation characteristics. The polarisation characteristics for 1% CO after 5 minutes exposure does not indicate any passivation, but only a small change of gradient. However, after 30 hours exposure, the passive region shown is small and not very distinct. Therefore, given enough time the corrosion reaction will be able to passivate the areas where passivity was interrupted by dislocations breaking through.

At 9% CO, the potential range before the change in gradient was fairly large compared to the same range after 30 hours of exposure. This is due to the shift in the corrosion potential to higher values. The current density in the passive region falls as the time of exposure is increased, so that the difference of current density for a passivated, and a freshly exposed surface is notable and would sustain cracking.

At 25% CO, the presence of passivity was already more noticeable after 5 minutes than the 9% CO gas mixture, although the difference in the current density was not very large. After 30 hours of exposure to the medium, the passivity was easily noted and it is clear that both the anodic as well as the cathodic reactions were inhibited by the passivation of the CO on the steel surface. There was not a significant shift in the corrosion potential of the steel after 30 hours of exposure. The potential range of passivity increased compared to 1 and 9% CO.

In the 50 % CO gas mixture after 5 minutes exposure, the steel showed passivity over a similar potential range than for the 25 % CO after 30 hours of exposure. The current density in this region also showed a considerable drop. After 30 hours of exposure, the passive potential range decreased, but the decrease in the current density increased. The smaller potential range was due to a shift in the corrosion potential.

At 75% CO after 30 hours exposure, the formation of the polarisation characteristics was very similar to the 50% CO gas mixture, but the whole curve shifted about 25 mV to the right. This indicated an increase in the nobility of the steel.

The polarisation characteristics for the 100% CO and 100% CO_2 indicate that there was a synergistic effect between the gas mixture of carbon monoxide and carbon dioxide, because the formation of the curves differed from those of the gas mixtures. For the 100 % CO_2, the corrosion potential moved to the left of the range tested.

The corrosion potential for most of these gas mixtures tested showed that there is a general shift to more noble potentials. However, for very long exposure times the corrosion potential showed a drop for the lower CO concentrations, which seem. This is in accordance with work done by Heusler and Cartledge[68] who noted that corrosion potential first became more noble and then decreased again slowly.

The kinetics of the passivation reaction is highlighted at 25°C, as seen for 25% CO in Figure 4-15 after 1 minute, the passive region was already noticeable and the current density was lowered in the passive region, but as time increased at 45°C the passivity increased more. However, the whole curve is moved to higher current densities than at 25°C. The progression of the corrosion potential shows an increase with time. The rate of passivation increased and the extent of passivation increased at the higher temperature.

With increased carbon monoxide concentrations the repeatability of the curves increased, and the stability of the curves, less scatter was found. In addition the stability of the passive region was also increased. However, this stability was not enough to inhibit cracking.

4.5 Conclusions

1. At 1% carbon monoxide the passive region did form and over time it decreased in current density, but required long holding times before it reached similar proportions to the higher concentrations.
2. At 9% carbon monoxide the passive region seen after a significant holding time, became very similar to that found at higher concentrations.
3. The temperature increased the kinetics involved, so that the same degree of passivation was found at faster rates.
4. An increase in the total pressure improved the passivation rate and the extent of the passive region.
5. The corrosion potentials were shifted to more noble potentials with exposure times.

6. The passivation rates determined might show some correlation with the crack propagation rates as related to the passivation at the crack tip.

CHAPTER 5

5 THE INFLUENCE OF CYCLIC LOADING IN A SYSTEM THAT PROMOTES STRESS-CORROSION CRACKING

5.1 Introduction

Slow strain-rate test and potentiodynamic polarization test results, have indicated that cracking of steel in this system occurs over a wide range of CO partial pressures and temperatures, which include the typical operating conditions for coal gasification plants. This indicated high susceptibility to stress-corrosion has not been found in the plant, where cracking is indeed limited to certain areas of the plant. Cracks found in the plant also indicated that in many cases, cracks initiated but then stopped propagating. Estimates based cracking occurrences in plants reflect this with crack propagation rates ranging from $1x10^{-11}$ $m.s^{-1}$ to $2x10^{-10}$ $m.s^{-1}$, according to Heaver[40]. Obviously, the experimental data discussed above cannot be used as life predictions on the plant where existing plants already operate for many years without failures.

As mentioned in Chapter 2 Heaver[40] used DCB specimens to obtain K_{ISCC} values. Unfortunately, no crack propagation could be measured on these samples while on the U-bend test specimens that he investigated he found cracking. It is proposed that the different behaviour of the specimens can possibly be ascribed to differences in strain rates at the crack tips due to the very different configurations of these two types of samples. It has been shown by Parkins[43], amongst others, that if film rupture is the rate-determining step in SCC a minimum strain-rate is needed to initiate and sustain stress-corrosion cracking. The strain-rate resulting from a step change in the stress typically decayed exponentially, with the result that a strain-rate high enough to sustain stress-corrosion cracking would only exist for a limited time. Therefore, with no crack initiation/propagation it might be possible that the stress fluctuation at the crack tip might not be significant resulting in a strain-rate that would not maintain crack propagation and thus cracking would cease. In order to investigate this was to sustain

the crack tip strain-rate, and doing this by cyclic perturbations of the stress, which would typically be present in an operating industrial plant (these stress conditions will be investigated and discussed in Chapter 11 and are shown in **Error! Reference source not found.**). The stress ratio of such perturbations in the plant conditions would be irregular or regular depending on the operating conditions of the components.

In this part of the study the influence of such stress perturbations on the cracking behaviour of steel in a CO-CO_2-H_2O system was investigated. However, the final aim of this study is to establish K_{ISCC} values that could be used for life predictions in industrial plants.

5.2 Experimental Procedure

5.2.1 Experimental set-up

The same autoclave setup was used which were previously indicated for the slow strain-rate setup. However, the load was applied with a hydraulic rig with a high pressure discharge system to ensure that the faster loading rates could be achieved. The load was controlled with a REX P250 controller, which meant that the stress increased during the test as the cracks propagated.

5.2.2 Samples

Cyclic loading tests were performed on smooth round tensile test specimens of type A516 steel, with the same chemical composition as shown in Table 3-1.

The samples were machined in the same direction as the rolling direction and the gauge lengths of specimens were ground to a 600 grit finish and cleaned in acetone before testing.

The first samples which were evaluated were performed on the same as the tensile samples, as mentioned. However, the second batch of samples contained a crack initiation point. This was created by applying a capacitive discharge weld using a steel electrode in the centre of the gauge length. A very small discharge was applied which created a small weld pool in the centre of the sample. These weld pool were created

along the circumference in the centre of the sample. The idea was to create an area where cracks would initiate from.

The shape of the specimens were the same as those used for the slow strain-rate analysis, as shown in Figure 3-2.

5.2.3 Environmental conditions

The tests were performed in a pressurised CO-CO_2-H_2O environment at 45°C. The test solution was prepared by de-aerating distilled water with nitrogen gas for 45 minutes. The water was then pressurised in an autoclave with a 25% CO - 75% CO_2 gas mixture to a pressure of 800 kPa. Each specimen under test was electrically isolated from the autoclave to prevent galvanic interactions.

5.2.4 Loading conditions

The samples were exposed to static as well as cyclic loading. One test was performed at static conditions at a load 70% of the tensile strength. The cyclic loading was done at various minimum stresses and R-ratios as indicated in Table 5-1 and Figure 5-1.

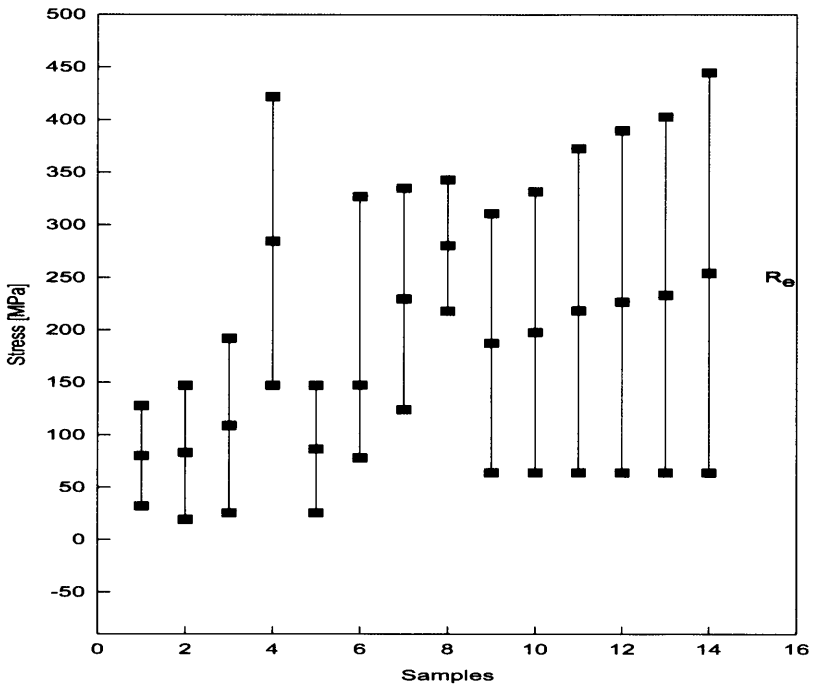

Figure 5-1. The maximum and minimum stresses used for testing A516 pressure vessel steel in CO-CO_2-H_2O environments.

The loading cycle is shown in Figure 5-2. The applied loading cycle used, was supposed to be as close as possible to a square wave but this was not always achievable at the higher frequencies, due to the limitations of the hydraulic test rig. At the higher frequencies the loading cycle more closely resembled the load cycle shown in Figure 5-2. But for most of the other frequencies, at much lower loading rates, the hydraulic rig followed the square wave very well. For specimens 10 to 16 though a square wave form was used with a loading time of about two seconds.

Table 5-1 Conditions of cyclic loading and static load tests for type A516 steel in CO-CO_2-H_2O.

Test No.	Frequency	t_{max}	t_{min}	R = $\sigma_{min}/\sigma_{max}$	σ_{max}	σ_{min}	Sample welded
	(Hz)	(s)	(s)		(MPa)	(MPa)	
1	0.0055	150	30	0.250	128	32	Yes
2	0.0055	150	30	0.130	147	19	Yes
3	0.0055	150	30	0.133	192	26	Yes
4	0.0055	150	30	0.348	422	147	No
5	0.00208	450	30	0.173	147	26	Yes
6	1.5	0.333	0.333	0.239	327	78	Yes
7	10	0.05	0.05	0.384	335	124	Yes
8	7.9	0.05	0.05	0.636	343	218	Yes
9	Tensile test in air				450	--	No
10	0.003	300	30	0.144	445	64	No
11	0.003	300	30	0.159	403	64	No
12	0.003	300	30	0.164	390	64	No
13	0.003	300	30	0.171	375	64	No
14	0.003	300	30	0.221	290	64	No
15	0.003	300	30	0.193	332	64	No
16	0.003	300	30	0.206	311	64	No

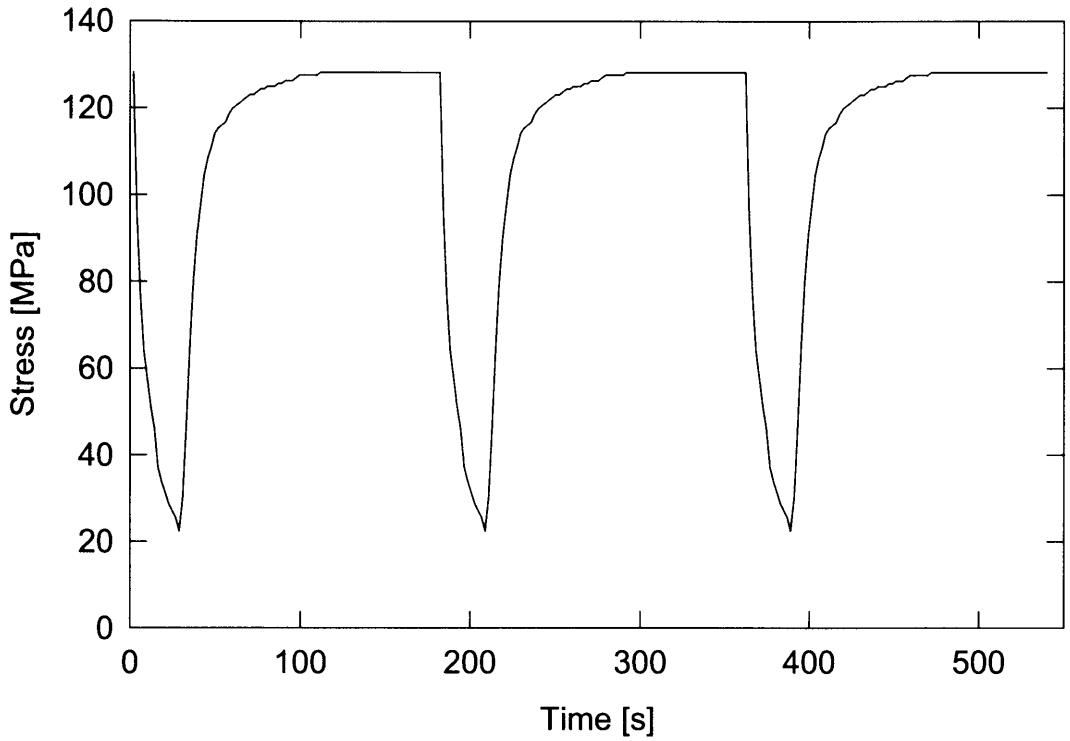

Figure 5-2. The cyclic load used for testing.

The higher maximum stress tests were performed at 0.003 Hz and most of tests with a maximum stress lower than the flow stress were done at 0.0056 Hz. The effect of frequency was evaluated at three other frequencies namely 0.00208, 1.5 and 10 Hz.

5.3 Results

5.3.1 Slow strain-rate test results

The stress-strain curve of a sample tested in a 25% CO 75% CO_2 water solution pressurised to 800 kPa at 45°C was compared with the same steel tested in air in Figure 5-3. The slow strain-rate results showed that the specimen exposed to

the environment was significantly embrittled. This result is included here to serve as a comparison with the cyclic stress results. The percentage elongation of the embrittled sample was 15% and the percentage reduction in area was 21% as compared to 29% and 70% respectively for the sample tested in air.

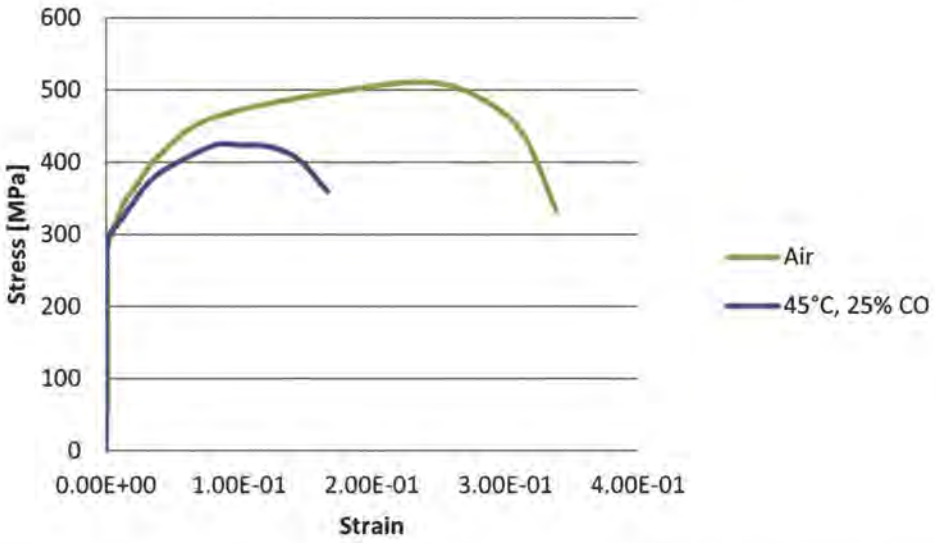

Figure 5-3. Slow strain-rate test result compared with a normal tensile test performed in air where no cracking is expected.

5.3.2 Cyclic test results

The severity of the cyclic tests is illustrated in Figure 5-4 with the insignificant reduction in area that was typical of most of the cyclic test samples. This specific sample showed only cracking in a concentrated position on the gauge length as a result of the cracking being concentrated in one position where the sample was spot welded.

Figure 5-4. An example of a sample after fracture as a result of the cyclic stress conditions, in a $CO/CO_2/H_2O$ environment after it failed with R = 0.348 and σ_{max} = 147.2.

The results of the cyclic tests are given in Table 5-2. Here it can be seen that some of the samples were spot welded, this contributed to the concentration of crack formation, which probably lead to crack coalescence, and increased growth. The final crack length was measured after the specimen failed and the fracture surface was studied to determine the extent of brittle cracks.

Table 5-2. Cyclic test results of A516 pressure vessel steel exposed to 25% CO – 75% CO_2 aqueous conditions at 45°C.

Test no	Frequency (Hz)	R = $\sigma_{min}/\sigma_{max}$	σ_{max} (MPa)	σ_{min} (MPa)	Spot welded	Time to failure (h)	No of cycles to failure	Final crack depth (mm)	Average crack propagation rate (mm/s)	Average crack propagation rate per cycle (mm/cycle)
No spot weld										
14	0.003	0.221	290	64	No	923	9963	1.95	$5.9x10^{-7}$	$2.0x10^{-4}$

Test no	Frequency (Hz)	R = $\sigma_{min}/\sigma_{max}$	σ_{max} (MPa)	σ_{min} (MPa)	Spot welded	Time to failure (h)	No of cycles to failure	Final crack depth (mm)	Average crack propagation rate (mm/s)	Average crack propagation rate per cycle (mm/cycle)
16	0.003	0.206	311	64	No	151	1631	1.75	$3.2x10^{-6}$	$1.1x10^{-3}$
15	0.003	0.193	332	64	No	51	549	1.00	$5.5x10^{-6}$	$1.8x10^{-3}$
13	0.003	0.171	375	64	No	65	702	1.15	$4.9x10^{-6}$	$1.6x10^{-3}$
12	0.003	0.164	390	64	No	85	922	0.75	$2.4x10^{-6}$	$8.1x10^{-4}$
11	0.003	0.159	403	64	No	108	1170	0.95	$2.4x10^{-6}$	$8.1x10^{-4}$
10	0.003	0.144	445	64	No	109	1189	0.10	$2.5x10^{-7}$	$8.4x10^{-5}$
Centre spot weld										
1	0.0055	0.250	128	32	Yes	499	11980	1.62	$9.0x10^{-7}$	$1.4x10^{-4}$
2	0.0055	0.130	147	19	Yes	289	5776	1.65	$1.6x10^{-6}$	$2.9x10^{-4}$
3	0.0055	0.133	192	26	Yes	341	6824	1.60	$1.3x10^{-6}$	$2.3x10^{-4}$
4	0.0055	0.348	422	147	No	618	12360		0	0
Lower frequency with a spot weld										
5	0.00208	0.173	147	26	Yes	681	4733	2.15	$8.8x10^{-7}$	$4.5x10^{-4}$
High frequency										
6	1.5	0.239	327	78	Yes	4	19548	1.40	$1.1x10^{-4}$	$7.2x10^{-5}$
7	10	0.384	335	124	Yes	4	126360	1.60	$1.3x10^{-4}$	$1.3x10^{-5}$
8	7.9	0.636	343	218	Yes	286	810680		0	0
Constant load										

Test no	Frequency (Hz)	R = $\sigma_{min}/\sigma_{max}$	σ_{max} (MPa)	σ_{min} (MPa)	Spot welded	Time to failure (h)	No of cycles to failure	Final crack depth (mm)	Average crack propagation rate (mm/s)	Average crack propagation rate per cycle (mm/cycle)
9	--	--	450	--	No	6888	--	0.24	9.7×10^{-9}	--

The test at static load of 70 % of the flow stress exposed to the same environment visually showed no cracking after 6 888 hours; the specimen was sectioned and etched to investigate for cracking. A section through the gauge length of this sample (Figure 5-5) showed a maximum crack depth of only 0.24 mm. This meant that the crack propagation rate was 9.7×10^{-9} $mm.s^{-1}$, if no incubation period was taken for crack initiation. An indication of the number of cracks that formed on the surface after constant loading is seen in the micrograph of the sectioned specimen in Figure 5-5. Figure 5-6 shows a fine branching crack, as well as a corroded crack approximately 0.15 mm apart, with fine cracks in the center of the micrograph.

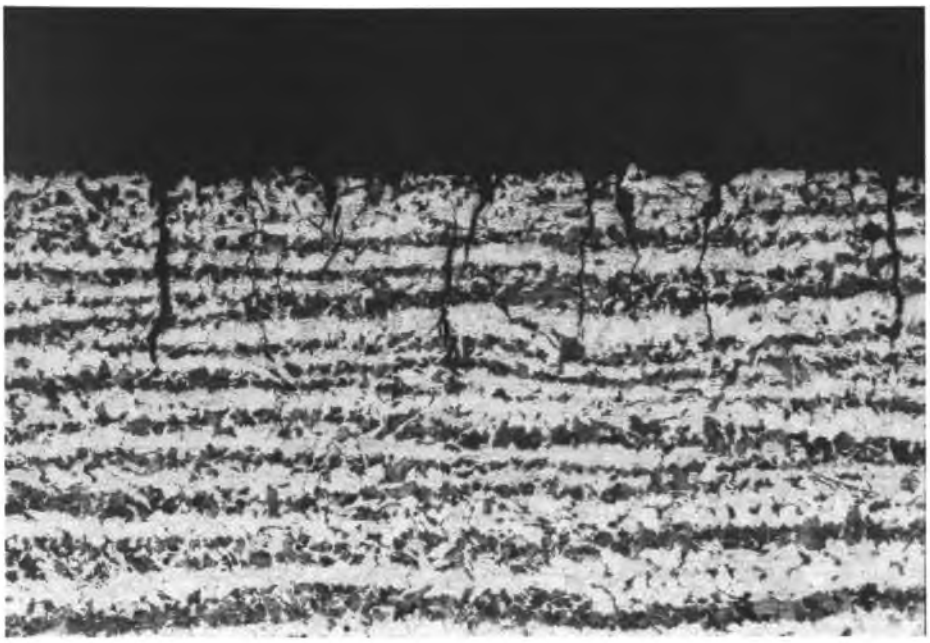

Figure 5-5. The sample exposed to a constant load after 6 888 hours at 25% CO, 45°C and 800 kPa.

Figure 5-6. Cracks found on a sample that was exposed to cyclic stresses, exposed to a 25% CO gas mixture at 800 kPa and 45°C..

A cross sectional micrograph in the region of cracking showed the fine cracks that were found on these samples.

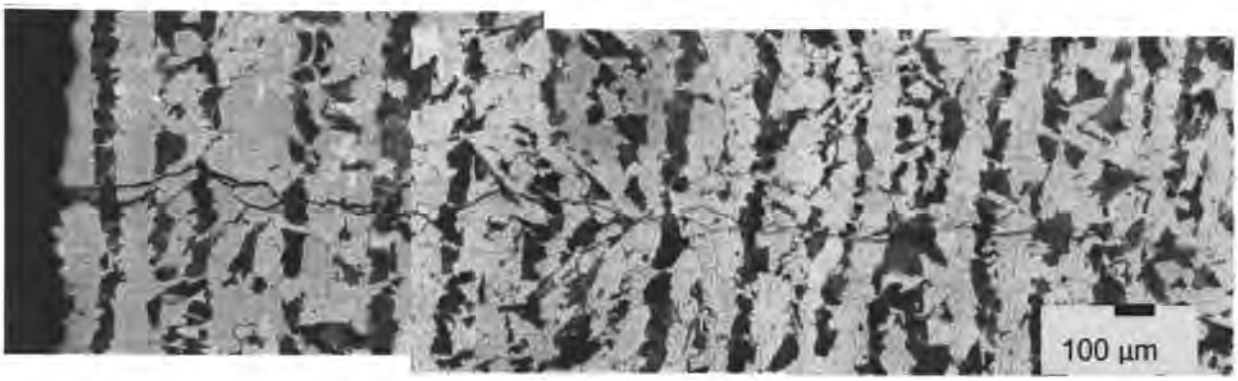

Figure 5-7. A micrograph indicating a very fine crack that formed during the cyclic stressing at the lowest maximum stress, exposed to a 25% CO gas mixture at 800 kPa and 45°C.

The extent of the fine crack shown in Figure 5-7 indicates how the crack tip was kept active by the cyclic stresses while the crack walls are kept passive with very little corrosion.

5.3.3 Cracking rate

5.3.3.1 Smooth specimens

Most of the tests on smooth specimens without a spot weld were done at high tensile stresses in order to see if the steel would be susceptible to cracking under cyclic loading conditions. This does not apply directly to practical applications, but does give a better understanding of the system of cracking. The time to crack propagation is shown in Figure 5-11 and it was obtained by measuring the displacement during the test and using the longest crack as reference point. All the samples with a maximum stress of more than the flow stress of the steel had a long incubation period, or a time where seemingly little or no cracking occurred. However, the second stage of deformation occurred rapidly. The total crack length measured at the end of the test as seen in Table 5-2 was not high, and increased with the lowering of the maximum

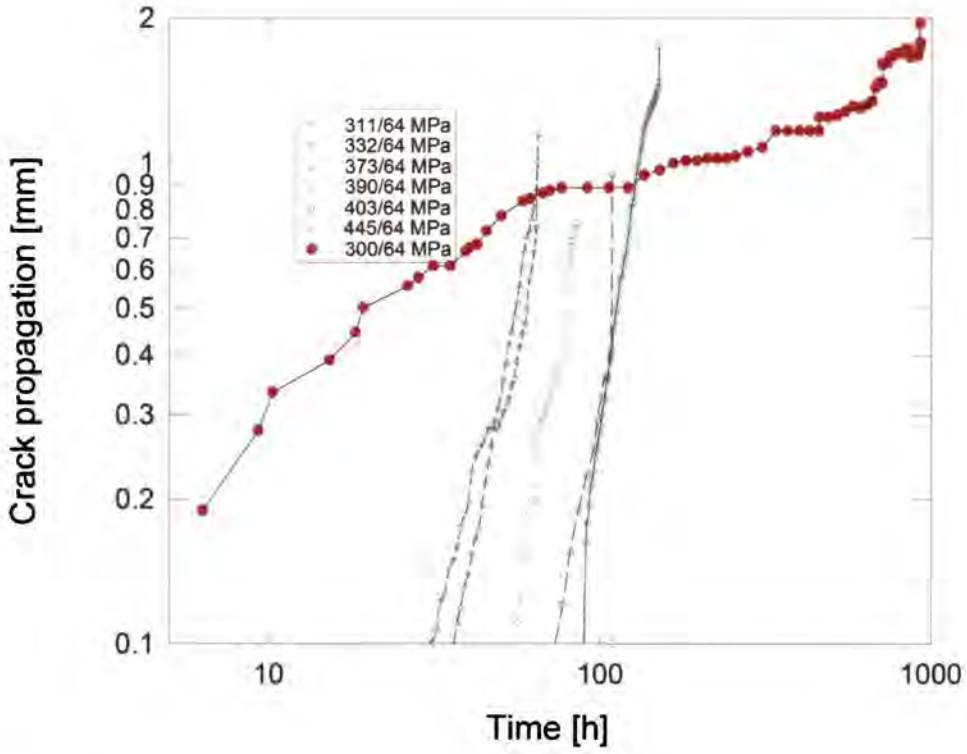

Figure 5-8. Measured displacement with time for cyclic loaded specimens.

stress, as it is expected due to the overloading of the remaining load bearing area. The test done below the yield strength (curve in red) showed a generally constant crack propagation rate for most of the test period, but the growth was somewhat discontinuous, occurring in growth spurts. The time to failure for this sample tested below the yield point, was also nearly an order of magnitude higher than for the other samples, and crack propagation rate was the lowest for this sample.

The elongation of the samples were measured during the test, and the measured displacement for the samples exposed to higher stress levels are shown in Figure 5-9.

More tests were done in the same environment with cyclic loading but these were not spot welded and the loading wave form was more of a square wave. The results were also summarised in Table 5-2, showing the higher maximum load that was used in the

former experiments. These results differ from the spot welded specimens in that the crack initiation took longer, but when propagation set in it was at a much faster rate than for the spot welded tests.

The times to failure of the non-spot-welded specimens were somewhat shorter than for the lower maximum stress specimens tested with the spot weld. Figure 5-9 shows the reduction in area for the low frequency tested specimens. A higher maximum stress level decreased the stress-corrosion cracking susceptibility.

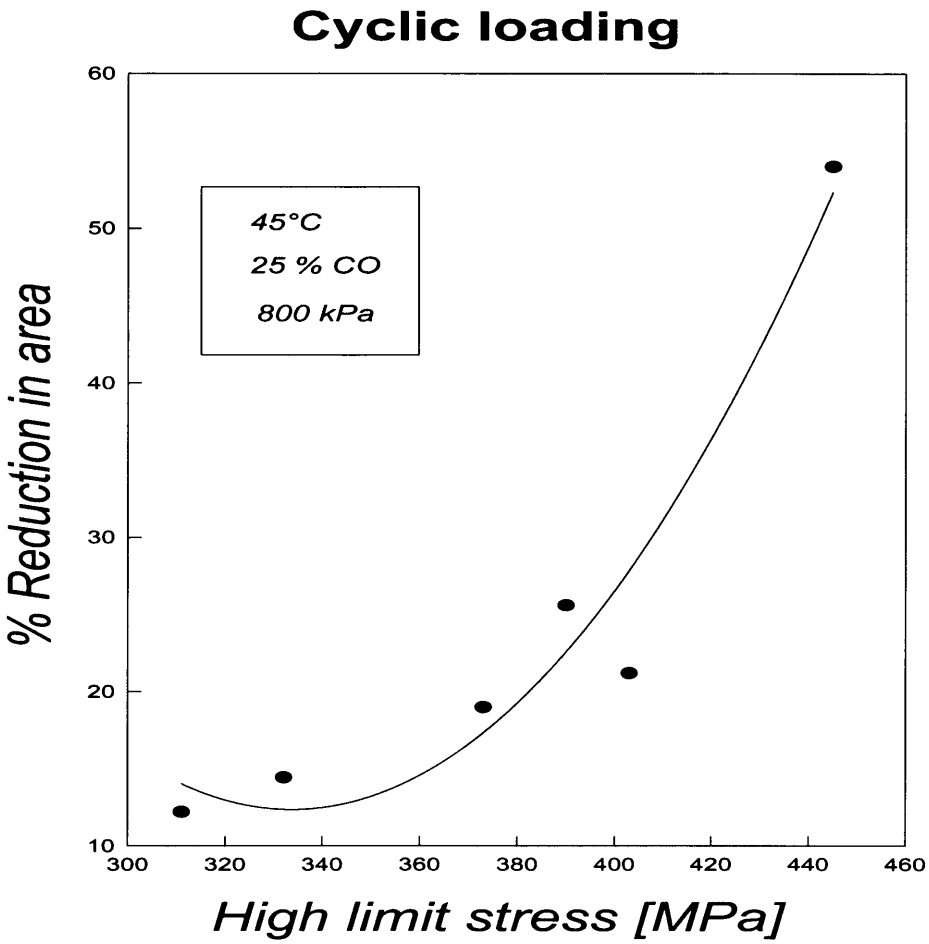

Figure 5-9. The influence of the high limit stress on the % reduction in area.

These tests were performed with more of a square wave than the other tests as mentioned before.

The higher maximum stresses may cause crack blunting that could have decreased the crack propagation rate. The crack tip was deformed to such an extent that the strain-rate was too high to sustain crack growth.

5.3.3.2 Spot welded specimens

All of the results of the spot-welded specimens, showed less than 10% reduction in area, making it very difficult to measure the reduction in area accurately. The tests performed with a maximum stress of below the yield strength generally showed a constant crack propagation rate for most of the test period, but the growth was somewhat discontinuous, occurring in growth spurts. The times to failure for these spot welded samples, tested below the yield point, were also nearly an order of magnitude higher than for the non-spot welded samples and crack propagation rates were the highest for these samples.

The micrograph in Figure 5-10, shows clearly the advantages of introducing a spot weld in order to have a more concentrated point of crack initiation. The time to failure for the smooth surface sample with the low maximum stress was greatly reduced with the introduction of the spot weld. It seems that a more continuous propagation rate was achieved when a sample was spot welded. This might be due to the fact that cracks propagated on the same level from around the circumference, because the spot welded region was circular. A number of small cracks initiated and then coalesced to increase the crack growth, but with a slow initiation process, the crack growth was slowed down, because little crack coalescence occurs. When cracks can initiate anywhere along the gauge length, the chances of having cracks on the same plane are reduced, which means that a crack must grow longer before an overload situation occurs.

The crack propagation in terms of the measured average displacement as a function of time for spot welded cyclically loaded specimens are shown in Figure 5-11 together with a specimen that was not spot welded. Therefore, with the spot weld the

repeatability of the test was much better. These three specimens were spot welded in the circumference of the centre of the gauge length. This seemed to have decreased the incubation period necessary for crack initiation. The crack growth occurred at a logarithmic rate. At the lower stress intensities, the crack growth rate decreased. Micrographic evaluation of the spot welded samples showed clearly the advantages of introducing a spot weld in order to establish a region of easy crack initiation. One sample was not spot-welded, and even at a high stress level, showed a low crack propagation rate. It seems that a more continuous crack propagation rate was achieved when a spot weld was introduced. As discussed above, when cracks initiated anywhere along the gauge length, the probability of a higher concentration of cracks around the same plane was lowered.

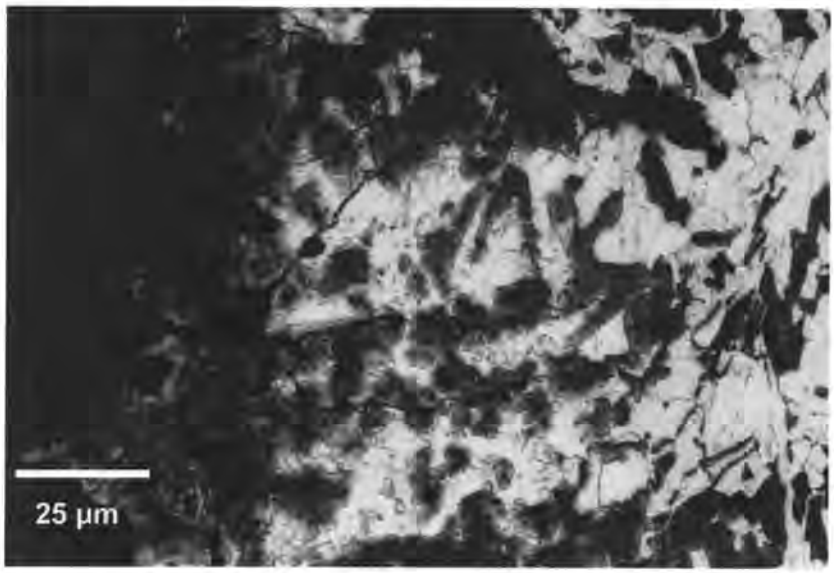

Figure 5-10. A cross sectional view of one of the spot-welded region after it was exposed to the cyclic stresses and the environment. Numerous cracks originated from this region.

Many fine cracks were visible, indicating the ease of crack initiation. These cracks did not form in a random direction, but formed perpendicular to the loading direction. On the spot welded region the more brittle phase - martensite - was seen after etching the specimen. Therefore, two features existed together at a spot welded point to initiate cracks under stress, the brittle phase as well as residual stresses that forms as the

molten pool solidifies. A slow strain-rate test was done on a specimen that was spot welded and it also fractured at the spot weld. Therefore, when the right conditions exist for crack propagation, whether cyclic or non-cyclic, the crack does initiate and propagates from this point.

The spot-welded samples were evaluated at lower maximum stress levels, below the yield point. The specimens shown in Figure 5-11 displayed a crack propagation rate with a constant rate for most of the test on a logarithmic scale.

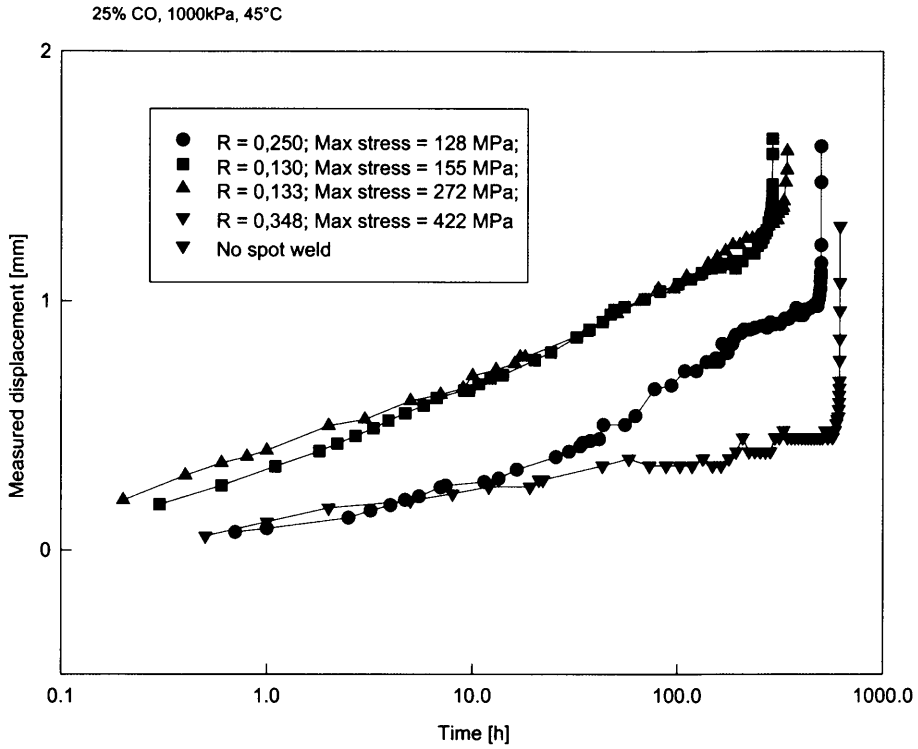

Figure 5-11. Four cyclic loading test results,25% CO, 1000 kPa and 45°C.

This crack growth can be described as:

$a = k\ ln\ (t) + l$.....5-1

$da/dt = k/t$.....5-2

Table 5-3 gives the parameters, *k* and *l*, for the four specimens shown in Figure 5-11:

Table 5-3. Parameters k and l for crack propagation.

Frequency Hz	R	σ_{max} MPa	*k* mm/h	*l* mm	Spot welded
0.00556	0.250	128	0.333	-0.375	Yes
0.00556	0.130	147	0.169	0.296	Yes
0.00556	0.133	192	0.158	0.375	Yes
0.00208	0.173	147	0.532	0.512	Yes
0.00556	0.348	422	0.058	0.100	No

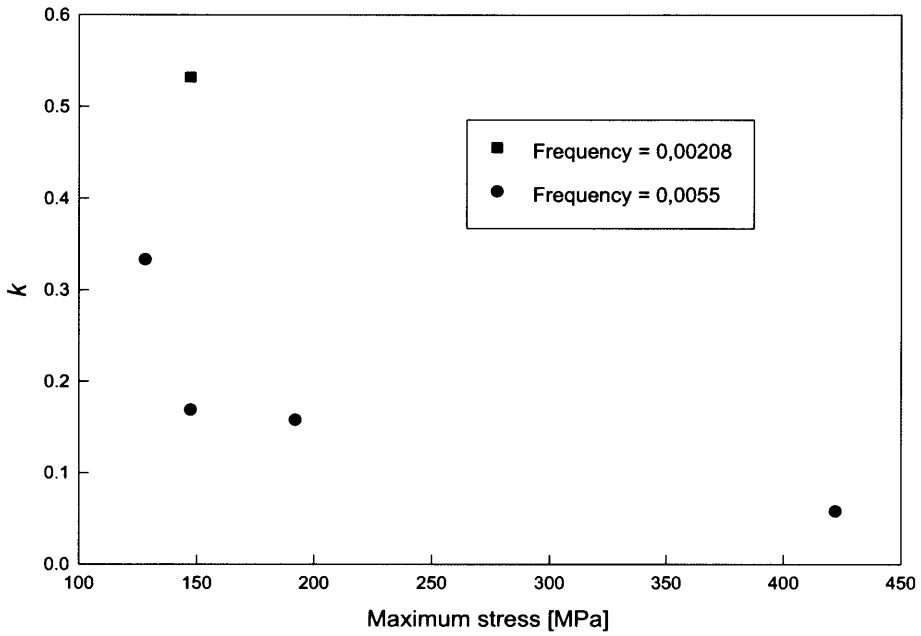

Figure 5-12. Parameter k plotted as a function of the maximum load.

When *k* is plotted as a function of the maximum stress, as seen in Figure 5-12, it increased with decreasing stress. It also increased as the frequency was lowered, while the other conditions stayed about the same. More information was needed to determine the threshold stress for cracking. A slow strain-rate test was done on a specimen with decreasing diameters, decreasing in steps of 0,5 mm from 6,0 mm to 4,0 mm. On each of these levels, the specimen was spot welded for easy crack initiation. Cracking did not occur at the 5,5 mm diameter and the maximum load applied to the sample was 315 kg, giving a stress level of more or less 120 MPa. However, more work needs to be done to establish this more accurately for cyclic loading.

The result of the test done at low frequency is shown in Figure 5-13. This specimen was also spot welded to decrease the incubation period. The crack growth rate decreased compared to similar conditions for higher frequencies.

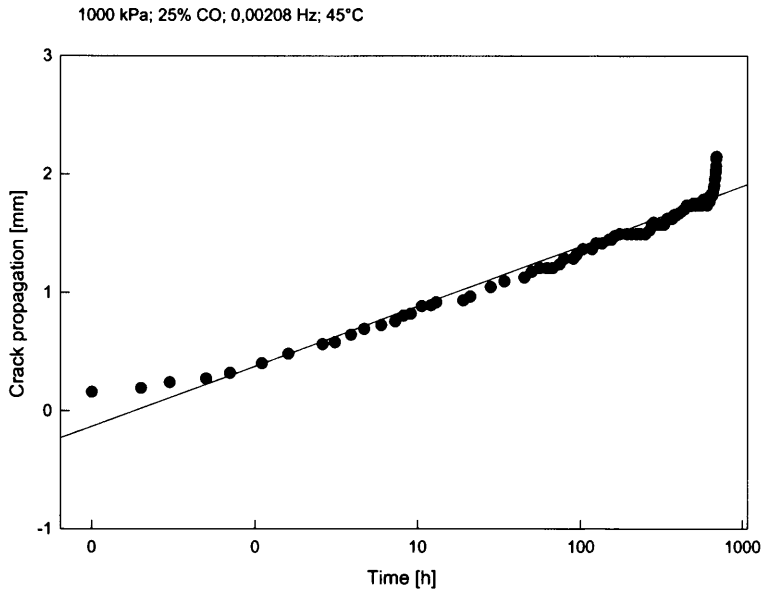

Figure 5-13. A low frequency, 0.00208 Hz, test of steel in water with 25%CO and 75% CO_2 at 1000 kPa.

When all of these results are combined in a S-N curve as in Figure 5-14, the difference is seen for spot welded and smooth specimens in that the latter had a much higher threshold. This indicates the effect of initiation time for cracking as it is known to play an important role in the fatigue life of a sample. The high frequency samples seems to lose the effect of the environment.

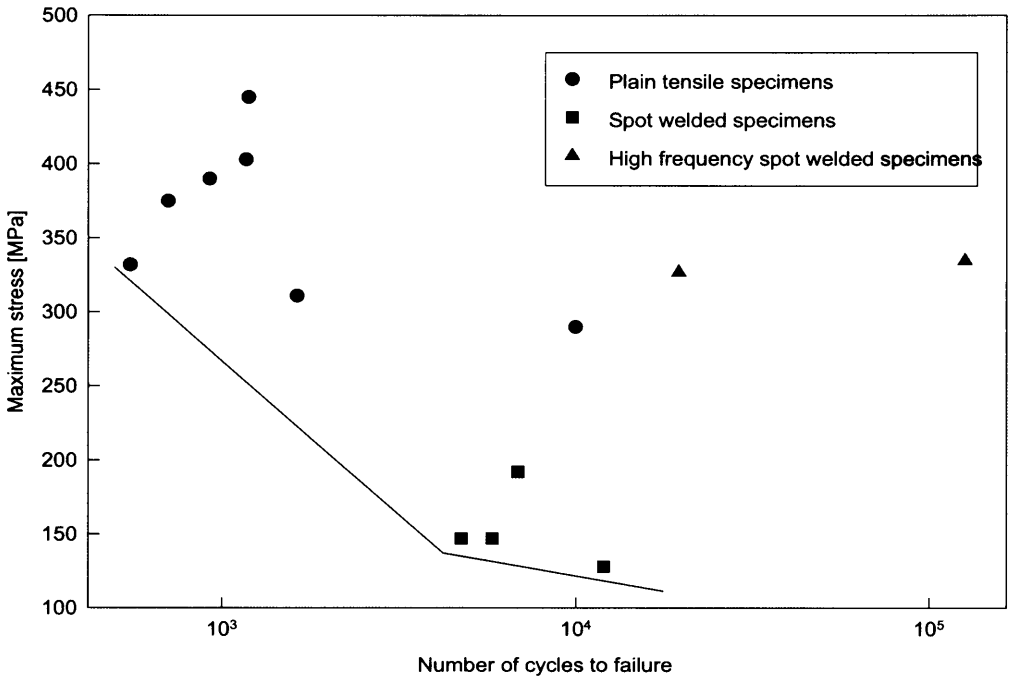

Figure 5-14. S-N curve for 25% CO at 45°C.

The lower frequency tests showed that the cracking process is more time dependent and showed a greater degree of embrittlement.

5.3.4 Fractography

Figure 5-15 shows a typical example of a spot welded specimen that failed during cyclic loading. The cracking was generally transgranular, in nature as shown in Figure 5-15 and 5-16. In Figure 5-15 pearlite colonies are seen on the crack surface after an etching effect of the medium. The micrograph in Figure 5-16 showed some striation marks, but this was the only specimen where this was observed. The striation spacing on the high magnification view of the fracture surface (Figure 5-16), was close to 1

micron in size which corresponds with the measured data. Scanning electron fracture graphs of the high frequency tested specimens showed a different brittle fracture than for the lower frequencies, indicating a crack mechanism that was not related to corrosion induced embrittlement, because of its more ductile nature.

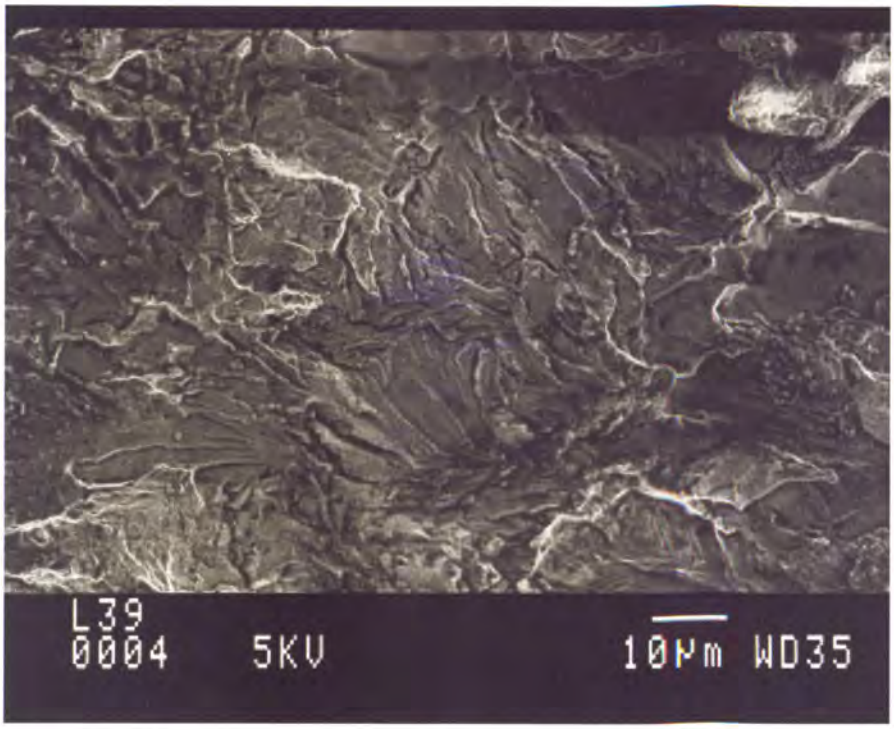

Figure 5-15. Fracture surface of a sample after it was exposed to a 25% CO gas mixture at 800 kPa and 45°C, with a cyclic maximum stress of 403 MPa at a frequency of 0.003 Hz.

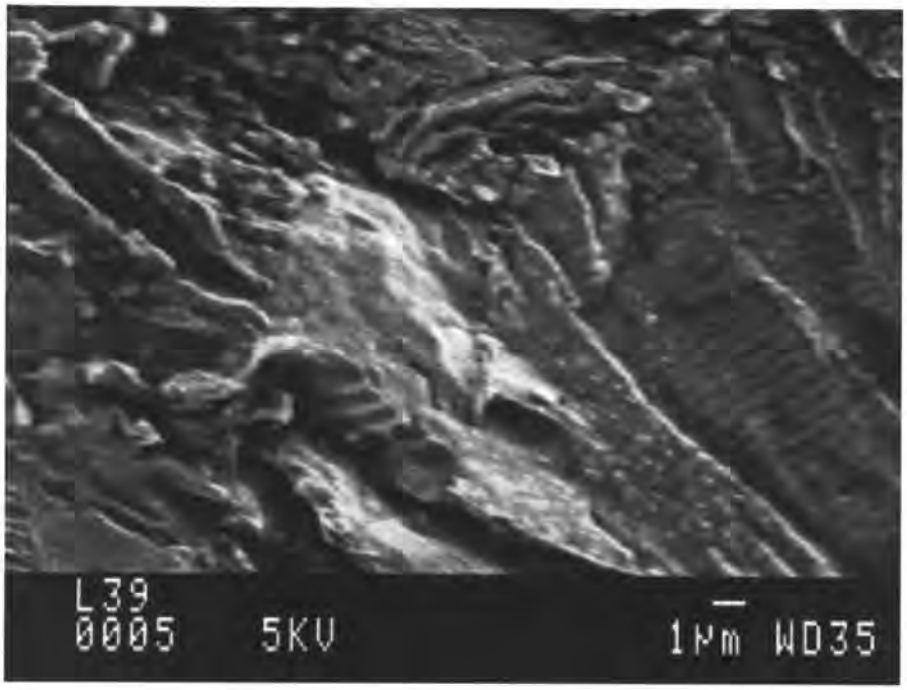

Figure 5-16. Fracture surface of a sample after it was exposed to a 25% CO gas mixture at 800 kPa and 45°C, with a cyclic maximum stress of 403 MPa at a frequency of 0.003 Hz.

The effect of the spot weld is illustrated by the micrograph in Figure 5-17. Here, a number of small cracks ran through the spot-welded area, and indicated the relative ease of crack initiation at these points. This ease of initiation was attributed to the high residual stresses present in the region where steel formed a molten pool. A slow strain-rate test was done with a specimen that was spot welded and it also fractured at the place where it was spot welded. Therefore, when the right conditions exist for crack propagation, whether cyclic or non-cyclic, the crack initiates there and propagates from this point. All of these cracks did not form in any random direction, but instead formed perpendicular to the loading direction.

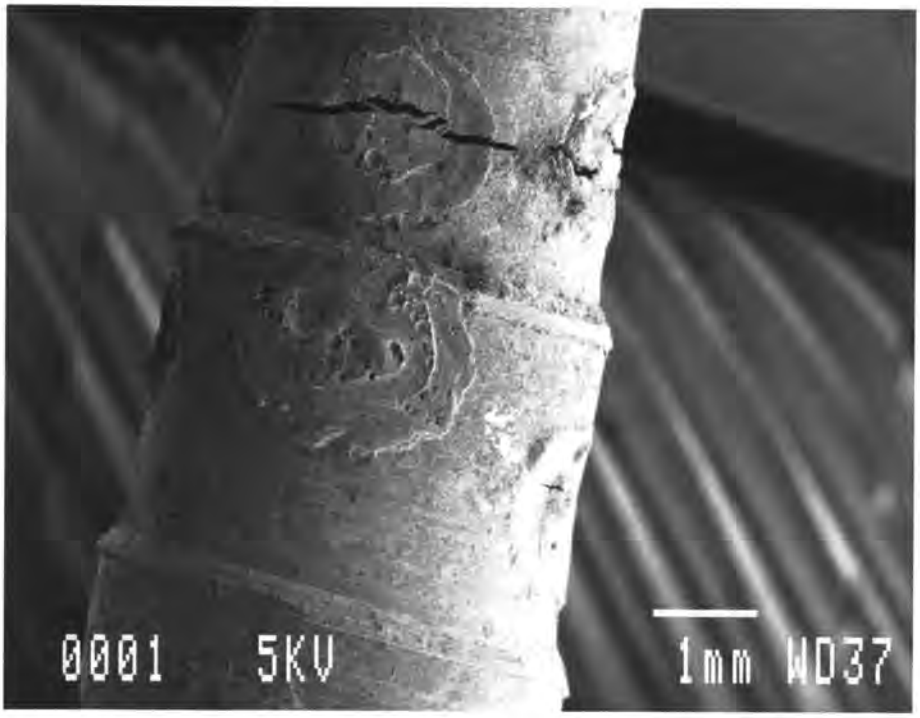

Figure 5-17. A cracked, spot-welded sample after it was exposed to a CO-CO_2-H_2O environment.

5.4 Discussion

5.4.1 Cyclic loading effect

The cyclic loading results showed a cause for the great increase in severity of cracking in the steel when stress fluctuations occur. The constant load test showed that crack initiation over an extended period is not a problem, but is a timeous process. The slow crack propagation of the specimen under the static condition indicated a situation of crack inhibition. However, the initiation process was easy as many small cracks were found, but how long the initiation process took was not established. For initiation to occur, the adsorbed passivating layer that forms on the surface of the steel needs to be broken by the strain of the metal surface underneath. This part of the stress-

corrosion cracking process depends on the time dependency of the stress condition in the steel, as well as the corrosion processes involved. This time dependency is demonstrated by the lower frequency test, where the number of cycles increased with a lower frequency. Shallow cracks and pits, or deeper and finer cracks form according to the aggressiveness of the environment, when the adsorbed passivating layer is not stable pits would form, but as passivity increases, cracks are more favourable to form. In the same way the rate of film breakage can influence crack growth and formation, as fresh steel matrix is exposed. The process of cracking is therefore rate-dependent and the loading rate has to correspond to the corrosion process rates, to produce the optimum conditions for fine cracks.

The tests at the higher frequencies required more cycles for failure, but the time span was shortened. At 10 Hz, it seemed that the cracking sensitivity decreased, because the corrosion rate of the cracking process could not keep up with the load frequency.

Table 5-3 shows that the indirect measured crack propagation rate (based on number of cycles to failure) of the lower frequency test is considerably higher for basically the same conditions. This underlines the importance of frequency in these tests. Although the time to failure increased for the lower frequency the number of cycles decreased. Thus, evaluation of the severity of cracking is difficult in terms of time to failure or number of cycles to failure, when different frequencies are tested. The similar value in terms of the cycles shows that the cracking process is dependent on the cyclic component of the test. It seems that crack growth was not enhanced by longer times at the maximum stress, but rather by the event of switching between the maximum and minimum stress.

5.4.2 Frequency dependency

Frequency does influence the response of the steel to the environment and hence cracking. Crack propagation is produced by the stress-corrosion cracking and corrosion fatigue. Wei[69] proposed a superposition model in which the corrosion fatigue crack propagation rate was equated with the sum of the stress-corrosion crack rate and the inert fatigue crack growth as shown in Equations 5-c and 5-d:

$(da/dt)/_{Total} = (da/dt)/_{SCC} + (da/dt)/_{CF}$.....5-3

$(da/dt)/_{CF} = (da/dN).(dN/dt) = f.(da/dN)$.....5-4

The crack propagation was influenced by primarily one of the factors or an overlapping effect. A weakness of the model is the lack of explanation for synergistic effects.

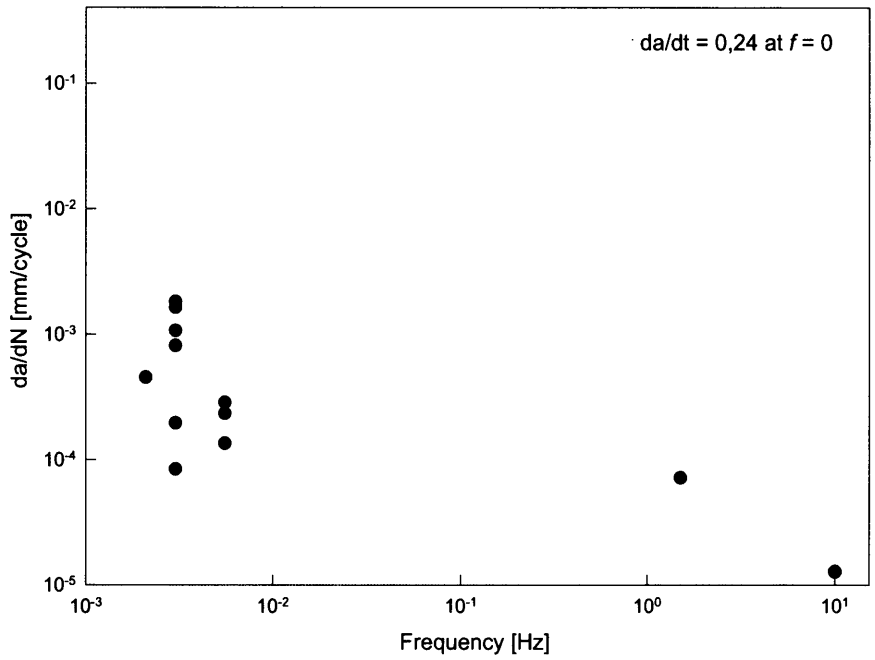

Figure 5-18. Frequency dependency of cracking, with cracking rate per cycle plotted as a function of the frequency.

When the frequency is very low, the cracking rate was predominately determined by the stress-corrosion cracking influence and the rate was limited by film rupture. At high frequencies, the corrosion rate was limited by chemical transport processes. The crack growth rate plotted as a function of the frequency gives an indication of the contribution of either SCC or corrosion fatigue. Figure 5-18 shows these data,

indicating the influence of the frequency given. On the high frequency side, the amount of cracking per cycle is lowest, and for the low cycles, the crack propagation per cycle increases. However, between the two extremes, the crack propagation varies only within an order of magnitude. The influence of frequency is important, because it is possible to determine whether cracking occurs through stress-corrosion or whether it is more of a corrosion fatigue phenomenon. The results of the low frequency test indicate that the cracking observed is more related to the stress-corrosion side of the spectrum. The similarity between the fractography of the slow strain-rate tests and the transgranular nature of the cracks seen on the fracture surface is a further confirmation of the greater presence of stress-corrosion. However, the result of the constant stress test makes it clear that some cyclic variation in the stress is necessary for faster or relevant crack propagation. The presence of striations on the fracture surface indicates the influence of corrosion fatigue type mechanisms in the cracking model.

It is important to note the difference between the tests done with the square wave form and those with the more sinusoidal form as shown in Figure 5-2. The tests show two different results for similar conditions, with the only large difference being the loading conditions. Therefore, the strain rate is an important parameter that needs more attention.

The plant tests performed that are shown in **Error! Reference source not found.**, and these were performed by MegChem in order to establish typical pipeline stresses that can be expected during normal operation. From their results it was clear that the high frequency loading events occurred at low stresses. However, there were instances of higher stresses, in the region of 12 MPa, and these occurred at significantly lower frequencies, only one or two instances over a period of 480 s. This type of frequency relates more to the frequencies that caused such severe sensitivity to cracking, that were considered in this chapter. However, the stress levels considered here were considerably higher than those found in the plant measurements. Possibly with the introduction of residual stresses during welding the stress conditions might be significantly different.

The effect of existing cracks and defects in a structure will affect the stress intensity, especially when these cracks start to propagate, and the next chapter will consider the influence of stress intensity on the crack propagation rates, as well as the rate of stress intensity change.

5.5 Conclusions

1. Stress-corrosion cracking was enhanced by cyclic loading, whereas cracking was not significant for the static load test.
2. Lower maximum stress enhanced crack propagation, although the crack propagation rate decreased, but the final rupture area was less.
3. Crack initiation was a large part of the time to failure and crack coalescence probably contributed to the faster crack propagation.
4. The frequency did influence crack propagation rate, at the higher frequencies the crack propagation was no longer under predominantly corrosion control.
5. At higher stresses crack propagation was more dependent upon the event of a stress discontinuation than time.
6. Crack propagation seems to be dependent upon the strain-rate.

Chapter 6

6 FRACTURE MECHANICS OF STEEL UNDER VARIOUS CONDITIONS OF CARBON MONOXIDE AND CARBON DIOXIDE IN WATER

6.1 Introduction

The fracture mechanics of a system such as steel exposed to CO-CO_2-H_2O can be of considerable benefit when considering the design of pressure vessels and pipelines, as well as the evaluation of 'fit-for-service' scenarios. In addition to this fracture mechanics gives more insight into the relationship between the crack propagation and the stress applied in the form of stress intensity. Important results are the K_{ISCC} and the constant crack propagation rate at higher stress intensities.

In this chapter the effect of carbon monoxide concentration on crack propagation rates will be investigated. The concentrations that will be considered are: 50%, 9% and 1% CO with CO_2 making up the balance. These gas concentrations were chosen for the following reasons; firstly, to determine the sensitivity to cracking of the steel to the nature of the environment in carbon monoxide rich concentrations and verifying the stress intensity threshold for stress-corrosion cracking. This threshold is important when considering post weld heat treatments that are applied to structures in order to lower residual stress conditions induced during welding and forming. Secondly, the effect of significantly lowering the carbon monoxide concentration to 9% to determine the influence of the temperature and the dissolved oxygen concentration at this gas composition, and to compare it with the carbon monoxide-rich gas mixtures. The emphasis of investigating these parameters was to determine if the mechanism of cracking of steel is similar to leaner carbon monoxide concentrations. Thirdly then, relating the results to carbon monoxide concentration at a relatively low level of 1% to the higher levels. It has been shown by other researchers[5,7] that the partial pressure necessary for the stress corrosion cracking to occur is very low. Experiments were performed to establish the amount of cracking at a low carbon monoxide concentration of 1% at 25 and 45°C. The influence of the dissolved oxygen concentration of the

water at these low CO concentrations can play a role in the crack propagation rate. Tests at this low CO concentration are important in order to evaluate the role of carbon monoxide during the cracking process.

In addition to the effect of CO concentration the influence of an externally applied potential was investigated. Brown et al.[5] did an extensive work on the influence of applied external electrochemical potential on the stress corrosion cracking with a total pressure of 7,9 bar and carbon monoxide with a partial pressure of 20 lb/in^2. They found cracking to occur within a potential band between -575 and -450 mV SCE, and cracking peaked at a value of -475 mV for all the gas mixtures that were tested. In order to establish crack propagation rates and stress intensity thresholds for cracking tests were performed to establish the fracture mechanical details when the samples were polarised. The samples were cathodically as well as anodically polarised in order to correlate it also with the polarisation data so that polarisation characteristics and crack growth rates can be compared.

This leads to the influence of the loading or straining rate and its interaction with the passivation reaction driven by carbon monoxide adsorption. Tests done on smooth samples showed that cracking occurred more readily when the load was not constant and cracking did occur during constant loading but the crack propagation rate was very low. The load applied to these samples was cyclic at low frequencies. Cyclic loading at the low frequency caused a high creep rate every time the sample was loaded and this caused a critical strain rate that produced a high crack propagation rate. The relationship of the loading rate and the crack propagation rate was not established because the crack propagation rate was not measured. With DCB specimens the crack length can be measure as the crack grows. Therefore, the influence of loading rate on the crack propagation could be determined.

The slow strain-rate tests also indicated that the crack propagation rate is influenced by the strain-rate. As shown earlier a minimum strain-rate exists for maximum stress corrosion cracking. Therefore a strain-rate exists which favours the processes that enhances cracking.

6.2 Experimental procedure

6.2.1 Water preparation

A low dissolved oxygen concentration was used by bubbling nitrogen through the water in the pressure vessel for at least 1 hour before the tests were started. In the case of high dissolved oxygen concentrations air was bubbled through the container until the appropriate level of 8 ppm was reached, this was confirmed with a dissolved oxygen meter. The water was then pressurised with the appropriate CO-CO_2 gas mixture. A temperature of 45°C or 25°C was used for the tests and the temperature was controlled by external heating of the autoclave in which the tests were done.

6.2.2 Specimen configuration and clamping

The experimental setup used where the double cantilever beam specimens were tested in an autoclave is shown in Figure 6-1.

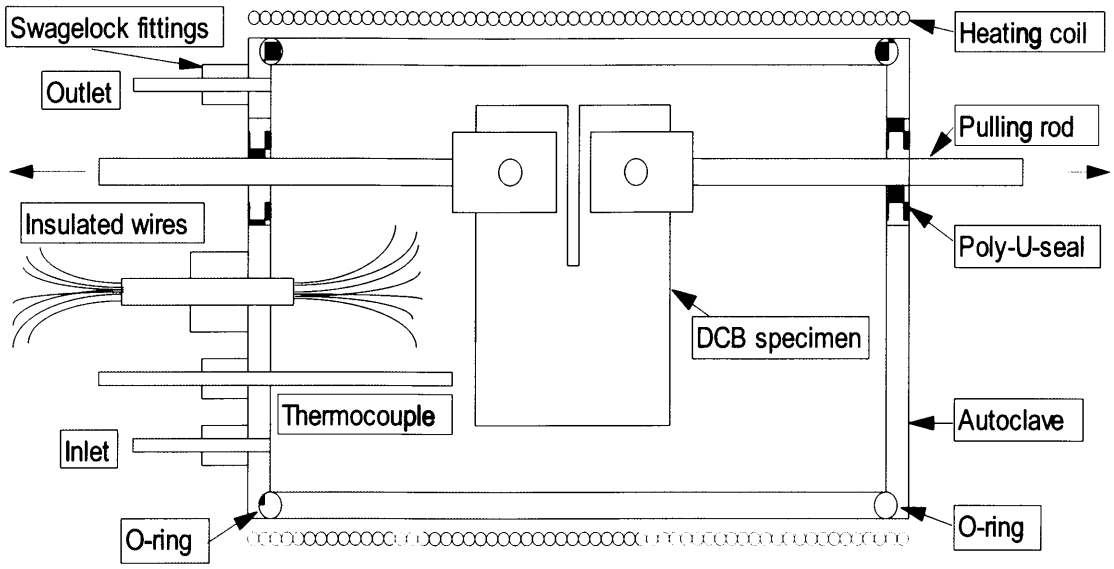

Figure 6-1. A schematic drawing of the autoclave in which experiments were performed.

The temperature of the test autoclave was controlled by using a heating element that was placed around the autoclave. This heating element was folded back on itself in order to avoid the generation of an electro-magnetic field. This was important because

the induced field influenced the crack depth measurements. When this was not done realistic crack measurements could not be made, as switching by the controller of the heating element caused the values to fluctuate.

The crack propagation was measured by the use of a potential drop method. This was done by maintaining a 1A current through the sample and measuring the potential drop on the top of the sample (as shown in Figure 6-2) and at the origin of the crack. The ratio of these two measurements was taken as an indication of crack length. This was calibrated to give the crack depth before the test was done.

The dimensions of the sample were below that normally required for a DCB specimen, but with the increased brittle behaviour caused by the nature of the environment the specimen configuration conformed to linear elastic fracture mechanics.

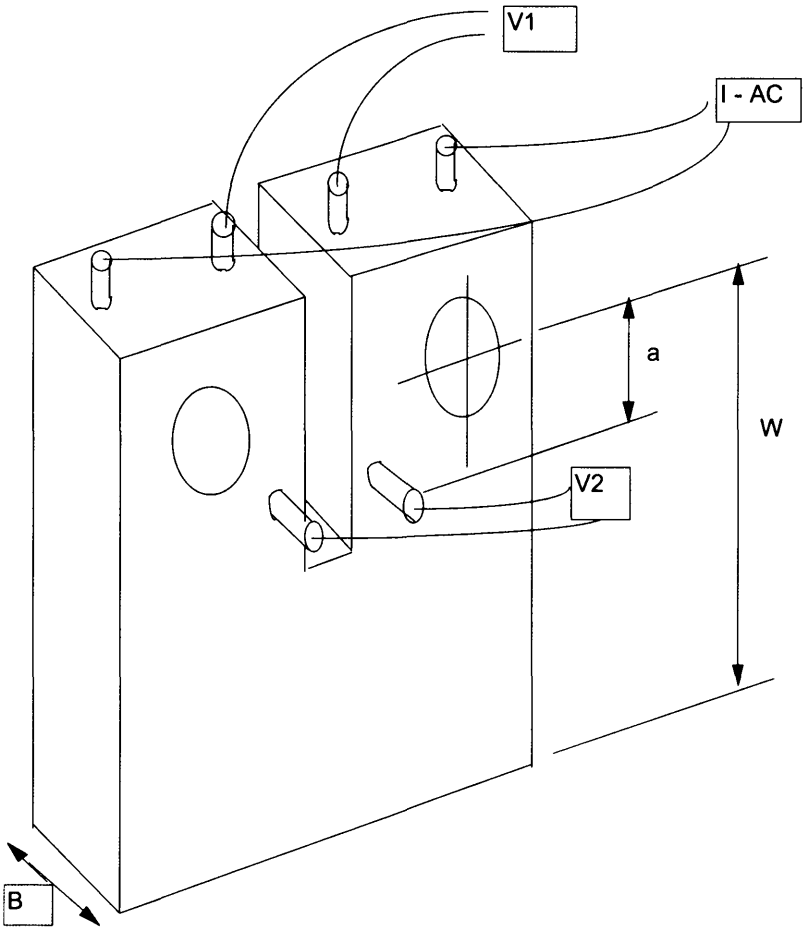

Figure 6-2. Crack propagation measurements as done with the potential drop method.

6.2.3 Stress intensity threshold determination

The same setup was used throughout for all the fracture mechanics tests, also for the current response tests that will be discussed in Chapter 7. The tests that were performed were done over a period of at least 14 hours, where the load was kept constant at the specified level.

6.2.4 Environmental variations

The 50% CO gas mixture was extensively researched with considerable number of test over the whole stress intensity spectrum. However, with the 9% and 1% carbon monoxide concentrations the emphasis was more on the influence of the environmental parameters, such as temperature and dissolved oxygen concentration. Two temperatures, 45°C and 25°C, as well as two dissolved oxygen concentrations, 8 and 0.1 ppm O_2, were selected, giving the test matrix shown in Table 6-1. A similar scenario was followed for 1% CO, but in this case the two environmental parameters were not as extensively researched and the emphasis was on the crack propagation rates.

Table 6-1. The experimental conditions that were used for the tests.

Test no.	Temperature (°C)	Dissolved oxygen concentration (ppm)
1.	25	8
2.	25	0,1
3.	45	8
4.	45	0,1

The influence of loading rate was also investigated for the 1% CO as well as 50% CO.

6.2.5 Applied potential

The setup as explained above was used and a platinum electrode was introduced into the autoclave so that the electrochemical potential could have been controlled when this was used as a counter electrode.

The samples were polarised to -620mV, -650mV and -490mV SSC.

6.2.6 Loading rate

At 25°C, the steel was tested in distilled water with a 50% CO and 50% CO_2 gas mixture, at a pressure of 800 kPa. The water was deoxygenated before the test was started, by purging with nitrogen for an hour, so that the water had an oxygen content of 0,1 ppm.

The crack length was measured as described in Section 6.2.2. As the load increased, the crack was pulled open and the crack sides did not touch. The measured crack length therefore increased as the load increased. This meant that the measured crack length was a virtual crack length and not the real crack length. However, at the same stress intensity, crack lengths were compared, and at a maximum crack length, the measured crack length could be taken as the real crack length. Therefore, the crack lengths increased from a maximum to another maximum, these were used to calculate a reliable value of crack growth.

These tests were performed on DCB test specimens with the configuration given in Section 6.2.2. Two test rates were used, firstly the load was increased from a low stress intensity and taken to a maximum. Secondly, the stress intensity was held at a maximum stress intensity and then the load was relaxed and the test was started at this lower stress intensity. The load was then increased at a certain rate, until the maximum stress intensity was reached again. With the latter test the same range of loading rates could be tested, but the general stress intensity was higher than the first kind of test.

6.3 Results and discussion

6.3.1 Fracture mechanics of steel in 50% CO- 50% CO_2 – H_2O

6.3.1.1 Results

The crack propagation rate against stress intensity was determined in order to establish the K_{ISCC} value. Figure 6-3 shows these results for tests done on different compact test specimens. The K_{ISCC} value was very low at 3 MPa.$m^{½}$ and the constant crack propagation rate was measured at $1x10^{-9}$ $m.s^{-1}$.

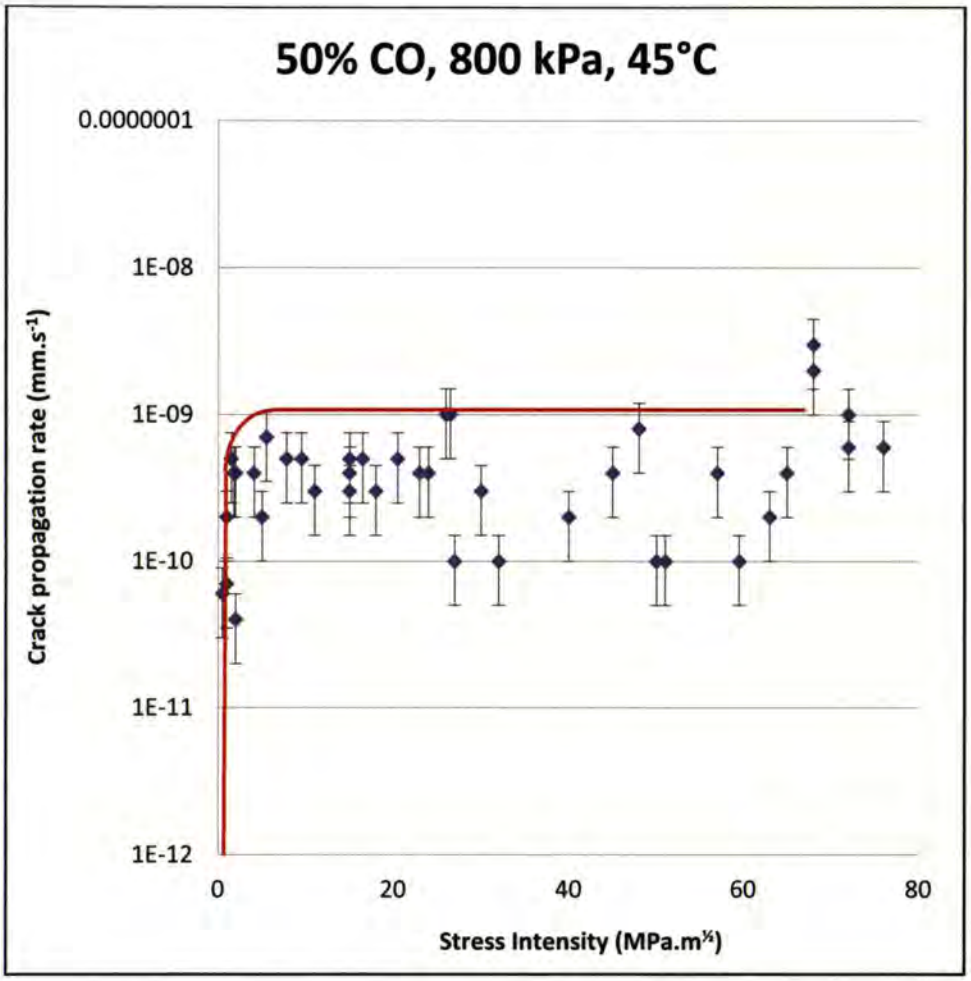

Figure 6-3. Crack propagation rate shown as a function of the stress intensity factor for steel exposed to water with 50% CO-50%CO_2 at 800 kPa and 45°C.

From around 3 to 78 MPa.m^{½}, the crack propagation rate was independent of the stress intensity. However, the crack propagation rate in this range of stress intensity showed a degree of variation.

When the loading rate was taken into consideration the crack propagation rates that were measured increased dramatically. Therefore, the crack propagation rates determined, was only measured after the specimens were loaded to exclude the enhanced crack propagation rate during the loading process. This phenomenon will be discussed in more detail in Section .6.3.4.

This very low stress intensity threshold for cracking is not typical for hydrogen embrittlement and a further indication of the stress corrosion type mechanism.

6.3.1.2 Discussion

The low value of the stress intensity threshold for cracking makes it very difficult to design structures and pressure vessels to operate at stress conditions below these threshold values. This low stress intensity threshold indicates the sensitivity of the steel to corrosion when exposed to carbon monoxide environment, with a significant instability of the passive layer formed by the carbon monoxide. Therefore, the slightest straining of the metal at the crack tip causes the film to be ruptured, corrosion occurs, and cracking is induced.

The crack propagation rate measured was relatively consistent, but with some variation which appeared to be as a result of the crack propagation rate that is also dependent upon the strain rate at the crack tip. This effect will be isolated and addressed separately. The rate of cracking also translates to 12 mm per year, which explains the severity of the cracking process in pipelines and pressure vessels.

The data from the current response measurements are indicating the same range for the stress intensity threshold for stress corrosion cracking as these results here.

6.3.2 Fracture mechanics of steel in 9% CO – 91% CO_2-H_2O

The critical stress intensity for stress corrosion cracking of the A516 pressure vessel steel exposed to water with 9% carbon monoxide was investigated at two temperatures, 25°C and 45°C, as well as two dissolved oxygen concentrations, 8 ppm and 0.1 ppm. Figure 6-4 and Figure 6-5 show the fracture mechanics characteristics determined in these environments, and the summarised results are shown in Table 6-2.

The subcritical crack propagation determined for the steel exposed to 9% CO, 8 ppm O_2, at 25°C showed a considerable scatter range in the order of $2x10^{-12}$ to $2x10^{-11}$. This was again seen for the same dissolved gas concentrations, but at 45°C that the subcritical crack propagation showed some variation above $1x10^{-10}$. These

tests were performed in order to determine the trend in the effect of temperature and dissolved oxygen concentration, however, more testing is required to give more definitive results.

Table 6-2. Fracture mechanics results from tests performed with 9% CO.

Temperature (°C)	CO (%)	CO_2 (%)	DO (ppm)	K_{ISCC} ($MPa.m^{½}$)	da/dt ($m.s^{-1}$)
25	9	91	0.1	20	2.00E-11
25	9	91	8	5	1.00E-11
45	9	91	0.1	15	3.00E-10
45	9	91	8	7	7.00E-10

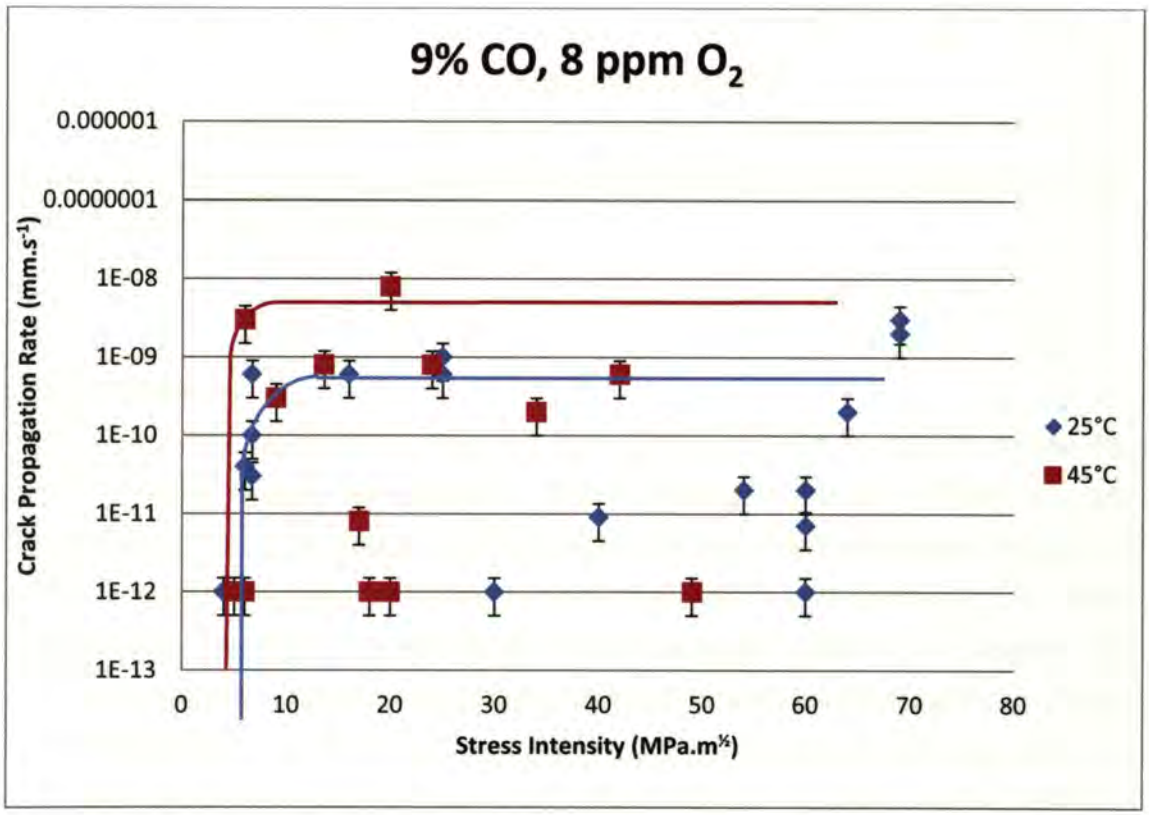

Figure 6-4. Crack propagation rate as a function of stress intensity of steel exposed to 9% CO-91% CO_2 with 8 ppm O_2 at 25°C and 45°C.

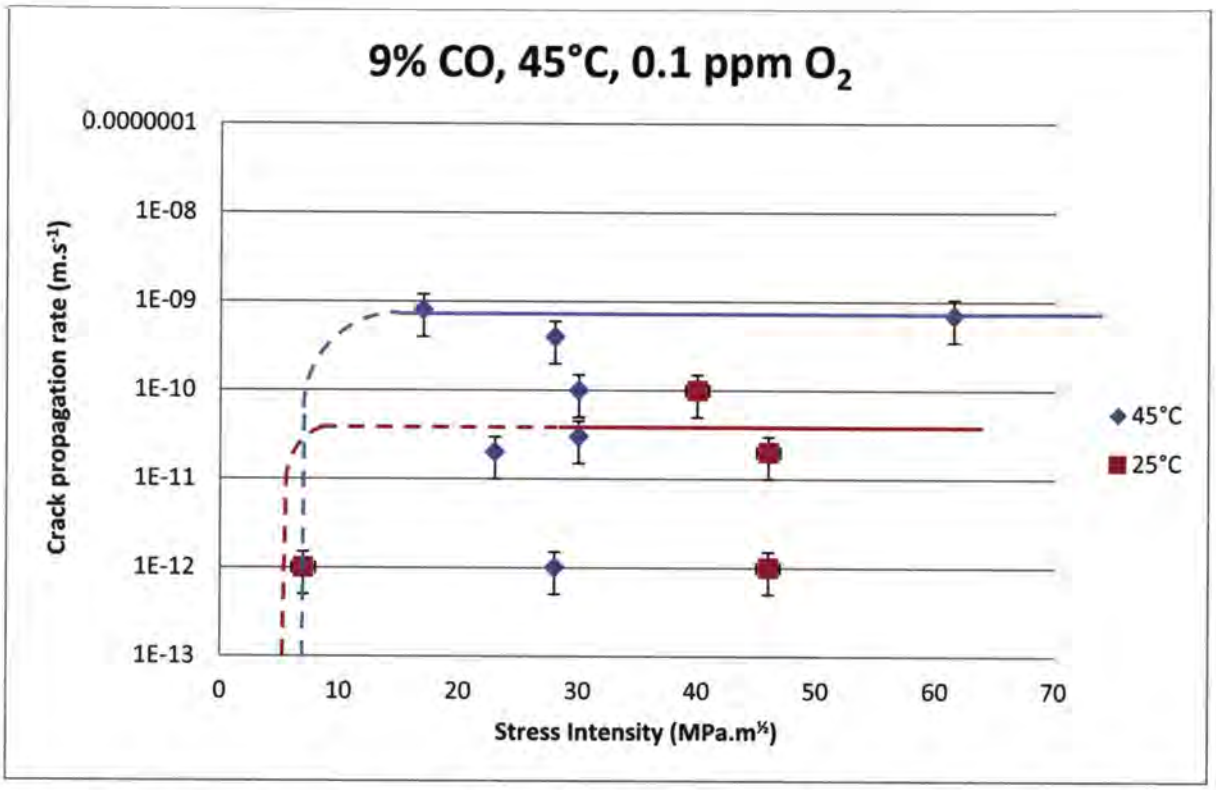

Figure 6-5. Crack propagation rate as a function of stress intensity of steel exposed to 9% CO-91% CO_2 with 0.1 ppm O_2 at 25°C and 45°C.

6.3.2.1 Discussion

The most severe situation that was considered was the higher temperature and the higher dissolved oxygen concentration. This was also the case for all the other gas mixtures that were investigated previously. At 25°C, the dissolved oxygen caused the stress intensity threshold for stress corrosion crack propagation to decrease considerably. However, the sub-critical crack propagation rate did not change with increased dissolved oxygen in the water, and some of the tests were even an order of magnitude below. At 45°C the dissolved oxygen again caused the K_{ISCC} value to decrease, and the sub-critical crack propagation rate did not show a large increase, although it increased with increased dissolved oxygen. At the dissolved oxygen level of 0.1 ppm, the temperature caused a decrease in the crack propagation rate of more than an order of magnitude. However, the threshold for cracking was nearly the same.

With the dissolved oxygen level at 8 ppm, the temperature did not affect the threshold stress intensity for stress corrosion cracking. However, with increased temperature, the sub-critical crack propagation rate increased dramatically.

The increase in the sub-critical crack propagation rate with increased temperature indicated the influence of the kinetics on the cracking process. Therefore, the reactions that took place at the crack tip inducing crack propagation were kinetically dependent as would be expected for corrosion controlled reactions.

6.3.3 1% Results

6.3.3.1 Fracture mechanics data

The temperature and the dissolved oxygen concentration in the water were varied so that three environments were tested. Firstly, at a temperature of 45°C the influence of the dissolved oxygen was ascertained by using water with a high and a low oxygen content. Secondly, with the third environment the influence of temperature was evaluated by using a water temperature of 25°C and keeping the oxygen content low at 0,1ppm.

Figure 6-6 shows the characteristics of the tests done at 45°C, for the low and high levels of dissolved oxygen. At 45°C and an oxygen concentration of 0.1 ppm, the K_{ISCC} value was 4 MPa.m^{½} . The range for subcritical cracking showed a crack propagation rate of $1x10^{-10}$ m.s^{-1}. A high crack growth rate was seen above 50 MPa.m^{½}, at around $3x10^{-9}$ m.s^{-1}.

Figure 6-7 shows the fracture mechanics characteristics for tests done at 25°C, showing the critical stress intensity for crack propagation, K_{ISCC}, was 13 MPa.m^{½}. The subcritical crack propagation rate was $8x10^{-10}$ m.s^{-1}, and then it increased to $3x10^{-9}$ m.s^{-1} at a stress intensity of 51 MPa.m^{½}. The extent of the crack propagation rates beyond this stress intensity is not known, as no tests were performed at higher stress intensities to verify it.

When the dissolved oxygen concentration was increased to 8 ppm, the K_{ISCC} value remained at 4 MPa.m^{½} as for the lower dissolved oxygen content. However, the level

of subcritical crack growth increased to $1x10^{-9}$ $m.s^{-1}$, which is an order of magnitude higher than for low oxygen content at the same temperature.

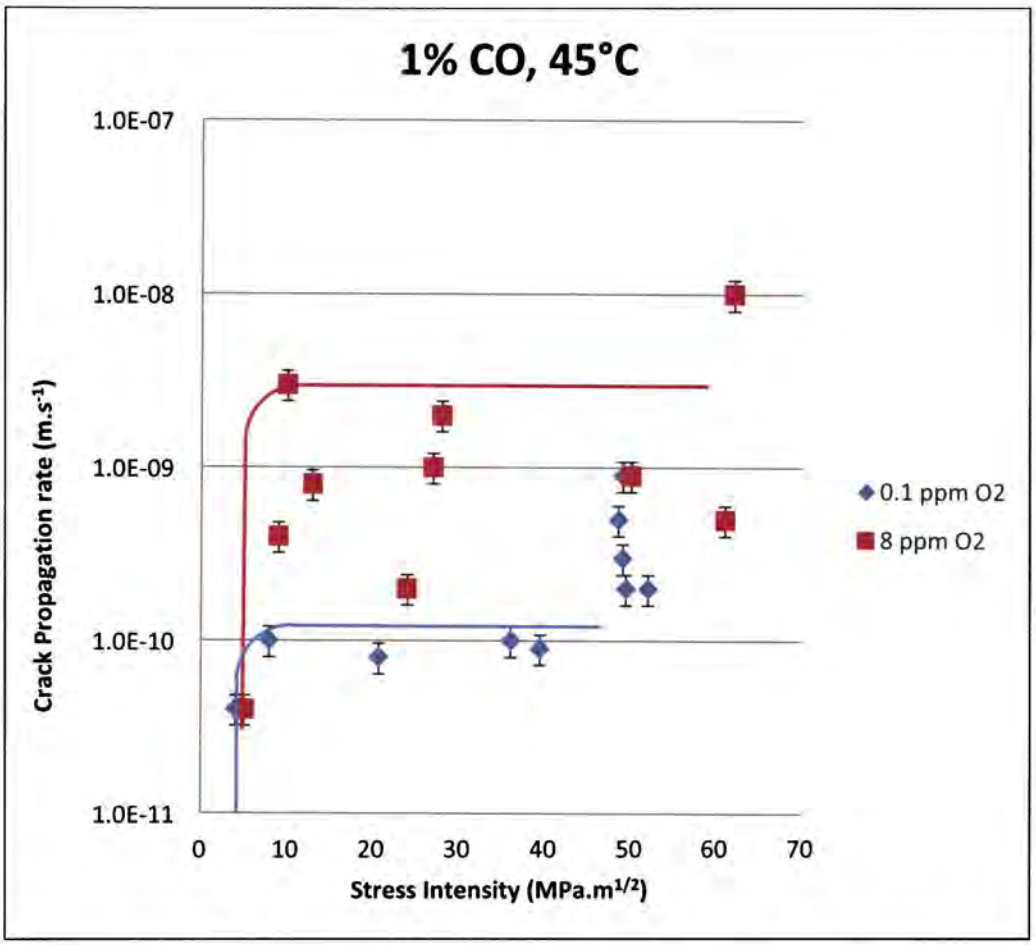

Figure 6-6. The fracture mechanical characterisics of the steel analysed in 1% CO – 99% CO_2 at 45°C and 0.1 ppm O_2 as well as 8 ppm O_2.

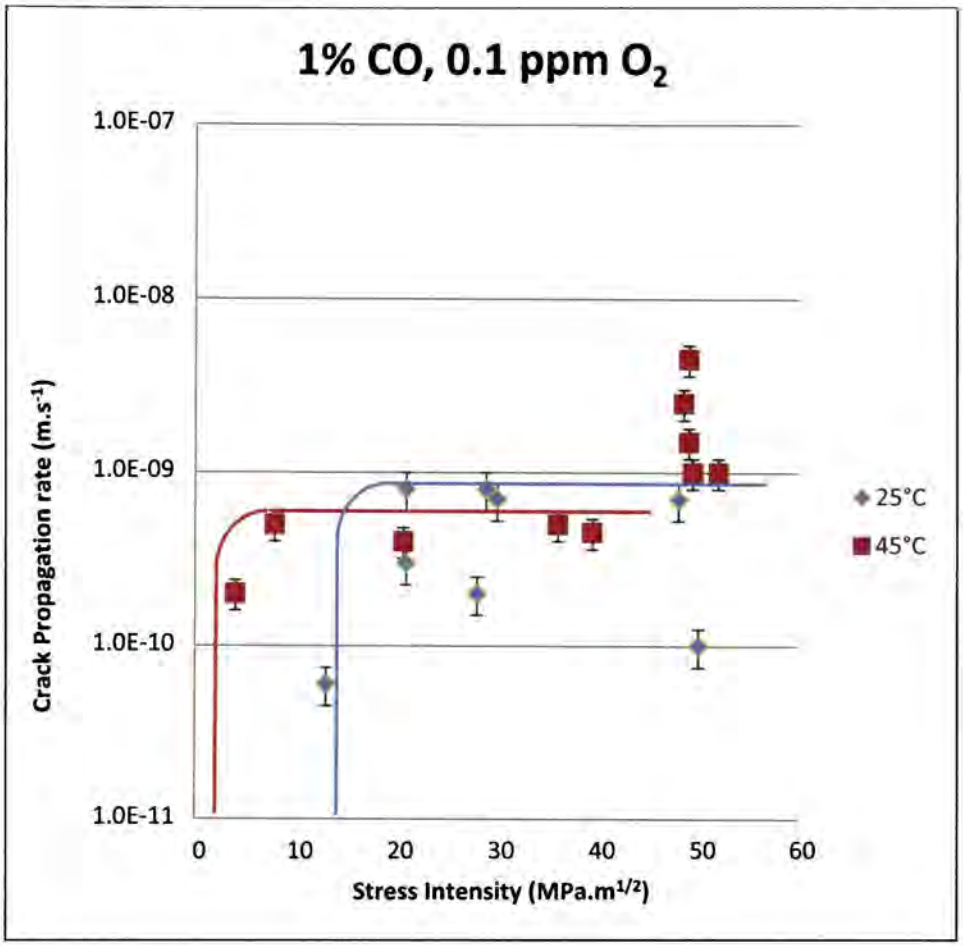

Figure 6-7. The fracture mechanical characterisics of the steel analysed in 1% CO – 99% CO_2 with 0.1 ppm O_2 at 45° and 25°C.

6.3.3.2 Discussion

The CO-CO_2 gas mixture is nearly pure carbon dioxide at 1% CO. The carbon monoxide was the only component that caused any inhibition to corrosion of the steel. According to the mechanism of stress corrosion cracking, this amount must be enough to provide adequate passivation for cracking to occur. However, if another mechanism of cracking was also at work, the CO_2 might have had a larger effect on the cracking process, as seen for hydrogen embrittlement.

The cracking process was increased by two main factors, namely the temperature and the dissolved oxygen concentration. These two components influenced the cracking process in two different ways; the temperature increased the K_{ISCC} value and the dissolved oxygen content increased the subcritical crack propagation rate that was found for stress intensities above the K_{ISCC} value. The increase of the subcritical crack propagation rate was nearly an order of magnitude higher at the higher dissolved oxygen concentration. At the lower temperature, the threshold stress intensity was lowered to nearly 16 MPa.m^{½}, but the subcritical crack propagation stayed at the same level.

Heaver and Sandenbergh[70] found that the process of corrosion inhibition of steel was nearly independent of carbon monoxide partial pressure. However, this was only true given sufficient time for the inhibition process to take place. They found that the anodic and cathodic curves of the polarisation characteristics settled to the same shape and current densities, regardless of the original gas mixture. This process of inhibition was found to be slower at low carbon monoxide concentrations. The passivation process is controlled by the kinetics of the reaction, and therefore is temperature dependent. The large influence of the temperature was shown in the increased stress intensity limit for crack growth. Thus, in order to increase the critical stress intensity, the rate of passivation has to be slowed down.

The higher dissolved oxygen content holds the free corrosion potential in the region of susceptibility to stress corrosion cracking. The effect of this is a greater crack growth rate, but has no effect on the critical stress intensity. Therefore, the lowering of the dissolved oxygen concentration does nothing to raise the stress intensity threshold for cracking. However, the lifespan of a component in this environment would increase, with an order of magnitude when the oxygen concentration was lowered. This apparent solution to cracking is a dangerous one, because there are other factors that influence cracking.

The rate of increase in the stress intensity seemed to be a factor that enhanced the crack propagation beyond the apparent limitations in the cracking environment. This is due to the critical strain rate at the crack tip that induced the film to break and enhanced the crack propagation rate beyond that of the influence of the other

parameters. This seemed to be the driving force for high crack propagation rates. Corrosion fatigue could have been the cause of cracking, but since the same crack propagation rate was achieved when the stress intensity was raised at the same rate showed that the stressing rate was the cause of cracking, and not corrosion fatigue.

6.3.4 Influence of Loading Rate

6.3.4.1 Results

The effect of loading rate was investigated for 50% carbon monoxide and 50% carbon dioxide with a nitrogen purge beforehand to establish low dissolved oxygen concentrations. The influence of the loading rate on the crack propagation rate is illustrated in Figure 6-8 and Figure 6-9. For the tests that were started at the lower stress intensity, the crack propagation rate increased as the loading rate was increased.

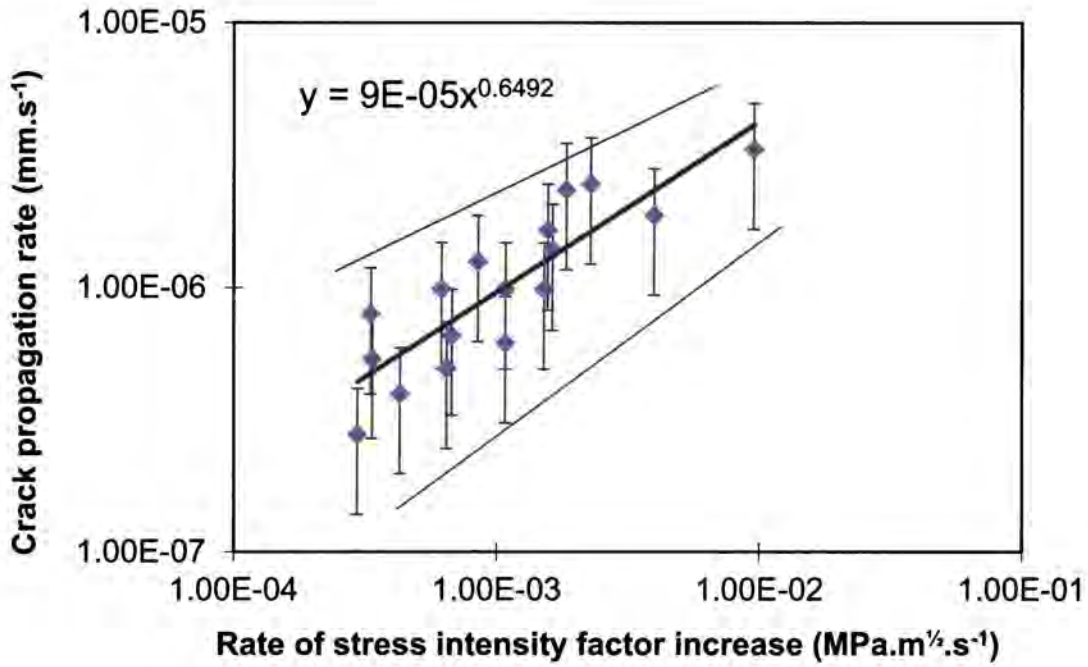

Figure 6-8. Crack propagation rate as a function of the stressing rate.

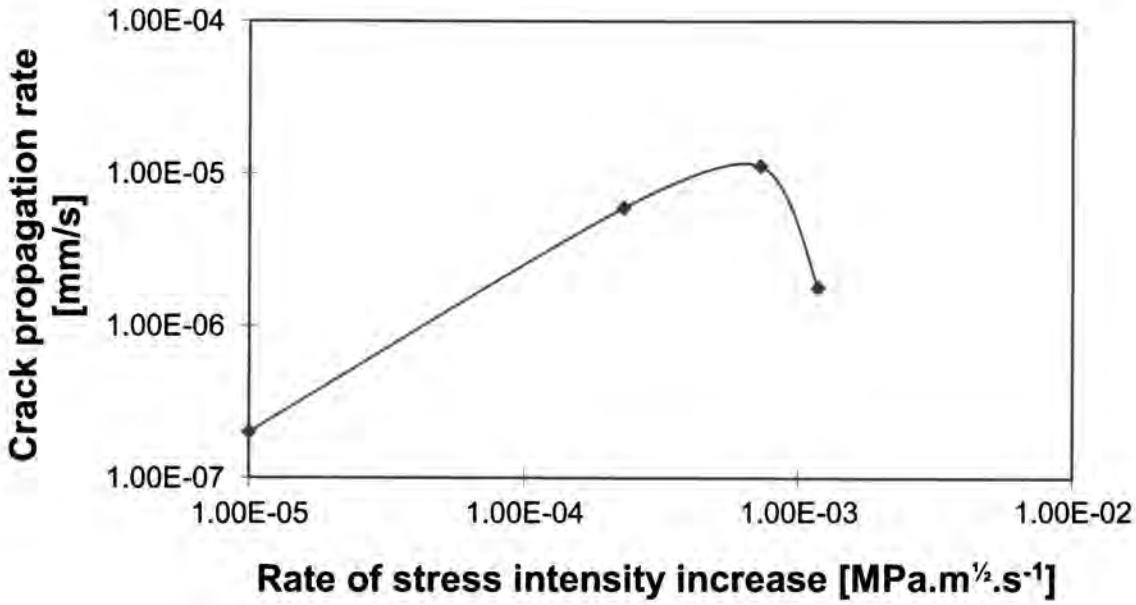

Figure 6-9. Crack propagation rate as a function of the stressing rate at higher stress intensities.

However, in Figure 6-9 the crack propagation rate decreased with the highest rate of stress intensity factor increase. This occurred at a stress intensity factor of 5×10^{-4} MPa.m^{½} and the crack propagation rate stayed a constant at a level of 2.5×10^{-6} mm.s^{-1} or 2.5×10^{-9} m.s^{-1}.

For the tests done at the higher stress intensity, the crack propagation rate increased (Figure 6-9). A point was reached where the loading rate was at a maximum for the highest crack propagation rate. The maximum crack propagation was 1.1×10^{-5} mm.s^{-1}, which was nearly an order of magnitude higher than the similar condition with the lower stress intensity condition (Figure 6-8).

6.3.4.2 Loading rate response in 1% CO – 99% CO_2

One of the factors that influence cracking is the rate of load increase. An example of the influence of this is seen in Figure 6-10, where the steel was exposed to water with 1%CO, 99%CO_2, and 0.1 ppm O_2 at 45°C. The load control of this particular test was not very good, and the stress intensity showed a variance of 1 MPa.m^{½}. Although, at 44 MPa.m^{½} the stress intensity was high, the crack propagation rate indicated on the chart of 3 x 10^{-6} mm.s^{-1} (3 x 10^{-9}m.s^{-1}) was much higher than expected from the rest of the data produced. Another test was performed at the same conditions, but the stress intensity was increased from a nearly no-load condition, and this is shown in Figure 6-11. The rate at which the stress intensity was increased was 0.0006 MPa.m^{½}.s^{-1} was approximately that of the individual cycles in the stress intensity shown in Figure 6-10 and the crack propagation rate was also 3 x 10^{-6}mm.s^{-1} (or 3 x 10^{-9} m.s^{-1}). Therefore, the effect of the stressing rate seemed to exceed the effect of the other parameters that enhanced cracking in this instance.

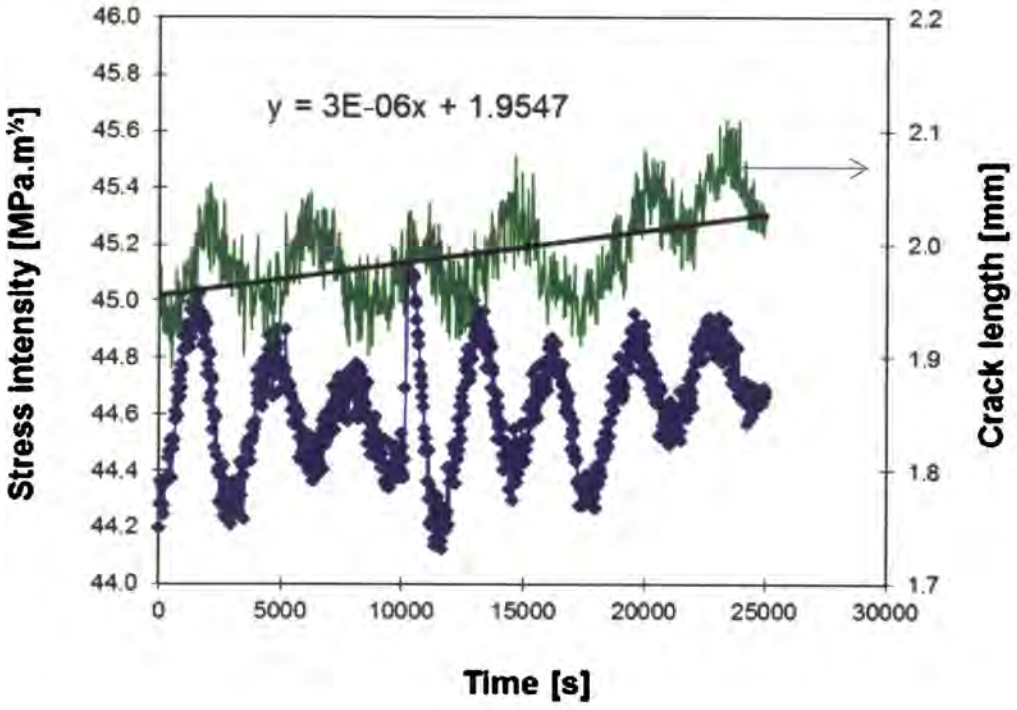

Figure 6-10. The stress intensity and crack length plotted against time at 25°C and 0.1 ppm O_2.

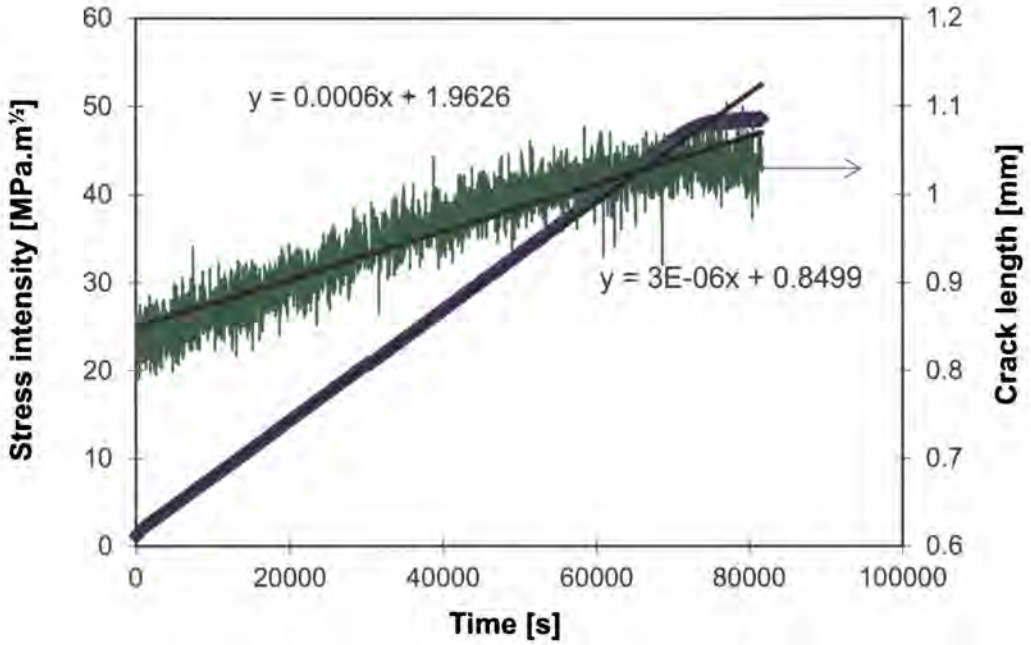

Figure 6-11. The stress intensity and the crack length is plotted against time for a test at 45°C and 0,1 ppm O_2.

6.3.4.3 Loading rate discussion

The influence of the loading rate on the crack propagation was very interesting because this might be the parameter that causes large increases in the crack propagation rate. The tests done at the higher stress intensity were also performed over a smaller stress intensity range than for the lower stress intensities. Therefore, the most severe condition was when the variance in the stress intensity was small – 2 MPa.m^{½} - and the recovery cycle an hour. This means that for stresses that occur in pipelines, only a small variance is necessary for high crack propagation rates to occur. However, when stress intensities are controlled at a constant value, the crack propagation is much lower.

The crack propagation for the tests with these varying loading rates performed at 25°C were higher than for the same environment at 45°C, but performed at constant stress intensities, shown in section 6.3.1. Generally, the reason for the higher crack propagation rates at higher temperatures is the higher rates of corrosion reactions that

take place on the surface of the steel, according to corrosion kinetic principles. The higher loading rate may have also caused a higher rate of the reactions that takes place on the surface. However, the rate of the adsorption reaction of the carbon monoxide on the steel remained the same. The rate at which bare metal was exposed to the environment was higher as the loading rate was increased. This means that there were more initiation sites from which cracking could occur.

The rate of passivation and the rate at which the bare metal surface was exposed are inter-related, and therefore contribute to the crack propagation.

6.3.5 Externally applied potential

6.3.5.1 Results

The polarisation of the specimens affected the crack propagation rate and the stress intensity threshold for stress-corrosion cracking. The fracture mechanics characteristics for the sample polarised to -490 mV (SSC) is shown in Figure 6-12, together with the results for samples polarised to -480 mV (SSC) and -620 mV (SSC). For the samples polarised to -490 mV (SSC) the stress intensity threshold for stress-corrosion cracking was at 15 MPa.m^{½} and the subcritical crack propagation rate is in the order of 2x10^{-10} m.s^{-1}. This was done at a temperature of 45°C. Two tests were performed at 47 MPa.m^{½} at lower electrochemical potentials of -470mV and -430mV. At -470mV the crack propagation rate was 1x10^{-10} m.s^{-1} and at -430 mV the crack propagation rate was 4x10^{-10} m.s^{-1}. At a polarisation of -480 mV the stress intensity threshold was slightly lower at around 10 MPa.m^{½} and the critical crack propagation rate at 1x10^{-9} m.s^{-1} or less. For the -620 mV polarisation the stress intensity threshold is again similar at around 15 MPa.m^{½} and the critical crack propagation rate 1x10^{-11} m.s^{-1}. The polarisation curve shown in Figure 4-16 in Chapter 4 was again shown here in Figure 6-13, illustrating the potential range where cracking would be expected. At -620 mV (SSC) the steel is definitely cathodic in nature, and at -480 and -490 mV (SSC) it would be anodic and within the passive range where cracking is expected. Figure 6-14 shows the influence of applied potential on the fracture mechanics of steel exposed to 50% CO at 25° and an overall pressure of 800 kPa.

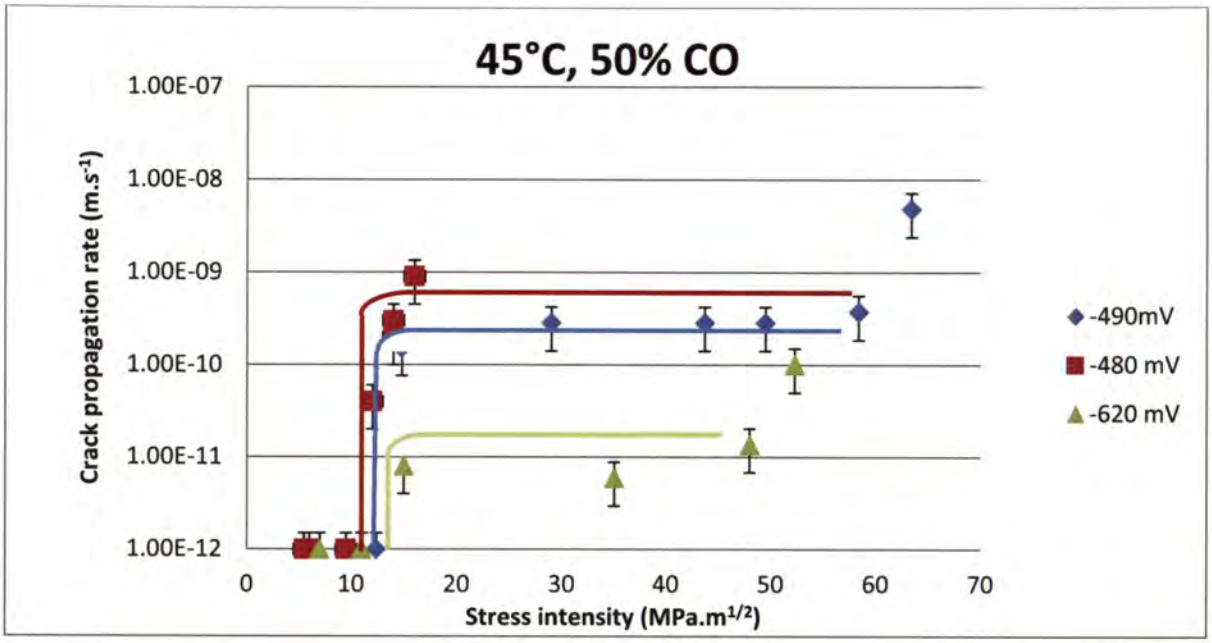

Figure 6-12. Effect of applied potential of steel exposed to 50% CO, at 800 kPa and 45°C.

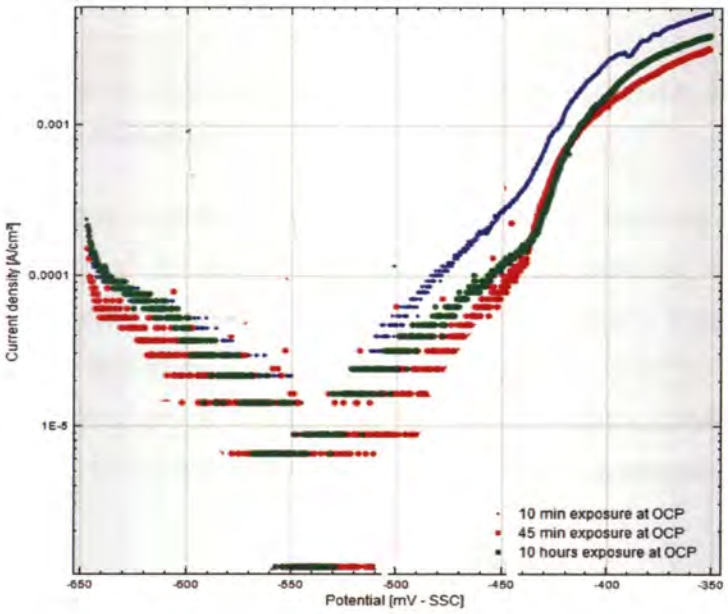

Figure 6-13. Polarisation characteristics of A516 pressure vessel steel exposed to 50% CO – 50% CO_2 at 45°C and 800 kPa, at a scan rate of 0.1 mV/s after it was held at open circuit potential (OCP) for various times from 10 minutes to 10 hours.

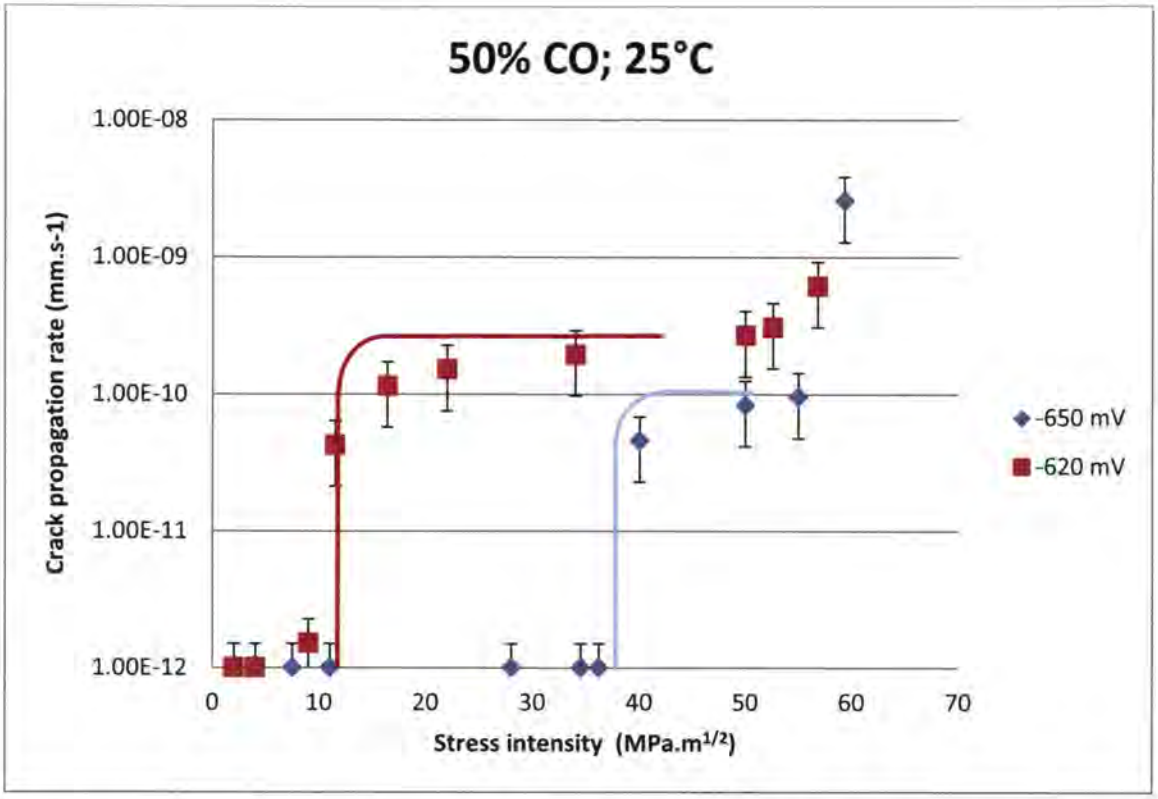

Figure 6-14. Effect of applied potential of steel exposed to 50% CO, at 800 kPa and 25°C, on fracture mechanics.

Note the significant increase in the stress intensity threshold for the steel from 11 MPa.m^{½} to above 35 MPa.m^{½}. In addition the critical crack propagation rate dropped from almost 2x10^{-10} m.s^{-1} to 1x10^{-10} m.s^{-1}. This critical crack propagation rate for the test at an applied potential of -620 mV at 25°C, is however slightly higher than the critical crack propagation rate for the same conditions at 45°C, which is more difficult to explain, unless another mechanism is operative.

Crack propagation rates were measured at a stress intensity of 20 MPa.m^{½} for a variety of applied potentials and these were plotted in Figure 6-15. The crack propagation rate showed a definite drop towards the lower potentials, while it increased on the anodic side of the polarisation. For both temperatures shown in Figure 6-15 the crack propagation rates were similar, although for the anodic potentials the propagation rates were significantly higher, which is an unexpected result.

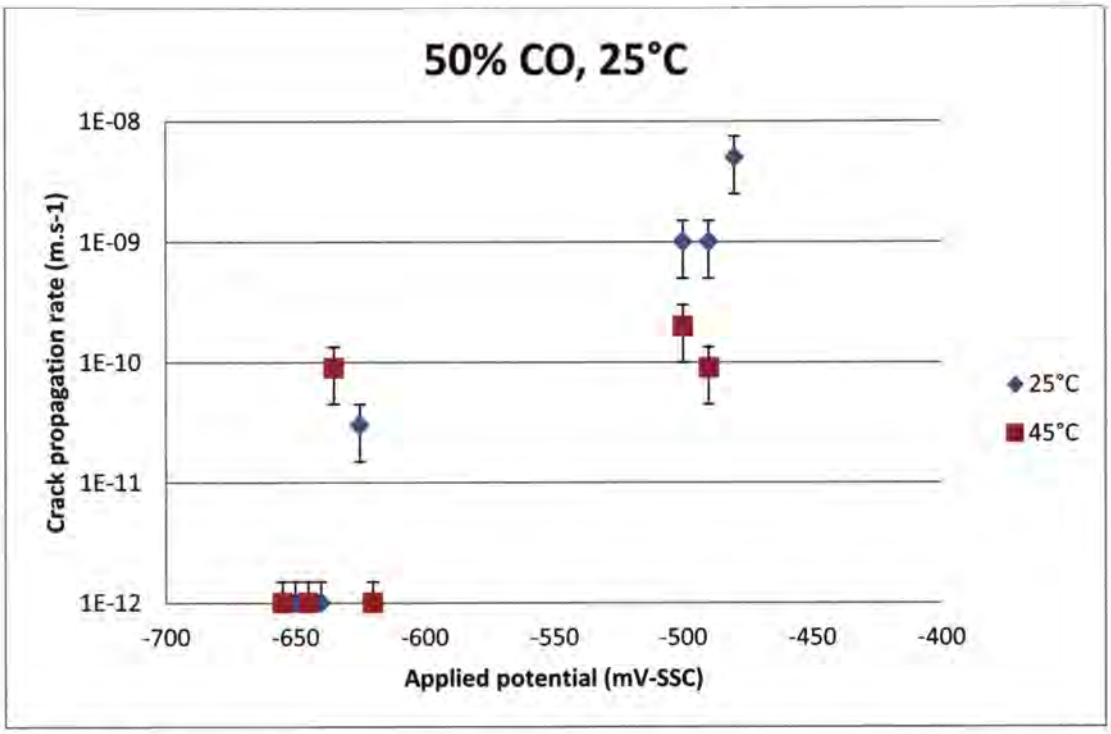

Figure 6-15. Effect of applied potential of steel stressed to 20 MPa.m^{½} and exposed to 50% CO, at 800 kPa and 45°C, on crack propagation rate.

6.3.5.2 Discussion – external potential

Both the cathodic as well as the anodic polarisation decreased the extent of cracking that occurred. However, the decrease in susceptibility to cracking differed. The subcritical crack propagation rate for all these scenarios was nearly the same at 1 to 2x10^{-10}m/s and this is a reduced propagation rate compared to the open circuit tests.

The K_{ISCC} value for the tests done at -490 mV was higher than for the open circuit tests, but the increase was more at -650 mV. With the small changes in the applied potential as shown, the crack propagation diminished quickly, even at a high stress intensity.

At the -650 mV applied potential, the K_{ISCC} value increased considerably, which indicated a safe range against stress-corrosion cracking, but the subcritical crack propagation was again at the same level as for the other potentials tested. The

process that enabled cracking at this potential might be the effect of the cathodic polarisation that enhanced the cathodic reaction at the crack tip, and possibly caused cracking enhanced by the presence of hydrogen.

6.4 Conclusions

6.4.1 50% CO – 50% CO_2

1. The K_{ISCC} value for cracking is 3 MPa.$m^{½}$.
2. The constant crack propagation in the order of $5x10^{-10}$ m/s above 3 MPa.$m^{½}$.
3. The current response data gave similar results for cracking.

6.4.2 1% CO – 99% CO_2

1. The K_{ISCC} value for 1%CO and 99%CO_2 in aqueous environments at 45°C was 1 MPa.$m^{½}$.
2. The dissolved oxygen concentration at 45°C caused the crack propagation rate to increase to $2x10^{-9}$m.s^{-1} from $1x10^{-10}$m.s^{-1}.
3. Crack propagation was enhanced by an induced strain rate.

6.4.3 9% Conclusion

1. The K_{ISCC} value decreases with increasing dissolved oxygen levels in the water.

2. The dissolved oxygen concentration of the water does not influence the subcritical crack propagation rate.

3. The temperature caused the sub-critical crack propagation rate to increase with an order of magnitude regardless of the dissolved oxygen level.

4. Temperature had little influence on the stress intensity threshold for stress corrosion crack propagation.

6.4.4 50-50 external potential

1. The K_{ISCC} value is moved to 35 MPa.$m^{½}$ when a potential of -650 mV, SSC is applied.

2. The K_{ISCC} value is moved to 15 MPa.$m^{½}$ when a potential of -490 mV, SSC is applied at 45°C.

3. The subcritical crack propagation rate is in the order of $2x10^{-10}$ m/s for the tests that were done.

4. Small changes in the applied potential above -490 mV, SSC increased the resistance to cracking.

6.4.5 Loading rate

1. The crack propagation rates for these tests are higher than tests done for constant loading.

2. The stressing rate enhances cracking to such an extent that the influence of temperature is overcome.

3. When the mean stress intensity is high the crack propagation is also higher.

CHAPTER 7

7 CURRENT RESPONSE MEASUREMENT DURING FRACTURE MECHANICAL TESTING IN A 50% CO-50%CO_2 AQEOUS SOLUTION

7.1 Introduction

The A516 pressure vessel steel in the H_2O-50%CO-50%CO_2 system was investigated to determine the fate of the current generated during crack growth. The usefulness of the current response as it followed the crack propagation and how it could be used to characterise the cracking processes was studied. The environmental conditions were kept constant, such as carbon monoxide concentration, temperature and total gas pressure, while the stress intensity and loading conditions were varied in order to establish the influence of the stress intensity on the cracking of the steel, as measure by the current response.

It was hoped to achieve similar results for the steel-carbon monoxide-carbon dioxide-water system, so that the K_{ISCC} value could easily be determined and be used as a less time-consuming way to determine the threshold for a variety of conditions. With the ability of monitoring the crack propagation more directly, the current response measurements could be followed more directly. Other factors that enhance cracking can be investigated at a closer level beyond the range limitations of crack measurements. The model of cracking is that dissolution at the crack tip results in the production of a positive current that flows out of the crack mouth on to the external surfaces. As charge is conserved, electrons are released through the steel. This current is consumed by the cathodic reaction on the external surfaces of the specimen and therefore the internal crack environment is coupled with the external specimen environment.

7.2 Experimental procedure

The external surface of each compact tension specimen was shielded from the environment by silicon rubber and a new external surface was created by separate steel pieces that were placed in close proximity on the opposite sides of the crack.

The whole sample was masked with the silicon rubber to ensure only a small area around the crack tip being exposed to the environment. This was done to reduce interference with the electrochemical noise measurements by the general corrosion occurring on the specimen surface.

The electrons produced at the crack tip were diverted through a zero-resistance ammeter (ZRA) to the new external surface. By attaching an insolated wire to the external surfaces, and taking it out of the autoclave in which the tests were done, it was connected to the ZRA, and the compact specimen was electrically linked to the ZRA. In this way, the electrons flowed from the compact specimen, through the ZRA, and back to the cathodic surface, where they contributed to reduction/oxidation reactions. Inserting the no-loss current measuring device in the circuit permitted the amount of current produced during the electro dissolution process to be measured. The distance over which positive current can travel, as it exists the crack mouth, was limited by the conductivity of the water, and therefore, the “cathodes” were placed in close proximity to the crack mouth as demonstrated in Figure 7-1.

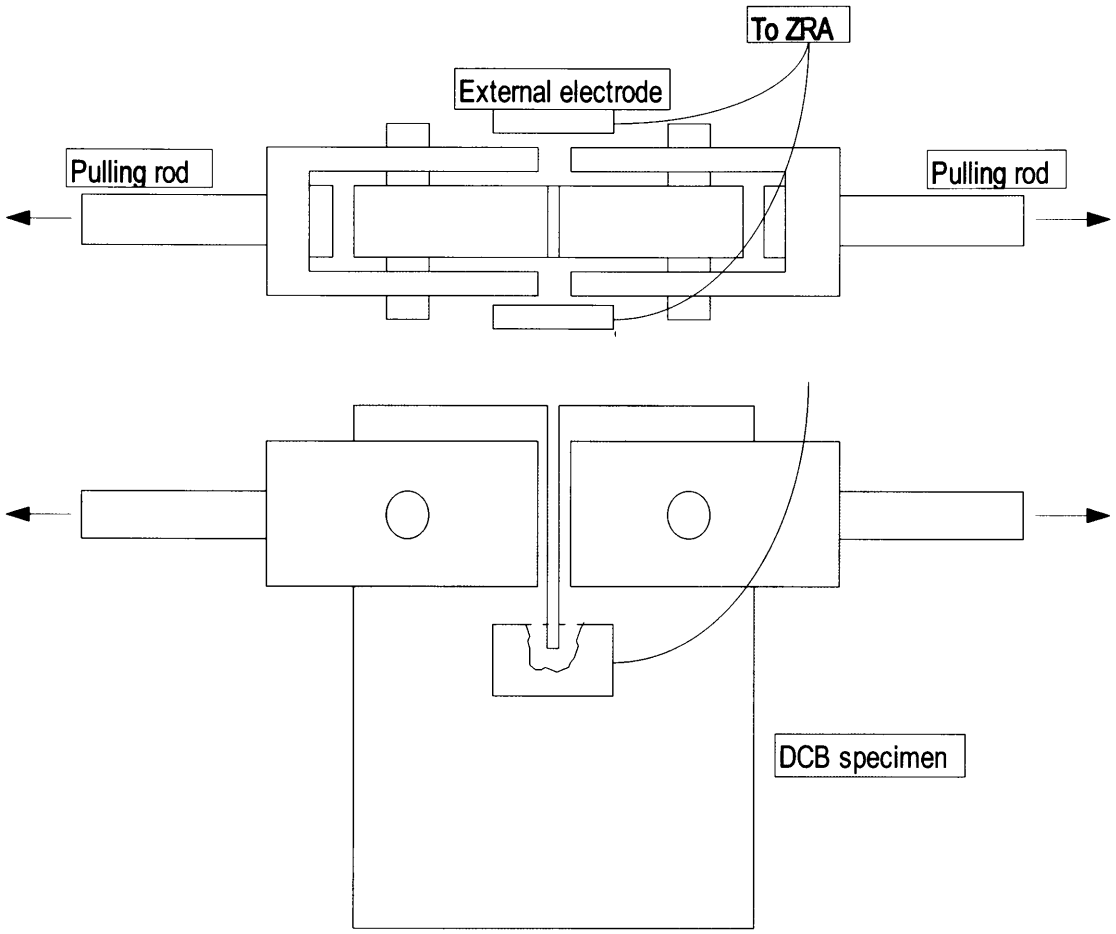

Figure 7-1. Schematic drawing of the double cantilever beam specimen showing the placement of the external electrode.

7.2.1 Test procedure

Distilled water was poured in the pressure vessel and it was then de-aerated by bubbling nitrogen through the water for one hour. The vessel was pressurized to 800 kPa with the 50% CO-50% CO_2 gas mixture. Then the pressurized water was released in to the test autoclave and the temperature was kept at 45°C. All the experiments were done at 45°C, except where otherwise noted.

These tests were done by raising the stress intensity to a specific value from a low-load condition. The stress intensity was kept at this level for an extended time shown in the results for each specific test. Next the stress intensity was lowered to a low-load condition for at least an hour and throughout this time, the current response was measured.

These ZRA measurements were of course performed in the high solution resistance distilled water environment and this could have masked the measurements. Because of corrosion products in solutions the conductivity of the environment would have changed slightly with the progression of the tests, assisting in the level of electrochemical noise measurements. However, this is problematic for the test environment, but would not have been the case for an industrial product.

7.3 Results

7.3.1 Introduction

The results of a number of tests are shown to indicate the various responses of the zero resistance ammeter (ZRA) signal as well as the repeatability of the measurements.

In Figure 7-2 the stress intensity was held at 1 MPa.m^{½} and then it was increased from 1 to 4 MPa.m^{½}; as it reached 4 MPa.m^{½} it decreased again to 3 MPa.m^{½} and then the load is applied to give a final stress intensity of 60 MPa.m^{½}.

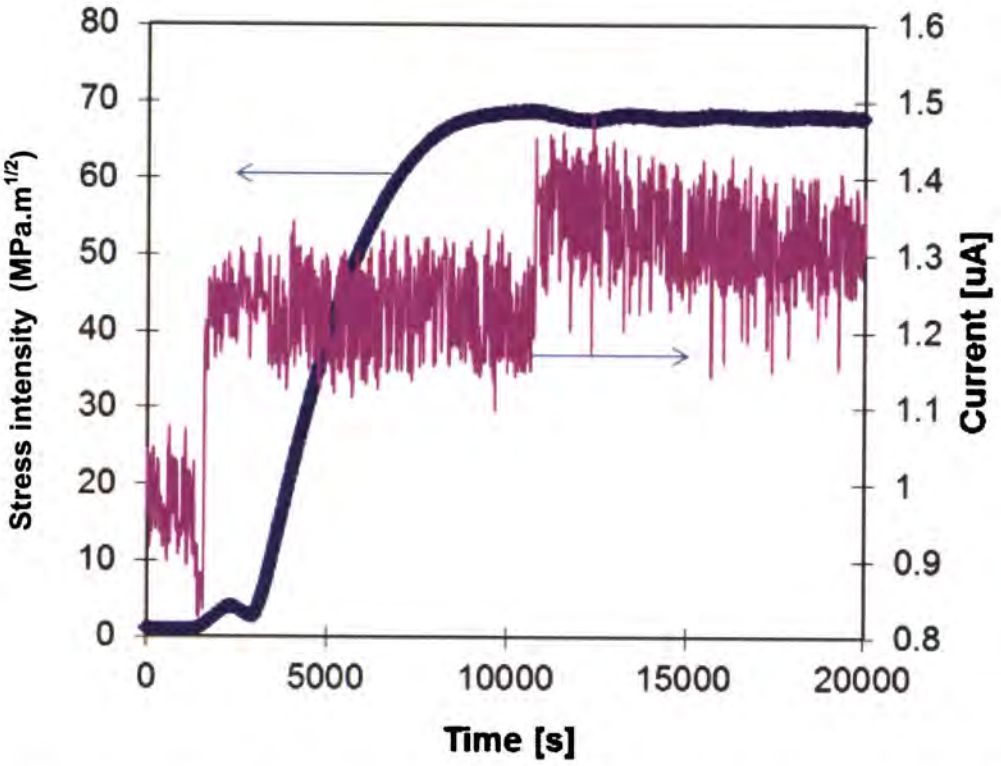

Figure 7-2. The stress intensity factor and the ZRA signal shown against time for a sample exposed to 50% CO – 50% CO_2 at 45°C and a pressure of 800 kPa.

The ZRA signal is plotted with the stress intensity in Figure 7-3 and two changes are seen in the mean of the ZRA signal. The first is when the stress intensity is raised from 1 to 4 MPa.m^{½}.

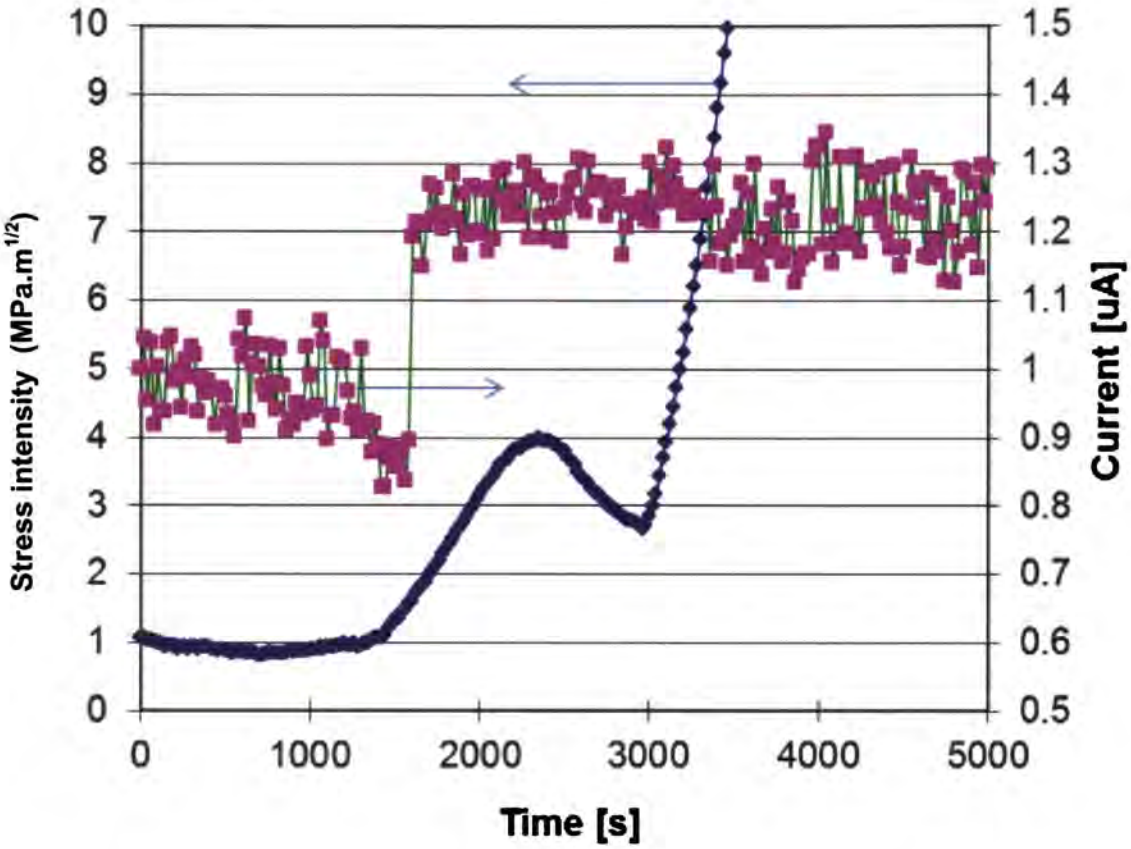

Figure 7-3. The stress intensity factor and the ZRA signal shown against time as shown in Figure 7-2 but localized at the region where the stress intensity started to increase a sample exposed to 50% CO – 50% CO_2 at 45°C and a pressure of 800 kPa.

In Figure 7-3, the first part of the increase in the stress intensity is shown and here the mean of the ZRA signal increased with nearly 0,4 µA when the stress intensity increased above 2 MPa.m^{½}. With this increase, the amplitude and frequency of the ZRA signal stayed the same. However, when the stress intensity increased for the second time, the amplitude of the ZRA signal increased slightly from 0,12 to 0,2 µA and this occurred at a stress intensity of 7 MPa.m^{½}. The frequency also increased slightly, although it was difficult to establish this with the measuring time that was used. The gradient of the increase in the stress intensity was 0,019 MPa.m^{½}.s^{-1} at 7 MPa.m^{½}. As the stress intensity reached 70 MPa.m^{½} the mean of the ZRA signal increased again by nearly 0,2 µA. This increase diminished over a period of 5 000 to 7 000 s.

The increase of the stress intensity is approximately 0-70 MPa.m^{½} in 5 400 s. At the second increase of the ZRA signal, the measured crack length showed an increase.

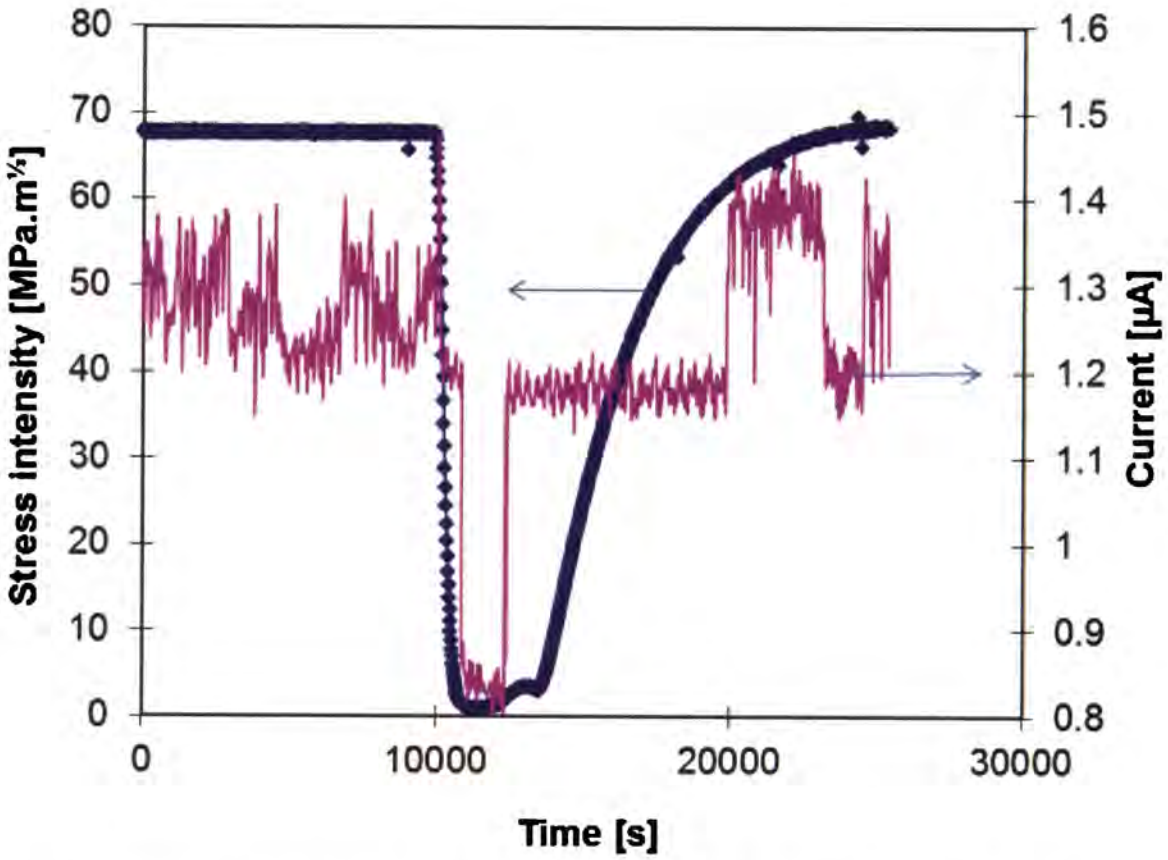

Figure 7-4. Stress intensity factor and the ZRA signal shown against time for a sample exposed to 50% CO – 50% CO_2 at 45°C and a pressure of 800 kPa..

The same was seen in Figure 7-4, where the ZRA signal oscillated at one level when the stress intensity was kept constant at 68 MPa.m^{½} and then it dropped to 0,8 µA as the stress intensity dropped to around 1 MPa.m^{½}. As soon as the stress intensity increased, the current increased again. At around 60 MPa.m^{½} the ZRA signal increased again but fell back to the original value as the stress intensity remains at 70 MPa.m^{½}. The instability in the ZRA signal responded to the growth of the measured crack length as seen in Figure 7-5. The mean value of the measured crack length increased from the first increase in the ZRA signal.

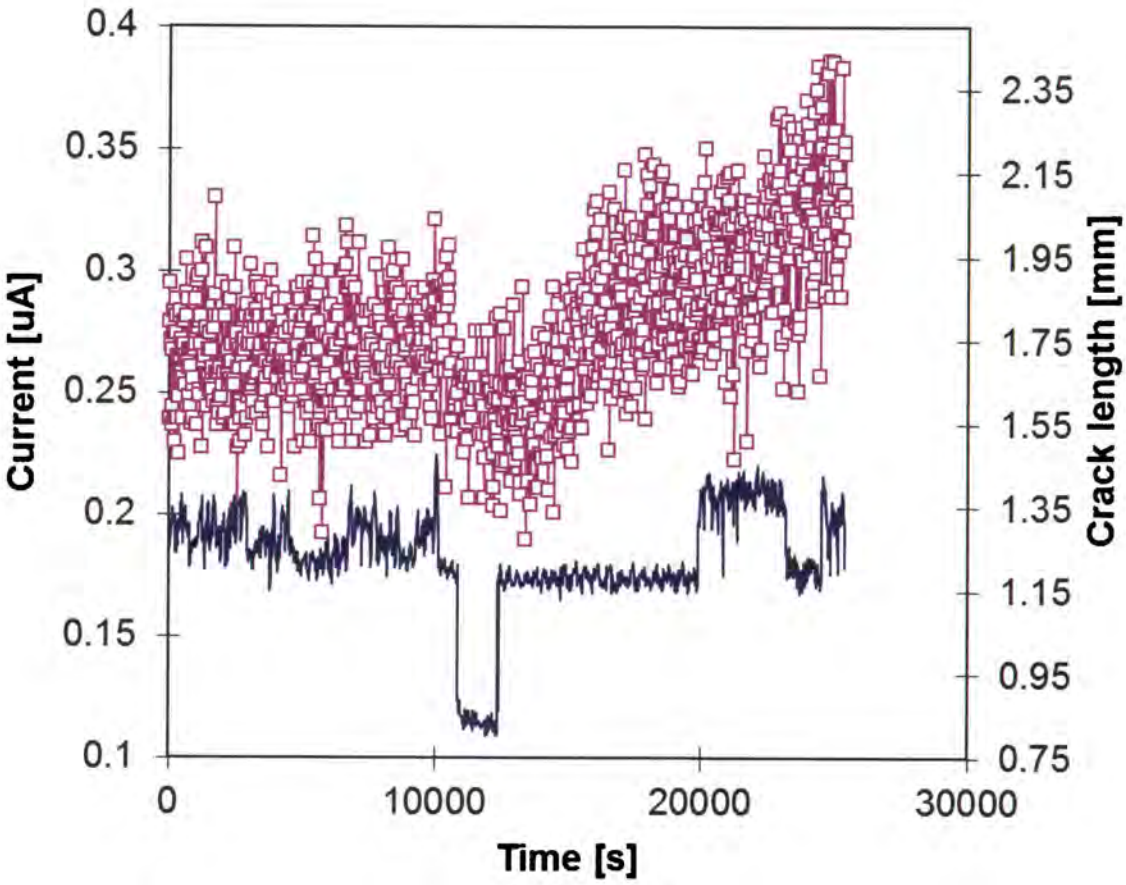

Figure 7-5. ZRA signal and the true crack length shown against time a sample exposed to 50% CO – 50% CO_2 at 45°C and a pressure of 800 kPa..

The crack length signal had a considerable amount of scatter on it.

7.3.2 ZRA signal response at low stress intensity levels

The stress intensity in Figure 7-6, is plotted with the ZRA signal against time. The stress intensity was kept at more or less 1 MPa.m^{½} and it was then raised to 3 MPa.m^{½}. As it was raised, the ZRA signal increased with about 0.25 µA indicating an increase in the activity at the crack tip. At this small increase in the stress intensity, the crack propagation rate could not be measured accurately. Crack growth was seen as the stress intensity was increased from 1 to 60 MPa.m^{½}, but the ZRA signal only

showed the increase as the stress intensity was raised beyond 1.2 MPa.m^{½}, and it stayed at the same level with the same amplitude. At the point where the mean value of the ZRA signal increased the amplitude of the ZRA signal stayed the same.

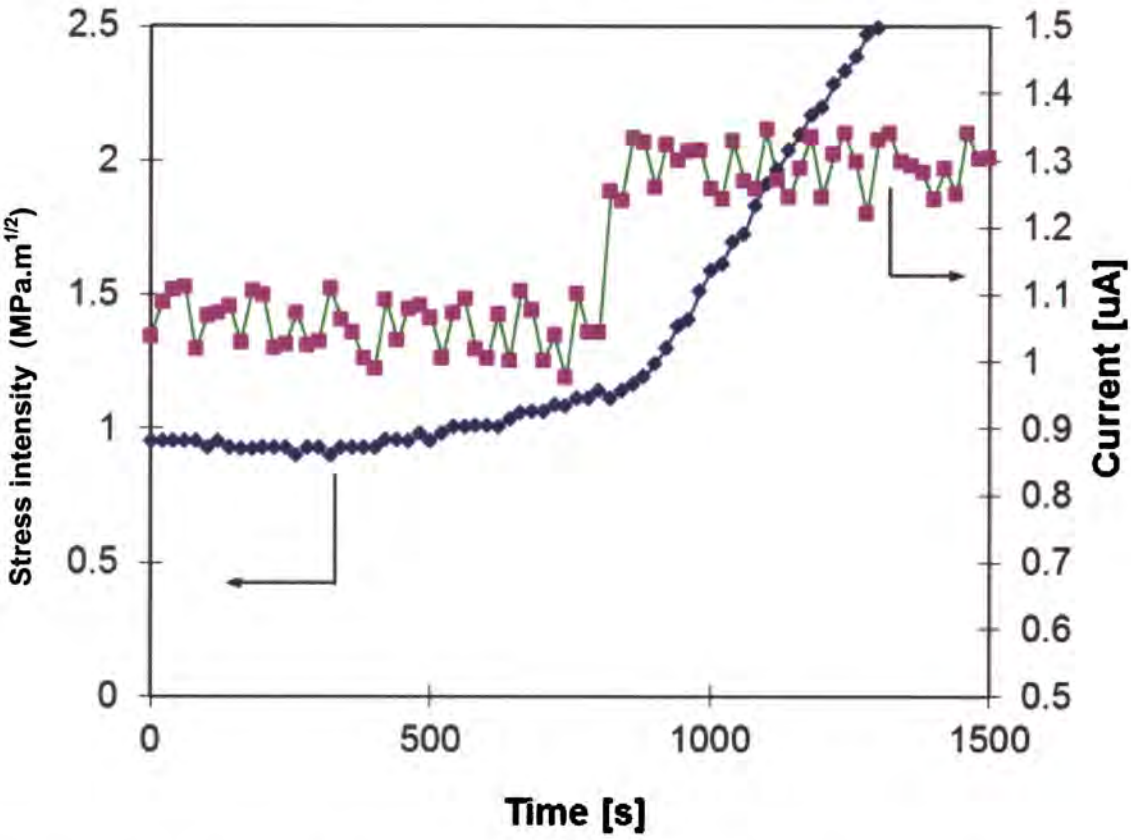

Figure 7-6. Stress intensity factor and the ZRA signal is plotted against time for a sample exposed to 50% CO – 50% CO_2 at 45°C and a pressure of 800 kPa.

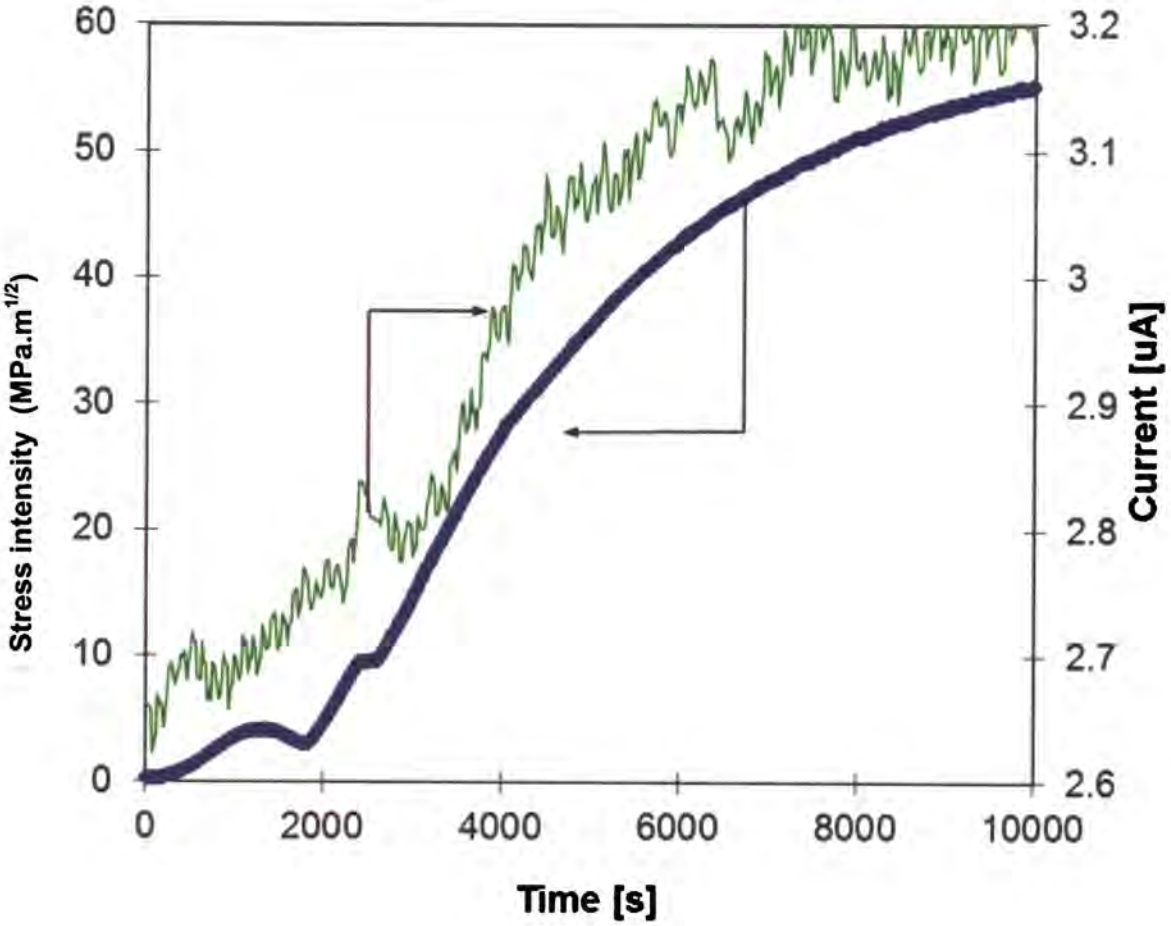

Figure 7-7. The stress intensity factor and the ZRA signal plotted against time for a sample exposed to 50% CO – 50% CO_2 at 45°C and a pressure of 800 kPa.

The ZRA response is shown in Figure 7-7 with the stress intensity against time. At the first increase in the stress intensity at 2 MPa.m^{½}, there was a slight increase in the ZRA signal. Then at 7 MPa.m^{½} another slight increase was seen. The gradient of the ZRA signal changed at 11 MPa.m^{½}, but decreased gradually as the stress intensity increased. A small amplitude was noted at 0,05 µA with a low frequency of 0,001 Hz.

Figure 7-8 is another example of how the ZRA signal increased as the stress intensity increased above 1 MPa.m^{½}. It is also seen how the gradient of the ZRA signal increased as the stress intensity is increased above 7 MPa.m^{½}.

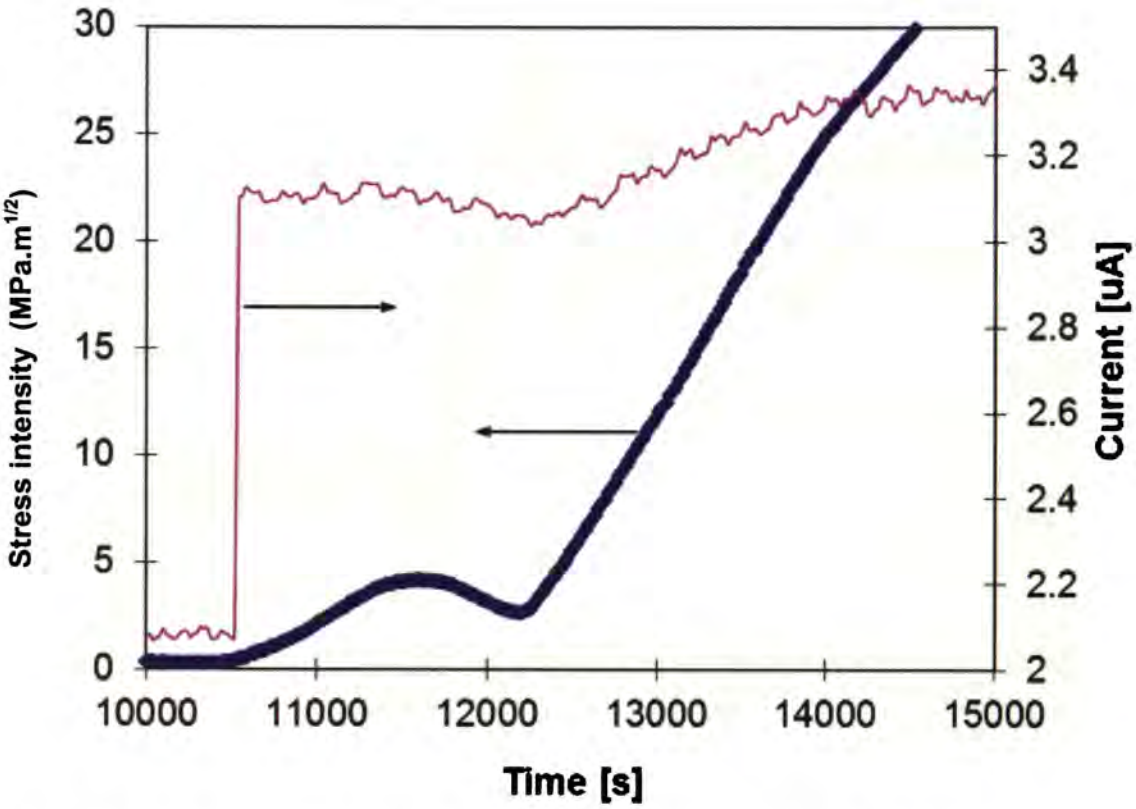

Figure 7-8. The stress intensity factor and ZRA signal plotted against time for a sample exposed to 50% CO – 50% CO_2 at 45°C and a pressure of 800 kPa.

The ZRA signal is plotted with the stress intensity in Figure 7-9. Here, the amplitude of the signal is 0,05 µA. The ZRA signal also followed with the increases in the stress intensity and two increases in the ZRA signal were seen. Firstly, as the stress intensity was raised to 4 MPa.m^{½} and secondly as it was raised above 7 MPa.m^{½}. After the first increase it stayed at 2,4 µA. With the second increase it reached 2,55 µA, but then it showed a slight decrease as the stress intensity was lowered, and then it stayed at a constant level as the stress intensity was also constant at 20MPa.m^{½}.

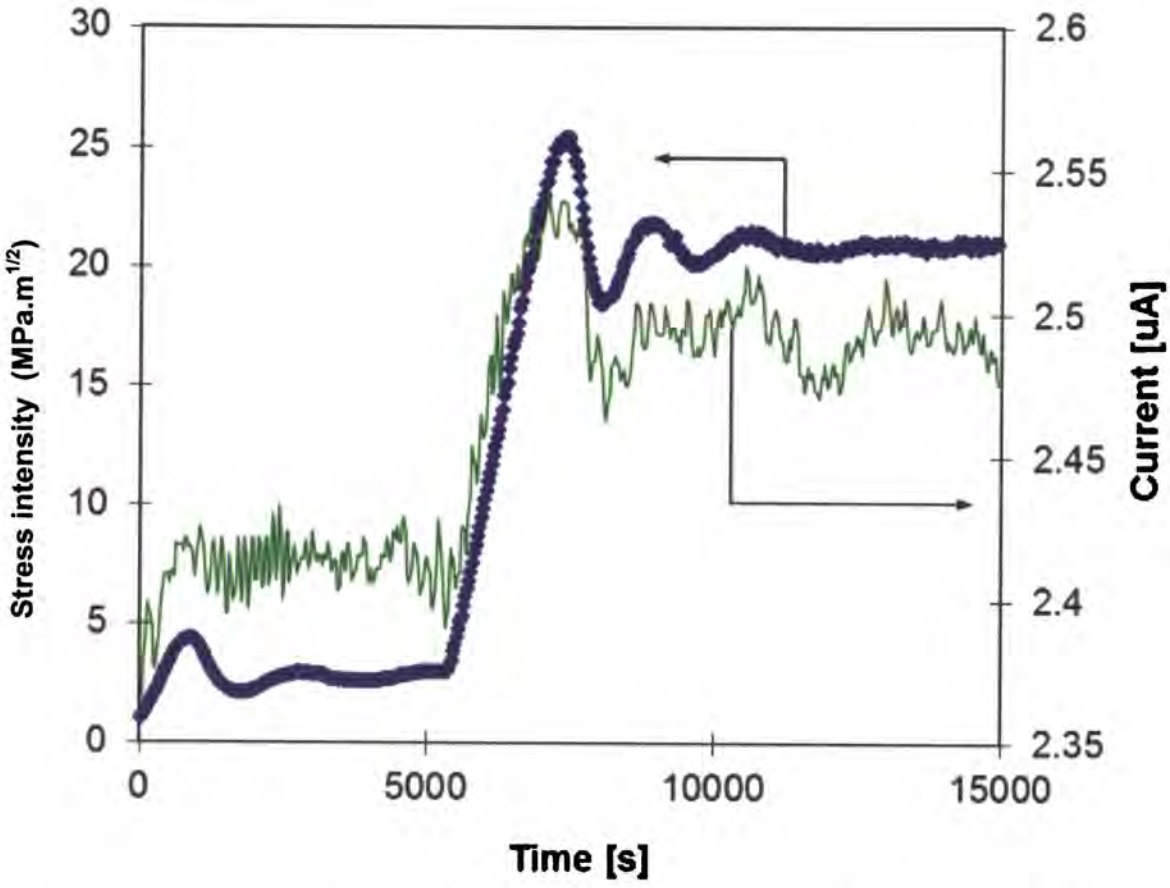

Figure 7-9. The stress intensity factor and the ZRA signal plotted against time for a sample exposed to 50% CO – 50% CO_2 at 45°C and a pressure of 800 kPa.

7.3.3 ZRA signal response as the stress intensity is lowered

The ZRA signal in Figure 7-10 had an amplitude of 0,06 µA. As the stress intensity was lowered from nearly 70 MPa.m^{½}, the ZRA signal dropped from 1,2 to 0,8 µA. As the stress intensity fell below 55 MPa.m^{½}, the ZRA signal increased suddenly, and then dropped exponentially over a period of 150 s.

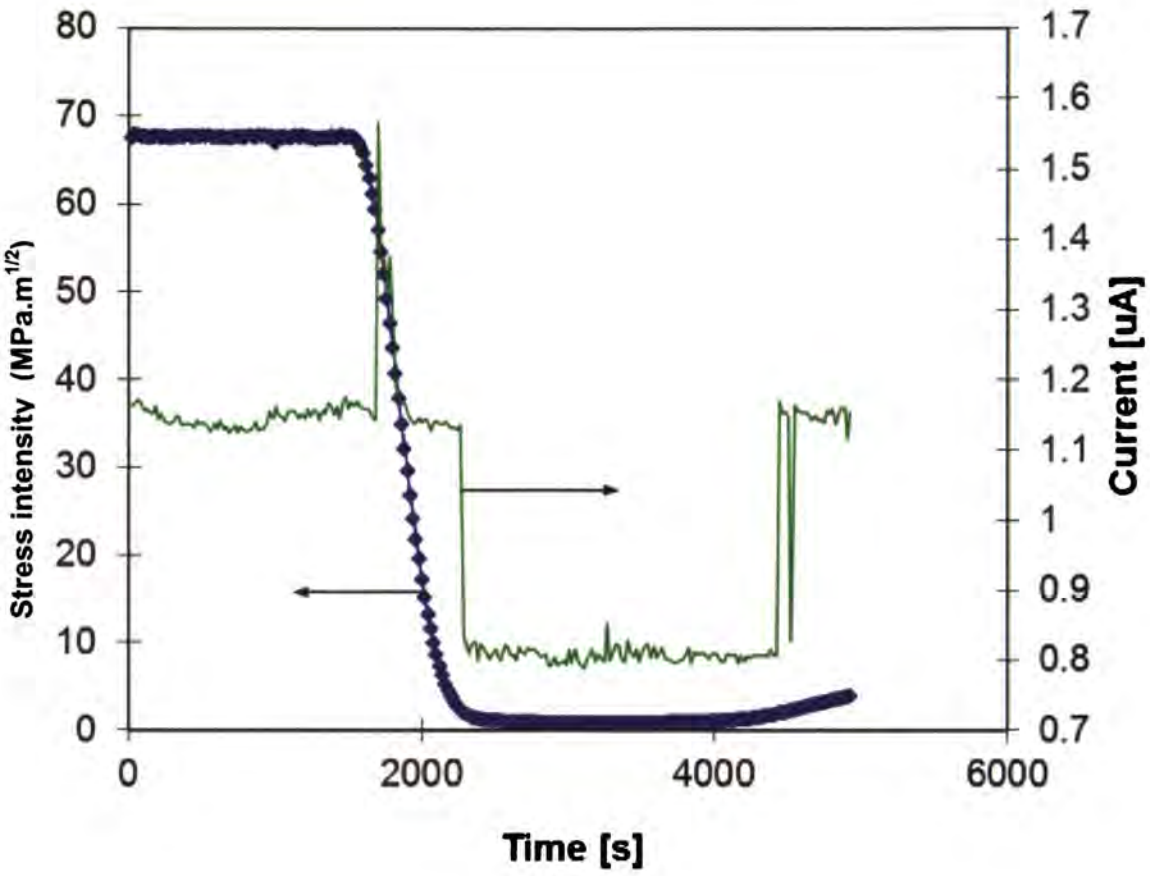

Figure 7-10. The stress intensity factor and the ZRA signal plotted against time for a sample exposed to 50% CO – 50% CO_2 at 45°C and a pressure of 800 kPa.

In Figure 7-11 as the stress intensity was lowered from 48 to 0 MPa.m^{½}, the ZRA signal decreased with the stress intensity at a certain gradient, but at 15 MPa.m^{½} the gradient lowered considerably and the mean value of the ZRA signal again increased slightly as the stress intensity was lowered. As the stress intensity dropped to nearly 0 MPa.m^{½}, the ZRA signal showed a sharp drop of 1 μA .

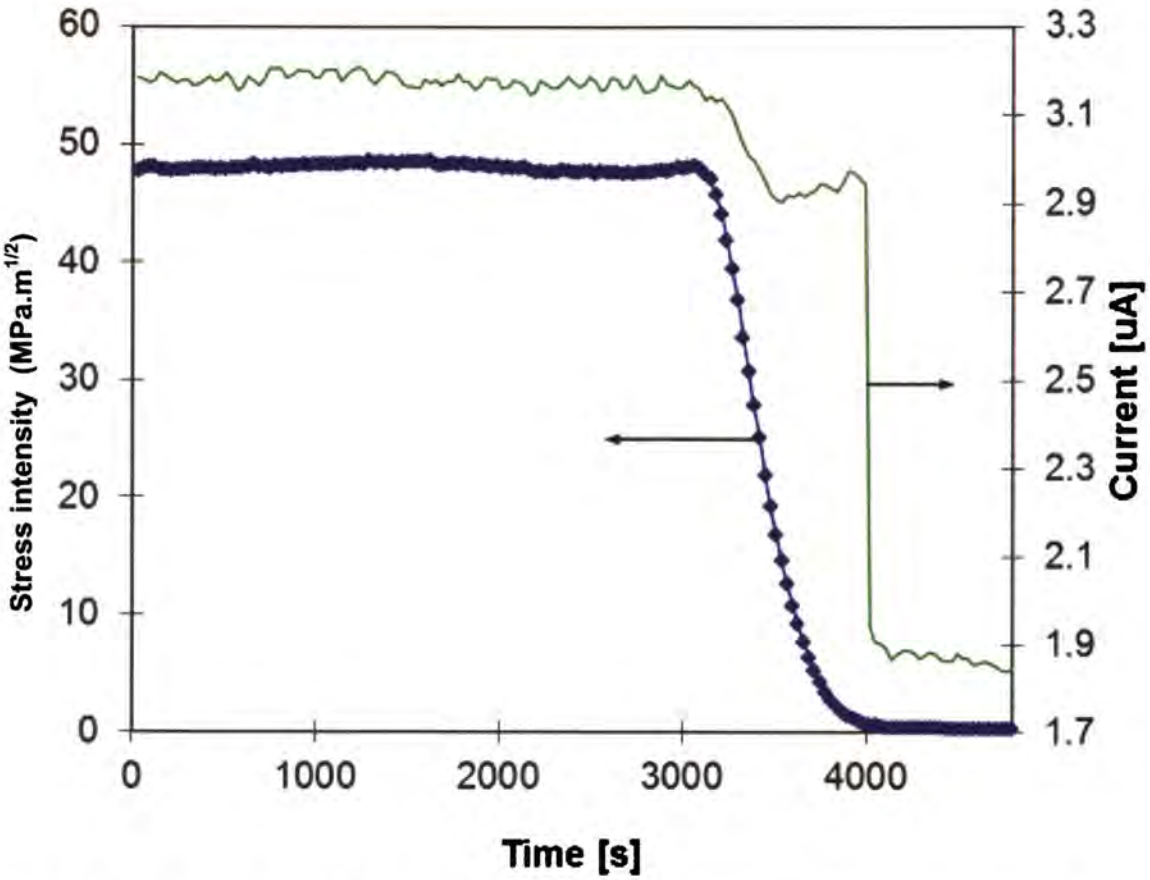

Figure 7-11. The stress intensity factor and ZRA signal plotted against time for a sample exposed to 50% CO – 50% CO_2 at 45°C and a pressure of 800 kPa.

7.3.4 Rate of stress intensity increase

The second increase of the ZRA signal in Figure 7-4 was looked at more closely, and it is shown in Figure 7-12.

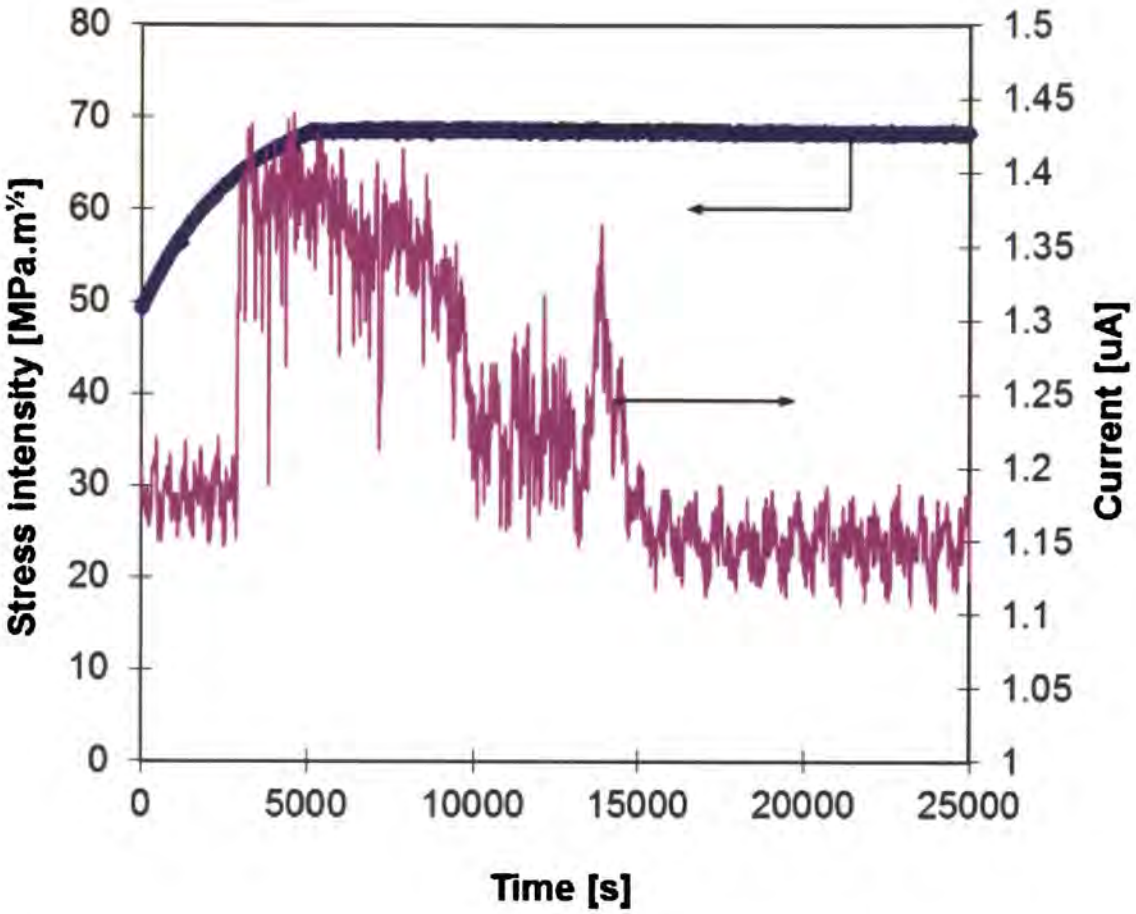

Figure 7-12. Stress intensity factor and ZRA signal plotted against time for a sample exposed to 50% CO – 50% CO_2 at 45°C and a pressure of 800 kPa.

The ZRA signal increased as the stress intensity was raised to 60 MPa.m^{½}. This increase is most likely explained by the rate at which the stress intensity was increased. This higher ZRA signal continued for more than 10 000 s and then it reverted back to the previous value. If the crack length was considered' it is seen that the crack length also increased in this region of a higher ZRA signal, as it was shown earlier (Figure 6-7). In Figure 7-12 the gradient of the increase in the stress intensity was shown to be 0,0036 MPa.m^{½}.s^{-1}. In the region 15 000 s to 25 000 s in Figure 6-15 the period of the ZRA signal was about 1 000 s or 16 minutes. The amplitude was in the range of 0.05 µA. However, the amount of crack growth in this region was difficult to measure, and nearly insignificant, when compared to that of the crack

growth, when the stress intensity was raised from 1 MPa.m^{½} to 60 MPa.m^{½}, as shown earlier (Figure 7-5).

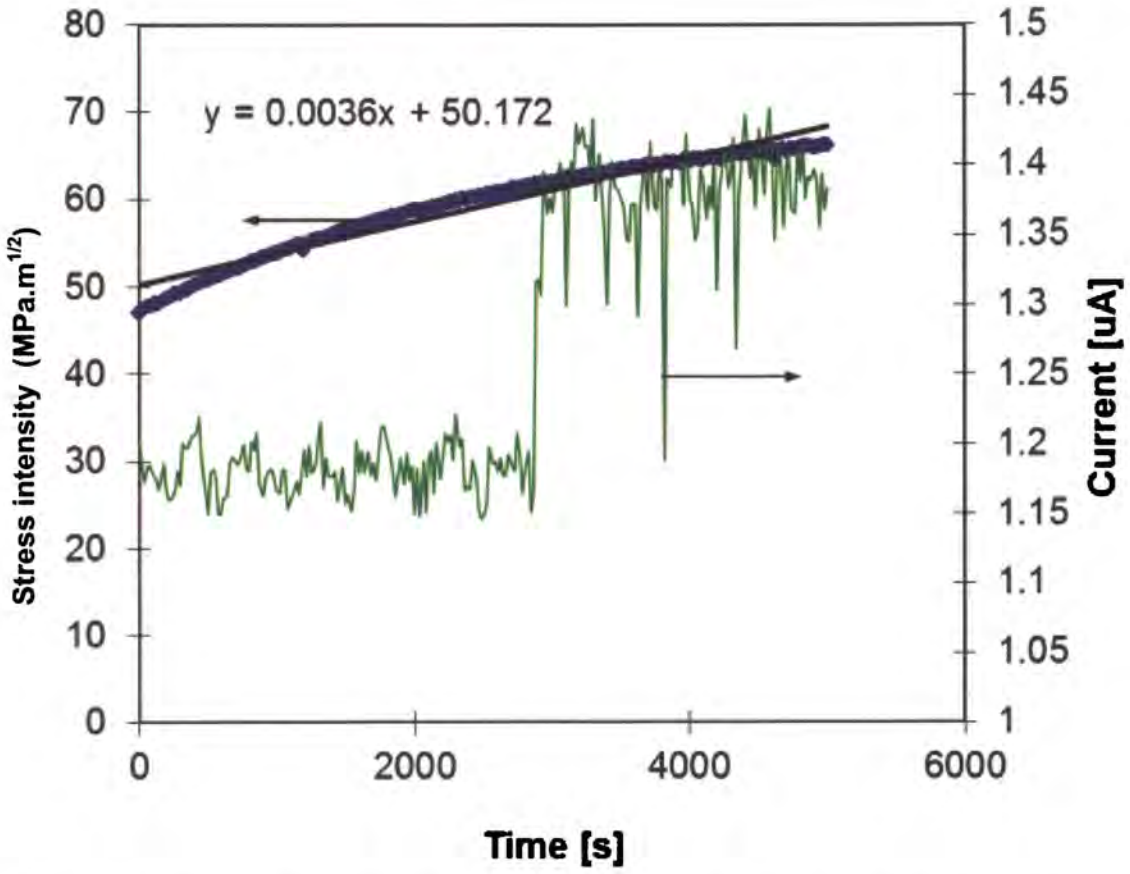

Figure 7-13. Stress intensity factor and the ZRA signal plotted against time for a sample exposed to 50% CO – 50% CO_2 at 45°C and a pressure of 800 kPa.

The ZRA signal is shown with the stress intensity against time in Figure 7-14 for a test done at 25°C.

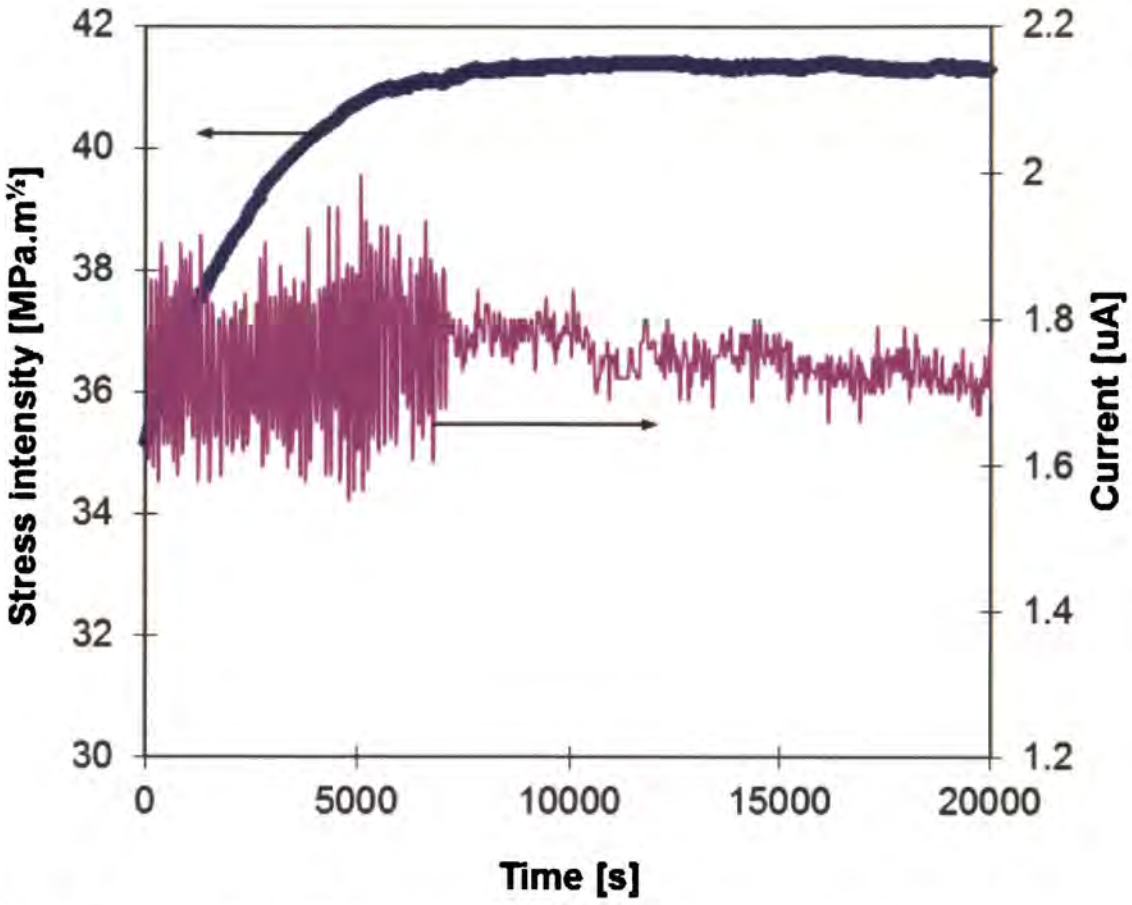

Figure 7-14. The stress intensity factor and the ZRA signal plotted against time for a sample exposed to 50% CO – 50% CO_2 at 25°C and a pressure of 800 kPa.

As the stress intensity was raised, the amplitude of the ZRA signal was high with a high frequency. As the loading rate decreased and the stress intensity stabilized the amplitude of the ZRA signal decreased and the frequency of the signal also lowered. However, the mean value of the ZRA signal stayed at a constant level of 1,8 µA. The crack growth is seen in Figure 7-15 and it shows that the crack propagation rate was higher from 0 to 8 000 s than in the region of 8 000 to 20 000 s, although the crack propagation rate was still relatively high in the latter region.

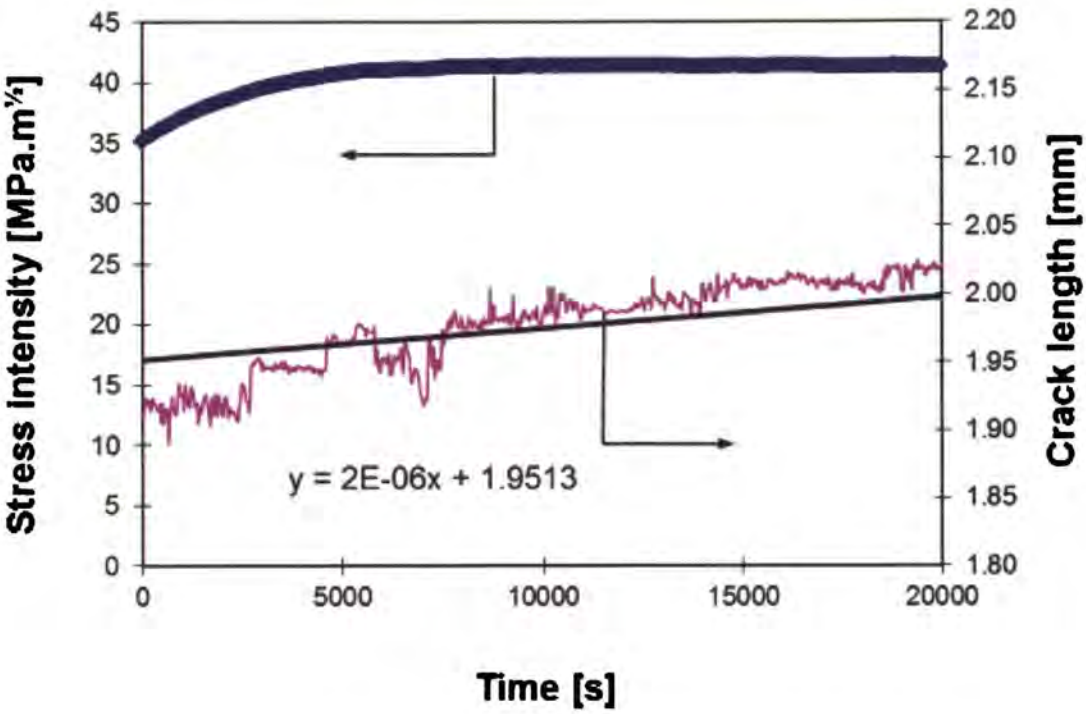

Figure 7-15. Stress intensity and the measured crack growth plotted against time for a sample exposed to 50% CO – 50% CO_2 at 45°C and a pressure of 800 kPa..

The current response is shown with the measured crack length against time in Figure 7-16 and the stress intensity and measured crack length against time in Figure 7-17.

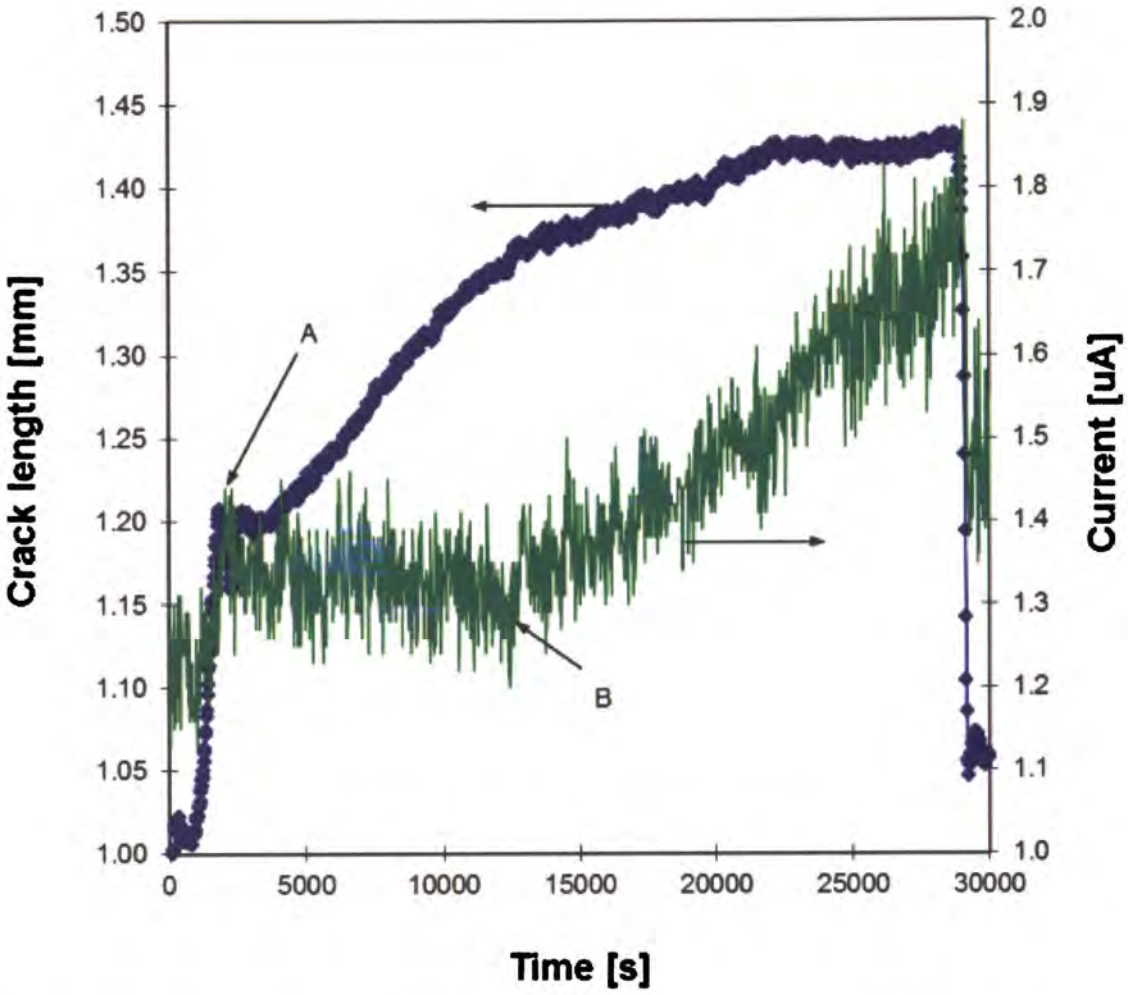

Figure 7-16. The measured crack length and the ZRA signal plotted against time for a sample exposed to 50% CO – 50% CO_2 at 25°C and a pressure of 800 kPa.

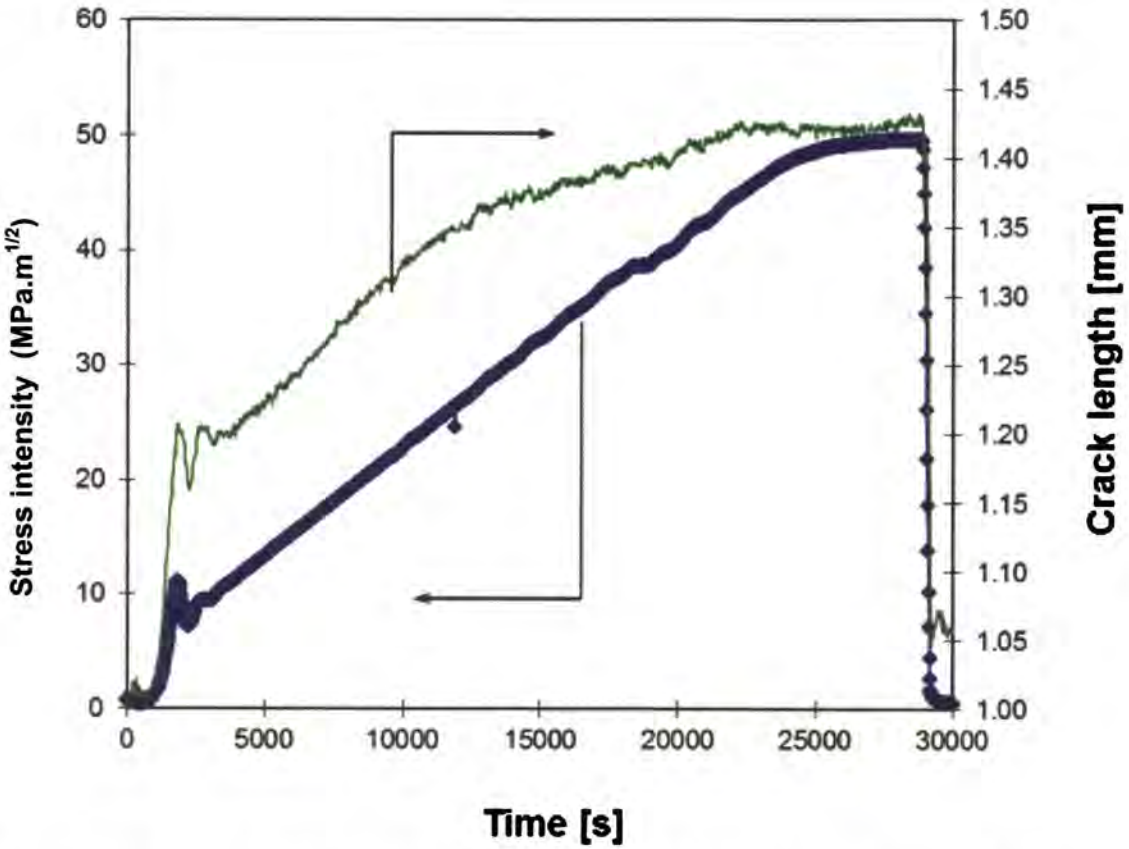

Figure 7-17. Stress intensity and the crack length plotted against time for a sample exposed to 50% CO – 50% CO_2 at 25°C and a pressure of 800 kPa.

The test was performed at 25°C, and the influence of loading rate on cracking was investigated, therefore the stress intensity was not constant. The measured crack length was therefore not the true crack length, because of the dependence of the measurements on the stress intensity. However, crack growth did occur when the crack length was more closely investigated, and it was also seen in the ZRA signal in Figure 7-16. At point A, the ZRA signal followed the increase in the crack length and the stress intensity and at point B there was an increase in the gradient of the ZRA signal.

7.3.5 ZRA signal response to variations in the stress intensity

In Figure 7-18 the stress intensity is shown against time together with the ZRA signal. The load control on the specimen became unstable and this lack of control caused an instability in the stress intensity. This instability at 40 MPa.m^{½} caused the amplitude and frequency of the ZRA signal to increase. The amplitude was raised from 0.08 µA to nearly 0.14 µA. After this incident of instability, the ZRA signal returned to its former dimensions.

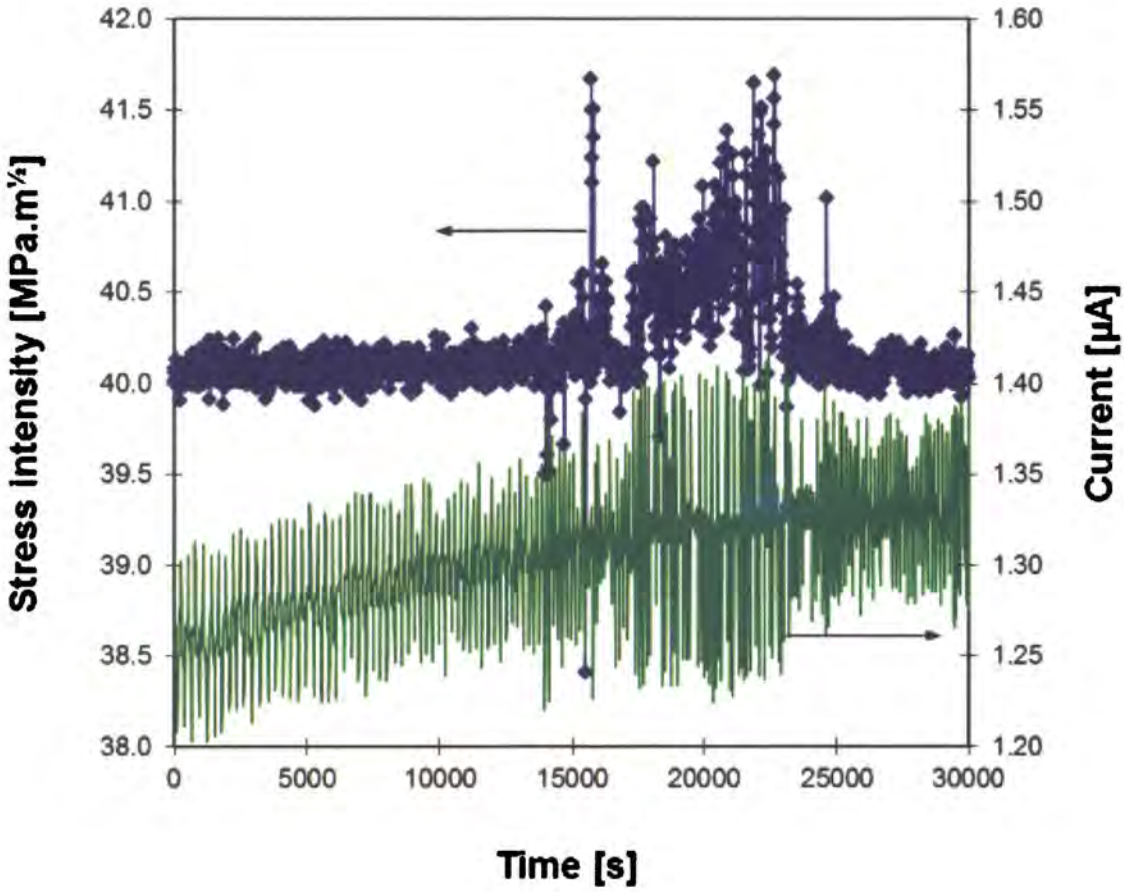

Figure 7-18. The stress intensity and the ZRA signal plotted against time for a sample exposed to 50% CO – 50% CO_2 at 45°C and a pressure of 800 kPa.

The ZRA signal in Figure 7-19 increased steadily from 2.4 to 2.65 µA as a result of a variance in the stress intensity. The stress intensity was held constant at

20.4 MPa.m^{½} and then it drops to 20.1 MPa.m^{½} and rises again to 20.4. At this point, a slight increase in the crack length was also seen.

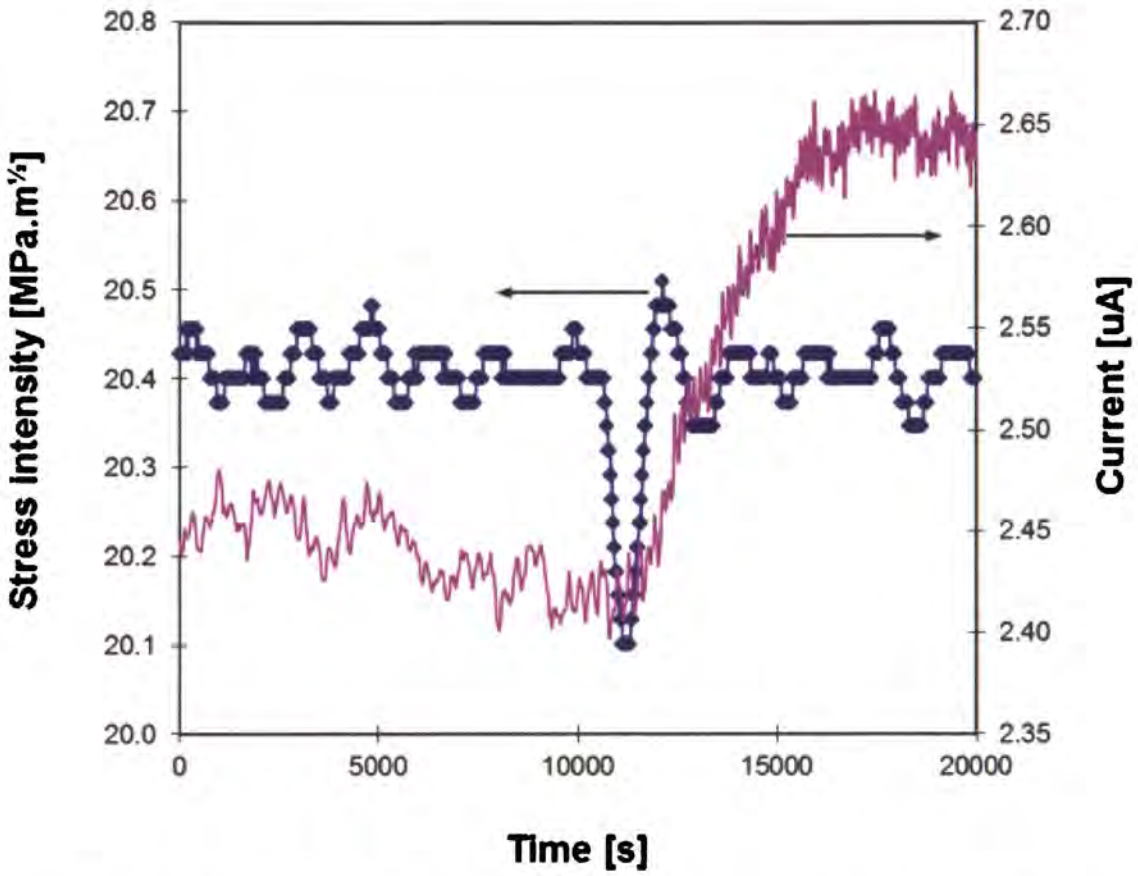

Figure 7-19. The stress intensity and the ZRA signal plotted against time for a sample exposed to 50% CO – 50% CO_2 at 45°C and a pressure of 800 kPa.

7.3.6 ZRA signal and the crack propagation rate

In Figure 7-20 the crack growth is plotted with a stress intensity of 15 MPa.m^{½}.

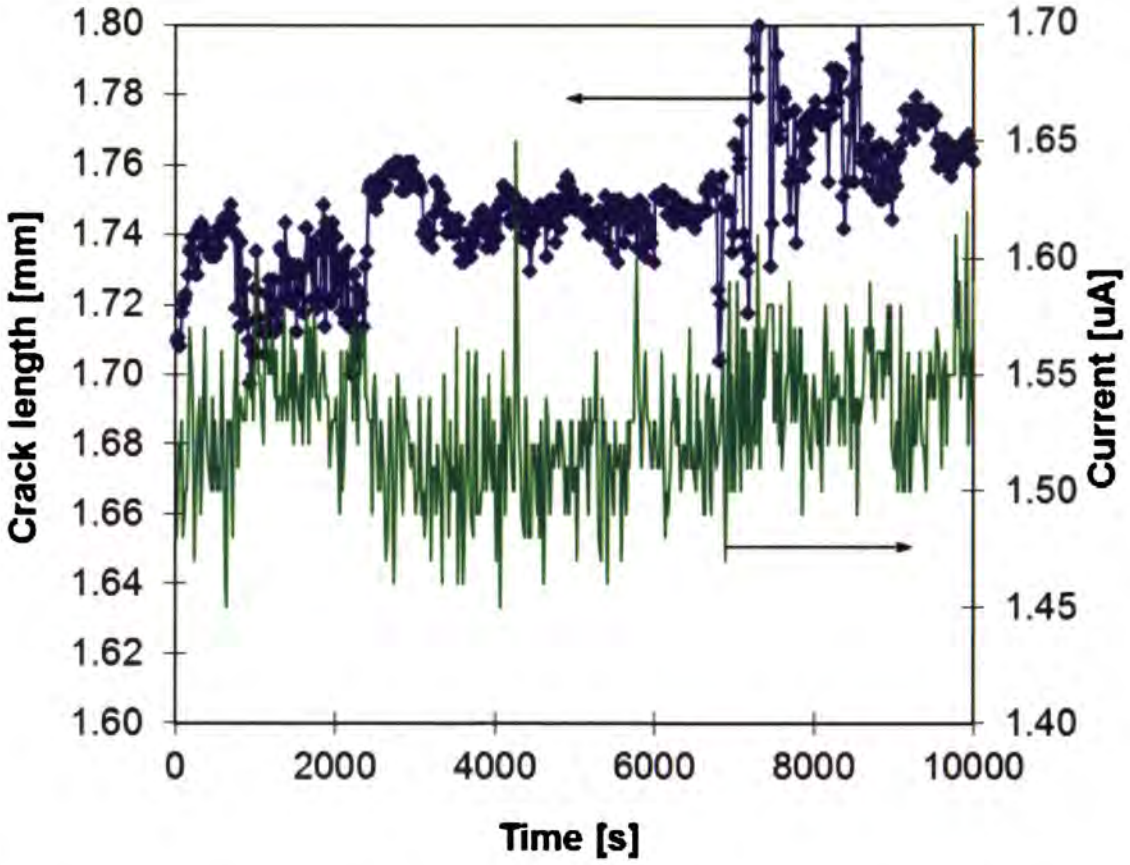

Figure 7-20. Crack length and the ZRA signal plotted against time, for a sample exposed to 50% CO – 50% CO_2 at 45°C and a pressure of 800 kPa.

The high crack growth rate at 25°C was due to the variance in the stress intensity which, was considered in Chapter 6. However, the ZRA signal is shown in Figure 7-20 together with the crack growth, and a polynomial function was fitted to the measured crack length. The measured crack length was differentiated to give the crack propagation rate and it was plotted against the ZRA signal as shown in Figure 7-21. The ZRA data did not change significantly in the order of 0,1 µA and was independent of the crack propagation rate. The crack propagation rate was in the range of 1 to $5x10^{-6}$ mms^{-1}.

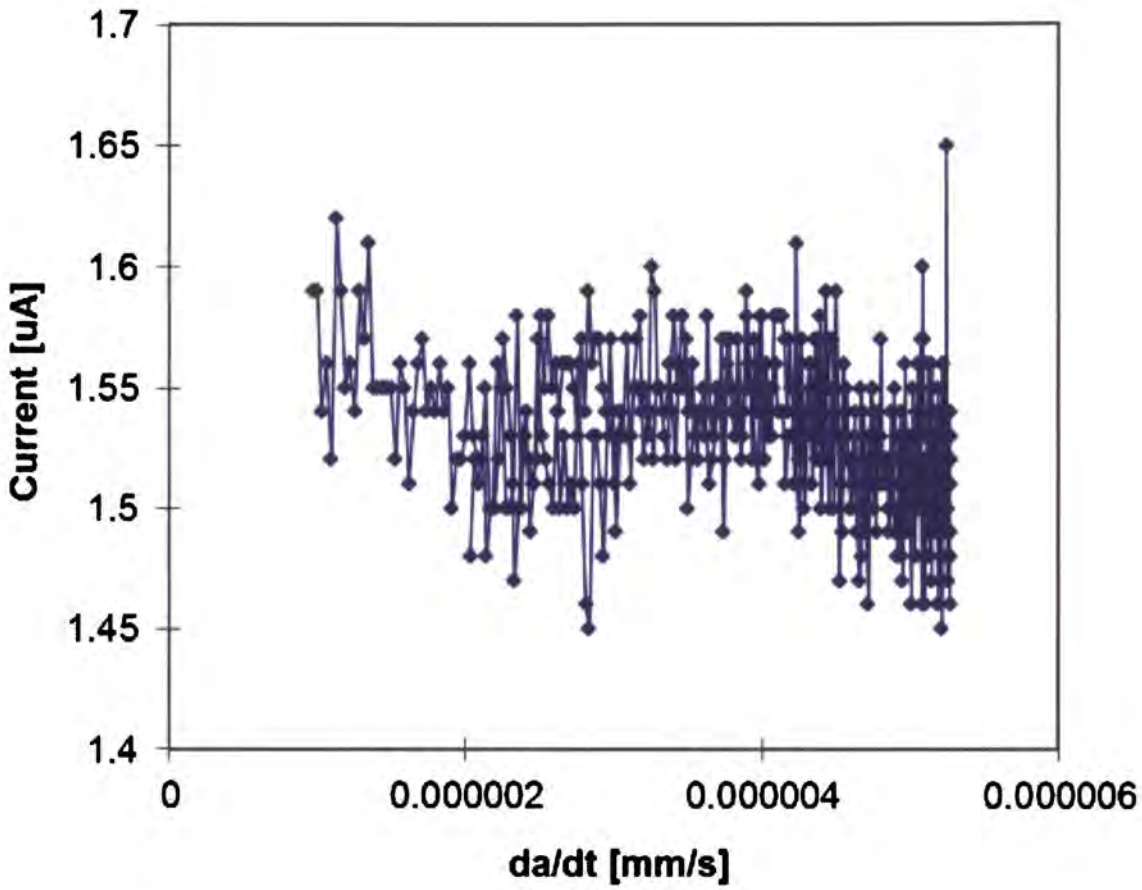

Figure 7-21. The ZRA signal plotted against the crack growth rate for a sample exposed to 50% CO – 50% CO_2 at 45°C and a pressure of 800 kPa.

In addition to this evaluation on the 50%CO-50%CO_2-H_2O environment and the response of current to the cracking process, the 1% CO gas mixture was initially investigated, but the current responses measured with a zero resistance ammeter showed a much smaller amplitude and were not further investigated.

7.4 Discussion

7.4.1 Compared to work of Manahan et al. [60]

If this particular system, steel exposed to CO-CO_2-H_2O, of stress corrosion cracking is to be compared with that which Manahan et al.[60] investigated, it is well to realise that it is two different systems and the mechanisms of cracking were not necessarily the same. This was indicated by the work of Hannah et al.[10], that the mechanism for cracking was different at high and low total pressures; at low pressures they proposed the hydrogen embrittlement model and at high pressures it seemed to follow the slip-step dissolution model or the hydrogen embrittlement model under cathodic control. However, considering the low strength of this steel and the very low stress intensity threshold for stress corrosion cracking hydrogen embrittlement is not a probable model. This means that the current response might take on different signals, depending on the type of reaction that takes place at the crack tip and this differs from the work done by Manaham and co-workers[60].

With the analysis of the given data the first question is whether the ZRA signal is at all significant. It would be very helpful to know whether the current response reacts to the change in stress intensity and its response to crack propagation rate, whether it would predict the crack propagation rate. It was shown that the current response that was measured could be correlated with the stress intensity, as well as the crack propagation and changes in these two parameters did cause the ZRA signal to respond accordingly. Therefore, the ZRA signal is significant, but to what extent is the next question. The meaning of current response its response to cracking is important and needs to be analysed. This would allow the current response to be used in an appropriate way to evaluate the cracking process.

The current responded to changes in stress intensity and the crack length in different ways which are:

a) the sudden increases and decreases of the mean value,

b) changes in the amplitude,

c) changes in the frequency,

d) the polarity and

e) the general gradient of the mean value of the ZRA signal.

The sudden increase of the ZRA signal as seen by Manaham[60] for the detection of the threshold value for cracking can be linked to this cracking system if the "slip-step dissolution model" is considered. This increase in the ZRA signal was due to the fracture of the passive layer at the crack tip as this is the only explanation for an increase when the stress intensity is raised. However, this would say that crack propagation occurs with the event of fracture of the passive layer according to the slip dissolution model. Therefore, the increase in the ZRA indicates the onset of crack propagation. The higher frequency of the ZRA signal indicated more events of rupturing of the adsorbed passivating layer that contributed to the overall crack growth. The higher amplitude might have indicated the extent of these events that took place at the crack tip. This higher amplitude seen in the work of Manahan et al. and was explained as higher crack growth after a period of incubation in which the crack had to propagate through the highly strained pre-cracked region. As the crack length exceeded this range, crack growth was easier and therefore the amplitude and the frequency of the ZRA signal increased beyond this region.

The sign of the ZRA signal indicated the nature of the process that was taking place at the crack tip and from this, the mechanism causing cracking could be established. It could be said that when the ZRA signal was positive the resultant reaction is anodic, and a cathodic reaction is typified with a negative ZRA signal, because of the flow of electrons to the cathode.

7.4.2 Factors that influenced cracking shown by the current response measurements

It appears that the crack propagation can be correlated by the ZRA signal or current measurements as a direct indication of the crack propagation. It was shown that the ZRA signal did not follow the crack growth, and the amplitude of the ZRA signal increased as cracking commenced, but there was not an increase in the gradient of the ZRA signal itself. If there would be any correlation the repeatability seems to be

poor, and dependent on a number of factors, such as the perfect conditions and alignment of the monitoring probe.

The determination of the stress intensity threshold for stress corrosion cracking is the important factor in the viability of the current response method. As it will be seen more clearly, the crack propagation depends not only on the stress intensity of the specimen, but also on the rate of increase in the stress intensity. With this in mind, it is more difficult to determine the stress intensity threshold at these conditions. However, the stress intensity threshold appears to be above 1,5 MPa.$m^{½}$ and below 7 MPa.$m^{½}$ as seen from the results in Figure 7-9. With the current response, it was possible to determine when cracking commenced and when it diminished. The crack length measurements fell in a band and crack propagation lower than 50 µm was more difficult to detect, therefore the current response measurements did give an indication of crack propagation that was more sensitive than the crack propagation measurement. It was seen that the crack propagation is not only dependent on the stress intensity, but the loading rate or the rate of increase of the stress intensity played an important role in crack growth, and this was seen by the current response measurements.

The variance in the stress intensity seemed to cause a greater possibility for cracking as the ZRA signal responded to this change. This response was due to the "fracture", or disruption, of the passive layer, because of an increased strain rate at the crack tip.

The current response measurements showed an increase even as the load was relaxed and the stress intensity dropped at a rate of 0.1 MPa.$m^{½}$/s. Therefore, cracking was enhanced even during unloading, which indicated a rate dependence of the crack propagation.

Based on the positive currents that were measured from the crack it would appear that in this system of cracking the only model of crack propagation was by slip step dissolution.

7.5 Concluding remarks

1. The current response measurements could be used to predict the threshold stress intensity for stress corrosion cracking, although the repeatability might be an issue.

2. The ZRA signal gave an indication of cracking that took place, but did not give a direct correlation of the crack growth.

3. Current response measurements could be used to highlight factors that indicate/identify cracking.

4. Where the crack length measurements could not be done accurately enough, the ZRA signal gave some indication whether cracking was taking place.

Chapter 8

8 MITIGATION OF STRESS CORROSION CRACKING

8.1 Introduction

The stress corrosion cracking can be mitigated by the addition of inhibitors. Berry and Payer[15] worked on stress corrosion cracking of pipeline steels undertaking screening tests of inhibitors for stress corrosion cracking in a 1 *N* Na_2CO_3 + 1*N* $NaHCO_3$. A whole range of inhibitors were tested at the potential of most severe SCC in the base solution. Those chemicals found to be effective were tested over a wide potential range to determine if they were true inhibitors or acted by simply shifting the critical potential range for SCC. They found several chromates, potassium silicate, and several phosphates were effective SCC inhibitors. Potassium bichromate inhibited cracking and although chromates are classified as "unsafe" corrosion inhibitors, where insufficient amounts accelerates corrosion, potassium bichromate was tested at low concentrations and no enhanced cracking was seen.

Heaver[70] worked on inhibitors that would specifically enhance the passivity of the steel, but the results were not satisfactory and only at 5000 ppm of Petrotec 1420 was cracking significantly inhibited.

Potassium bichromate as an inhibitor would not be the best solution for an industrial application, but it was selected here to investigate the required passivity to completely inhibit stress corrosion.

8.2 Experimental procedure

The slow strain-rate test technique was used as a screening test to establish whether any inhibition of cracking occurred or not for varying inhibitor concentrations. Tensile test samples were prepared for testing as described in chapter 3.

The tests were done in 25% carbon monoxide and 75% carbon dioxide at 800kPa and 45°C. Distilled water was used and was not de-aerated. This environment was

chosen as a sufficiently severe environment for stress corrosion cracking susceptibility, as was seen from the work in Chapter 3.

8.3 Resutls

8.3.1 Inhibitor concentrations

Tests were performed over a range of inhibitor concentrations from 10 to 1000 ppm potasium bichromate as shown in Table 8-1. No cracking occurred for the concentrations higher than 500 ppm $K_2Cr_2O_7$, severe cracking occurred for concentrations of lower than 80 ppm and above 100 ppm the cracking decreases dramatically.

Table 8-1. The results of the slow strain-rate tests performed in 25%CO-75%CO_2-H_2O at 45°C.

$K_2Cr_2O_7$ [ppm]	Elongation (%)	Reduction in area (%)
1000	29	70
100	31	70
87	22	42
73	19	26
60	20	23
30	19	38
10	16	30
200	20	44

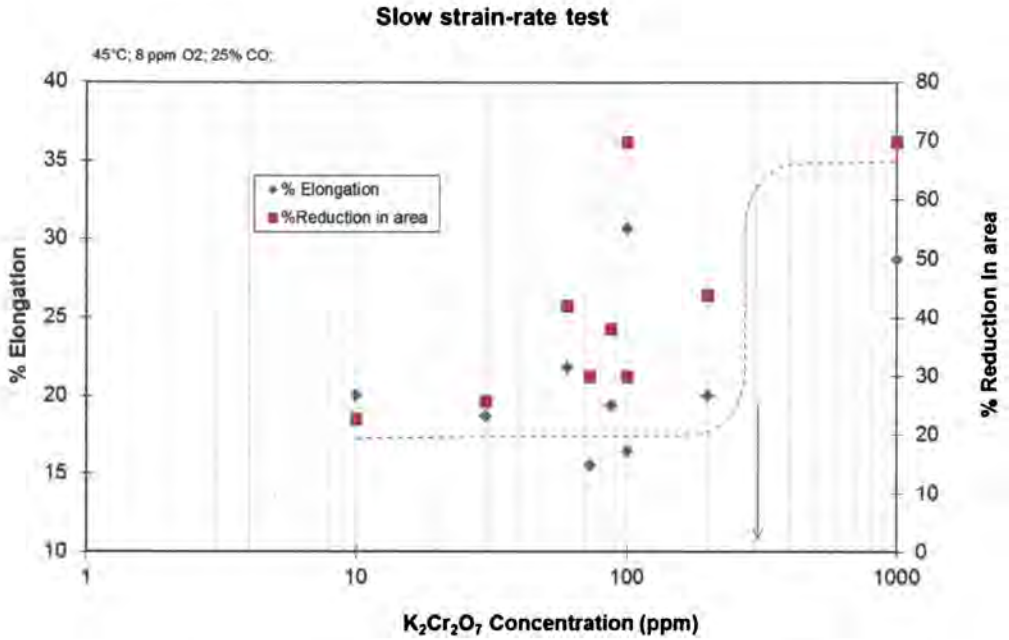

Figure 8-1. The results of slow strain-rate tests that was done at 45°C and 8 ppm O_2 with different potassium bichromate levels.

8.3.2 Polarisation characteristics

The influence of environment on the passivity of the steel was investigated by the use of polarisation characteristics in order to determine if this could give any insight into the cracking process as shown by Brown et al.[5]. Therefore, the extent of the passive region as well as the corrosion potential was investigated with varying concentrations of the appropriate inhibitor.

The water was not de-aerated and the same levels of potassium bichromate were used as for the slow strain rate tests. Additionally 0,007 N ClO_4^- was used to lower the solution resistance. A scan rate of 0,1 $mV.s^{-1}$ was used. In Figure 8-2 the polarisation characteristics are shown for both types of tests that were performed; those with inhibitor and those without. The polarisation characteristics of the A516 steel tested in varying degrees of added inhibitor are shown. The increased inhibitor concentration decreased the current density measured for the corresponding electrochemical

potential. However, the corrosion potential for these tests also increased with increasing inhibitor concentration. The decrease in the current density was significant for the inhibited steel.

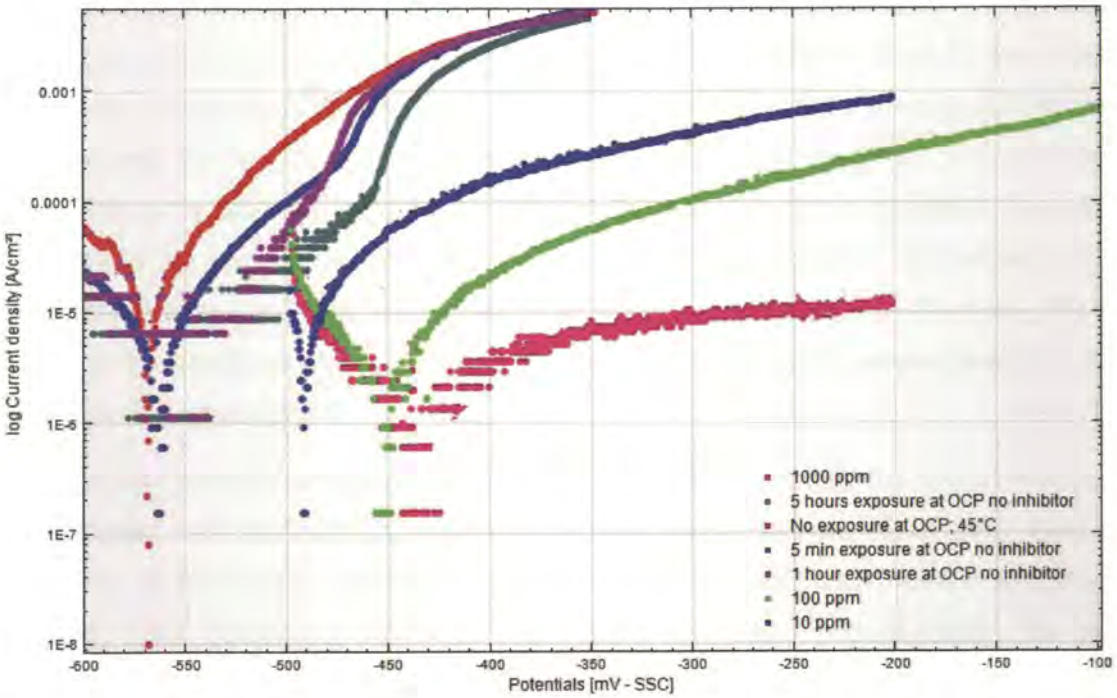

Figure 8-2. The polarization characteristics of a 25% CO gas mixture with varying amounts of inhibitor. The curves without inhibitor are same as those shown in Figure 4-7, performed in a low dissolved oxygen concentration.

8.4 Discussion

The inhibitors trials showed a remarkable increase in resistance to stress-corrosion cracking, after significant passivation had taken place.

Potassium bichromate was included as a classical passivator which means that the anodic reaction was greatly retarded, but it can also be classified as a mixed inhibitor because the cathodic reaction also was retarded. The reduction of bichromate ions only started at potentials more negative than -0,6 to -0,8 V, rather than at the values that might have been expected on the basis of the oxidation-reduction potential of the reaction:

$$Cr_2O_7^{2-} + 14H^+ + 6e^- \Leftrightarrow 2Cr^{3+} + 7H_2O. \quad \text{.....8-1}$$

The equilibrium potential of this reaction is $\varphi^0_{pH=0} = +1{,}33V$; however, the reaction proceeded with a large overpotential. The anodic polarisation of steel in a solution containing 0.1g/l of potassium bichromate was more negative than in the initial electrolyte. The rates of dissolution of steel at given potentials in the range 0.25 to 0.5 V, increased by two or three orders of magnitude, as a result of a preliminary adsorption of potassium bichromate (1.5 g/l or more) and the electrode potential remained in the passive region as the current density was reduced. The effect of the chromates was due to retardation of the rates of both electrochemical reactions, but in particular the anodic reaction. Thus, chromates can be classified electrochemically as inhibitors of the mixed type.

The inhibition process caused two reactions to take place. Firstly, the anodic reaction was inhibited, and secondly, the electrochemical potential was moved to more positive potentials. It would seem that both of these reactions are necessary for the mitigation process. The passivation observed from these tests was considerable. As the inhibitor concentration was increased by an order of magnitude, the level of the passivated anodic current density also decreased by almost an order of magnitude, to as low as $2x10^{-6}A/cm^2$ for an inhibitor concentration of 1000 ppm. As seen from the results of the slow strain-rate tests, no stress corrosion cracking was seen with potassium bichromate additions of more than 400 ppm, and it decreased with concentrations above 100 ppm. The necessity for crack inhibition was seen in the difference of these three polarisation characteristics. The polarisation characteristics of the steel that was introduced into the medium and held at the open circuit potential for a specific period showed a definite time dependence in the polarisaion characteristics.

However, from the work of Heaver[40] Petrotec 1420 was the only inhibitor that mitigated cracking effectively, although at a high concentration of 5000 ppm, the polarisation characteristics of this inhibitor showed that the corrosion potential was moved nearly 150 mV more positive. Whereas, for the other inhibitors that were tested, they influenced only the passivity of the steel in the solution, and not also the corrosion

potential. This could have polarised the steel out of the stress-corrosion sensitivity region.

The inhibiting properties of chromates consist not so much in a retardation of the reduction of oxygen, as in the ability to reduce the rate of the anodic reaction. This passivation reaction was strongly driven to inhibit the corrosion reaction on the surface of the steel as enhanced by the presence of carbonic acid. However, due to the fact that the chromate ions also acted as an inhibiting agent, the stress corrosion reaction was enhanced when inhibition did not occur completely. Thus, the reaction may even be aggravated in the presence of low concentrations of potassium bichromate, as indicated by polarisation of the anodic curve. In consequence, potassium bichromate was considered to be a dangerous inhibitor.

8.5 Concluding remarks

1. A concentration of more than 200 to 1000 ppm potasium bichromate is required to mitigate stress corrosion cracking of carbon steel in wet CO/CO_2 environments.
2. The passivation that occurred significantly lowered the passive current density.
3. The inhibition of stress-corrosion was achieved only after an order of magnitude reduction in the current density of the passive region.

Chapter 9

9 SLOW STRAIN-RATE AND C-RING ANALYSES OF THE SUSCEPTIBILITY OF CARBON STEEL EXPOSED TO INDUSTRIAL APPLICATIONS

9.1 Introduction

9.1.1 Introduction - SSRT

The stress-corrosion cracking of carbon steel in CO-CO_2-H_2O investigated here correlates directly with industrial environments related to the petrochemical industry in South Africa. The gas conditions investigated in this study can be applied in a number of similar conditions where carbon monoxide and carbon dioxide are present to cause the type of cracking that have been studied here. In the petrochemical industry, water is contaminated by the combustion of coal, which causes the formation of a by-product water which either contains a carbon monoxide rich concentration at around 13% or a leaner gas mixture with the carbon monoxide at around 3%, with the balance made up of mostly carbon dioxide, but also other contaminants such as HCN that could also contribute to passivation of the steel and cracking, Buchholtz and Pusch[71] have attributed the cyanide ion with causing transgranular stress corrosion in carbon steels. This chapter will consider the effect of stress conditions in these two industrial applications by studying C-ring specimens. In the first application, the leaner by-product water was to be introduced as a cooling agent. However, with the presence of carbon monoxide and carbon dioxide, it was expected that carbon steel would be susceptible to stress-corrosion cracking. This was due to previous plant experience where equipment had failed after exposure to this environment, and because this water by-product also contains traces of HCN that would further enhance the susceptibility to cracking. However, at an operating temperature of 90°C, the likelihood of cracking was low as demonstrated in Section 3.4.4 for samples evaluated in only water with carbon monoxide and carbon dioxide. Thus, a slow strain-rate test was

initially performed to establish the baseline for sensitivity to cracking. The slow strain-rate test was selected as the starting point to evaluate the steel in these environments, because of its relatively fast evaluation procedure. It was expected that in these environments a protective film would also form on the surface of the steel.

To summarise, the stress corrosion was studied in the leaner water by-product as well as the carbon monoxide 'rich' water by-product. Slow strain-rate tests were only performed in the leaner water by-product, and the influence of stress was evaluated with constant strain tests for both gas concentration conditions.

9.1.2 Lean gas by-product water

The corrosion resistance of carbon steel in lean gas by-product water was in question because of the proposed use of this by-product water as a cooling medium in a certain section of the plant. Carbon steel is likely to show cracking in lean gas by-product water because of a number of factors that usually contribute to cracking in a system. Firstly, the carbon steel is protected from high corrosion rates by the presence of a passive layer that forms on the surface of the steel. This is why the corrosion rate of the carbon steel in lean gas by-product water is low. The passive layer that exists in lean gas by-product water consists of carbon monoxide and cyanide that adsorbs onto the surface of the steel as discussed in Chapter 2. Carbon monoxide possesses an electronic structure similar to cyanide, and it is a reproducing complexing ligand, and bonds with the metal atom via the carbon atom. The weak electron donor properties of the molecule and the vacant orbitals of the metal are involved. Secondly, the Lean gas by-product water also contains other components that will increase the corrosion rate of the carbon steel once the passive layer has been broken by emerging slip steps on the solution-steel interface. The components that enhance the corrosion process are carbonic acid and chloride ions.

It was therefore expected that cracking would occur and it was necessary to determine the actual stress dependency of the cracking process, because when a structure is welded, the residual stresses can be in the order of the yield strength of the material.

However, with post weld stress relieving heat treatments, it is possible to lower the stress levels of the steel. Therefore, in order to establish the necessity of stress relieving of the welded section, it was decided to undertake tests that would indicate the stress corrosion cracking susceptibility of the steel at a range of stress levels. The C-ring test was chosen for the evaluation of the influence of stress on the susceptibility to cracking. This test is a constant deflection, or constant strain test, which means that the strain on the specimen remains constant, while the stress would change during crack propagation. The initial stress of the specimen was known, but when the sample cracked the stress at the crack tip was lowered. Therefore, is it only possible to work from a maximum stress which correlates with the initial pre-loaded stress on the C-ring.

9.1.3 Rich gas by-product water

The stress corrosion cracking resistance of carbon steel was also evaluated in by-product water containing the richer gas mixture, in a similar way as with the constant strain tests. However, in this instance, a more thorough procedure was followed in order to determine the extent of cracking and the crack initiation, as well as propagation rates with time related to stress levels.

Carbon steel is likely to show cracking in this rich gas by-product water for the same reasons as the lean gas by-product water.

Stress-corrosion cracking occurs as a result of the combination of a stressed structure exposed to a specific environment which is dependent upon the material used for the structure. If the stress is removed from the structure the cracking process will be terminated.

During the installation of pipelines the structure is welded and during welding residual stresses are induced which contribute to the cracking process. By reducing these stresses through post-weld heat treatments it has been believed that the cracking process can be limited and mitigated. However, throughout this study, it was shown that cracking occurred at very low stress levels, and to further evaluate this, the stress conditions were carefully determined and evaluated.

It was necessary to determine the actual stress dependency of the cracking process, because when a structure is welded, the residual stresses are in the order of the yield strength of the material. However, with post-weld stress relieving heat treatments, it is possible to lower the stress level of the steel. Therefore, in order to establish the necessity and the degree of stress relieving of the welded section, it was decided to do tests that would indicate the stress corrosion cracking susceptibility of the steel at a range of different stress levels. The C-ring test was again chosen for the evaluation of the influence of stress on the susceptibility to cracking. The initial stress of the specimen is known, but when the sample cracks the stress at the crack tip is lowered. Therefore, is it only possible to work from a maximum stress that correlates with the initial stress of the C-ring, and so this testing procedure is more valuable with regard to crack initiation, since the stress threshold for crack initiation can be established.

9.2 Experimental

9.2.1 Experimental setup - SSRT

A test was performed in air to simulate the normal properties of the material when stress corrosion cracking had no influence. The other tests were performed inside an autoclave. A schematic drawing of the experimental setup is shown in Figure 9-1. A schematic drawing of the sample is shown in Figure 9-2. A sample of the CO-rich by-product water was taken from the plant in a sampling bomb. In order to maintain the pressure that was seen in the plant the by-product water was pressurised with nitrogen to a pressure of 900 kPa. Nitrogen was used as it is an inert gas that does not affect the corrosion process. The autoclave with the sample was heated with a heating element wrapped around it and the temperature was measured with a J-type thermocouple. This setup simulates stagnant by-product water at 900 kPa. The sample was tested in this environment at a strain rate of 10^{-6} s^{-1}, chosen as a proven strain rate to simulate severe stress-corrosion cracking conditions.

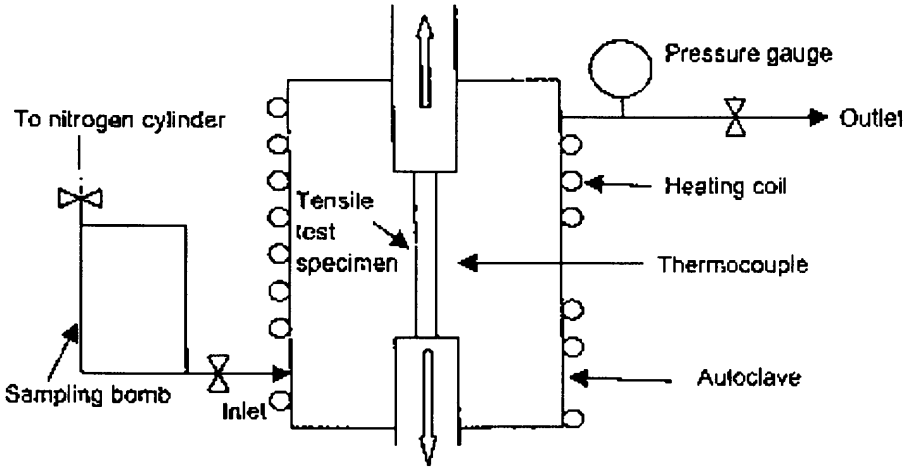

Figure 9-1. Experimental setup that was used for the slow strain rate tests.

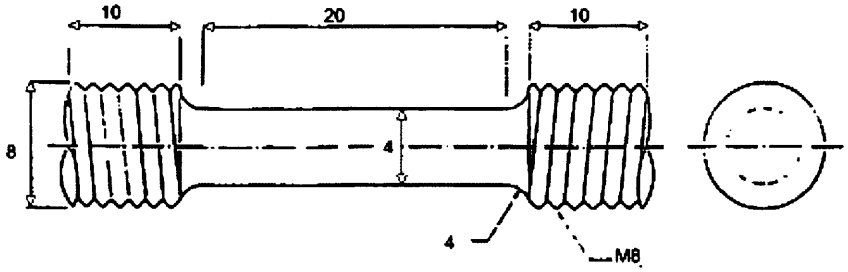

Figure 9-2. Schematic drawing of the sample.

From the initial and final gauge lengths and diameters the % elongation and % reduction in area can be determined as described in Section 2.12.1.

9.2.2 Experimental procedure - Lean gas by-product water

It was decided to stress the C-ring specimens at different stress levels in order to establish the effect of stress on the cracking process. With these results, it would have been possible to establish whether a residual stress level below which no cracking will

occur, existed. The tests that were proposed are shown in Table 9-2, for not welded specimens and Table 9-2 for welded specimens. The yield strength of the carbon steel pipe used in the test was measured at 361 MPa.

Table 9-1. Stresses applied to the C-ring specimens.

Sample no.	Stress level (% yield strength)	Stress level (MPa)
C1	100	361
C2	90	325
C3	79	285
C4	68	242
C5	56	202
C6	42	152
C7	30	108
C8	20	72

Table 9-2. Stresses applied to the welded C-ring specimens.

Sample no	Stress level (% yield strength)	Stress level (MPa)
W1	80	289
W2	65	235
W3	50	181
W4	35	126

The specimens were tested in autoclaves at 90°C and a pressure of 900 kPa to simulate the plant conditions. The pressure was achieved by introducing nitrogen gas into the system, which is an inert gas that does not interfere with the electrochemical reactions. The initial test ran for 300 hours, after which the specimens were examined and replaced in the autoclaves for another 300 hours, and again examined and replaced for 400 hours. After the cumulative 1000 hours that the samples were immersed in lean gas by-product water, they were investigated using an optical and scanning electron microscope. The samples underwent a magnetic particle test to detect any possible surface cracking.

9.2.3 Experimental procedure – Richer gas by-product water

The samples were sectioned according to ASTM G48 and the outer surface was polished to a 1 micron finish. A strain gauge was mounted on the convex surface at the centre between the bolt holes, with the strain gauge oriented to measure the hoop stress. Each C-ring was individually stressed and the stress measured with the strain gauge. When the desired stress was reached, the nuts were fastened and secured in place to ensure that it would not be loosened during the exposure.

The stress levels for the C-ring specimens are shown in Table 9-3. A tensile test was performed on the particular steel pipe sample that was used, and the yield strength of the carbon steel pipe used in the test was measured at 322 MPa. Three samples were used per pre-stress level these were exposed for, 465 h, 816 h and 1,272 h respectively. This was done to ensure that samples could be removed after each period, and then sectioned and examined for the crack length. The sectioned samples were not further exposed to the environment. This introduced some error into the experiment, because it was not the same crack that was investigated from the initial exposure, but three different samples with three different cracks.

Table 9-3. Stresses applied to the C-ring specimens exposed to the richer gas by-product water.

Sample no	**Pre-stress level**	**Stress**
	(% of yield strength)]	(MPa)
S1,M1,L1	100	321
S2, M2, L2	90	289
S3, M, L3	80	255
S4, M4, L4	70	225
S5, M5, L5	60	193
S6, M6, L6	50	161
S7, M7, L7	40	128
S8, M8, L8	30	96
S9, M9, L9	20	64

The specimens were tested in autoclaves at 65°C and a pressure of 900 kPa. The pressure was achieved by nitrogen gas as an injection system, which is inert, without interfering with the electrochemical reactions.

The samples underwent a magnetic particle test to detect any possible surface cracking before being subjected to the microscopic evaluation.

9.3 Results and Discussion

9.3.1 Results - SSRT

The results of the test done in air, as well as the tests done at 90°C and 50°C are shown in Table 9-4.

Table 9-4. The results of the tensile tests.

Sample no	Environment	Temperature	Gauge Length	Diameter	Final Length	Final diameter
		(°C)	(mm)	(mm)	(mm)	(mm)
1	Air	25	20	4	25.5	2.45
2	SGL	90°C	20	4	23.2	3.4
3	SGL	50°C	20	4	23.76	3.15

The results are shown in Table 9-5. The elongation and reduction in area of the specimen tested in Lean gas by-product water at 90°C was well below that of the specimen tested in the air.

Table 9-5. The elongation and reduction in area of the tested samples.

Temperature	Environment	Elongation	Reduction in Area	Elongation index to SCC	Reduction in area index to SCC
(°C)		(%)	(%)	(%)	(%)
25	Air	27.5	62.5	1.00	1.00
90°C	By-product water	16.0	27.8	0.58	0.44
50°C	By-product water	18.8	38.0	0.68	0.61

The index to stress corrosion cracking gave an indication of how susceptible the steel was to stress-corrosion cracking in the environment tested. The sample tested in air and the samples tested in Lean gas by-product water at 90°C are shown in Figure 9-3.

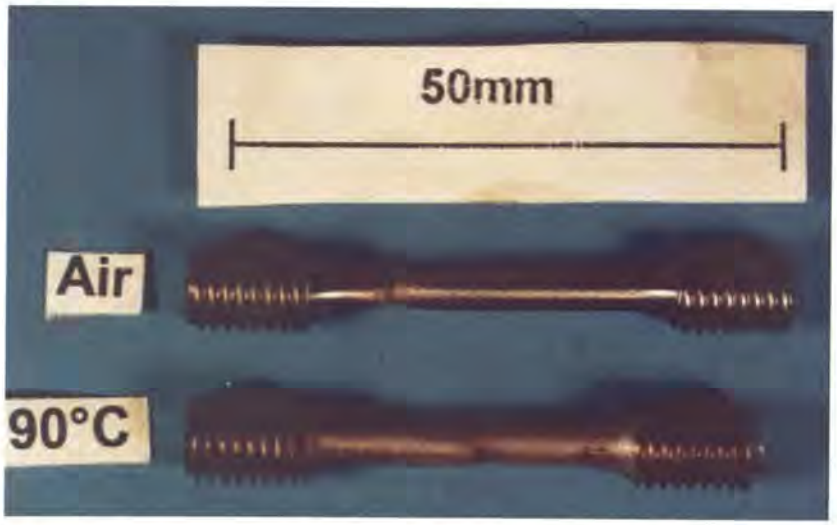

Figure 9-3. Comparison of the slow strain-rate test sample exposed to the by-product water at 90°C with a sample stressed in air where no stress-corrosion occurred.

Note the marked difference in elongation on the two samples indicated in Figure 9-3, illustrating the effect of stress-corrosion cracks. The stress-strain curves for the three tests are shown in Figure 9-4. Surface cracks were found on the sample tested in the by-product water at 90°C.

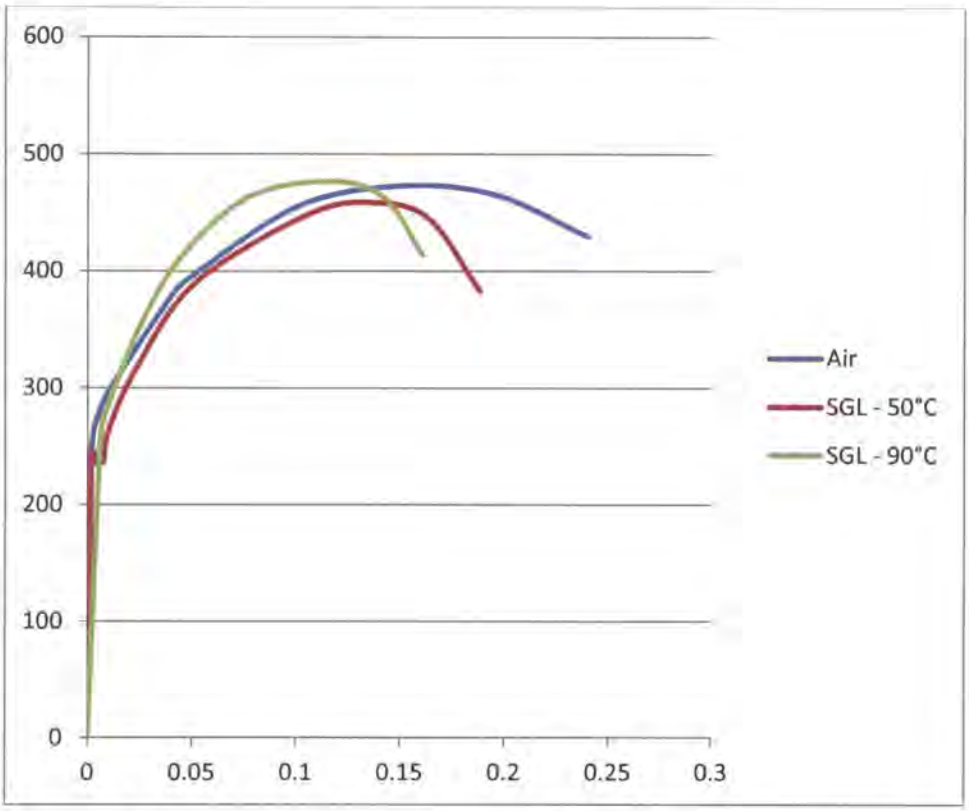

Figure 9-4. Slow strain-rate test results for the samples tested in by-product water at 50°C and 90°C.

Note the sample evaluated at 50°C failed after slightly lower total strain than the sample evaluated at 90°C. This is in contrast to trend of the results found earlier, shown in section 3.4.4, where the stress corrosion was evaluated only up to 75°C, but the trend of those results showed that the most severe stress-corrosion was found around 40°C to 50°C.

9.3.2 Discussion - SSRT

From the results of the two tests performed, it can be seen that the carbon steel was susceptible to stress-corrosion cracking in by-product water at 90°C, as well as at 50°C. It is difficult to give an exact measure of the susceptibility of the steel, but it is clear from the index to stress corrosion cracking that the carbon steel was susceptible to stress corrosion cracking in this medium. Although the reduction in area and the elongation were not exactly the same, the index to stress corrosion cracking susceptibility calculated from these two parameters was lower for the test done in by-product water at 90°C than at 50°C. These results indicate that the stress corrosion cracking of the steel is enhanced with an increase in temperature. This is contrary to what was expected originally from the test results shown in section 3.4.4. The explanation for this phenomenon might be the more significant influence of cyanides than that of carbon dioxide and carbon monoxide. Cotton and Wilkinson[33] found that the cyanide ion possesses an electron donor property and complexing ability similar to that of carbon monoxide. Therefore, the ion appears capable of adsorption and inducing stress corrosion cracks similar to carbon monoxide and with the presence of both components in the environment it would be possible to increase the susceptibility as seen here. For stress corrosion cracking of carbon steel in carbon dioxide-carbon monoxide environments, temperature plays a prominent role due to the fugacity (solubility) of the gasses at higher temperatures as seen in section 3.4.4, (however, note that temperatures only up to 75°C were tested, but the trend showed that at higher temperatures the severity of cracking decreased).

9.3.3 Results – Lean gas by-product water

9.3.3.1 Magnetic particle test

The specimens that were welded did not show any cracking, while the specimens that were not welded did show cracks. The results of the magnetic particle tests conducted on the samples are in Table 9-6 and Table 9-7, and the pictures of the C-ring samples after 1 000 hours are shown in **Error! Reference source not found.**.

Table 9-6. Stressed C-ring specimens that showed cracking after 300 hours and 1,000 hours exposed to lean gas by-product water at 90°C.

Sample	C-ring specimen stress (MPa)	% yield	Outcome after 300 hours exposure	Outcome after 1,000 hours exposure
C1.	361	100	No cracks	Cracks
C2.	325	90	No cracks	Cracks
C3.	285	79	Cracks	Cracks
C4.	245	68	No cracks	Cracks
C5.	202	56	Cracks	Cracks
C6.	152	42	Cracks	Cracks
C7.	108	30	Cracks	Cracks
C8.	72	20	No cracks	Cracks

Some of the samples showed only one prominent crack whereas others showed two or more surface cracks as shown in **Error! Reference source not found.**.

Table 9-7. Stressed welded C-ring specimens that showed no cracking after 300 hours as well as 1 000 hours exposed to lean gas by-product water at 90°C.

Sample	C-ring specimen stress (MPa)	% yield (%)	Outcome after 300 hours exposure	Outcome after 1 000 hours exposure
C1.	289	80	No cracks	No cracks
C2.	235	65	No cracks	No cracks
C3.	181	50	No cracks	No cracks
C4.	126	35	No cracks	No cracks

The absence of cracking on the welded samples was seen for the samples exposed to both 300 hours as well as 1 000 hours.

9.3.3.2 Optical microscopy and scanning electron microscopy

The surfaces of the C-ring specimens were examined under the stereo microscope and the results are shown in **Error! Reference source not found.**. In Figure 9-5 two cracks are shown for the specimen tested at 20% yield strength.

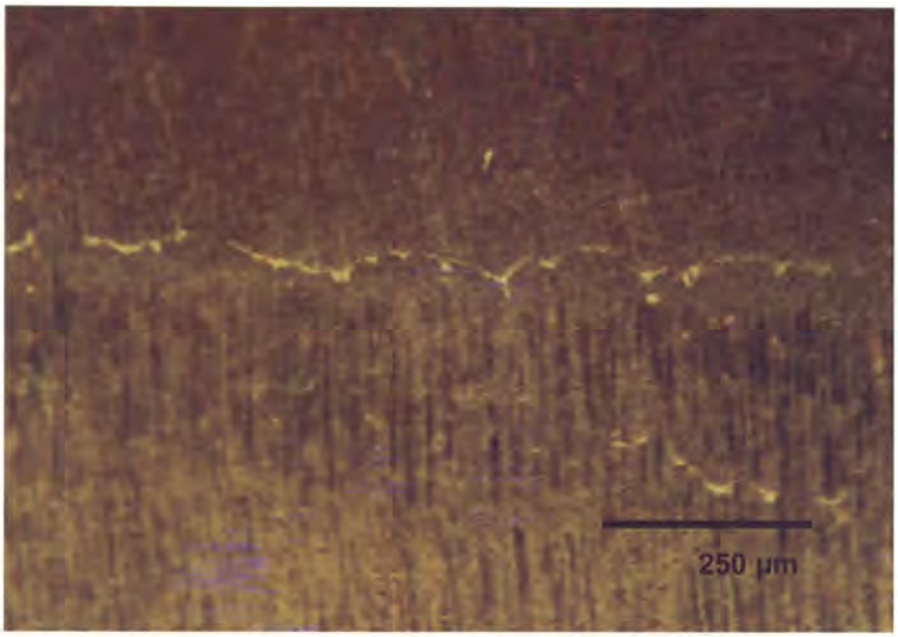

Figure 9-5. Two cracks found on the specimen stressed to 20% of the yield strength.

On the other unwelded specimens stressed at 30%, 42%, 56%,68%, 79% and 100% of the yield strength, cracks were found after 1 000 hours, as shown in **Error! Reference source not found.**. Only the 90% stressed specimen showed no evidence of cracking.

9.3.3.3 Cross sections of the cracks

Cross sections of the C-ring specimens were made, and the depths of the cracks that were seen on the surface were measured. These cracks are shown in Figure 9-6 to Figure 9-12. The depths of these cracks are presented in Table 9-8, together with the crack propagation rates of the cracks.

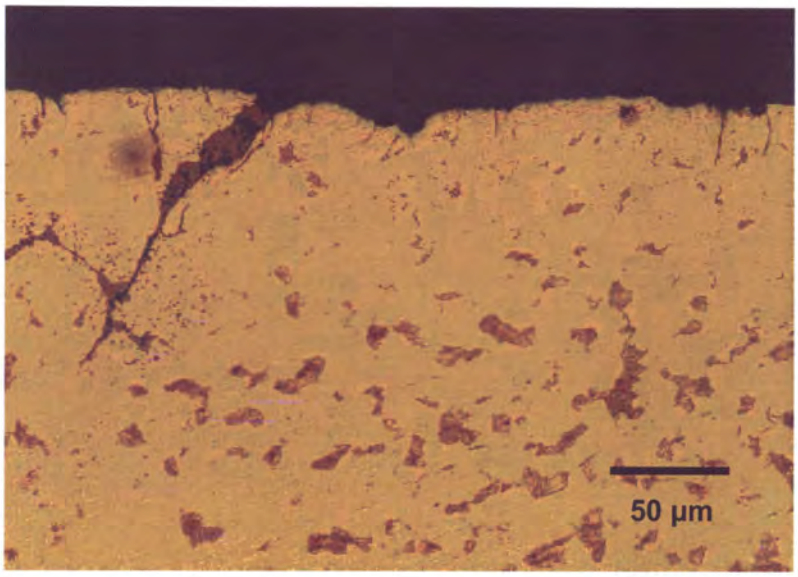

Figure 9-6. Cracks on the specimen stressed to 20% of the yield strength exposed to leaner gas by-product water for 1,000 hours, showing cracks.

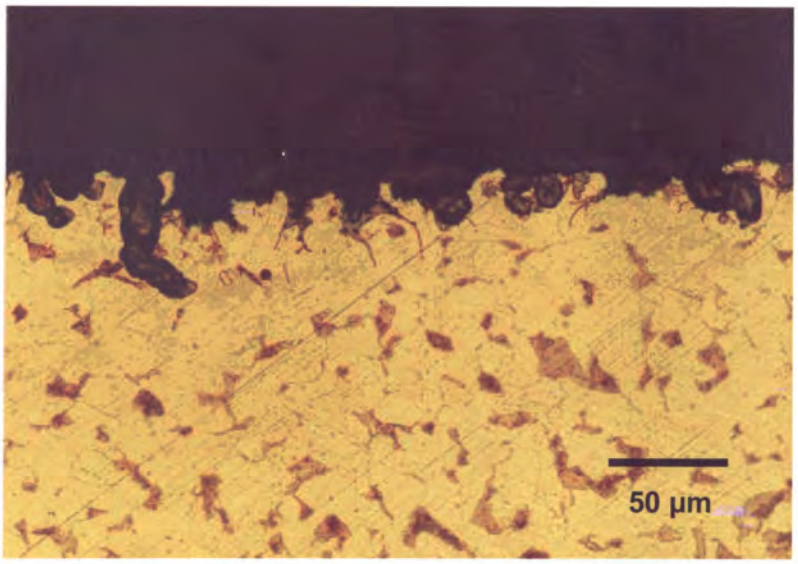

Figure 9-7. Pitted surface of the specimen stressed to 20% of the yield strength exposed to leaner gas by-product water for 1,000 hours, showing cracks.

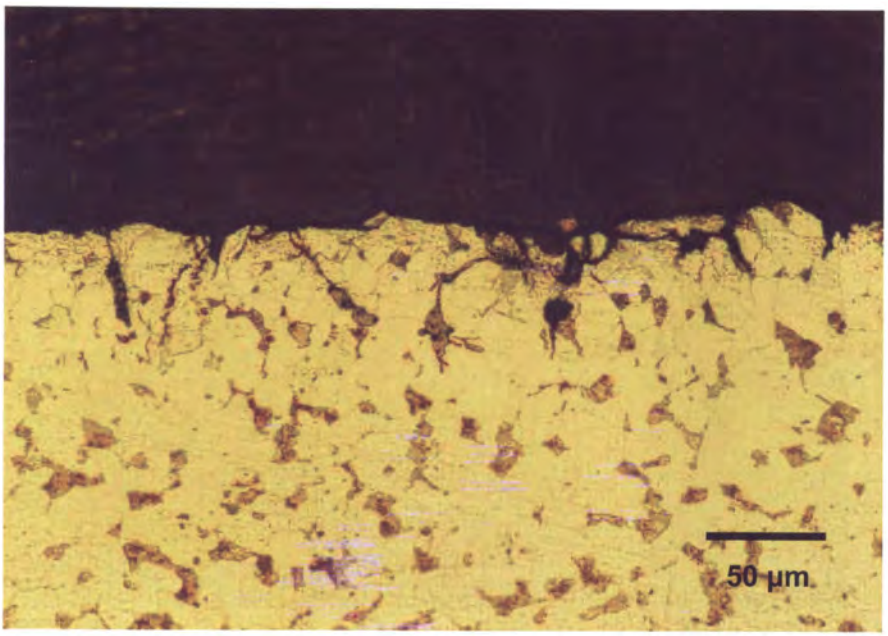

Figure 9-8. Cracks on the specimen stressed to 30% of the yield strength exposed to leaner gas by-product water for 1,000 hours, showing cracks.

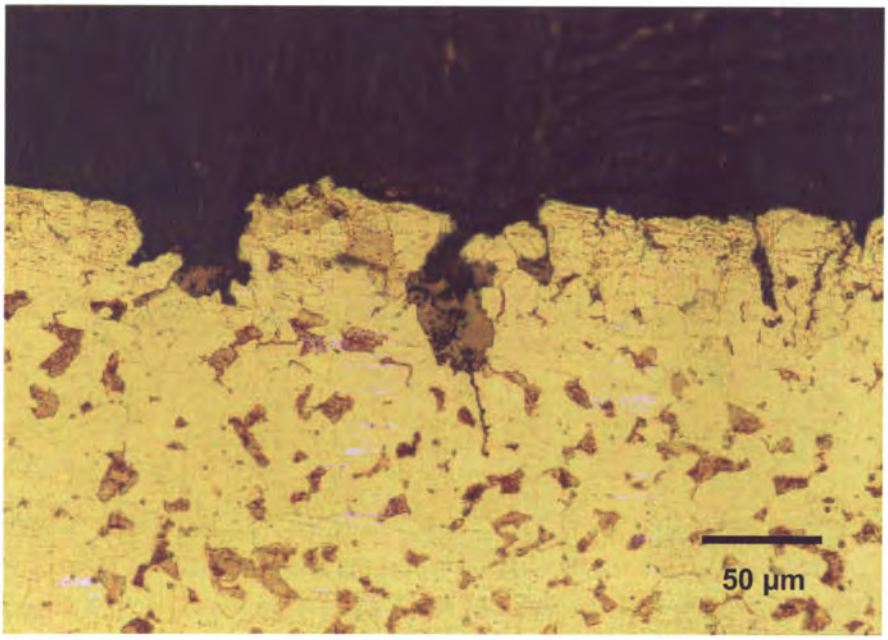

Figure 9-9. Cracks on the specimen stressed to 30% of the yield strength that initiated from a pit exposed to leaner gas by-product water for 1,000 hours.

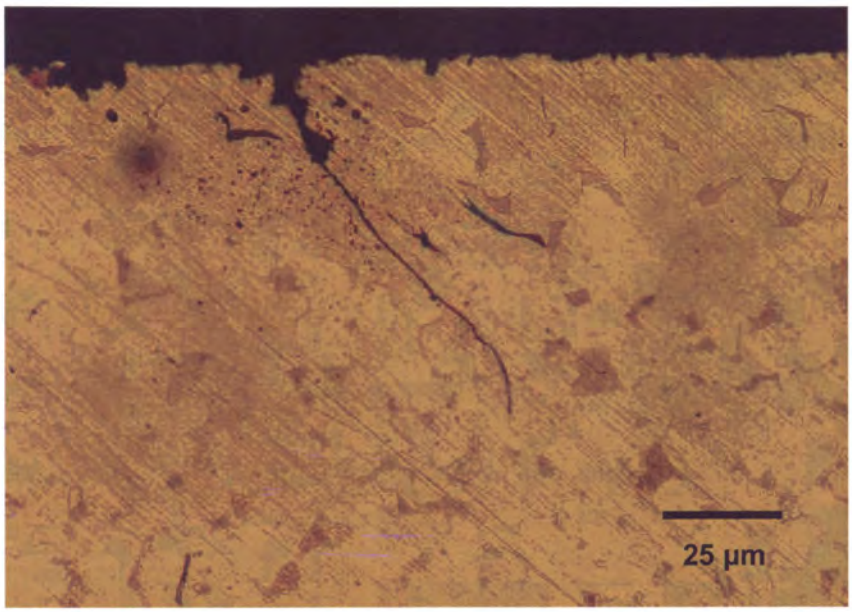

Figure 9-10. A crack on the specimen stressed to 42% of the yield strength exposed to leaner gas by-product water for 1,000 hours.

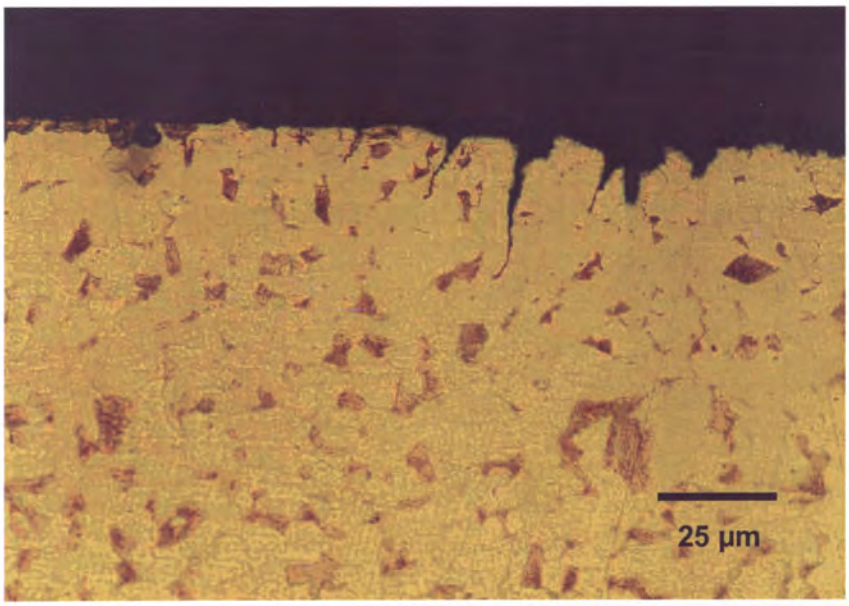

Figure 9-11. Cracks on the specimen stressed to 79 % of the yield strength exposed to leaner gas by-product water for 1,000 hours.

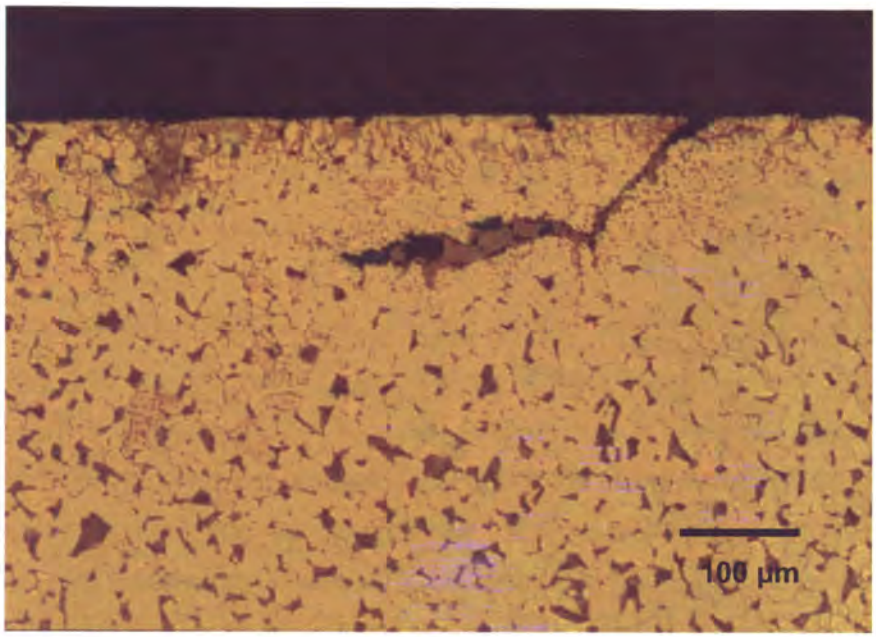

Figure 9-12. A crack on the specimen stressed to 100% of the yield strength exposed to leaner gas by-product water for 1,000 hours.

Table 9-8.The measured crack lengths and corrosion rates on the C-ring specimens.

Sample no.	Stressed to % yield strength (%)	Measured crack length (µm)	Crack propagation rate as calculated over 1,000 hours ($m.s^{-1}$)
C1.	100	40	$1.11x10^{-11}$
C3.	79	130	$3.61x10^{-11}$
C6.	42	130	$3.61x10^{-11}$
C7.	30	40	$1.11x10^{-11}$
C8.	20	120	$3.33x10^{-11}$

Error! Reference source not found. shows a fine crack that was found on the specimen stressed to 20% of the yield strength. Also seen on this specimen were small pits, as shown in **Error! Reference source not found.**. Cracks that were found on the specimen stressed to 30% of the yield are shown in **Error! Reference source not found.**, and in **Error! Reference source not found.**, a crack is shown that initiated from a pit. A crack found on the specimen stressed to 42% of the yield strength is shown in **Error! Reference source not found.**. A crack found on the specimen stressed to 79% of the yield strength is shown in **Error! Reference source not found.** with several smaller cracks also originating in the same area. A crack found on the specimen stressed to 100% of the yield is shown in **Error! Reference source not found.**, this crack grew perpendicular to the C-ring surface, and then grew parallel to the surface, which does seem contrary to what is expected.

9.3.4 Discussion of lean gas by-product water results

All the unwelded specimens showed some degree of cracking. The threshold stress found for the unwelded specimens, according to these results, was more than the yield point, but this should not be considered as an accurate representation of the susceptibility to cracking. It is possible that the residual stress condition was such that it actually inhibited the cracking of these welded samples.

Figure 9-13 show the measured crack propagation as a function of the initially applied stress, and it is clear that the applied stress did not influence the crack propagation rate significantly, the crack propagation rate remained constant.

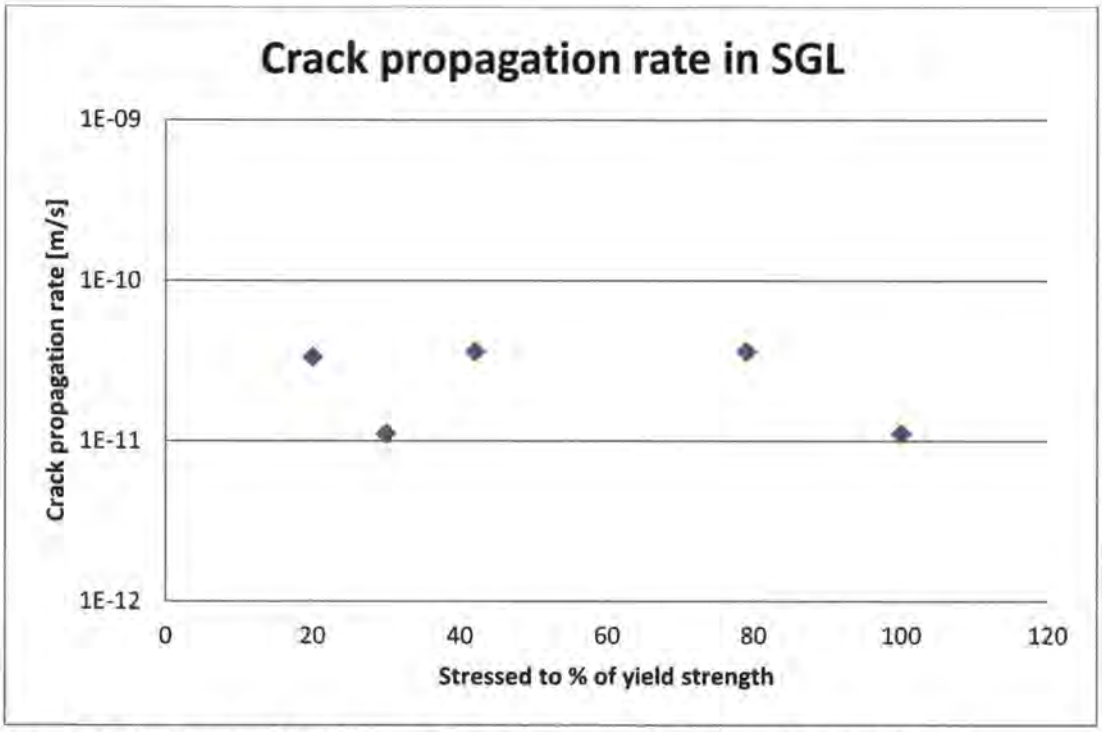

Figure 9-13. Relationship between the crack propagation rate and the initial stress.

It has to be remembered that the stress-corrosion cracks that formed during the slow strain rate test, formed at a much faster strain-rate than those that formed during the C-ring test. As seen from the previous results in the foregoing chapters, cracking of the steel was more dependent upon the straining of the specimen than the stress. The straining of the surface therefore enhanced the cracking process. The cracking process was also rate dependent, which meant that a critical strain-rate exists for greater sensitivity to cracking. Therefore, the strain rate at which these C-rings were exposed to was probably less than this critical strain rate. The strain rate of the slow strain-rate test was again above the maximum, and also did not show the maximum crack propagation rates that can be achieved. This is in according to tests shown in Chapter 6, regarding the strain-rate. This maximum strain-rate was in the order of 10^{-7} s^{-1} to 10^{-8} s^{-1}, and the slow strain-rate test was done at a strain-rate of 10^{-6} s^{-1}. The strain-rate that will be experienced on the pipelines is difficult to quantify, and would probably be closer to the strain-rates that were found on the C-ring specimens. However, fluctuations in the stress levels in the pipelines at a low frequency would also

give a slow strain-rate. The crack propagation rates that were measured are very low, and would not be of great concern, even over the long term. It is also possible that the cracks arrested during the test. However, the crack propagation rate that was found previously (Section 9.3.1) on the slow strain-rate test was high enough to be of concern. The welded C-ring specimens did not show any sign of cracking. This could have been due to a different metallurgy that was induced by the welding process, or because of the difference in the strain-rate that was found at a specific stress, or as mentioned the state of stress before stressing the samples in the form of residual stresses. The heat affected zone should not be of concern, because the samples evaluated for the cyclic stresses in Section 5.3.3.2, actually showed a sensitivity to crack initiation.

9.3.5 Results and Discussion – Rich gas by-product water

9.3.5.1 Magnetic particle test

The results of the magnetic particle tests on the C-ring specimens are shown in **Error! Reference source not found.** and are tabulated inTable 9-9.

The highest density of cracks was seen on the specimens stressed from 50% to 80% of the yield strength. Some of the C-ring specimens were not cracked on the centre of the specimen where the stress was the highest, but had cracked closer to the tensioning bolt, as clearly shown in **Error! Reference source not found.**.

Table 9-9. C-ring specimens that showed cracking or apparent cracking from the magnetic particle test.

Sample	Coring specimen stress		Condition after exposure period (Visible cracks - Yes/No)		
	(MPa)	% of yield	After 465 h	816 h	1272 h
S1,M1,L1	321	100	No	No	Yes
S2, M2, L2	289	90	Yes	No	No
S3, M3, L3	255	80	No	Yes	Yes
S4, M4, L4	225	70	Yes	Yes	No
S5. MS, L5	193	60	Yes	Yes	Yes
S6, M6, L6	161	50	Yes	Yes	Yes
S7, M7, L7	128	40	Yes	Yes	Yes
S8, M8, L8	96	30	Yes	Yes	Yes
S9, M9, L9	64	20	Yes	Yes	Yes

9.3.5.2 Cross sections of the cracks

Cross sections of the C-ring specimens were made and the depths of the cracks detected on the surface by the magnetic particle test were measured. These cracks are shown in Figure 9-14 to Figure 9-38. Figure 9-14 shows a slight pit that was found on the surface of the C-ring specimen stressed at 100% of the yield strength. At 90% (after 456 hours), a crack formed and the crack growth terminated, but continued again with a fine crack propagating from the crack, as shown in Figure 9-15. The specimen stressed to 80% after 456 hours showed a small fine crack (Figure 9-16). Figure 9-17 shows a fine secondary crack found on the larger crack for a specimen stressed to 70% of the yield strength after 456 hours exposure. The end of a fine crack from a specimen exposed to 60% of the yield strength after 456 hours exposure is shown in

Figure 9-18. Similar cracks are shown in Figure 9-19 to Figure 9-22, for the specimens stressed from 50 to 20% of the yield after 456 hours. No cracks were found on the specimen exposed for 861 hours, stressed to 100% of the yield strength. Shallow pits were found on the surface of the specimen stressed to 90% of the yield strength exposed for 861 hours, shown in Figure 9-23. The small crack found on the specimen exposed for 861 hours, stressed to 80% of the yield strength is shown in Figure 9-24.

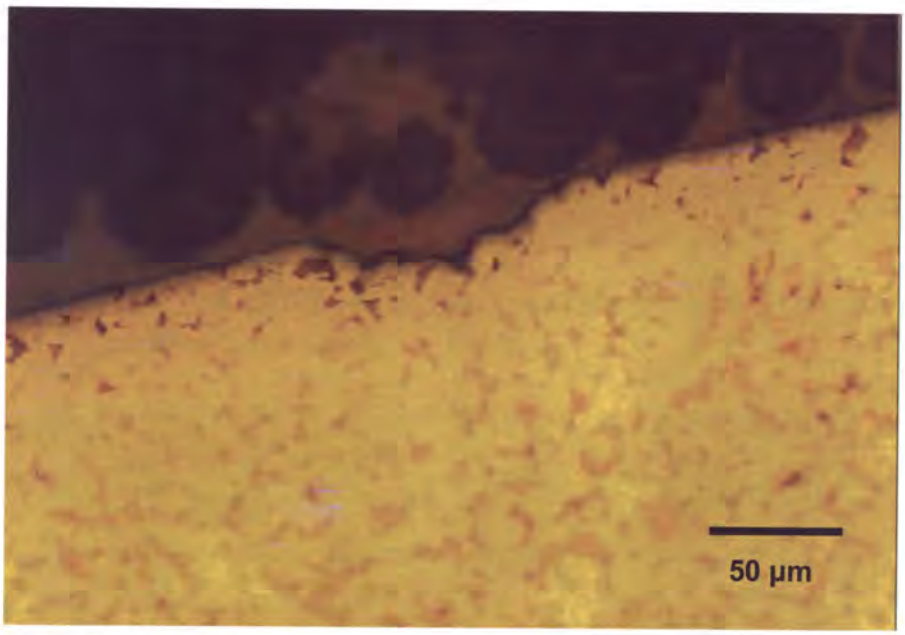

Figure 9-14. Shallow pit on the surface of the specimen stressed to 100% of the yield strength exposed to the rich gas by-product water for 456 hours.

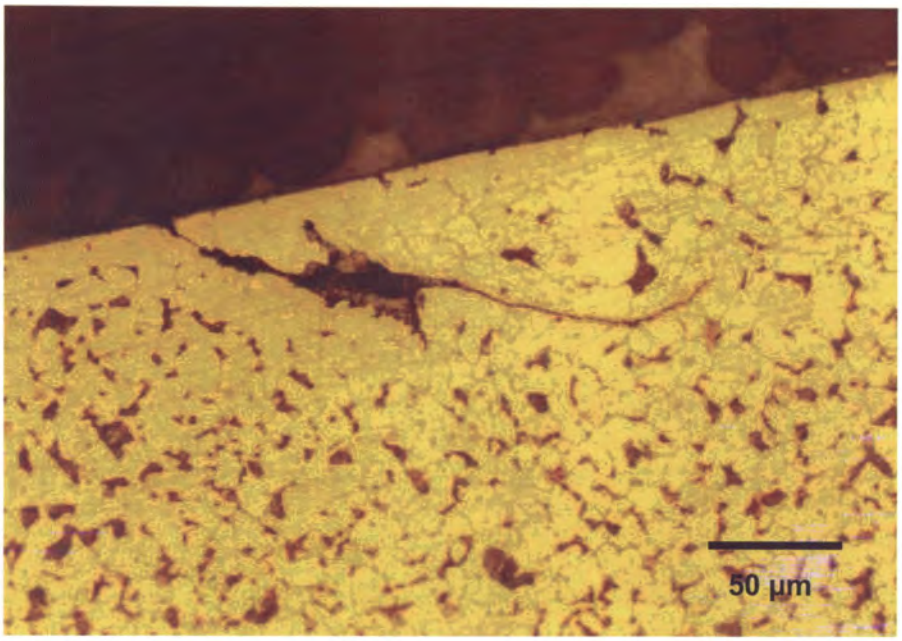

Figure 9-15. A crack on the C-ring specimen stressed to 90% of the yield strength, exposed to the rich gas by-product water for 456 hours.

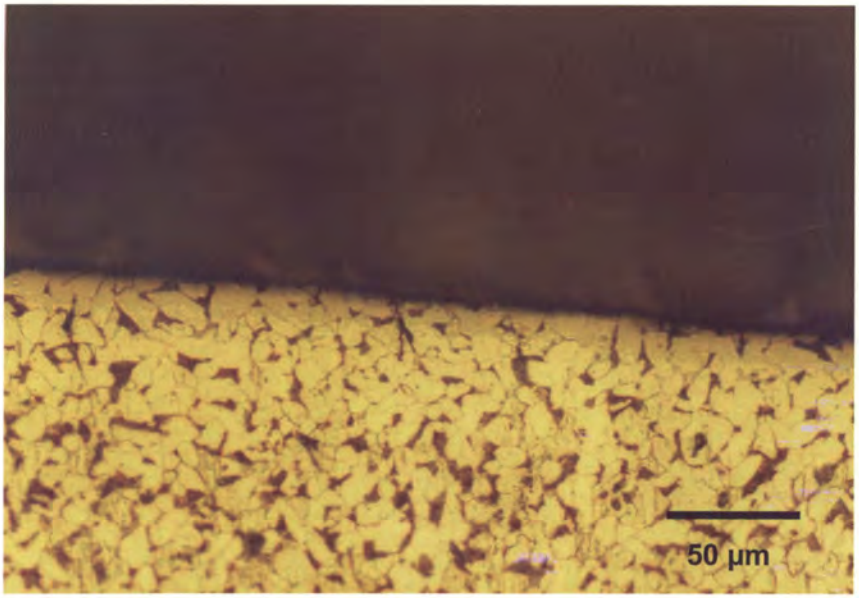

Figure 9-16. A fine crack on the C-ring specimen stressed to 80% of the yield strength, exposed to the rich gas by-product water for 456 hours.

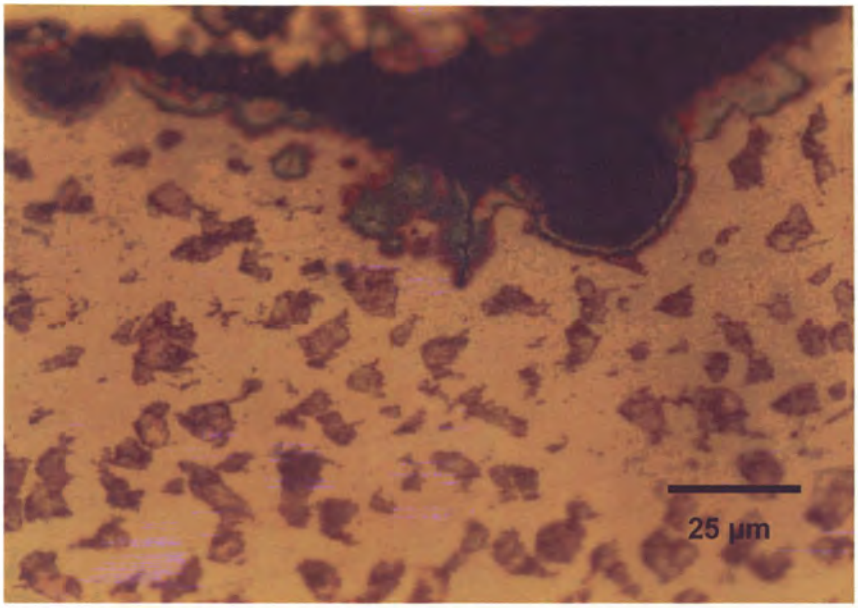

Figure 9-17. A fine crack on the C-ring specimen stressed to 70% of the yield strength, exposed to the rich gas by-product water for 456 hours.

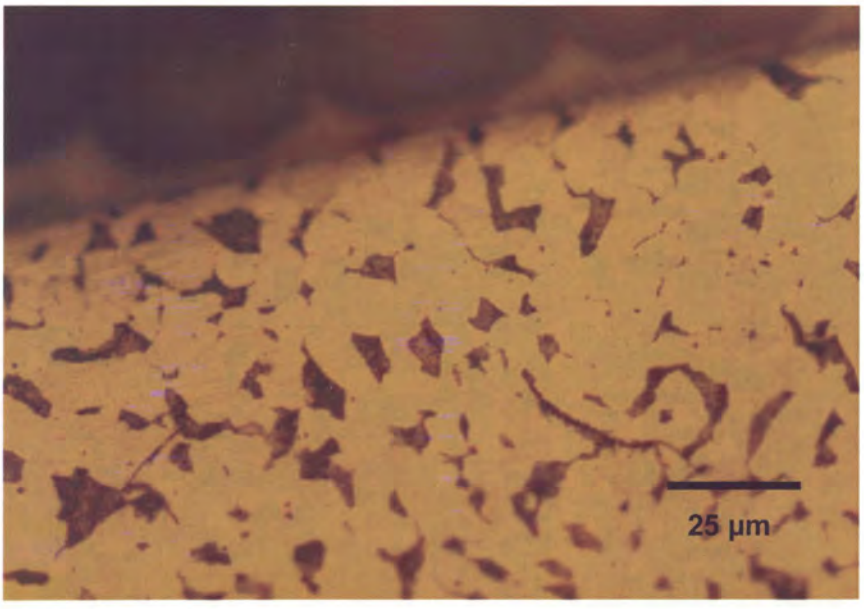

Figure 9-18. Fine cracks emerging under the surface, on the C-ring specimen stressed to 60% of the yield strength, exposed to the rich gas by-product water for 456 hours.

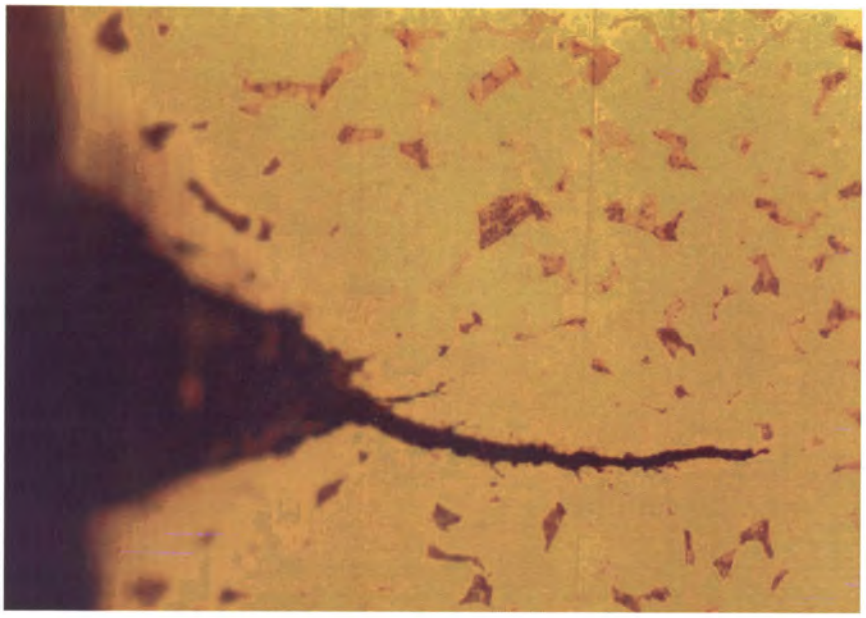

Figure 9-19. A crack on the C-ring specimen stressed to 50% of the yield strength, exposed to the rich gas by-product water for 456 hours.

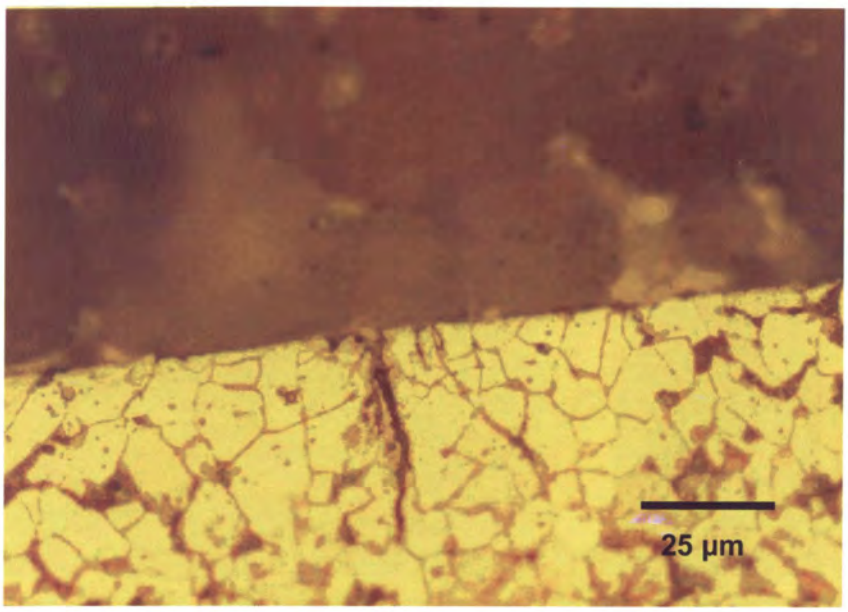

Figure 9-20. Cracks on the C-ring specimen stressed to 40% of the yield strength, exposed to the rich gas by-product water for 456 hours.

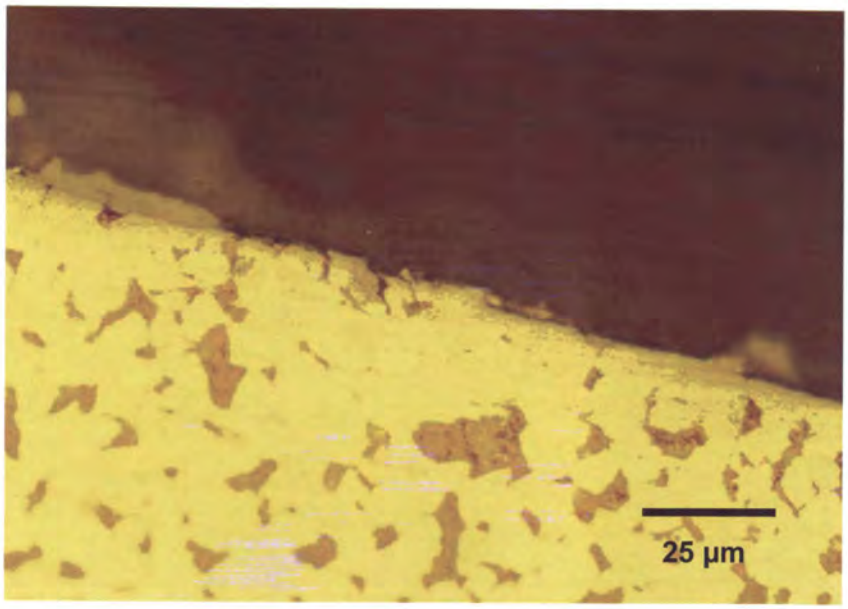

Figure 9-21. Fine cracks on the C-ring specimen stressed to 30% of the yield strength, exposed to the rich gas by-product water for 456 hours.

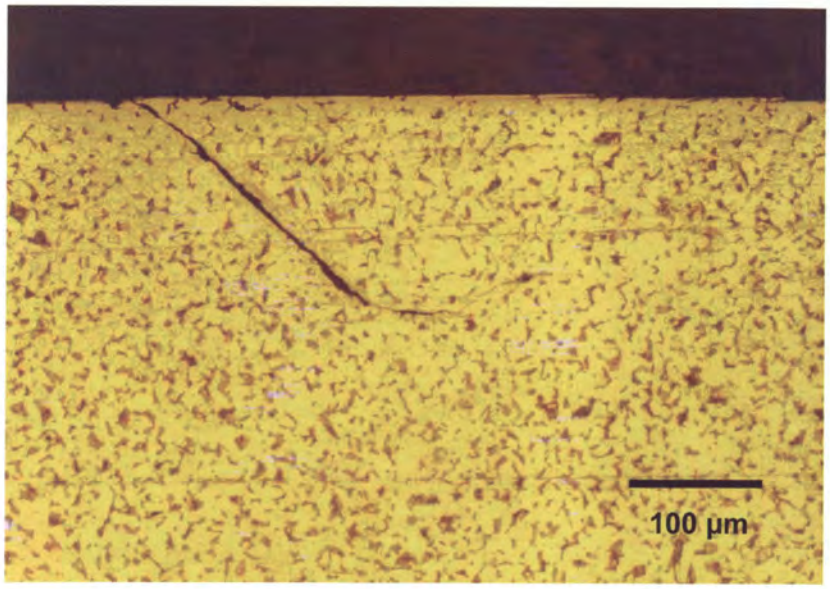

Figure 9-22. A crack on the C-ring specimen stressed to 20% of the yield strength, exposed to the rich gas by-product water for 456 hours.

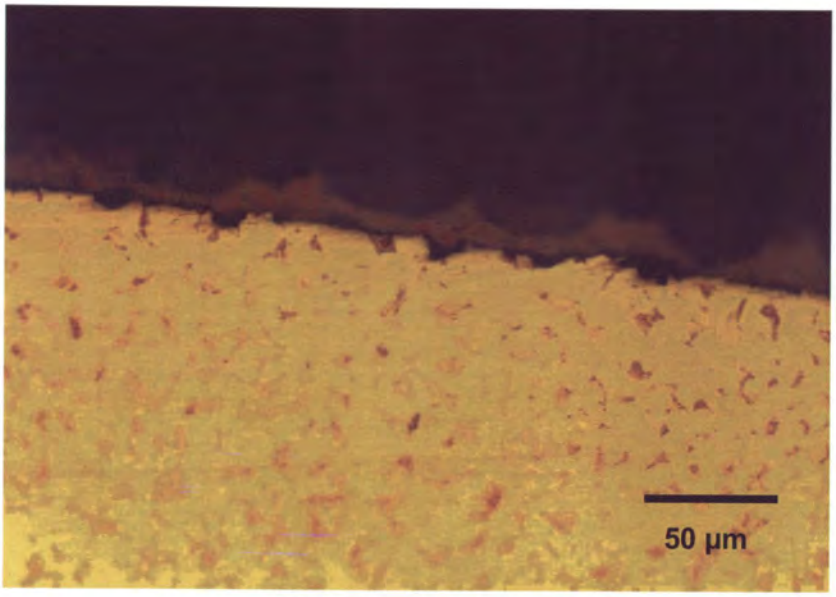

Figure 9-23. A fine crack on the C-ring specimen stressed to 90% of the yield strength, exposed to the rich gas by-product water for 861 hours.

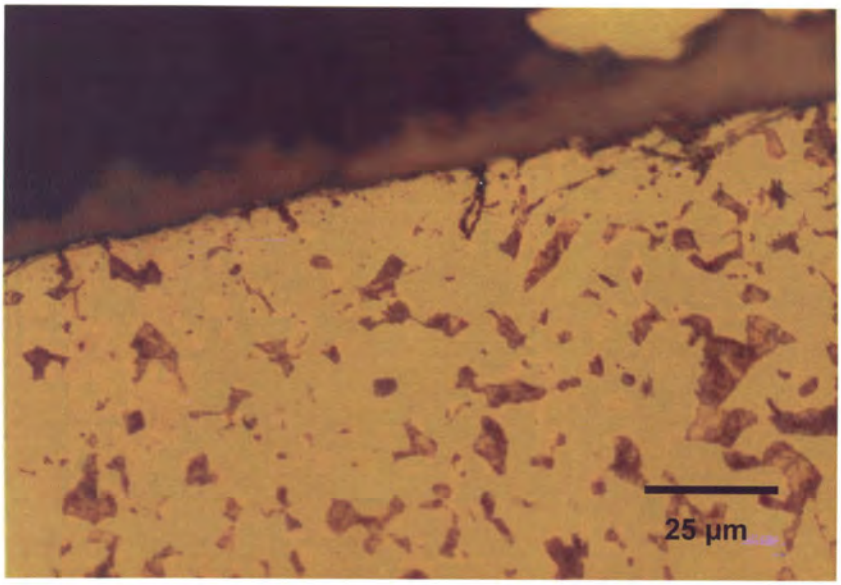

Figure 9-24. A fine crack on the C-ring specimen stressed to 80% of the yield strength, exposed to the rich gas by-product water for 861 hours.

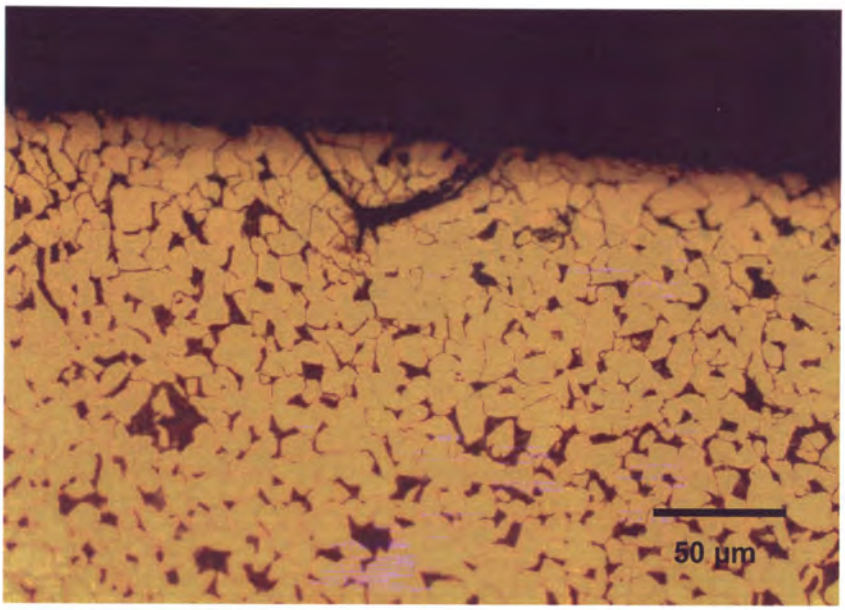

Figure 9-25. A crack on the C-ring specimen stressed to 70% of the yield strength, exposed to the rich gas by-product water for 861 hours.

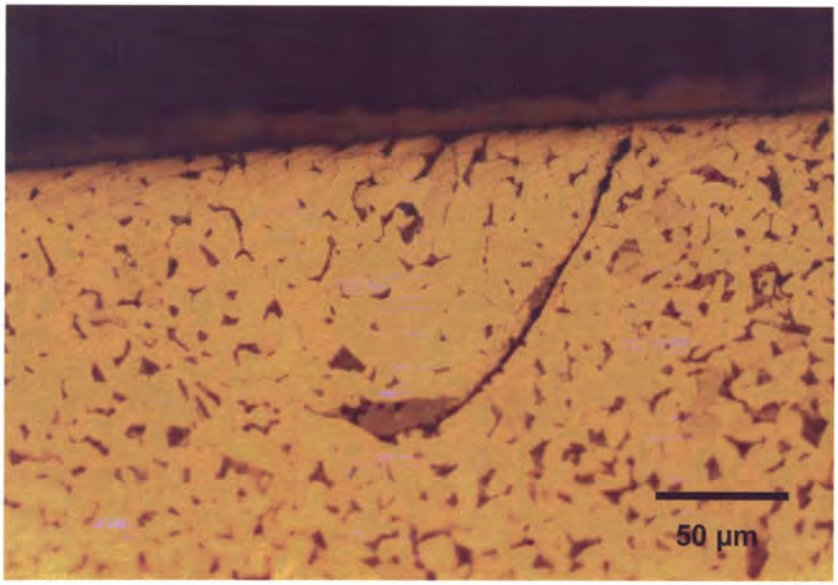

Figure 9-26. A crack on the C-ring specimen stressed to 60% of the yield strength, exposed to the rich gas by-product water for 861 hours.

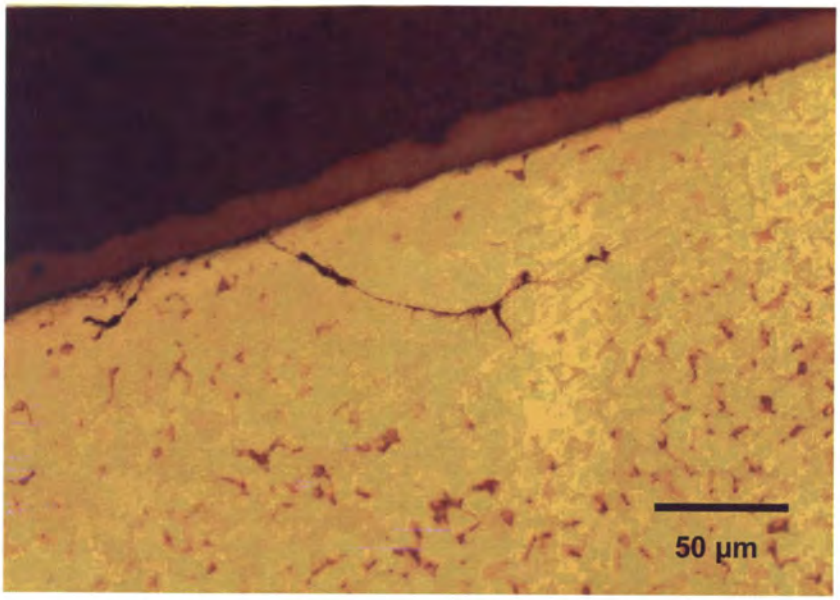

Figure 9-27. Fine cracks on the C-ring specimen stressed to 50% of the yield strength, exposed to the rich gas by-product water for 861 hours.

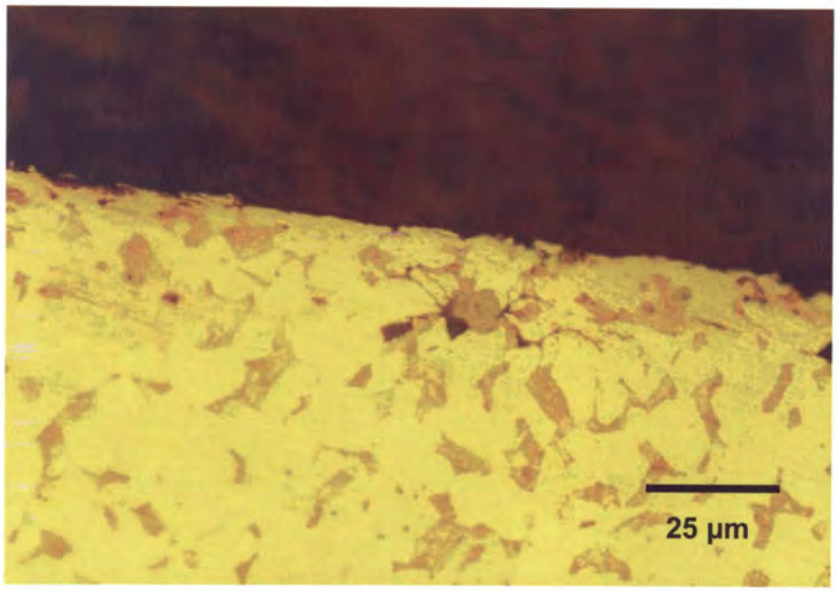

Figure 9-28. Fine cracks on the C-ring specimen stressed to 40% of the yield strength, exposed to the rich gas by-product water for 861 hours.

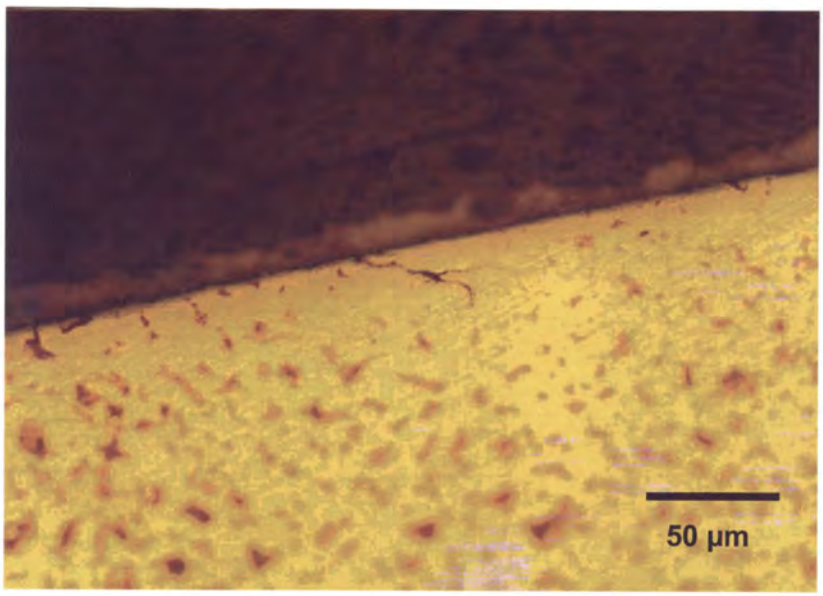

Figure 9-29. A fine crack on the C-ring specimen stressed to 30% of the yield strength, exposed to the rich gas by-product water for 861 hours.

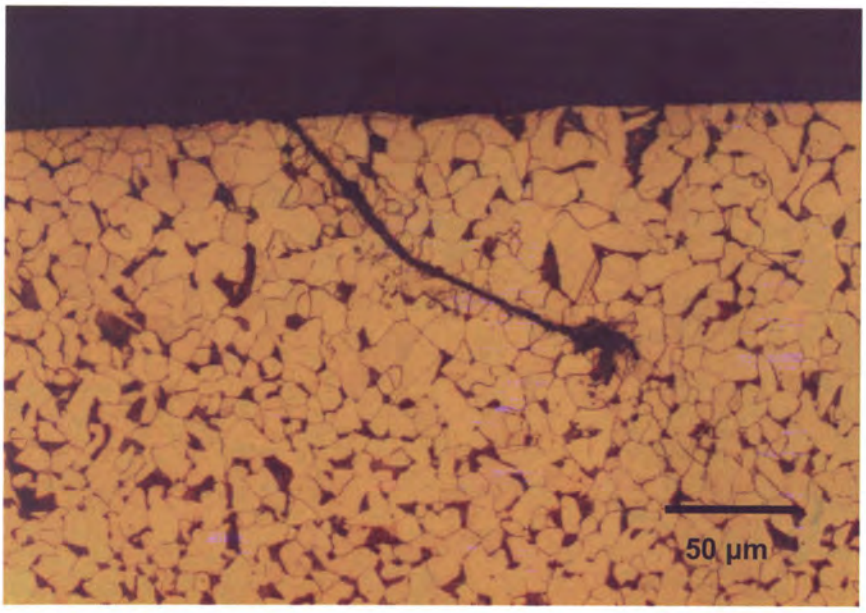

Figure 9-30. A crack on the C-ring specimen stressed to 20% of the yield strength, exposed to the rich gas by-product water for 861 hours.

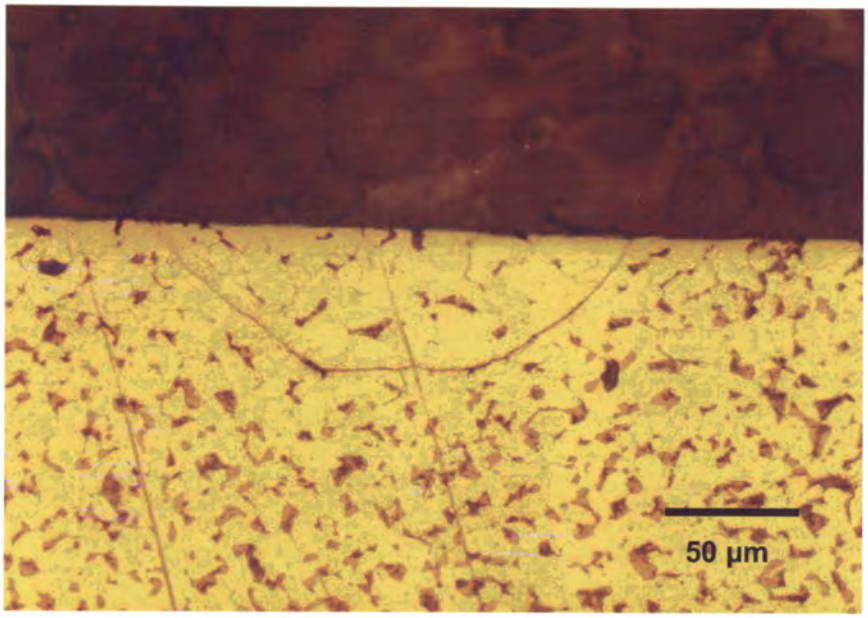

Figure 9-31. A fine crack on the C-ring specimen stressed to 100% of the yield strength, exposed to the rich gas by-product water for 1,272 hours.

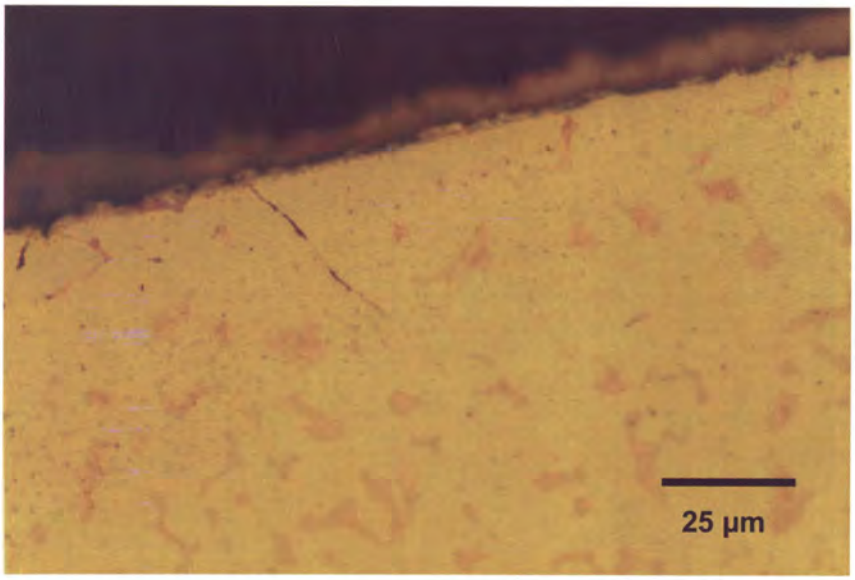

Figure 9-32. A fine crack on the C-ring specimen stressed to 80% of the yield strength, exposed to the rich gas by-product water for 1,272 hours.

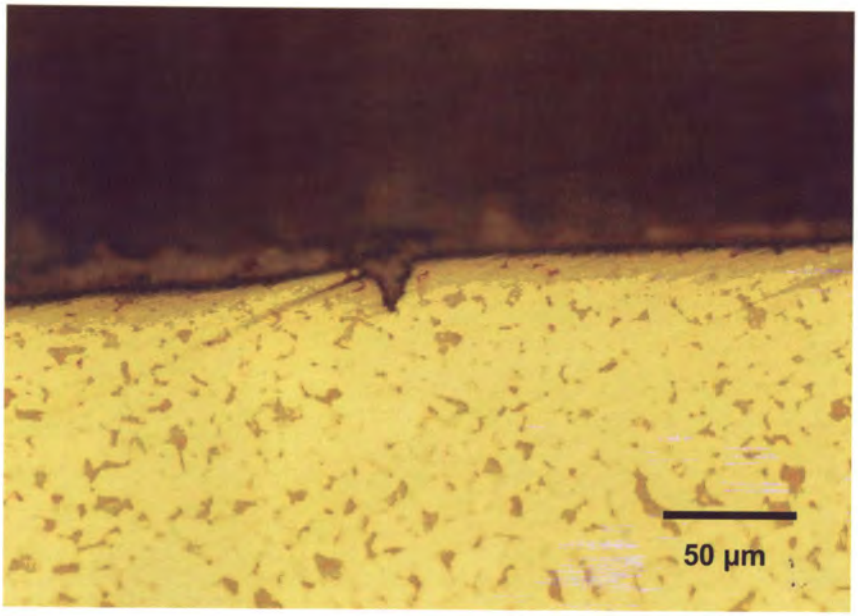

Figure 9-33. A crack on the C-ring specimen stressed to 70% of the yield strength, exposed to the rich gas by-product water for 1,272 hours.

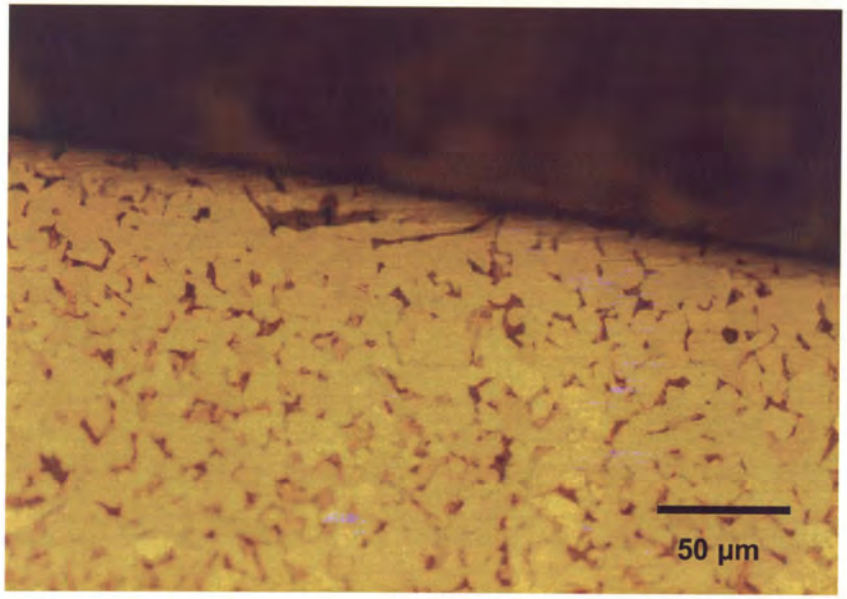

Figure 9-34. A crack on the C-ring specimen stressed to 60% of the yield strength, exposed to the rich gas by-product water for 1,272 hours.

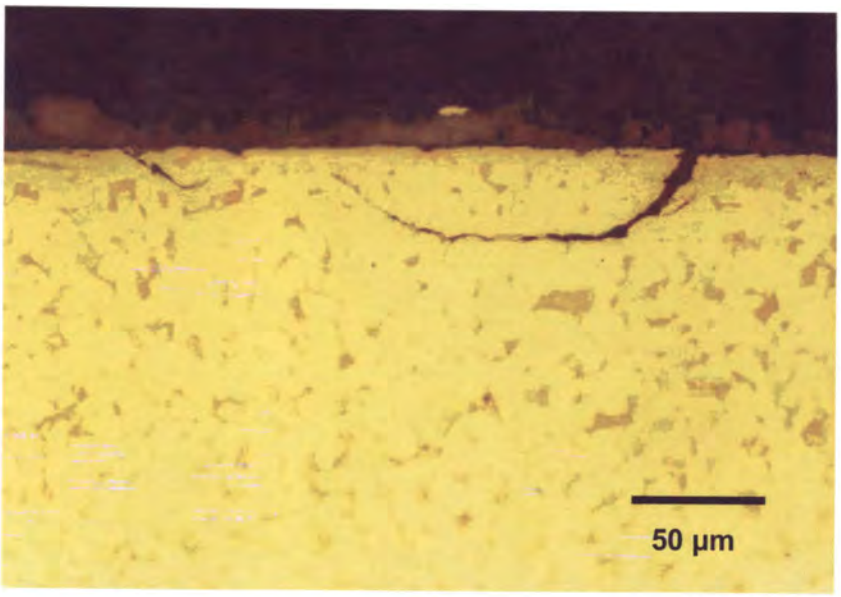

Figure 9-35. Cracks on the C-ring specimen stressed to 50% of the yield strength, exposed to the rich gas by-product water for 1,272 hours.

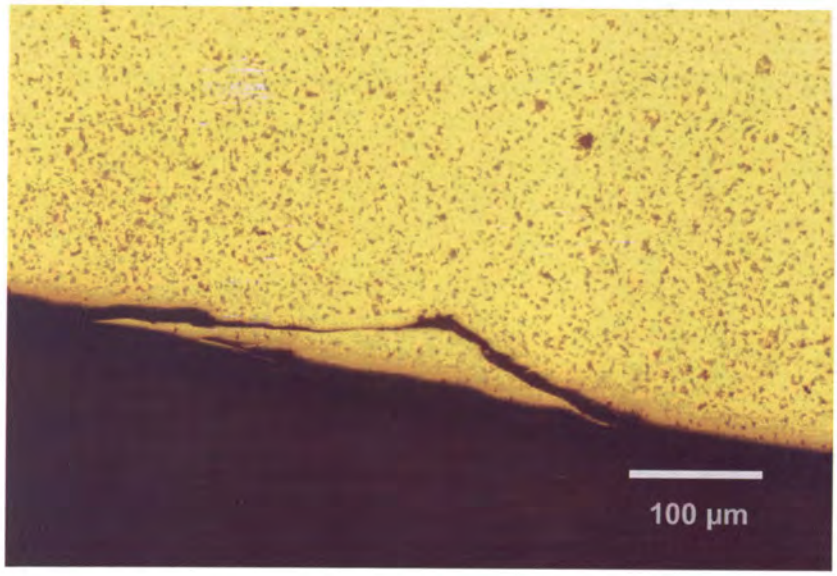

Figure 9-36. A crack on the C-ring specimen stressed to 40% of the yield strength, exposed to the rich gas by-product water for 1,272 hours.

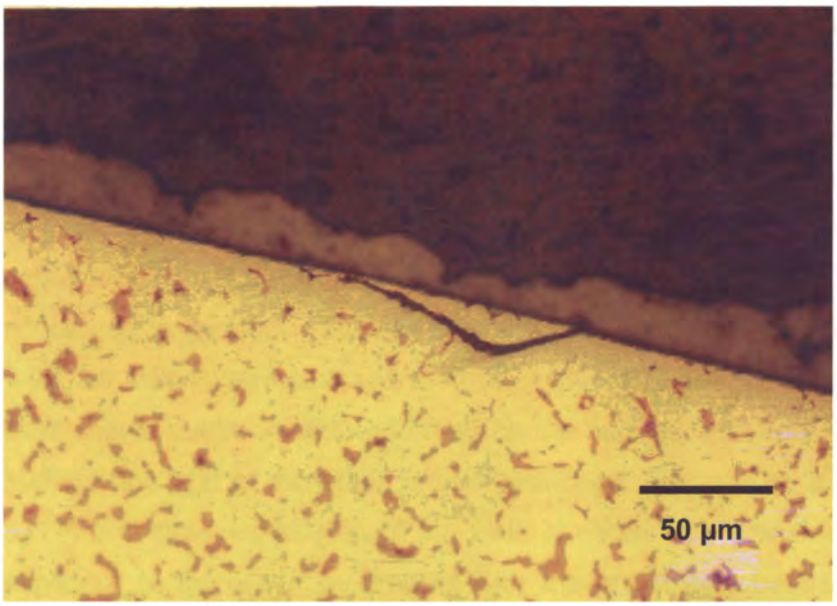

Figure 9-37. A crack on the C-ring specimen stressed to 30% of the yield strength, exposed to the rich gas by-product water for 1,272 hours.

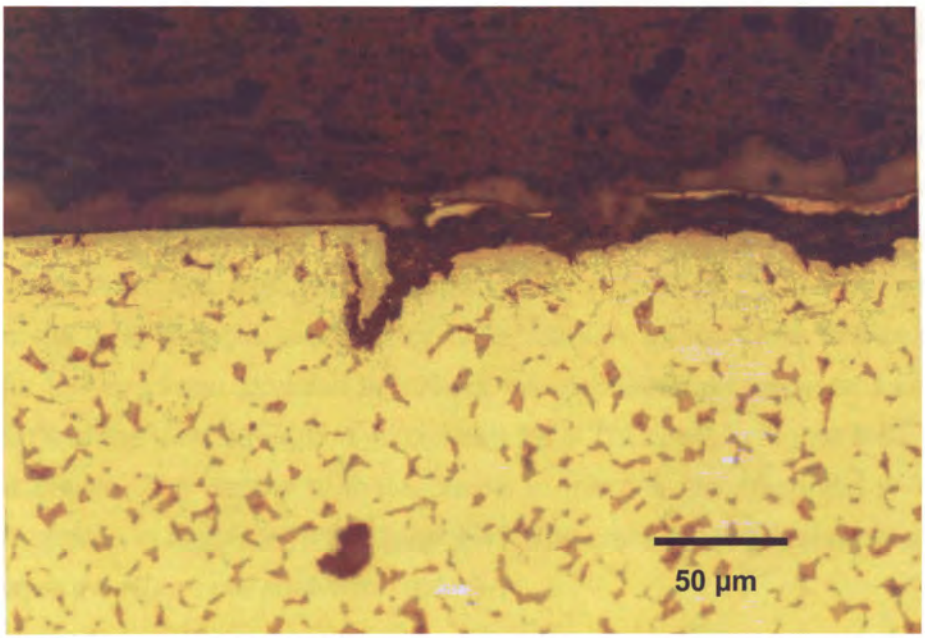

Figure 9-38. A crack on the C-ring specimen stressed to 20% of the yield strength, exposed to the rich gas by-product water for 1,272 hours.

Figure 9-25 shows the crack on the specimen exposed to the gas liquour for 861 hours, stressed to 70% of the yield strength. Figure 9-26 shows a fine crack on a specimen stressed to 60% of the yield strength exposed for 861 hours, the crack initiated perpendicularly to the surface, but the crack tip was nearly parallel to the surface. The fine crack shown in Figure 9-27 is surrounded by a region of depleted cementite. This was on a specimen stressed to 50% of the yield strength exposed to richer gas by-product water for 861 hours. A branched crack can be seen in Figure 9-28, on a specimen stressed to 40% of the yield and exposed for 861 hours. Figure 9-29 shows a fine crack that formed on the surface, in a near parallel direction to the surface, the end of the crack is also branched, this was on a specimen exposed for 861 hours stressed to 30% of the yield strength. The crack seen after 861 hours of exposure to the water by-product with the specimen stressed to 20% of the yield strength is shown in Figure 9-30. A half round crack was found on the specimen stressed to 100% of the yield strength exposed for 1 272 hours, shown in Figure 9-31. The specimen stressed to 80% of the yield strength, exposed for 1 272 hours showed a crack at a 45° angle in Figure 9-32. A small pit is shown in Figure 9-33 on the surface of the specimen exposed for 1272 hours, stressed to 70% of the yield strength. At 60% of the yield strength, and exposed for 1 272 hours a crack more parallel to the surface of the specimen is seen in Figure 9-34. A more circular crack is shown in Figure 9-35 for the specimen stressed to 50% of the yield strength, exposed for 1 272 hours. A large surface crack is shown in Figure 9-36 for the specimen stressed to 40% of the yield strength, exposed for 1272 hours. A smaller crack is shown in Figure 9-37 for the specimen stressed to 30% of the yield strength, exposed for 1 272 hours. At 20% of the yield strength and exposed for 1 272 hours in Figure 9-38, a surface crack is shown. The depths of these cracks in microns are presented in Table 9-10, and illustrated in Figure 9-39 to Figure 9-41. The crack propagation rates of the cracks that were measured are shown in Table 9-11.

Table 9-10. Measured crack lengths and corrosion rates on the C-ring specimens in richer gas by-product water.

Stressed to % of yield strength		**Measured crack length (m)**		
% Yield	**Stress (MPa)**	**456 hours**	**816 hours**	**1272 hours**
20	64	7.00E-04	2.60E-04	4.30E-04
30	96	3.00E-05	9.50E-05	2.30E-04
40	129	7.00E-05	3.10E-04	1.15E-03
50	161	2.40E-04	2.50E-04	3.00E-04
60	193	1.50E-04	4.70E-04	1.90E-04
70	225	9.00E-05	1.10E-04	
80	257	4.00E-05	9.00E-05	1.70E-02
90	289	3.50E-04		
100	321			4.00E-04

Unfortunately some of these cracks look like it could have been laps in the steel, but mostly these were similar to stress corrosion cracks.

Table 9-11. Crack propagation rates calculated from the crack lengths shown in Table 9-10.

Stressed to % of yield strength		Crack propagation rate as calculated from the exposure time (m/s)		
% Yield	Stress (MPa)	465 hours	816 hours	1272 hours
20	64	4.30E-10	8.90E-11	9.40E-11
30	96	1.80E-11	3.20E-11	5.00E-11
40	129	4.30E-11		2.50E-10
50	161	1.50E-10	8.50E-11	6.60E-11
60	193	9.10E-11	1.60E-10	4.10E-11
70	225	5.50E-11	3.70E-11	
80	257	2.40E-11	3.10E-11	3.70E-11
90	289	2.10E-10		
100	321			8.70E-11

The results shown in Table 9-11 and are illustrated in

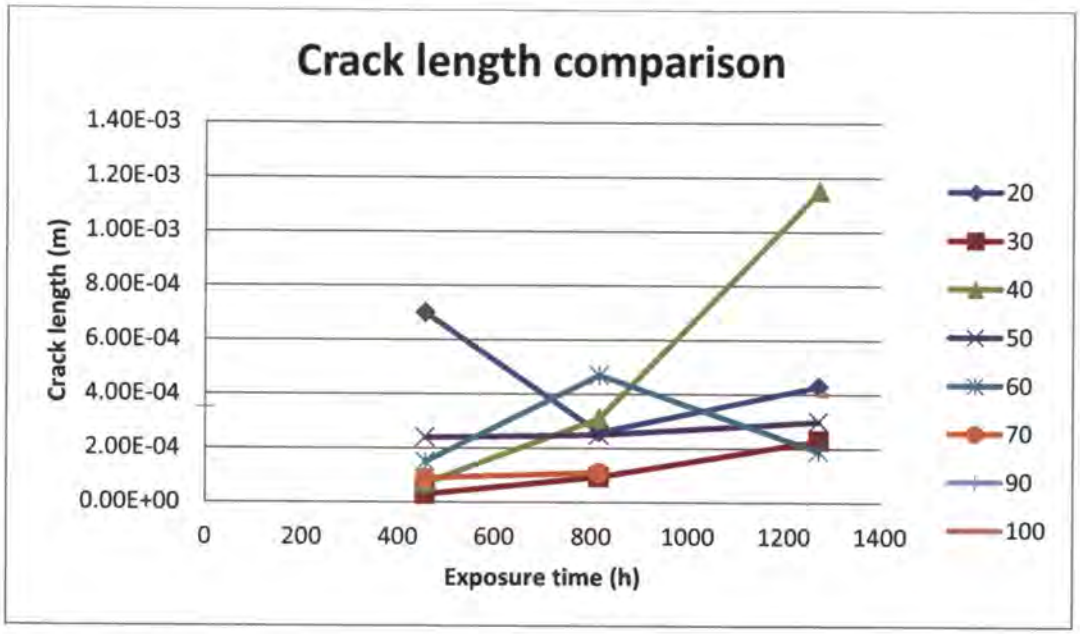

Figure 9-39., note the slight increase in most of the stress levels, but a decrease in some and also not a significant increase as would be expected. This is further clarified in Figure 9-40 where the crack growth rate decrease is seen for the longer exposure times. The only specimen that clearly does not follow this trend is the C-ring stressed to 60% of the yield.

The values for the crack propagation rates shown in Table 9-11 were taken for each period and the average crack propagation rates for each stress condition were calculated, and are shown in Table 9-12 and Figure 9-41. From these it is clear that again the crack propagation rate stayed constant for all the stress conditions tested, except for the sample stressed to 20% of the yield strength.

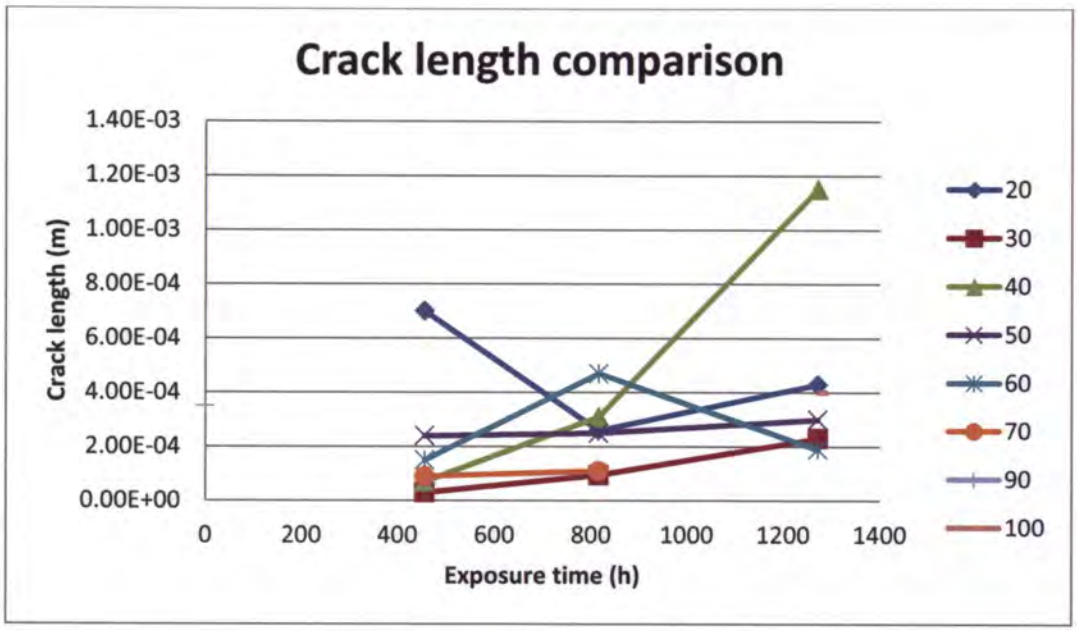

Figure 9-39. The variation of the crack length with exposure time.

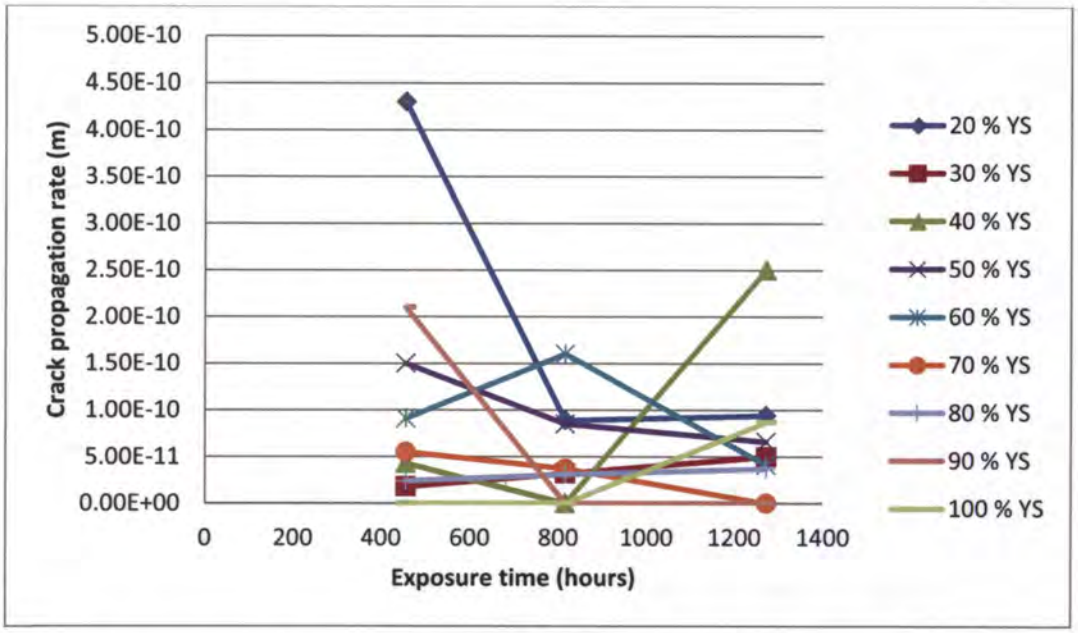

Figure 9-40. Variation in crack propagation rate over exposure time for the C-ring specimens tested in the rich gas water by-product.

Table 9-12. The average crack propagation rates determined from the data shown in Table 9-11.

% Yield strength (MPa)	Crack propagation rate ($m.s^{-1}$)
20	1.00E-10
30	4.00E-11
40	2.00E-10
50	8.00E-11
60	8.00E-11
70	1.00E-11
80	3.00E-11
90	2.00E-11
100	6.00E-11

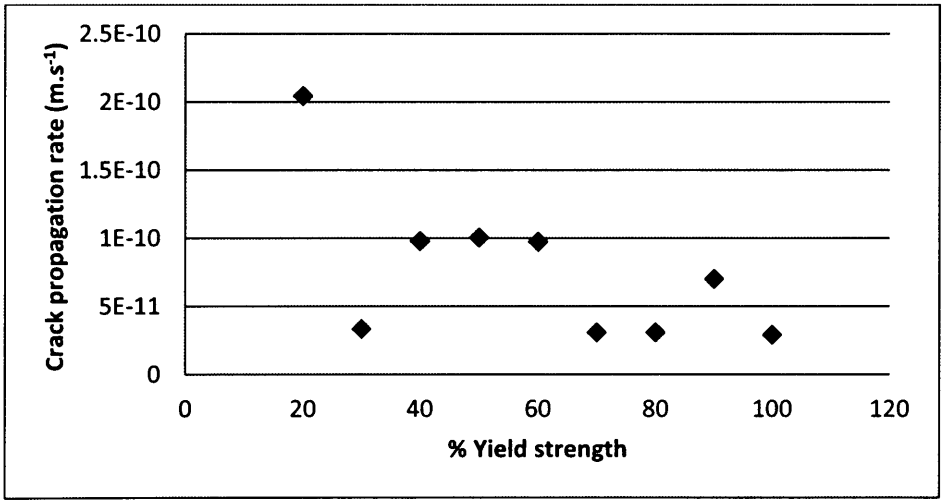

Figure 9-41. The average crack propagation rate measured over time for the differently stressed C-ring specimens exposed to the rich gas water by-product.

9.3.6 Discussion

The results indicate that cracking occurred over a wide range of stress levels. It would even appear that the crack propagation rate was higher at lower stress levels, which is surprising.

The crack propagation rates which were measured on the specimens were at a maximum at the lowest stress over the shortest time, 4.3 $x10^{-10}$ $m.s^{-1}$. The lowest propagation rate was measured at the very next stress level (30% of the yield strength) at $1.8x10^{-11}$ m/s. This would indicate some inconsistency in the propagation rate measured. The other measurements that were taken averaged $1.3x10^{-10}$ $m.s^{-1}$, giving a propagation rate of around 4.1 mm/year. However, the nature of the cracks was not always perpendicular to the surface and therefore, this does not represent an exact penetration rate for cracking.

At none of the exposure times did the crack depth follow the stress level increase or decrease, and the crack depth stayed constant. The comparison of the three exposure times also indicated a constant crack depth. The crack propagation rates determined from the exposure time and the crack depth indicated that the crack propagation rate remains constant over time. Therefore, the crack growth is not characterised by growth spurts. However, the graphs for the data according to the stress indicated that most growth occurred at 40% of the yield strength during the last period of the exposure. For the rest of the stresses, the crack growths were constant, but lowered for the stresses close to the yield strength of the material. Cracking was more likely to take place at the lower stresses, as seen on the C-ring specimens that were stressed to 100% of the yield strength where the cracking occurred close to the stressing bolt, where the stress would be much lower than in the centre of the C-ring.

When considering the C-ring test stress condition, the following stress analyses were performed on the C-ring with finite element anlaysis, and the results are shown in Figure 9-42 to Figure 9-46. The C-ring of course would have a compressive stress on the inside surface, in Figure 9-42 the green area denotes the highest negative compressive stress of 322 MPa for a maximum stress of 231 MPa – tensile on the

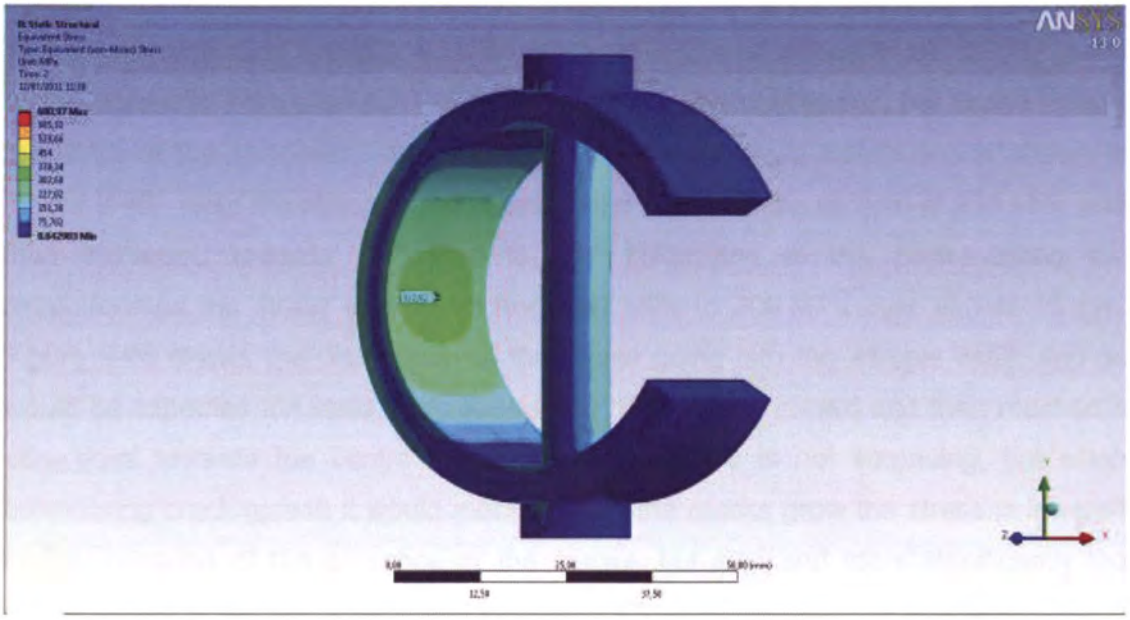

Figure 9-42. Finite element analysis of a stressed C-ring, showing the stress condition on the inside of the C-ring.

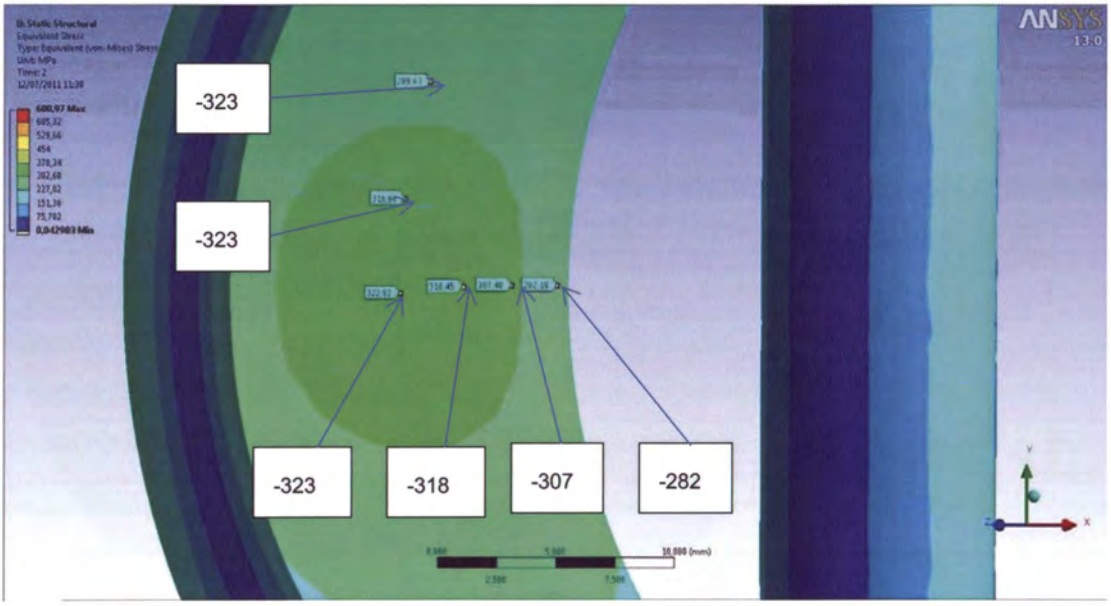

Figure 9-43. Compressive stresses found on the inside of the C-ring when it was stressed to 231 MPa on the external surface. (The values shown are in MPa)

external surface. The stress gradient on the inside is shown in Figure 9-43, with the stress slowly increasing from the centre, and the highest stress occurring at the edge. The external surface analysis showed again the highest stress levels in the green region shown in Figure 9-44. The stress pattern is not continuous, but varied across the width of the specimen. A closer analysis of this stress distribution is shown in Figure 9-45. Note the stress is the lowest in the centre of the sample at 231 MPa and then increased towards the edge to 287 MPa, and in the centre along the circumference the stress decreased from 287 MPa to 200 MPa over almost 10 mm. Figure 9-46 shows the distribution of the stress going into the sample itself, and as would be expected the stress decreased from the surface inward and then reached a zero point towards the centre of the thickness. This is not surprising, but when considering crack growth it would mean that as the cracks grow the stress is lowered slightly because of the presence of the cracks, but also and more significantly the actual stress at the crack tip would decrease constantly as the crack grows. This is probably not significant for short term exposures, but explains the reduced crack

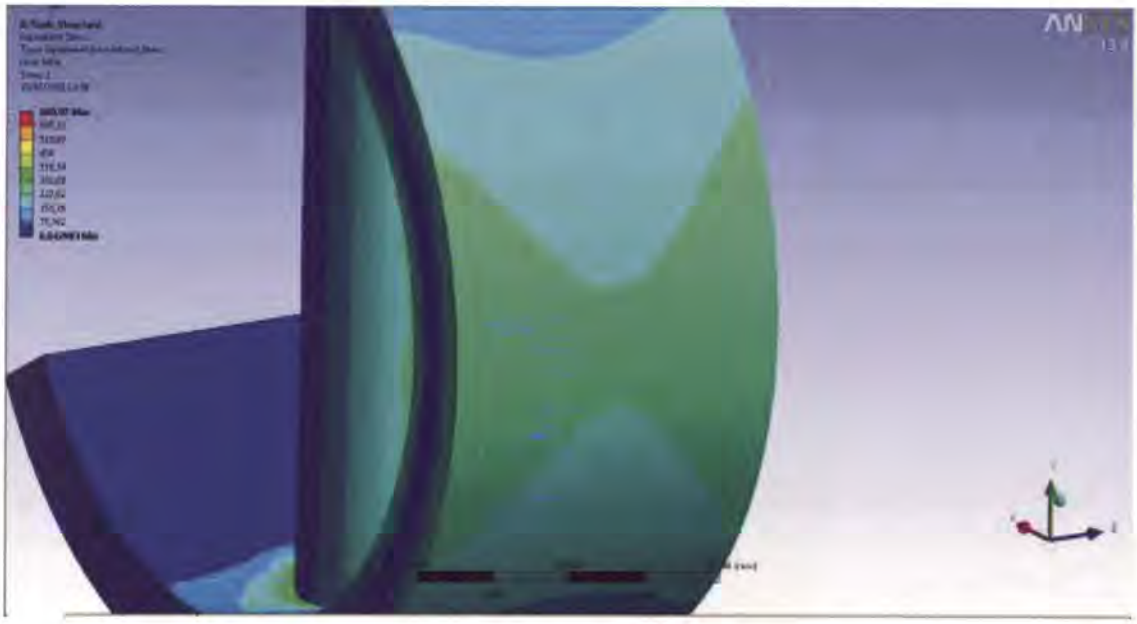

Figure 9-44. Finite element analysis of a C-ring, showing the external surface where the highest stresses are expected.

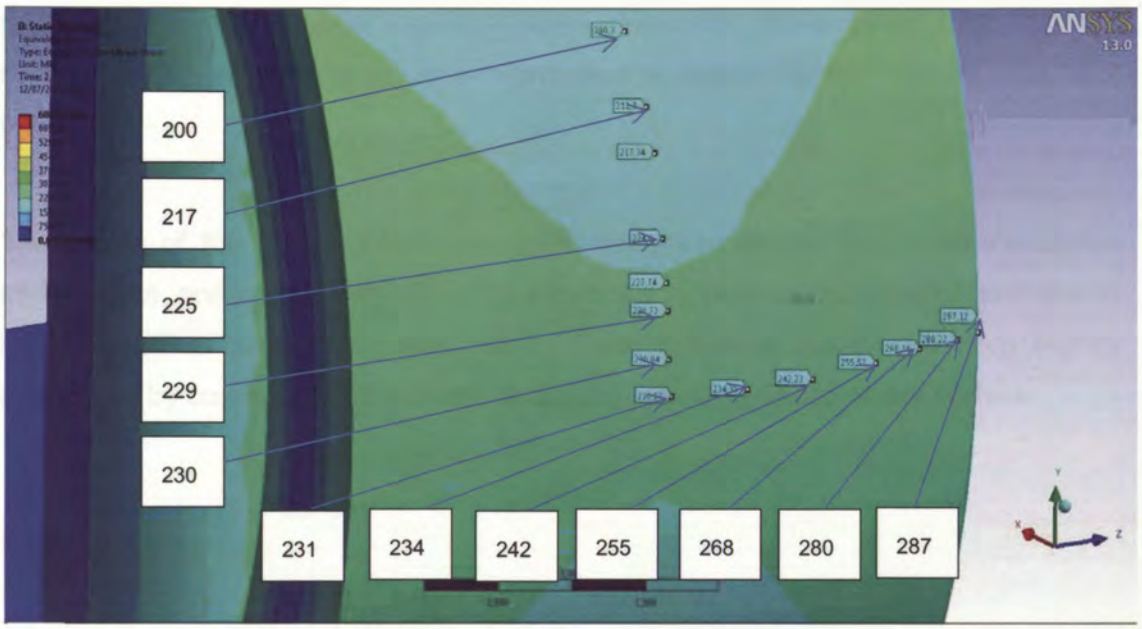

Figure 9-45. Finite element analysis of a C-ring, showing the stress distribution along the width, as well as the stresses along the circumference, starting at the centre where the stress will be at its highest. (The values shown are in MPa)

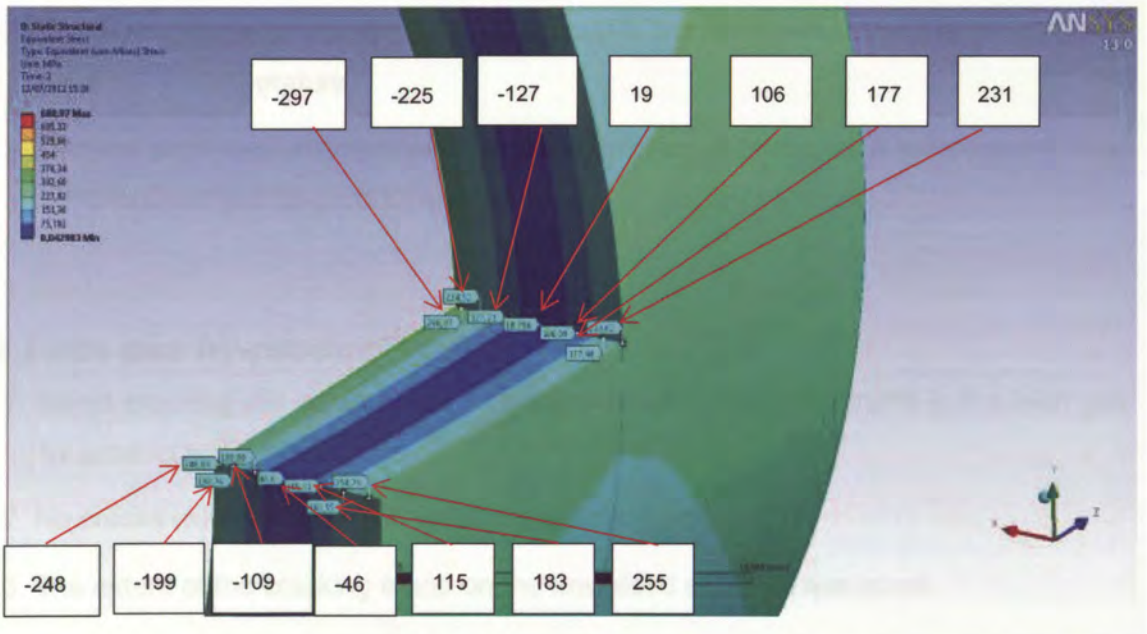

Figure 9-46. Finite element analysis of the C-ring showing the stress distribution through the thickness in the centre where the highest stresses are. (The values shown are in MPa)

growth rates over the longer exposure times. However, this does not make this test method invalid, as it gives valuable information on crack initiation, and its relation to the stress.

The nature of the cracking was completely transgranular as seen from the optical micrographs, and relates well with what was found in the previous chapter, and also in literature. The cracks were fine, but in some instances the cracks were slightly broadened by corrosion, and in some cases only pits were found on the surface.

9.4 Conclusion

9.4.1 Slow strain-rate tests

1. The C-Mn steel was susceptible to stress corrosion cracking in the lean gas by-product water at 90°C according to the slow strain rate test.
2. The susceptibility to cracking of carbon steel in this environment was enhanced with increase in temperature.
3. Carbon steel was susceptible to stress corrosion cracking at a temperature from 50°C in Lean gas by-product water.

9.4.2 Lean gas by-product water

1. Some cracking did occur on all of the unwelded C-ring specimens in the lean gas by-product water at 90°C.
2. No cracks were found on the welded specimens.
3. The extent of the cracking found on the unwelded samples was small.
4. The measured crack propagation rates for the unwelded specimens were in the order of $3x10^{-11}$ $m.s^{-1}$.

9.4.3 Rich gas by-product water

1. Cracking occurred at all stress levels that were tested.
2. The crack propagation rate did not alter significantly with the stress level as a percentage of the yield strength.
3. The crack propagation rate decreased slightly with increasing stress level, taking a linear interpolation for each stress level.
4. Crack initiation was possible at all the stress levels evaluated.

CHAPTER 10

10 DISCUSSION AND CONCLUSIONS

10.1 Discussion

Stress-corrosion cracking of steel exposed to CO-CO_2-H_2O appears to be very dependent upon the carbon monoxide adsorption on the steel surface. With the increase of temperature the solubility of both carbon monoxide and carbon dioxide decrease (at a constant overall pressure) and therefore decreasing sensitivity to cracking was found at higher temperatures. A similar decrease in sensitivity to cracking was found at the lower temperatures. However, the effect of temperature was moved to higher temperatures for the higher carbon monoxide concentration, therefore indicating the importance of the higher carbon monoxide concentration. This increased passivation of the steel by the higher carbon monoxide concentrations was probably also the case for the industrial product evaluated in Chapter 9. However, for the industrial product the presence of cyanide contributed to the passivation of the steel and therefore, increased the passivation kinetics at higher temperatures, and therefore increasing the sensitivity to cracking. Schutt[72] confirmed an increase in transgranular cracking of ASTM A516-70 steel exposed to 0.21% thiosulphate when cyanide was added.

With the slow strain-rate tests influence of the gas was further highlighted by the effect of higher total gas pressures. This confirms what Malik and Nawaz[37] found for tests performed at atmospheric pressures.

The slow strain-rate tests of steel in the carbon monoxide–carbon dioxide environment also revealed that an increased exposure time of the specimen to the environment before the test was started caused an unexpected increased sensitivity to cracking of the steel, which highlighted the critical dependence of the cracking process on the passivation of the steel, the passivation rate, and the presence of carbon monoxide. Furthermore, the effect of exposure time before the test illustrates the dependence upon the adsorption of the carbon monoxide on the steel interface. This time dependent adsorption was demonstrated by Heaver[73] illustrating the effect of the

passivation of the steel as a result of exposure time to a carbon monoxide containing environment. Therefore, when the time dependency of the embrittlement is considered it has to be ascribed to the adsorption reaction of the carbon monoxide. The other parameters that were investigated did not show the same level of significantly embrittling effects. The orientation of the samples and grinding marks on the surface of the samples both did not have a very significant effect, although these parameters showed some contribution to cracking. In terms of crack initiation however, it was found that secondary cracks formed on the grinding marks and would have contributed to the cracking process. It was seen on the slow strain-rate specimens that cracks originated on fine machining marks oriented at a certain angle. An almost linear relationship was found when considering surface roughness, produced by grinding marks and sensitivity to cracking. For a higher surface roughness the sensitivity to cracking was also the highest. This is a significant finding, because crack initiation is such an important part of the life of a component sensitive to cracking. Therefore, if the component surface can be kept free from deep grinding marks the cracking will also be slowed.

The slow strain-rate tests also showed that the applied potential caused a significant effect on cracking with a definite potential range where cracking was enhanced. The minimum potential to this crack sensitive range corresponded with the corrosion potential and showed insensitivity towards hydrogen charging, whereas the maximum approximately corresponded to the transpassive potential of the pseudo passive region. This confirms the importance of the passivation and the passivation kinetics on the crack propagation and confirms the slip step dissolution model.

Temperature had an influence on the cracking of the steel, and the carbon steel was most sensitive to cracking at around 40 – 50°C. This was consistent for both 25% and 50% carbon monoxide and a pressure of 800 kPa, however at 50% this region of minimum resistance moved to a slightly higher temperature range, around 60°C. These measurements showed a considerable amount of scatter though, which could have resulted because of varying exposure times. However, there was a clear trend with decreasing sensitivity to cracking for both lower and higher temperatures, probably based on the corrosion kinetics at the lower temperatures and the

concentration of the dissolved gasses at the higher temperatures. Together with the influence of the temperature the effect of the rolling direction was investigated, but no significant trend was found beyond the scatter of the results. However, a parameter that showed a significant effect on the stress-corrosion resistance of the steel was the influence of the total gas pressure, as the pressure was decreased the susceptibility to cracking also decreased markedly, and this would of course be a way to inhibit cracking for plant conditions.

Therefore, from the slow strain-rate results it would appear that the environmental conditions played a more important role than the metallurgical condition of the steel. Another important result was the effect of strain-rate on the stress-corrosion sensitivity, where it was shown that at very slow strain-rates the sensitivity decreases. Berry and Payer[15] showed that sensitivity to cracking increases with decreasing strain rates, but they did not perform the tests at below $3x10^{-7}$ $m.s^{-1}$, and therefore did not find the strain-rate for maximum cracking sensitivity. (Based on this one could consider that the strain-rate used for the slow strain-rate tests might have been too fast, but the number of tests that had to be performed and the fact that cracking did occur is enough evidence to suggest that the strain-rate employed was slow enough.) This finding is important because it indicates that stress-corrosion cracking is the preferred mechanism of cracking, as opposed to the mechanism of hydrogen embrittlement, because sensitivity to hydrogen embrittlement increases with lower strain-rates.

Since the exposure time before the slow strain-rate tests had such a significant influence on the results, the kinetic properties of the corrosion reactions were the logical next step to investigate with electrochemical techniques. Here the influence of gas composition and exposure time as well as temperature and gas pressure were investigated. These characteristics were performed for a number of environments ranging from low carbon monoxide concentrations to relatively high levels. The interesting part of these results was the presence of the passive region, even at low carbon monoxide levels. The extent of the passivity was initially not significant at 1%, but with exposure time the passive region increased, and became prominent. For the other carbon monoxide concentrations, the passive region was seen, and these were very similar, after long enough exposure times, for all the carbon monoxide levels

except at 1%. However, the presence of the passive region after exposure even at low concentrations, indicated why stress-corrosion is also witnessed at these levels. The very slow passivation kinetics at room temperature, as compared to the higher passivation kinetics found at 45°C, indicated why the susceptibility to cracking increased with temperature. Clearly a fine balance exists between the passivation kinetics and sensitivity to cracking.

From slow strain-rate test data it was clear that steel was more embrittled at 45°C than 20°C when exposed to 25% CO. When looking at these results for 50% CO the temperature range of greatest sensitivity to cracking increased to around 60°C. Considering the passivation rates for these instances, it would be possible to determine the role that passivation rate plays in the cracking process, if passivation rate was to be the most important parameter. For the two scenarios it is clear that the curves moved to more active potentials at the higher temperature, and there is a slight increase in the current densities in the passive regions. At the short exposure time when the steel is still active the current densities are also higher at 45°C. However, the time to get to the same relative passivity is much shorter at the higher temperature.

It would seem that the importance of passivation is not so much in the first hour, but the degree of passivation after this as seen at the long exposure times. Here the passive region that forms is very prominent and significantly different from the lower temperatures over shorter exposures. As mentioned above slow strain-rate tests showed an increased embrittlement when the samples were exposed to the environment prior to testing (in the order of 48 hours), therefore there was time for the steel to passivate and especially with the passive region shown after 30 hours.

How would passivation rate be related to cracking and crack propagation rate and then strain rate? There is a link, but at first the relationship is not obvious. Strain rate increases the susceptibility to cracking, and the corrosion reaction is rate related, but passivation is even more rate dependent as seen from these experimental results and there is the effect of temperature and the effect of CO concentration. Both of these parameters were varied to establish the effect on passivation and passivation rate. Therefore if it is possible to quantify the effect of temperature and/or CO concentration in terms of sensitivity to cracking and then relate that back to the passivation rate, it

might be possible to get some correlation between these. The problem with the slow strain-rate results are that these are, although performed at fixed strain rates, not always giving a fixed crack tip strain rate, which makes these results irrelevant for significant crack growth correlations. However, the effect of CO and temperature was measured for fracture mechanical tests which could be used to get an indication of correlation. These tests were performed for 50% CO at 45°C, 9% CO at 25° and 45°C and 1% CO at 25° and 45°C. The results were as follows:

Table 10-1. Fracture mechanical data for A516 pressure vessel steel exposed to CO-CO_2-H_2O environments.

% CO	Temperature (°C)	K_{ISCC} (MPa.$m^{½}$)	da/dt (m.s^{-1})
50	45	3	$4x10^{-10}$
9	45	≈10	$8x10^{-10}$
9	25	7	$5x10^{-11}$
1	45	4	$1x10^{-10}$
1	25	13	$8x10^{-10}$

From these results it can be seen that the stress intensity threshold is very similar for the 1% and 50% CO at 45°C. The results for 9% and 1% CO at 25°C are similar with higher K_{ISCC} values. Therefore, looking at the trend of the K_{ISCC} values at different CO concentrations but the same temperature (45°C) it was found that although 9% CO has the highest value there is not a significant difference between these. At 25°C it would appear that the K_{ISCC} values are slightly higher (at least the minimum and maximum values.

The crack propagation rates at 25°C are spread widely from $5x10^{-11}$ to $8x10^{-10}$ m.s^{-1}. However, at 45°C for the various CO concentrations a similar order of magnitude was

measured, especially when considering the error margin of the measurements. From this it becomes clear that carbon monoxide concentration has very little influence on the crack propagation rates. When these results are then compared to the results of the potentiodynamic scans it would explain the similarity. Since the results found after long enough exposure times the degree of passivation was independent of CO concentration. Therefore, cracking under constant conditions appear to be similar for the various CO concentrations. When the strain rate at the crack tip is varied it would interfere with the passivation rate, and therefore increase the possibility for localised corrosion and crack growth.

From the fracture mechanical data it is clear that the strain rate, and therefore indirectly the passivation rate, plays a role in the crack propagation rate of the steel, since higher crack propagation rates were achieved at increased strain rates of the crack tip.

Further, based on the passivation characteristics, and the sensitivity to strain-rate for related systems as pointed out by Parkins[43], the cyclic stresses at low frequencies were investigated, and showed dramatic loss in ductility of steel. At first, the cyclic stresses were evaluated at relatively high levels of above the yield point to establish whether cracking would occur. Once sensitivity to cracking of low frequency cyclic stresses was established, the stress levels were lowered to below the yield point, and the crack propagation still occurred. The very low frequencies employed did not necessarily cause corrosion fatigue, but only caused an enhanced strain-rate at the crack tip, providing a severe stress-corrosion cracking condition. This would have contributed to the low stresses that still caused significant crack propagation rates. From these results it was clear that the stress threshold for cracking had to be determined, with a measure that could be used for design purposes such as fracture mechanics.

The fracture mechanics analysis is very important, and troublesome, as Heaver[40] found that no cracking occurred on his specimens. This resistance to cracking can probably also be attributed to the effect of strain-rate, in this instance probably very low strain-rates. For the tests performed in this study very low stress intensity thresholds were found, even for the low carbon monoxide concentration of 1%. This is a

significant finding in terms of the crack propagation rate that can be expected and the influence of the post weld heat treatment on the inhibition of cracking. Since post weld heat treatments would not ensure that the residual stresses are reduced to below these critical stress intensities. At the higher carbon monoxide concentrations tested it would seem that the stress-corrosion threshold drops to 3 $MPa.m^{½}$ whereas at the lower carbon monoxide concentration of 1 and 9% the threshold is closer to 8 $MPa.m^{½}$, except in 1% carbon monoxide with a low dissolved oxygen content. The subcritical crack growth rates varied between $1x10^{-10}$ and $1x10^{-9}$ $m.s^{-1}$, except at around 45°C and with high dissolved oxygen concentrations.

On the fracture mechanical results, the effect of strain-rate was found to be significant, and caused a dramatic increase in the crack propagation rate. However, an increase in the strain-rate showed a certain maximum strain-rate for maximum crack propagation rates. These results confirmed what was found on the cyclically loaded tensile specimens where a high strain rate was maintained through the fluctuation in load.

The influence of the applied potential showed an increase in the stress intensity threshold when potentials were polarised more cathodically, which is in agreement with the results from the slow strain-rate tests where it was found that the stress-corrosion mechanism would be the main mechanism of cracking rather than hydrogen embrittlement.

The crack propagation rates measured during the fracture mechanical tests related to growing cracks, but not to crack initiation. Therefore, the C-ring tests in the industrial application are an important conclusion of the picture that describes not only propagation, but also crack initiation. The C-ring tests were performed over a range of stresses, and therefore give a clear indication of the susceptibility to crack initiation over a range of stresses in fractions of the yield strength. The initial crack propagation rates measured showed a reasonable agreement with the fracture mechanical data. However, when the crack propagation rate was measured over a longer period, or measured over intervals to ensure the continued growth of the cracks it was found that the crack propagation rate decreased. The stress conditions of the C-ring specimens were evaluated by finite element analysis, and clarified the cracking behaviour that

was found with the stress condition varying significantly in all the dimensions, especially through the wall thickness of the C-ring. This of course influences crack propagation significantly since the stress diminishes through the thickness of the sample even before cracking commences. Therefore, the C-ring test gives a beneficial indication of the crack initiation, but not really of crack propagation.

From all of these results it would seem that the carbon steel investigated cracked readily in these environments, especially under certain stress conditions. Although some material or specimen related parameters contributed to cracking, such as the surface roughness, cracking was mostly influenced by the environmental conditions, and especially the passivation reaction. This contributed to stress-corrosion mechanism and it was found that cracking occurred even at very low carbon monoxide levels due to the passivation of steel. Cracking occurred at low stress and stress intensity levels since the cracking was controlled by the influence of the strain rate and its relationship with the passivation reaction. When strain rates increased the crack propagation rates also increased, and it could have been strain rate controlled rather than stress controlled as such.

10.2 Conclusions

One of the most important conclusions that can be made from this work is the question of whether post weld heat treatment will be a required procedure to reduce crack initiation and propagation in environments containing water with carbon monoxide and carbon dioxide, and it was found that based on the very low stress intensity thresholds for cracking post weld heat treatments would not significantly reduce cracking.

Secondly, with the sensitivity of cracking to the strain rate of the underlying metal and the passivation rate induced by the carbon monoxide the cracking procedure was greatly enhanced by strain inducing phenomena.

The cracking was controlled by strain rate rather than stress.

Gas mixtures showed a slight variation in the stress intensity threshold for stress corrosion cracking, but the crack propagation rates were very similar.

At low carbon monoxide concentrations at 45°C the presence of dissolved oxygen concentration caused the crack propagation rate to increase from $1x10^{-10}$m.s^{-1} to $2x10^{-9}$m.s^{-1}, but the stress intensity threshold for stress corrosion stayed constant.

Decreasing the applied potential increase the stress intensity threshold for cracking and decreased the crack propagation rates.

Smooth stress raiser free surfaces exposed to industrial environments showed irregular crack initiation and propagation over a range of stresses below the yield point of the steel.

Hydrogen embrittlement was suggested in the earlier literature as a possible mechanism for crack propagation and this was investigated extensively. The slow strain-rate results showed that during cathodic polarisation no cracking occurred and this was again confirmed for the fracture mechanics, the threshold stress increased and the crack propagation rate decreased with the application of a cathodic potential. The steel also did not show a high ultimate tensile strength and hydrogen embrittlement would not be expected. Therefore, it is possible to rule out the possibility of a hydrogen embrittlement mechanism.

10.3 Recommendations

Although stress-corrosion tests were performed over a spectrum of carbon monoxide levels, more can be done in terms of the higher levels of carbon monoxide. However, these are not always encountered for industrial applications. In addition the combination of H_2S and cyanides together with carbon monoxide and carbon dioxide needs to be investigated further. Ideally it would be beneficial to evaluate the influence of cyanide and hydrogen sulphide individually with a fixed CO-CO_2 gas mixture. Because of the nature of these components it might also be beneficial to look at the effect of different strength steels and their sensitivity to cracking. The presence of cyanide in the industrial product probably produced an increase in the passivity and therefore cracking was sustained at higher temperatures. Therefore this is a component that has to be further evaluated.

Unfortunately, the influence of gas composition at high carbon monoxide concentrations was not investigated and it is important to complete the picture of the higher carbon monoxide concentrations in terms of crack sensitivity.

A probe should be developed for the evaluation of steel exposed to these types of environments in order to establish whether cracking has occurred or not.

Once cracks have been found in components the crack propagation rates can be used for determining remaining life.

11 REFERENCES

1 Kowaka, M. and Nagata, S., (1968). Transgranular stress-corrosion cracking of mild steels and low-alloy steels in H_2-CO-CO_2 systems. Corrosion, 24, No. 12, pp. 427 – 429.

2 Jones, D.A., (1996). Principles and Prevention of Corrosion. 2nd ed. Prentice-Hall Inc.; 1996.

3 Buchholtz, H., and Pursh, R., (1942). Stahl u. Eisen, **62**, p.21.

4 Logan, H.L., and Yolken, H.T., (1966). Proceedings of the second international congress on metallic corrosion, NACE, p.109.

5 Brown, A., Harrison, J.T. and Wilkins, R. Corrosion Science, 10, p. 547, 1970.

6 Kowaka, M. and Nagata, S., Corrosion, 24, p. 427, 1968.

7 Kowaka, M., and Nagata, S., (1976). Stress corrosion cracking of mild and low alloy steels in CO-CO_2-H_2O environments. Corrosion, **32**, No. 10, p.396.

8 Bowman, R.W., Dunlop, A.K., and Tralmer, J.P., (1977). CO/CO_2 cracking in inert gas miscible flooding. Corrosion, **16**, p.28.

9 Brown, A., Harrison, J.T., and Wilkins, R., (1973). Electrochemical investigations of stress corrosion cracking of plain carbon steel in the carbon dioxide -carbon monoxide - water system. Conference on the stress corrosion cracking and hydrogen embrittlement of iron base alloys, Unieux-France, p.686-695.

10 Hannah, I.M., Newman, R.C., and Procter, R.P.M., (1990). Environmental cracking of C-Mn steels in aqueous CO-CO_2 environments. Proceedings of the 4th interntional conference on the effect of hydrogen on the behaviour of materials. Edited by Moody, N.R., and Thompson, A.W., p. 965.

11 Parkins, R.N., Blanchard Jr., W.K., and Delanty, B.S., (1994). Transgranular stress corrosion cracking of high-pressure pipelines in contact with solutions near neutral pH. Corrosion, **50**, No. 5, p.394-408.

12 Kowaka, M., (1991). Metal corrosion damage and protection technology, Allerton Press, p.255.

13 Spahn, H., Wagner, G.H. and Steinhoff, U., (1977). Proceedings of internatiol conference on stress corrosion cracking and hydrogen embrittlement of iron base alloys, NACE, Houston, Texas (Unieux Firminy) p. 80

14 Dunlop, A.K., and Olson, E.E., (1975). Inhibition of stress corrosion cracking of steel in aqueous CO/CO_2 environments. Proceedings of the sixth international congress on metallic corrosion. p332-342.

15 Berry, W.E., and Payer, J.H., (1979). Internal stress corrosion cracking by aqueous solutions of CO and CO_2. The sixth symposium on line pipe research; Pipeline Research Committee of American Gas Association, Houston Texas, p. 251-268.

16 Schmitt, G., and Rothman, B., (1978). Corrosion of unalloyed and low alloyed steels in carbonic acid solutions. Werkstoffe und Korrosion, Vol 29, p237.

17 Schmitt, G., (1983). Fundamental aspects of CO_2 corrosion. Corrosion'83, paper 43.

18 Whitman, G.W., Russel, R.P., Altieri, V.J., (1924). Ind. Eng. Chem., **16**, No.7, p.665.

19 Rothmann, B., (1977). PhD Thesis, Technical university of Aachen.

20 Schmitt, G., (1981). gwf-gas/erdgas, **122**, No.2, p.49.

21 Schmitt, G., and Rothmann, B., (1977). Werkstoffe und Korrosion, **28**, p.816.

22 Urbach, H.B., Adams, L.G., Smith, R.E., (1974). J. Electrochem. Soc., **55**, p391.

23 De Waard, C., and Milliams, D.E., (1975). 1st International conference on the internal and external protection of pipes, Durham, England, Paper F1.

24 De Waard, C., and Milliams, D.E., (1975). Corrosion, **31**, No. 5, p.177.

25 Prange, E.A., (1959). Corrosion, **15**, No. 2, p.49t.

26 Lange, K.H., and Pöpperling, R.K., (1980). 12th Annual offshore technology conference, Houston, Texas, OTC3890.

27 DeBerry, D.W., Clark, W.S., and Yost, A., (1980). Corrosion due to the use of carbon dioxide for enhanced oil recovery, Final report, SumX No. 78-003, SumX Corporation, Austin, Texas, DOE/MC/08442-1, Corrosion abstract, **19**, p.342.

28 Rhodes, F.H., and Clark, J.M., (1936). Ind. Eng. Chem., **41**, p.1078.

29 The Field Testing of 32 Alloys in the Flow Streams of Seven Condensate Wells. National Association of Corrosion Engineers, Publication 50-3, July 1950.

30 Hudgins, C.M., McGlasson, R.L., Mehdizadeh, P., and Roborough, W.M., (1966). Corrosion, **22**, p.236.

31 Schmitt, G., Schlerkmann, H., and Aachen, F.R.G., (1981). Corrosion cracking of steel in the system CO_2/H_2O. Proceedings of the eighth international congress on metallic corrosion, p.426-431.

32 Heusler, K.E., and Cartledge, G.H., (1961). The influence of iodide ions and carbon monoxide on the anodic dissolution of active iron. Journal of the electrochemical society, **108**, No. 8, p.732-740.

33 Cotton, F.A., and Wilkinson, G., (1968). Advanced inorganic chemistry, **611**, Interscience.

34 Trabanelli, G., Zucchi, F., and Zucchini, G.I., (1968). Influence du mono-oxyde de carbone sur les processus de dissolution des mètaux. Corrosion - Traitement protection finition, **16**, No. 7, p. 335-345.

35 Durrant, J.P, and Durrant, B., (1962). Introduction to advanced inorganic chemistry, Longmans, London.

36 King, C.V., and Rau, E., (1956). Journal of the electrochemical society, **103**, p331.

37 Malik, H., and Nawaz, F., (2005). Stress corrosion cracking and electrochemistry of C-Mn steels in CO-CO_2-H_2O environments. Anti-Corrosion Methods and Materials, **52**, pp. 259-265.

38 Gräffen, H., and Schlecker, H., (1985). Stress corrosion cracking (SCC) of unalloyed steels exposed to CO-CO_2-H_2O systems. Int. Report, Bayer, Leverkussen.

39 Traversa, E., and Calderón, T., (1991). Electrochemical investigation on carbon steel behaviour in CO-CO_2-H_2O environment for the interpretation of the scc mechanism, Werkstoffe und Korrosion, **42**, p.35-40.

40 Heaver, E.E., (1994). Stress corrosion cracking of steels in industrial process environments, PhD thesis.

41 Parkins, R.N., (1979). Development of strain-rate testing and its implications in stress-corrosion cracking – The slow strain-rate technique, STP 665. Ugiansky, G. M. and Payer, J.H. Ed. American Society for Testings and Materials, p. 82-93.

42 Tanimura, M., Nishimura, T., Nakazawa, T., (1974). SCC of high strength steels in CO-CO_2 gas. Nippon Kokan Technical Report Overseas, No.19, 9, pp9-16; Chem. Abstr. 84, 48416.

43 Parkins, R.N., (1990). Strain rate effects in stress corrosion cracking. Corrosion, **46**, No. 3, p178-189.

44 Parkins, R.N., and Singh P.M., (1990). Stress corrosion crack coalescence, Corrosion, **46**, No. 6, p.485-499.

45 Kitagawa, H., Fugita, T., and Miyazawa, K., (1978). Corrosion Fatigue Technology, ed. Craig Jr., H.L., Crooker, T.W., and Hoeppner, D.W., ASTM STP 642 (Philadelphia, PA ASTM 1978), p.98.

46 Parkins R.N., (1989). The application of stress corrosion crack growth kinetics to predicting lifetimes of structures, Corrosion Science, **29**, No. 8, p. 1019-1038.

47 Brown, B.F. and Beacham, D.C., (1965). A study of the stress factor in corrosion cracking by the use of the precracked Cantilever-Beam Specimen. Corrosion Science, **5**, p.

48 Kowaka, M., and Nagata, S., (1968). Transgranular stress corrosion cracking of mild steels and low alloy steels in the H_2O-CO-CO_2 system, Corrosion, **24**, No. 12, p.427-429.

49 Nakagawa, K., Kenjo, T., and Kawamoto, T., (1980). Proceedings of `80 annual spring meeting of Japanese society of corrosion engineering, p.54.

50 Hinton, B.R.W., and Procter, R.P.M., (1983). The effect of strain-rate and cathodic potential on the tensile ductility of X-65 pipeline steel, Corrosion Science, **23**, No.2, p.101-123.

51 Vosikovsky, O., (1975). Trans. ASME Jnl. Engng. Mater. Tech, **97**, p298.

52 Hinton, B.R.W., (1980). University of Manchester, PhD Thesis.

53 Hoar, T.P. and West, J.M., (1962). Proc. Royal Soc., A268, 304.

54 Parkins, R.N. (1975). Proceedings of the NATO Advanced Study Institute on Stress Corrosion Research, Stress-corrosion research. Sijthoff and Noordhoff, p 1 – 17.

55 Parkins, R.N., Predictive approaches to stress corrosion cracking failure. Corrosion Science, Vol 20, 1980, p.147 – 166.

56 Metal Corrosion, Erosion, and Wear, Vol. 03.02, Section 3, Annual Book of ASTM Standards, ASTM.

57 Smith, H.R., and Piper, D.E., Stress Corrosion Testing with Precracked Specimens, Stress Corrosion Cracking in High Strength Steels and in Titanium and Aluminium Alloys, Brown, B.F. Ed., Naval Research Laboratory, 1972, pp. 17 – 78.

58 Standard Method Test for Plane-strain Fracture Toughness Testing of Metallic Materials, E 399, Annual Book of ASTM Standards, Vol. 03-01, ASTM.

59 Sprowls, D.O. Evaluation of Stress-Corrosion Cracking. In: Jones, R.H.,editor. Stress-Corrosion Cracking. Ohio:ASM International; (1992). p. 363-416.

60 Manahan, Sr, M.P., Macdonalld, D.D., and Peterson, A.J., (1994). Determination of the fate of the current in the stress corrosion cracking of sensitzed type 304 stainless steel in high temperature aqueous systems, Corrosion science, **37**, No. 1, pp. 189-208.

61 Macdonald, D.D., and Urquidi-Macdonald, M., (1991). A coupled environment model for stress corrosion cracking in sensitized type 304 stainless steel in LWR environments. Corrosion Science, **32**, No. 1, pp.51-81.

61 Chung, P.C., Cragnolino, G., and Macdonald, D.D., (1985). Corrosion, **41**, p 179.

63 Metal Corrosion, Erosion and Wear, Vol. 03.02, Section 3, Annual Book of ASTM Standards, ASTM.

64 Turnbull, A., (1992). Test methods for environment assisted cracking. British Corrosion Journal, vol 27, no 4 p.275.

65 Itoh, G., (1977). Ko-atsu gas (J. Inst. Safety High-Pressure Gas Eng.), **14**, 19.

66 Kim, C.D., and Wilde, B.E., (1979). A review of Constant Strain-Rate Stress Corrosion Cracking Test, Stress Corrosion Cracking – The Slow Strain Rate Technique, STP 665. G.M. Ugianski and J.H. Payer, Ed., American Society for Testing and Materials, p 97 -112.

67 Staehle, R.W., Royuela, J.J., Serrate, E., Morin, C.R. and Farrar, R.V., (1970). Effect of alloy composition on stress corrosion cracking of Fe-Cr-Ni base alloys. Corrosion, 26, pp. 451-486.

68 Heusler, K.E., and Cartledge, G.H., (1961). The influence of iodide ions and carbon monoxide on the anodic dissolution of active iron. Journal of the electrochemical Society, **108**, No. 8, pp.732-740.

69 Wei, R.P., and Landes, J.D., (1969). Material Research Standards, **9**, p.25.

70 Heaver, E.E., and Sandenbergh, R.F., (1993). Inhibition of stress corrosion cracking of carbon manganese steels in the CO_2-H_2O system, Progress in the understanding and prevention of corrosion, Ed. J M Costa and A D Mercer, vol. **2**, p.1562-1572.

71 Buchholtz, H., and Pusch, R., (1942). Stahl u Eisen, **62**, p. 21.

72 Schutt, H.U., (1988). New aspects of stress corrosion cracking in monoethanolamine solutions. Materials Performance, **27**, pp. 53-58.

73 Heaver E.E., (1994). Stress corrosion cracking of steels in industrial process environments, PhD thesis.

APPENDIX A. – MegChem Vibration Analysis Report

REPORT

MEGCHEM
ENGINEERING AND DRAFTING
SERVICES (PTY) LTD
Reg no.: 93/00296/07

VIBRATION ANALYSIS ON TOTAL FEED GAS LINE - UNIT 220

Date: 19 November 1996

Author: DE Botha

Designation: Senior Engineer

JOB PARTICULARS

Equipment number	:	220-LN-1012 CC
Equipment	:	Total Feed Gas Line
Plant	:	Synthol East
Client	:	W. Binkowski Tel: (017) 610-2554
Electronic File	:	C:\MyFiles\FEA Final Reports DEB\Total Feed Gas line vibrations.wpd
Date	:	19 November 1996
Revision number	:	01
Complied By	:	DE Botha Tel: (017) 619-2436 Fax:(017) 619-2525

SIGNED: DATE: 21/11/96

APPROVED: DATE: 21/11/96

CONTENTS

1. INTRODUCTION

Excessive vibrations on the pump-around structures lead to the modification of the total feed gas line supporting mechanism to the structure. This modification proved to be successful in that it reduced the pump-around structure vibration satisfactorily. Concern however was raised regarding the influence of the modification to the pipe line itself. This lead to this investigation which is aimed at accessing the fatigue loading of the pipe line.

2. DESIGN DATA

Design Pressure	:	3300 kPa
Design Temperature	:	245 °C
Operating Pressure	:	2540 kPa
Operating Temperature	:	175°C
Material	:	API-SL-B
Design Code		

3. ANALYSIS

This analysis was conducted in three phases. The first phase was a finite element analysis which was done to reveal the points of high stresses and to obtain a global picture of the stress distribution in the pipe line. The second phase was to do vibration measurements using accelerometers in order to establish which frequencies were excited in the pipe. Finally two strain gauges were applied onto one of the elbows which would firstly provide a means of scaling the finite element analysis modal stresses and also to provide stress cycle information (range pair counting).

4 . RESULTS & DISCUSSION

A normal mode dynamic analysis (eigen values) was done which shows the modal stresses for each mode (refer to the figures attached). From the vibration measurements and the strain gauge measurements (refer to the graphs attached) it is clear that the active modes are in the vicinity of 2 Hz. These modes are more closely observes in the elbow at which the strain gauges were applied. The measurements from the accelerometers, measured on the fourth elbow from the left end of the pipe (refer to the attached figures) are seen to correspond quite closely to the measurements of the strain gauges (which were attached to the second elbow in the direction of flow) with the main activity at approximately 2 Hz. From the accelerometer measurements it can be observed that the east-west movement is highest, followed by the north-south movement while the vertical movement in the vicinity of 2 Hz is practically absent. This would imply (looking at the difference between the mode shapes of modes 2 and 3 which are close to 2 Hz) that the most active mode in this case seems to be mode 3. Mode 2 has virtually no lateral movement at the fourth elbow while mode 3 has significant movement in the lateral directions and little movement in the vertical direction.

It can be seen from the strain gauge measurements that the stresses on the inner radius (IR) of the elbow are much higher than at the outer radius (OR) which is expected. Referring to figure 2(d), it is observed that the strain gauges measure stresses in the same direction as the maximum principal stresses for mode 3. From the finite element results (figure 2(b)) the ratio of inner radius stress to outer radius stress is approximately 4.03/1.07=3 .8. Referring to the frequency responses of strain gauge measurements the ratio is approximately 0.16/0.043=3.7. Once again mode 3 is confirmed to be the significant mode of movement.

In general all results indicate low stress levels. The stresses that are given by the finite element analysis are modal stresses which only give relative information depending on the amount with which the modes are excited. The finite element analysis can however provide stress distribution information which a strain gauge cannot give and therefore the stresses measured by the strain gauge are used to scale the finite element analysis results. For fatigue purposes it is appropriate to observe the maximum shear stresses (which is equal to the algebraic difference betwee11 the maximum and the minimum principal stresses). From figure 2(a) the maximum shear stress on the inner radius is 0.14 MPa compared to the strain gauge reading at the same position of 0.16 MPa at 2Hz. This position (inner radius) is however not the worst spot on the elbow. The top and bottom positions have a modal stress (figure 2(a)) of 2.09 MPa which means that the values from the strain gauge measurements would have to be scaled by a factor of 2.09/0.14*0.16 = 2.4 in order to arrive at a suitable stress range for fatigue calculations. From the stress cycle count graph, the maximum stress range recorded is less than 5 MPa which when multiplied by 2.4 gives less than 12 MPa. From the fatigue curves in ASME VIII Div 2 this stress range is far below the limits of the graph which implies that no risk of fatigue exists (stress levels are below the endurance limit).

5. CONCLUSION

Stress levels are lower than the endurance limit and fatigue failure is not expected in this pipe line due to its vibration. ·The integrity of the pipe is not threatened by the modification to the supports

MODAL STRESSES AND SHAPES FOR THE FIRST 6 MODES

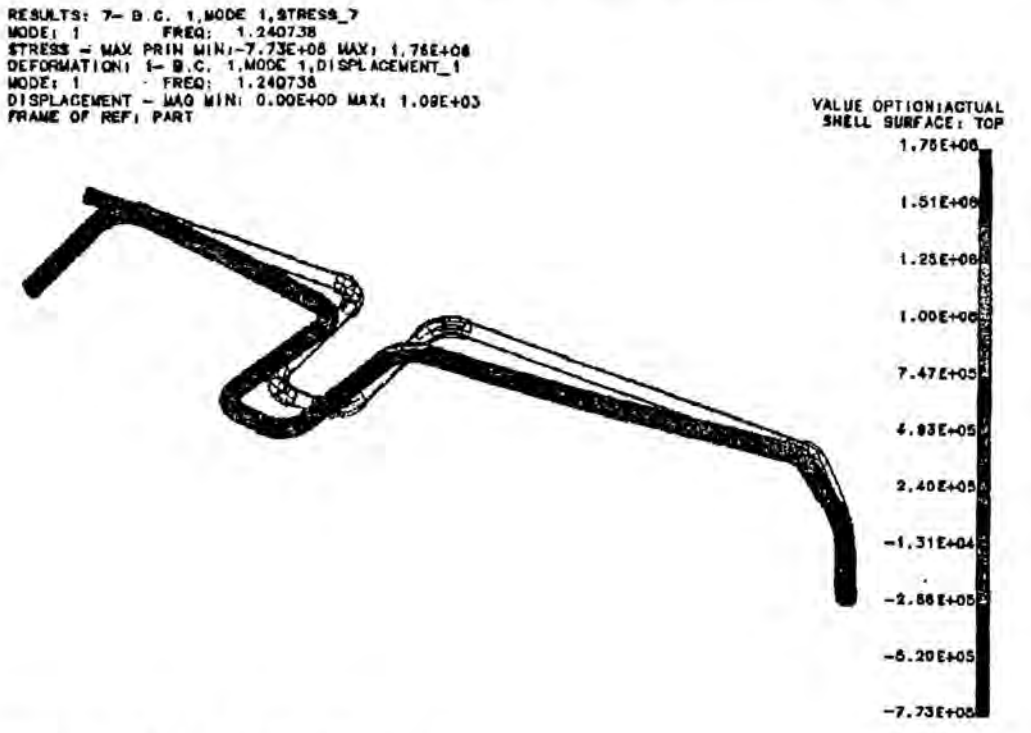

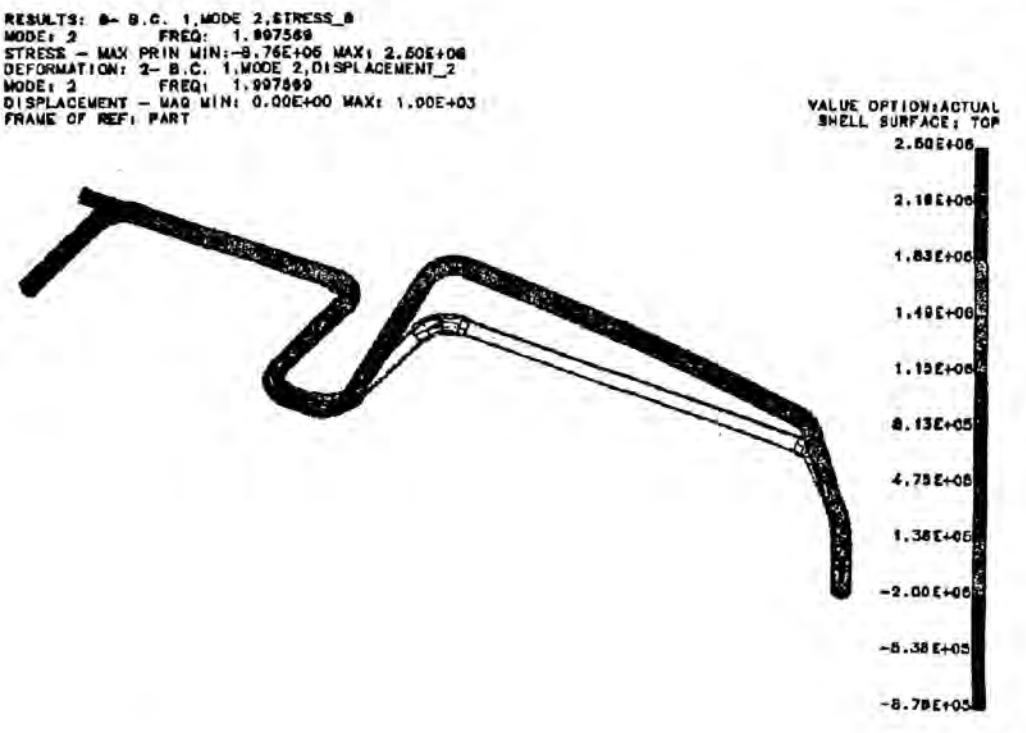

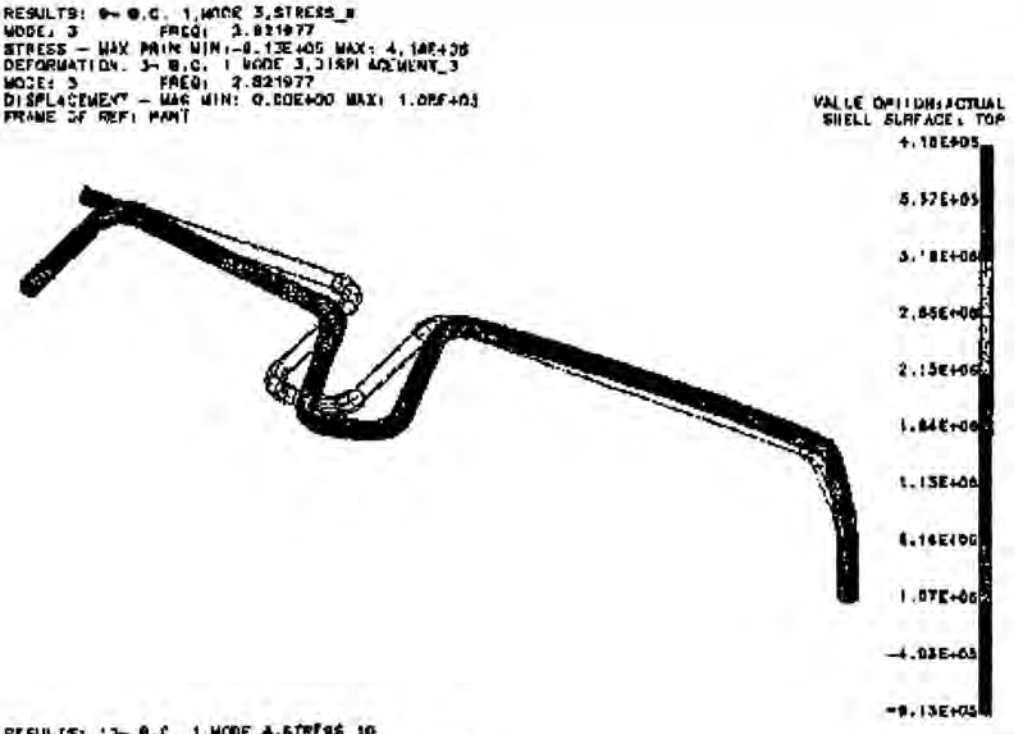

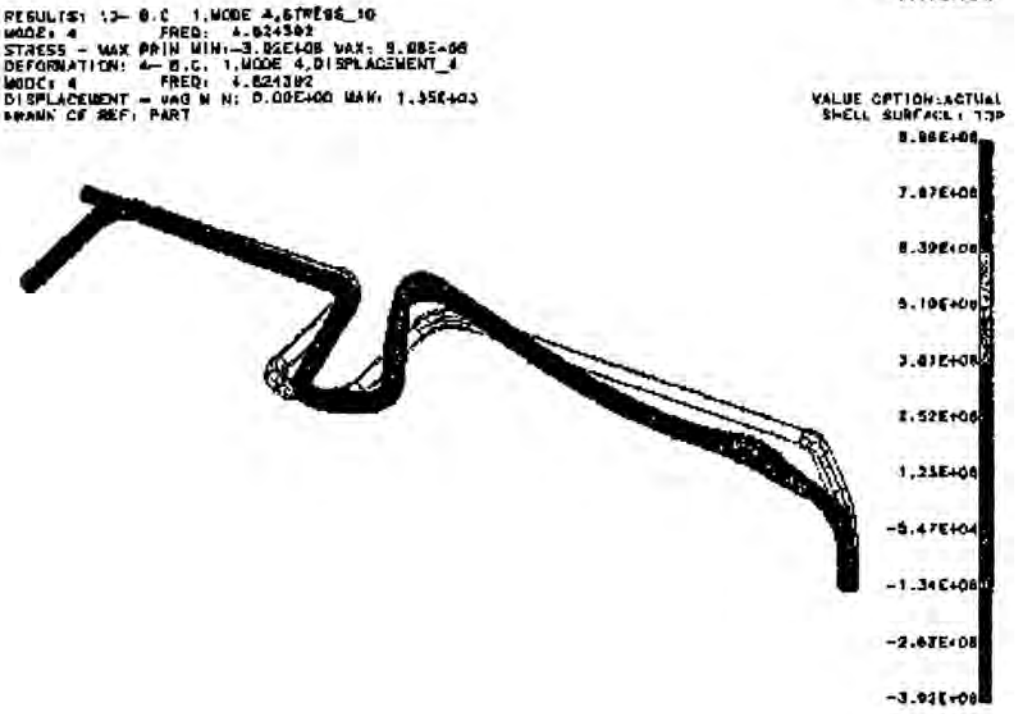

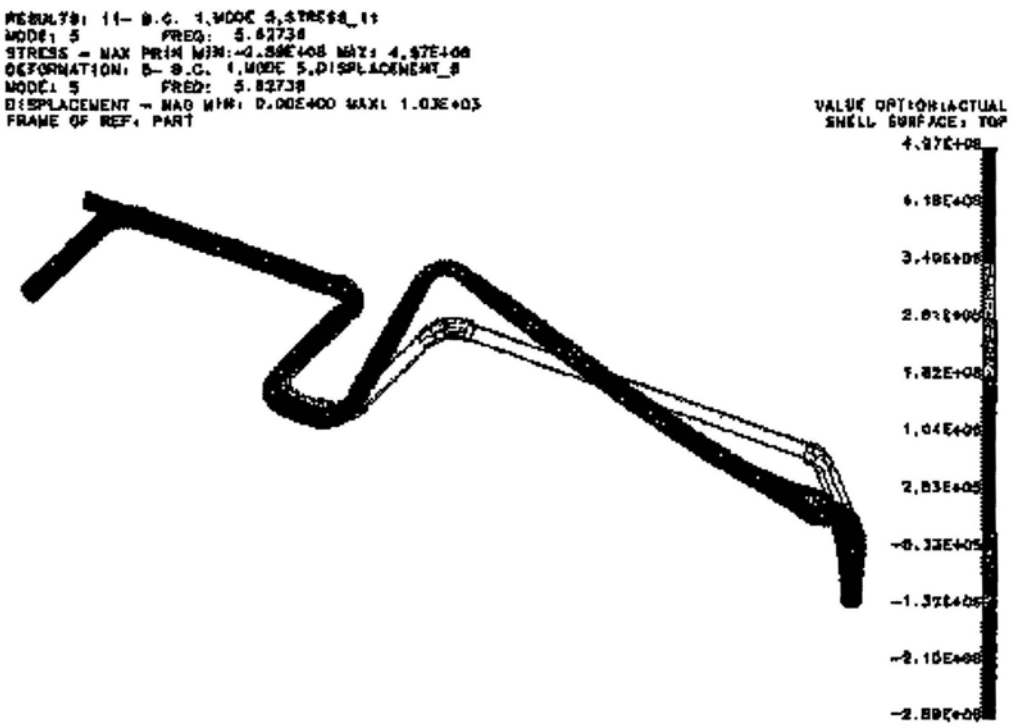

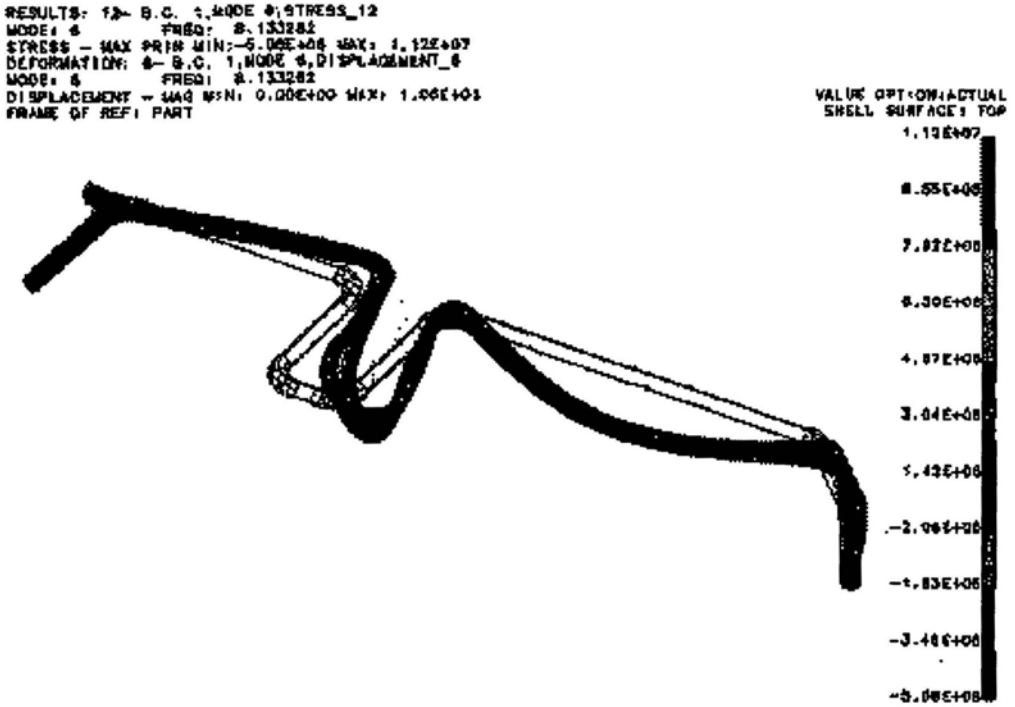

ZOOMED VIEWS OF STRESSES ON ELBOW (#4)

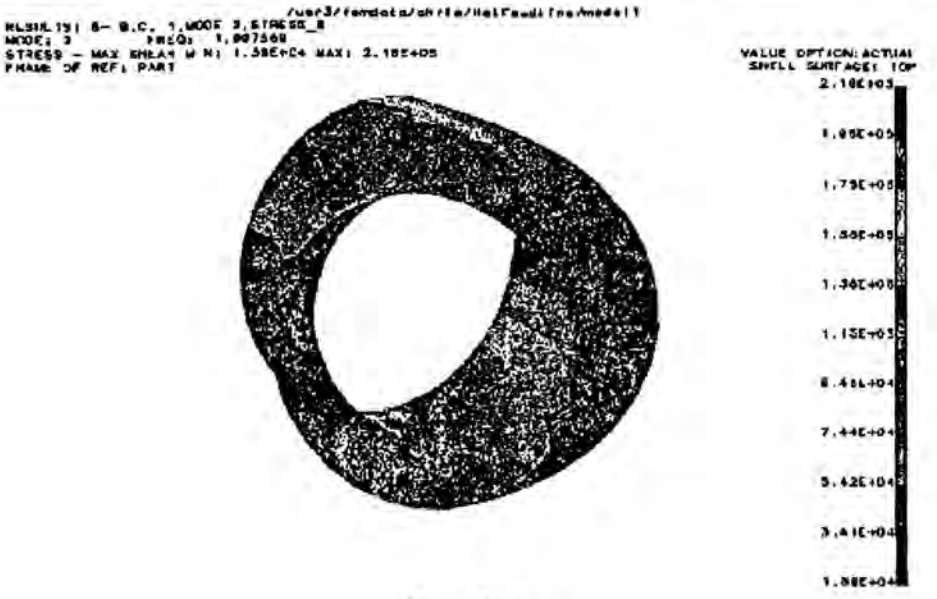

Figure 1(a)

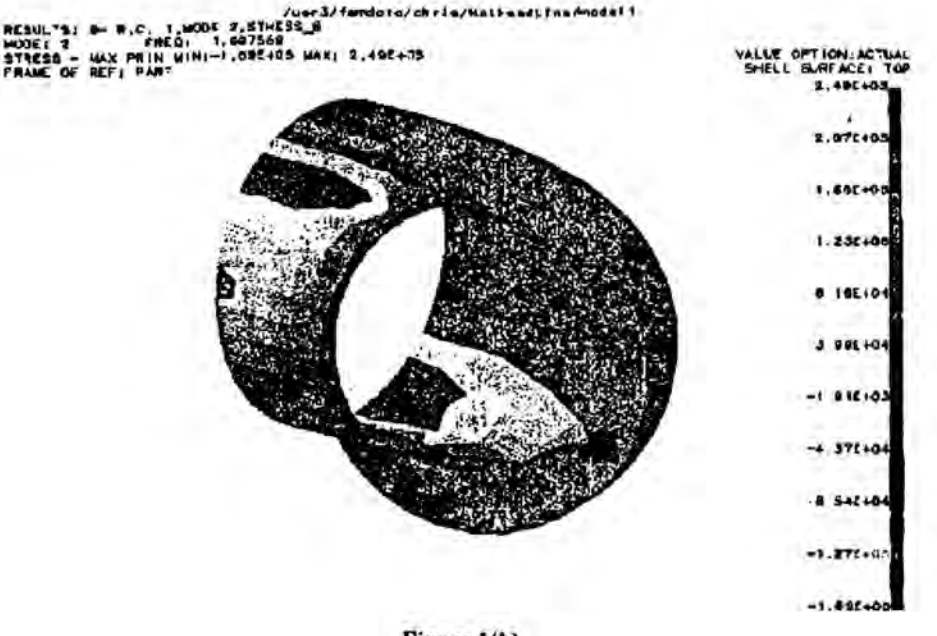

Figure 1(b)

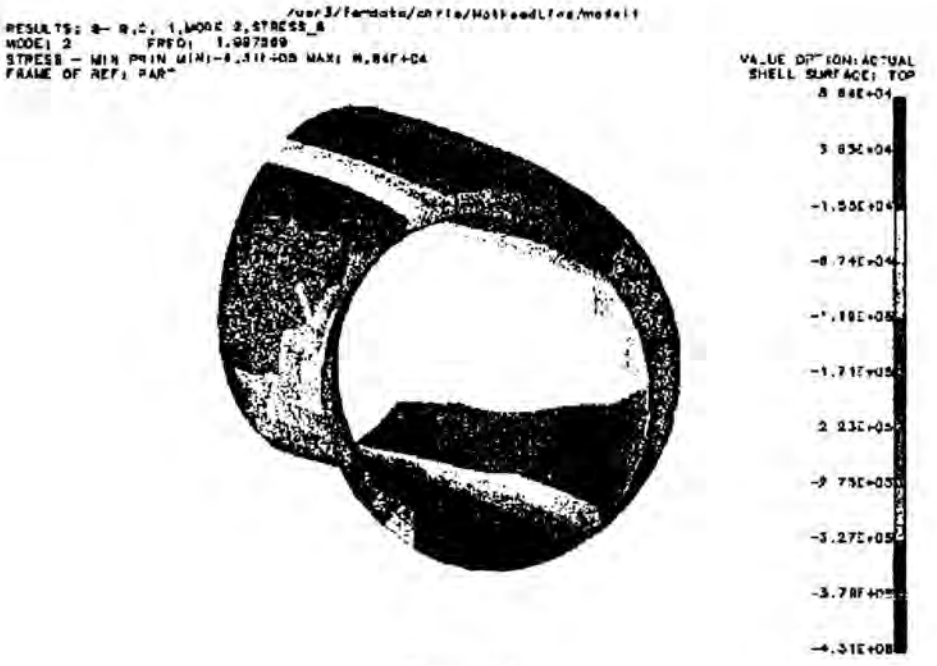

Figure 1(c)

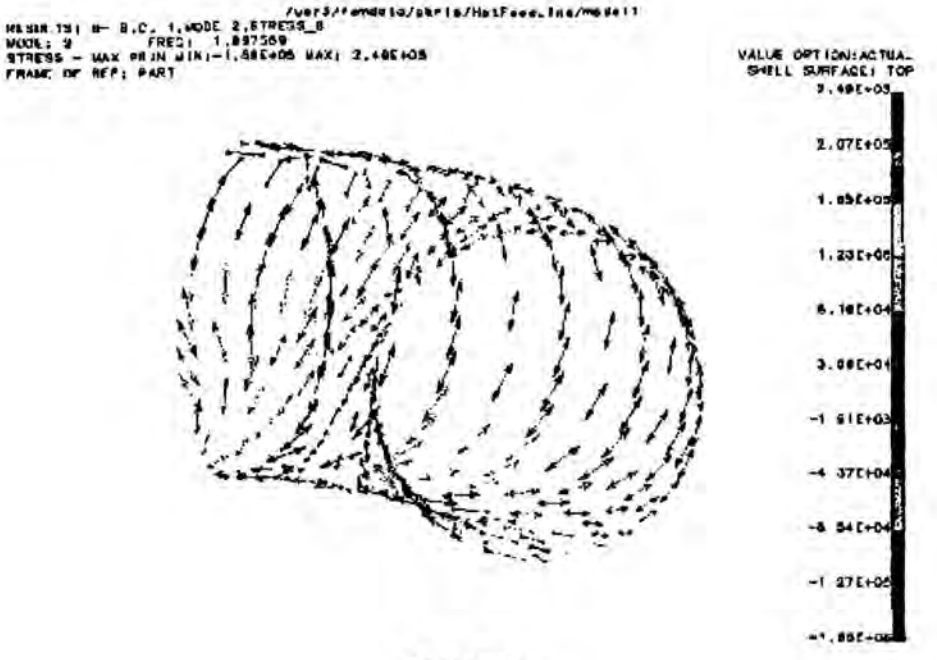

Figure 1(d)

Figure 1(e)

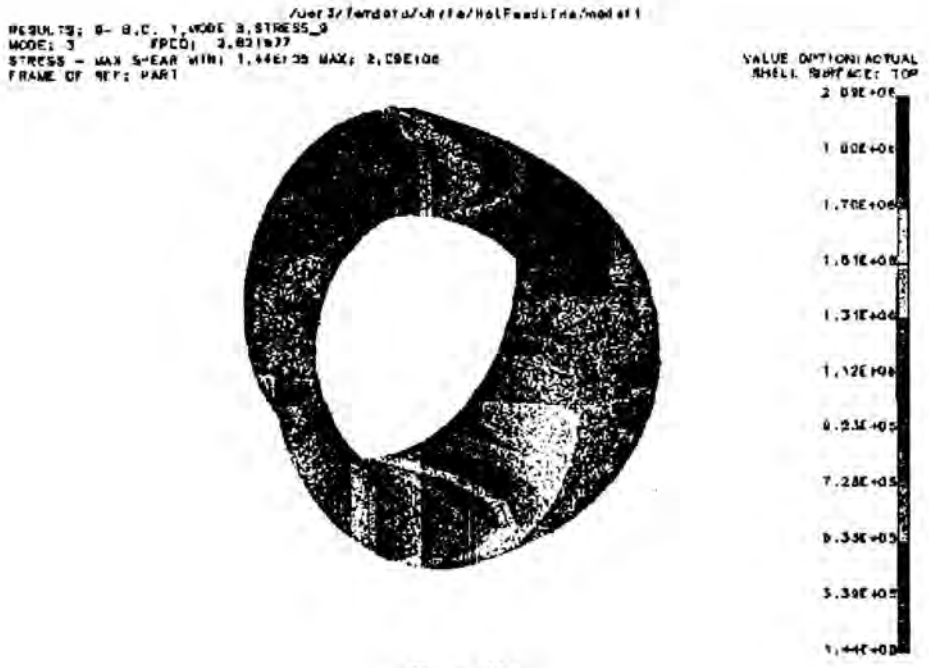

Figure 2(a)

Figure 2(b)

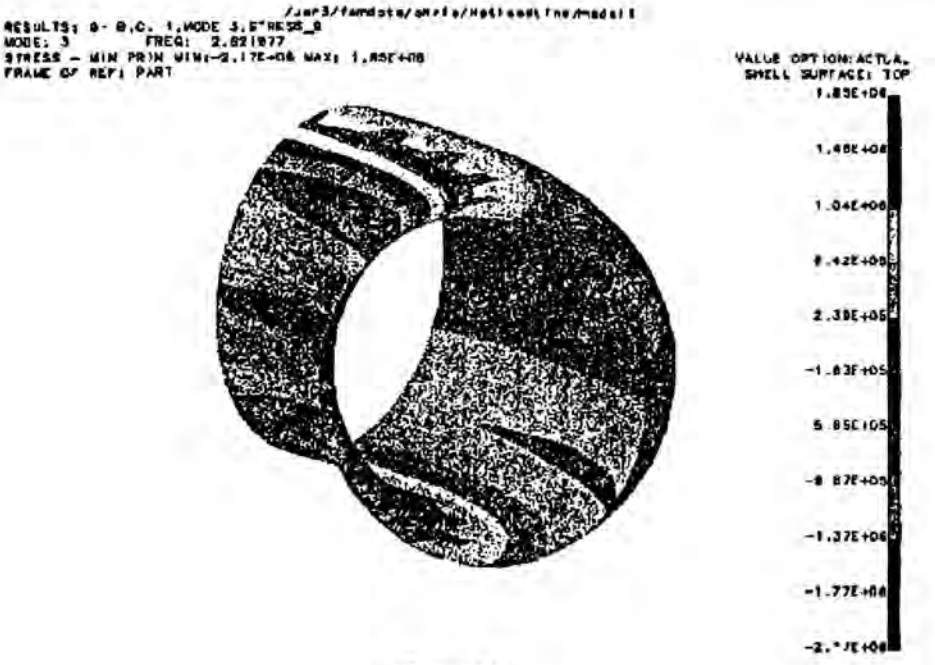

Figure 2(c)

Figure 2(d)

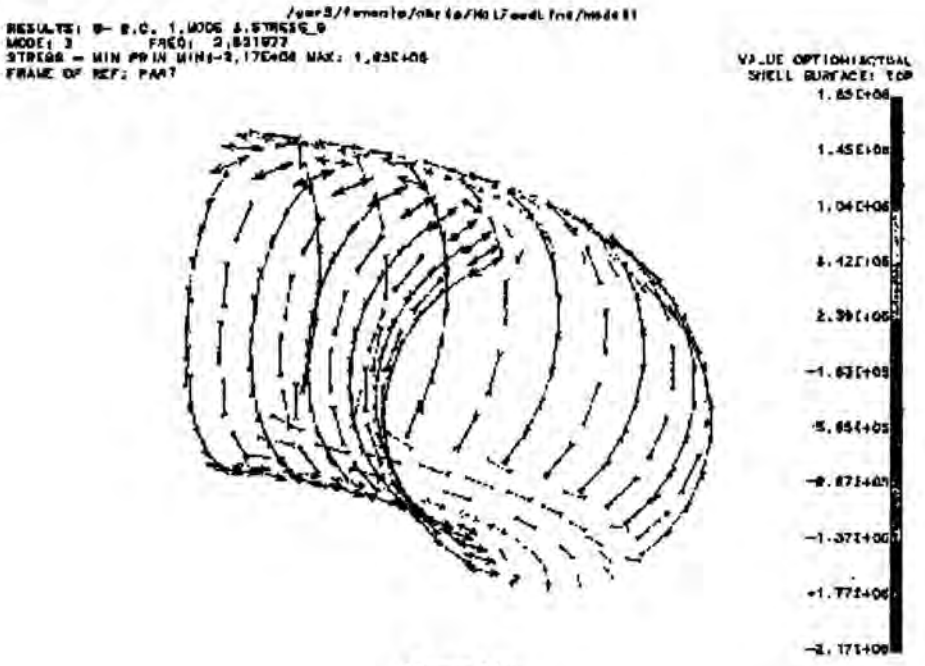

Figure 2(e)

VIBRATION MEASUREMENT RESULTS

TOTAL FEEDGAS LINE TRAIN 1 ON EXPANSION LOOP SOUTH WEST ELBOW

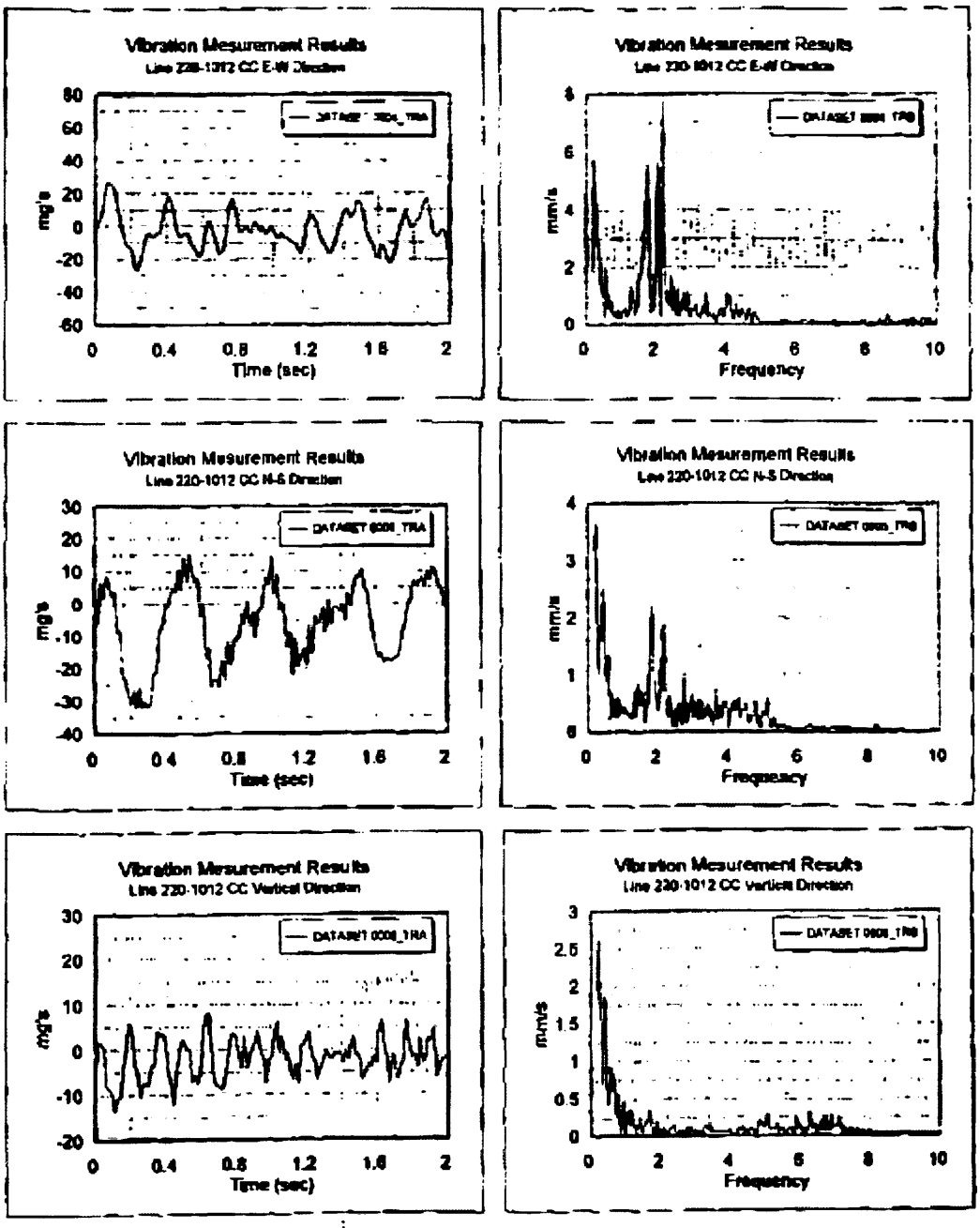

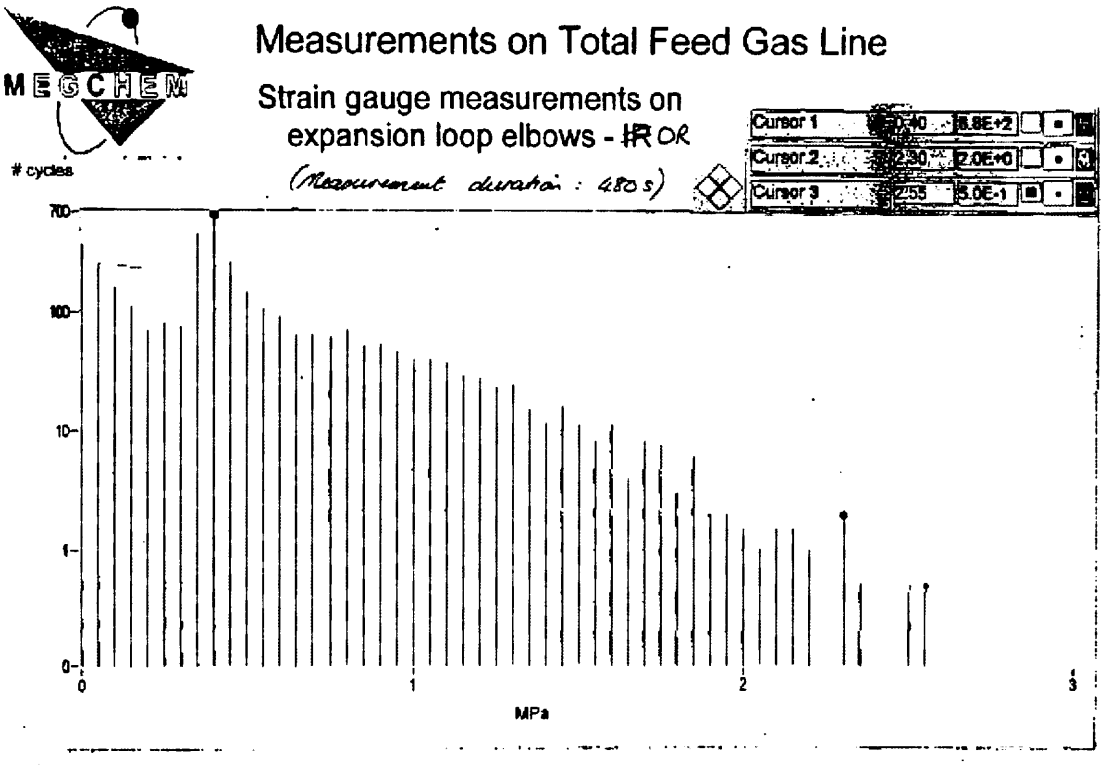

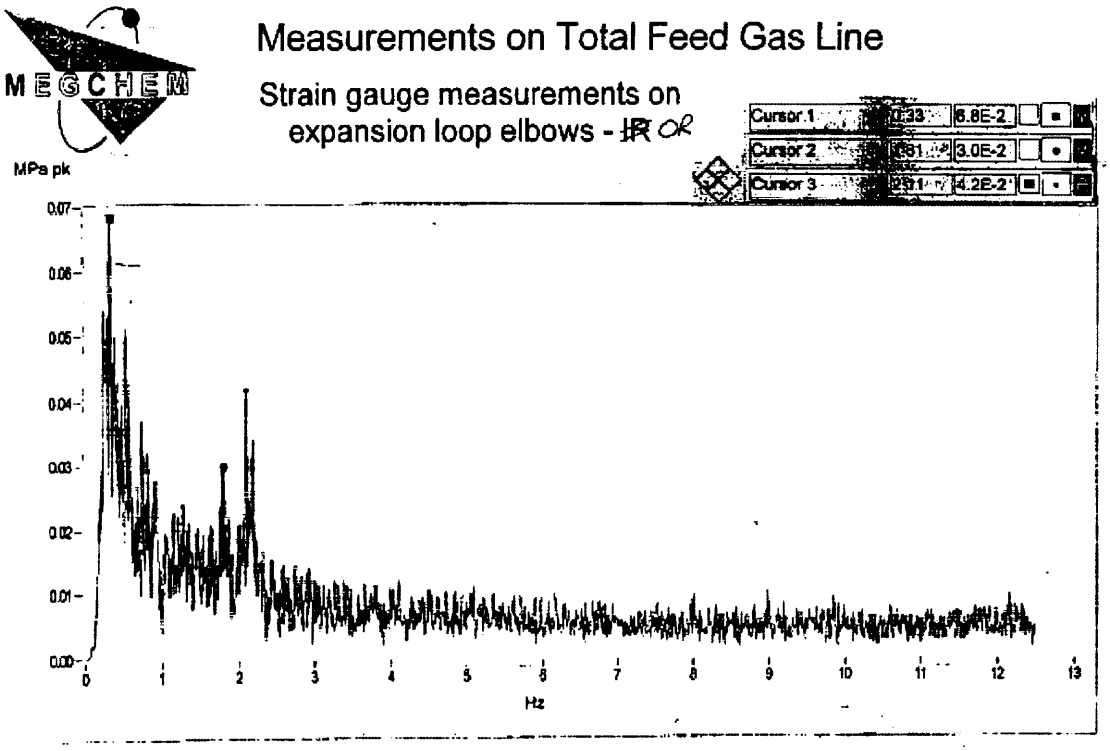

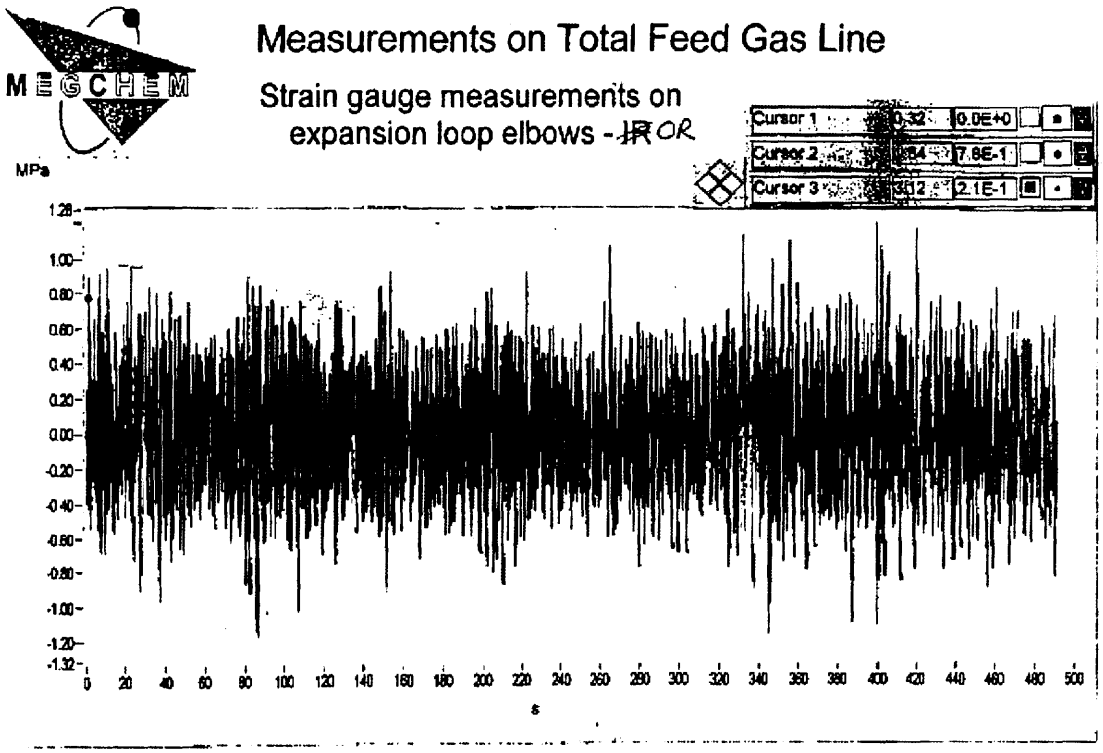

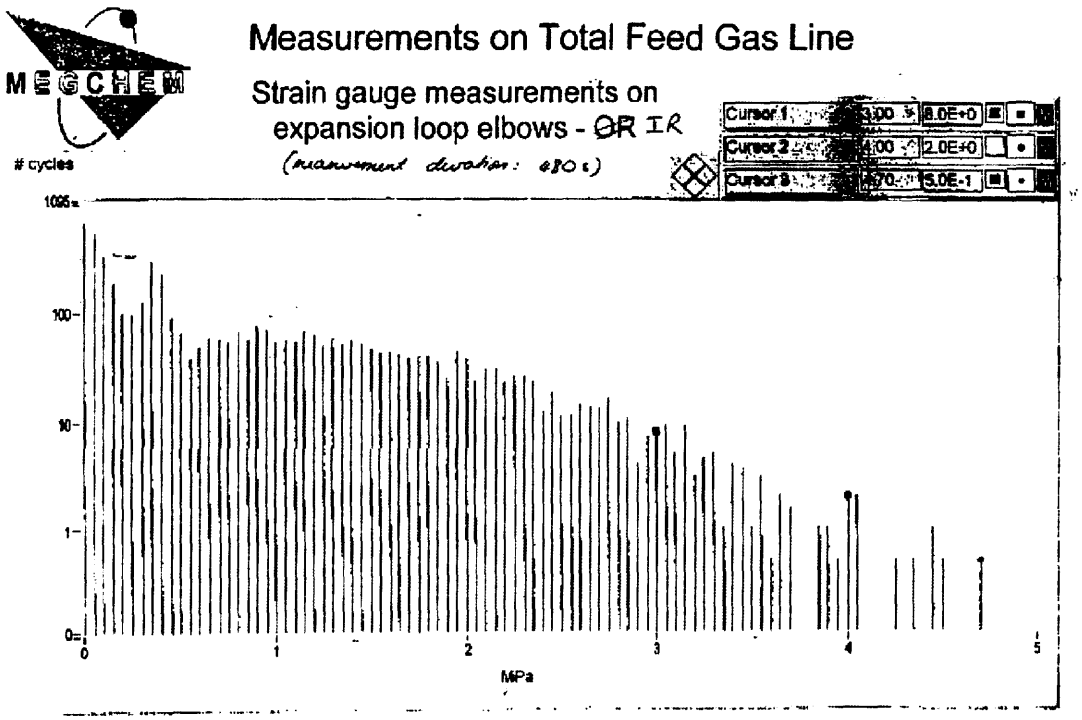

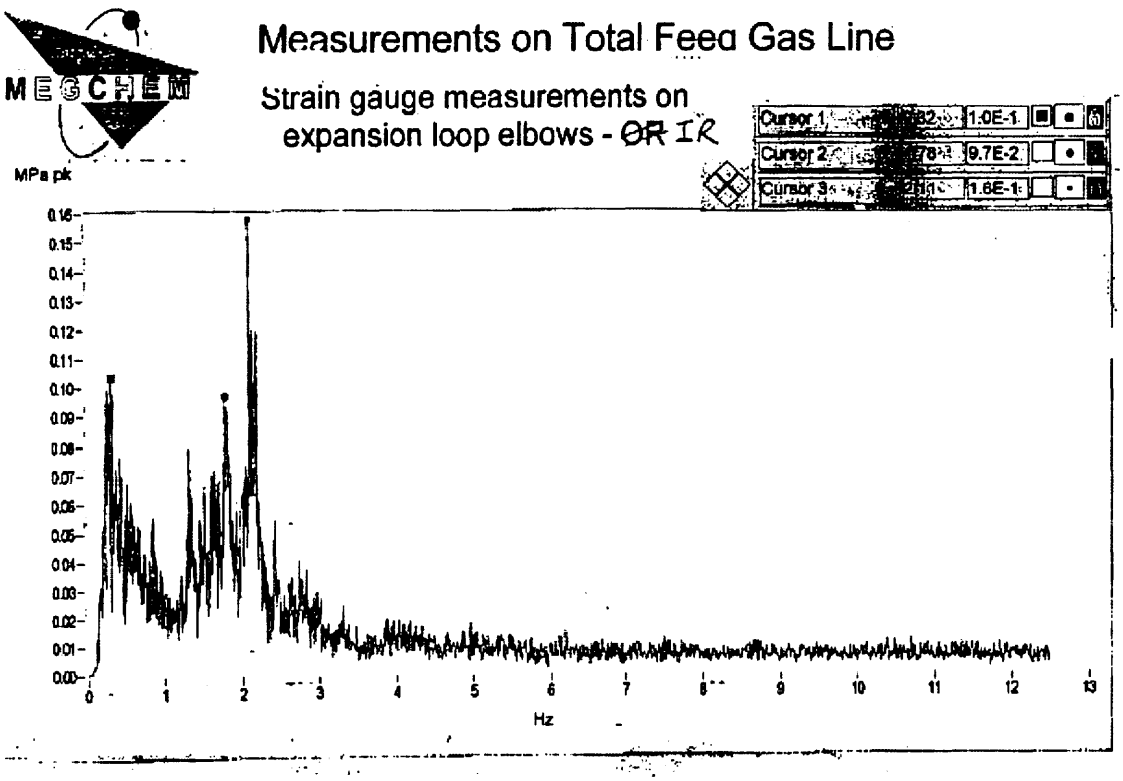

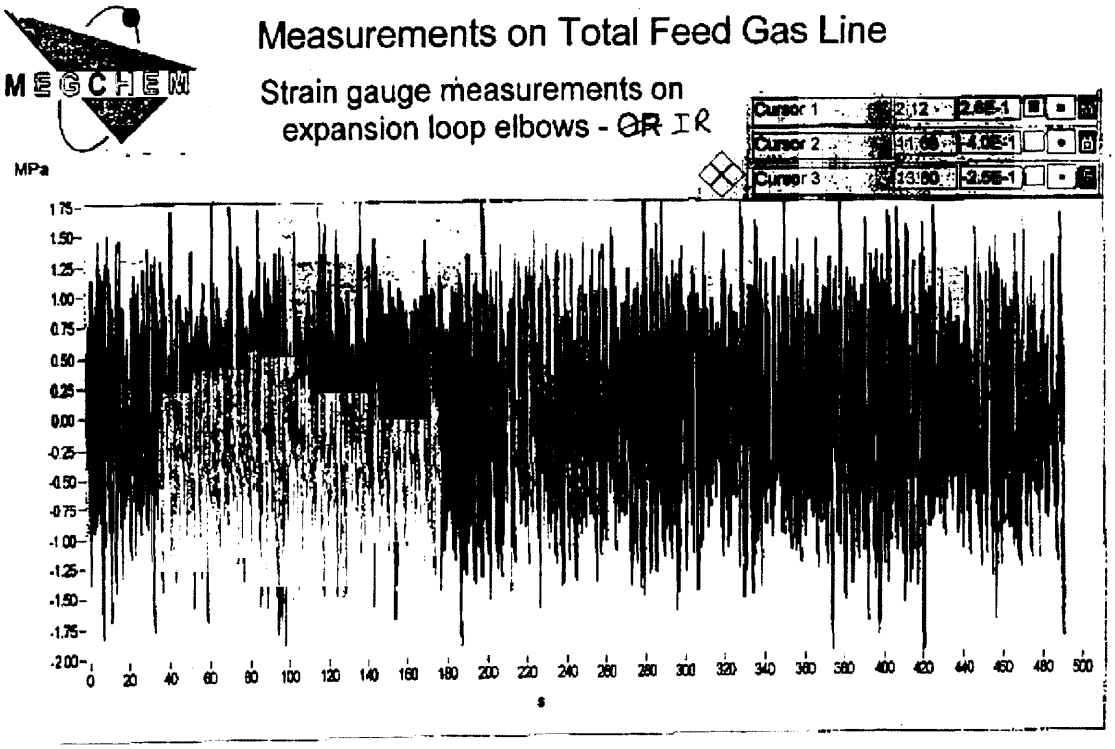

VIBRATION MEASUREMENT RESULTS

TOTAL FEEDGAS LINE TRAIN 1 ON EXPANSION LOOP SOUTH WEST ELBOW

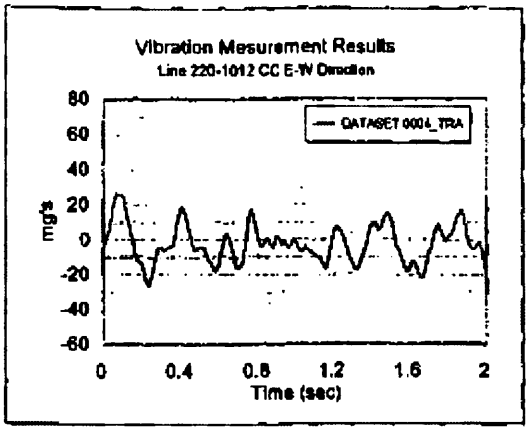

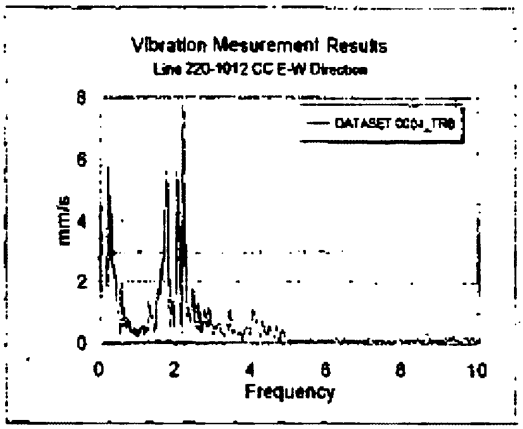

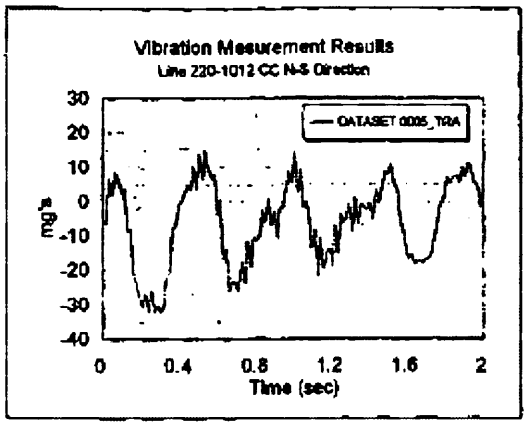

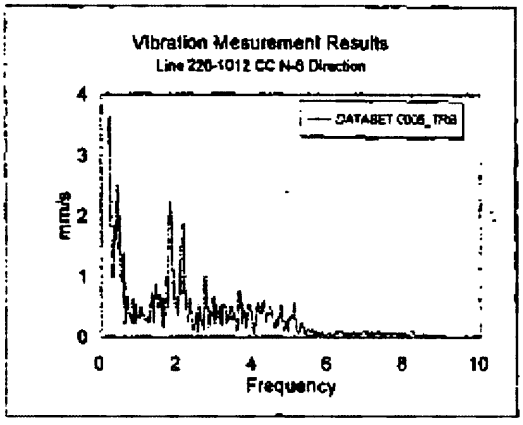

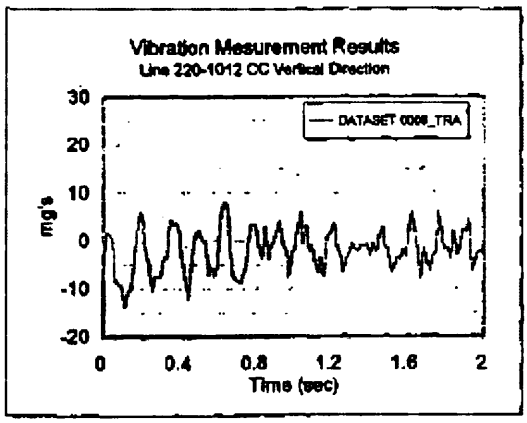

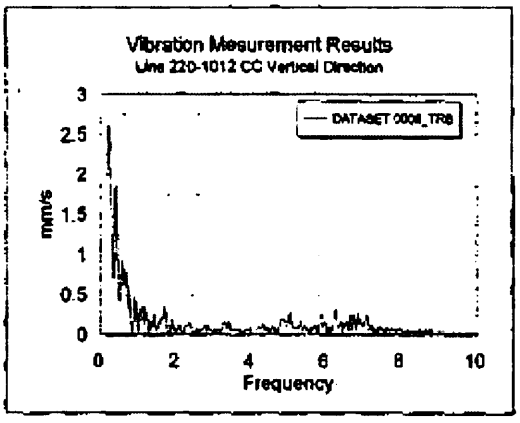

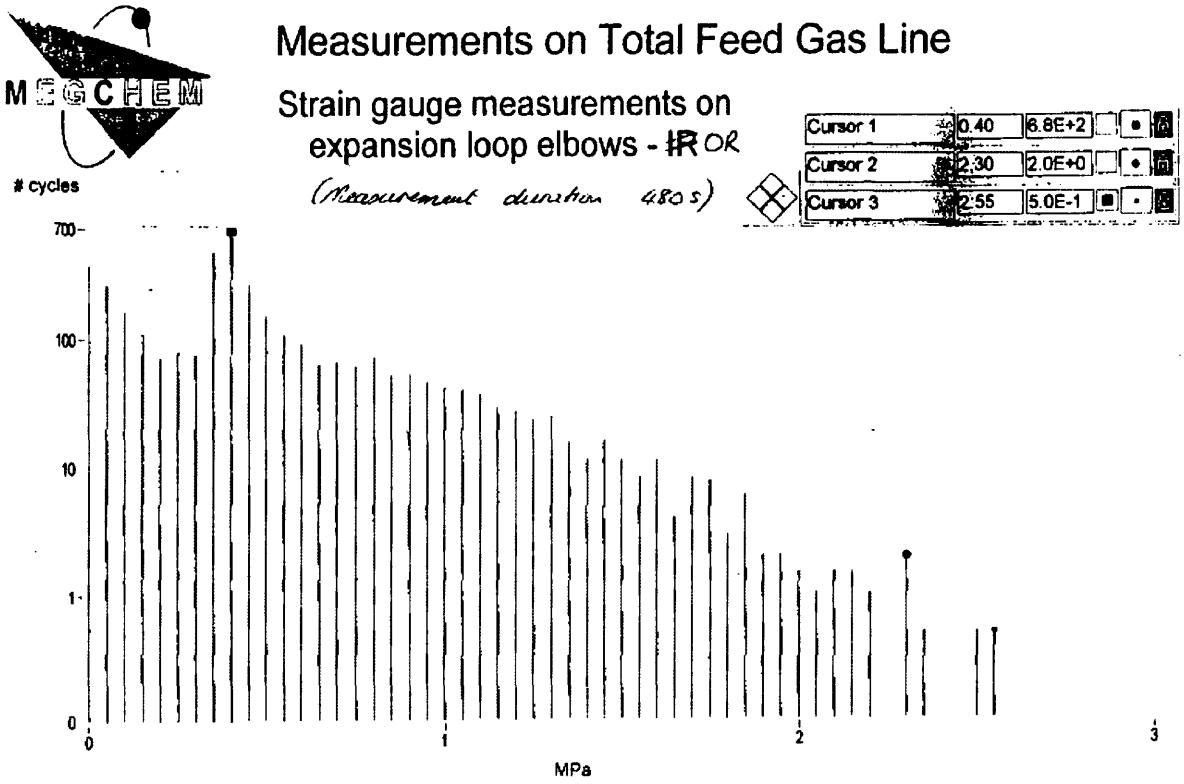

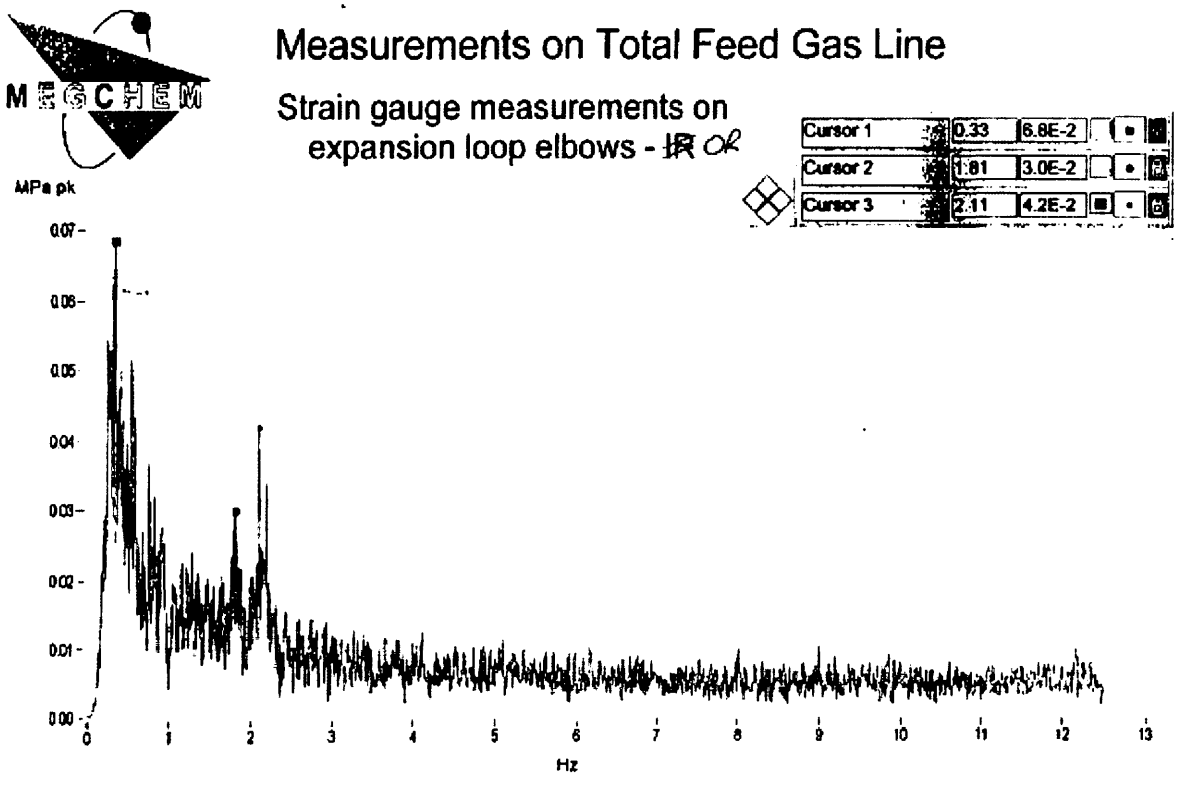

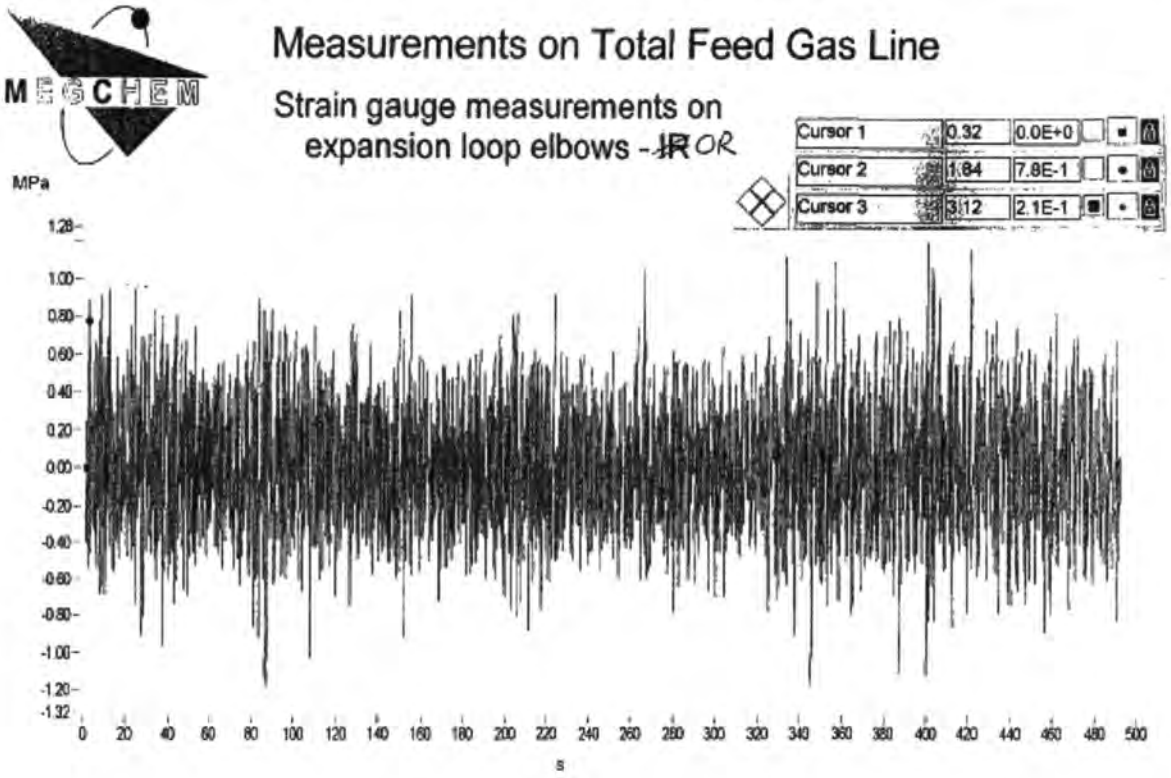

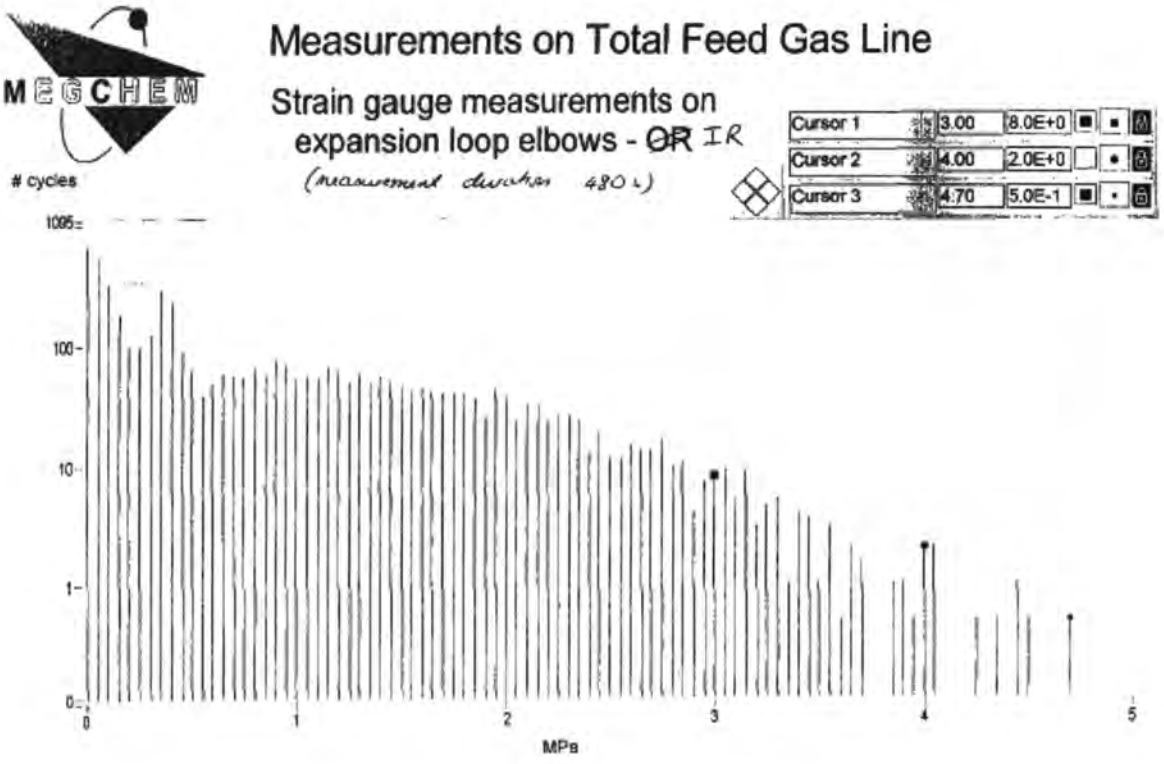

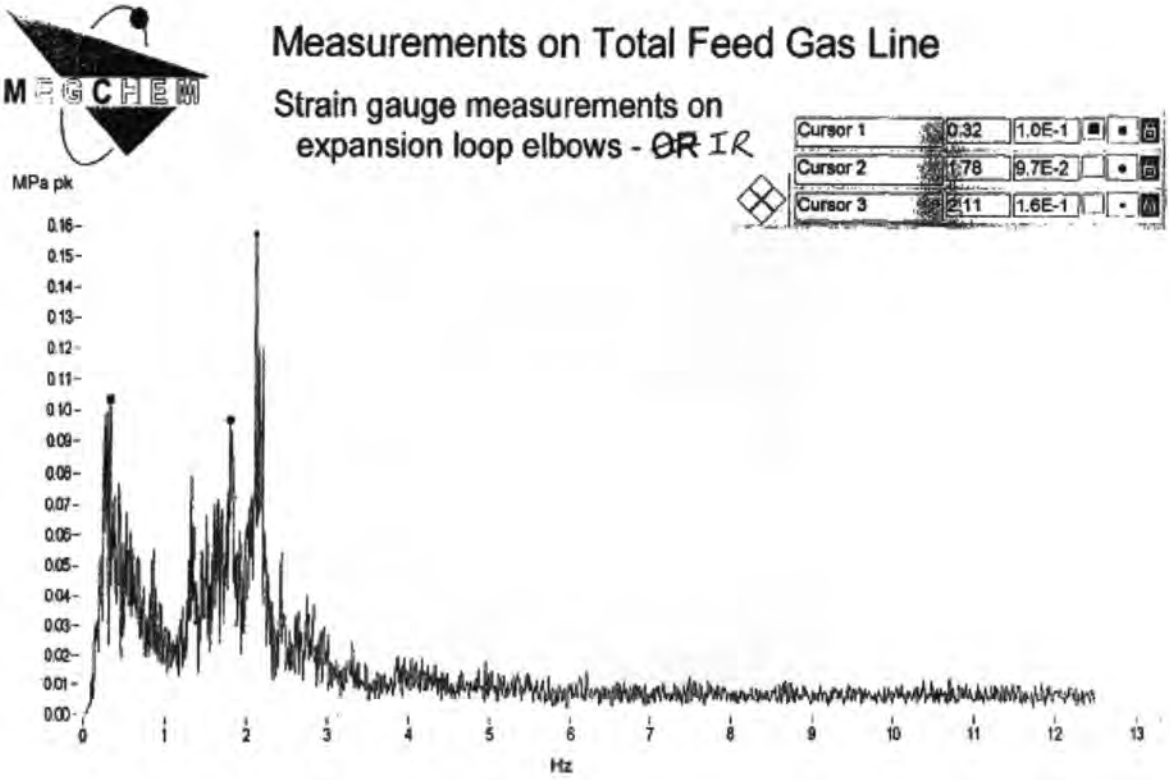

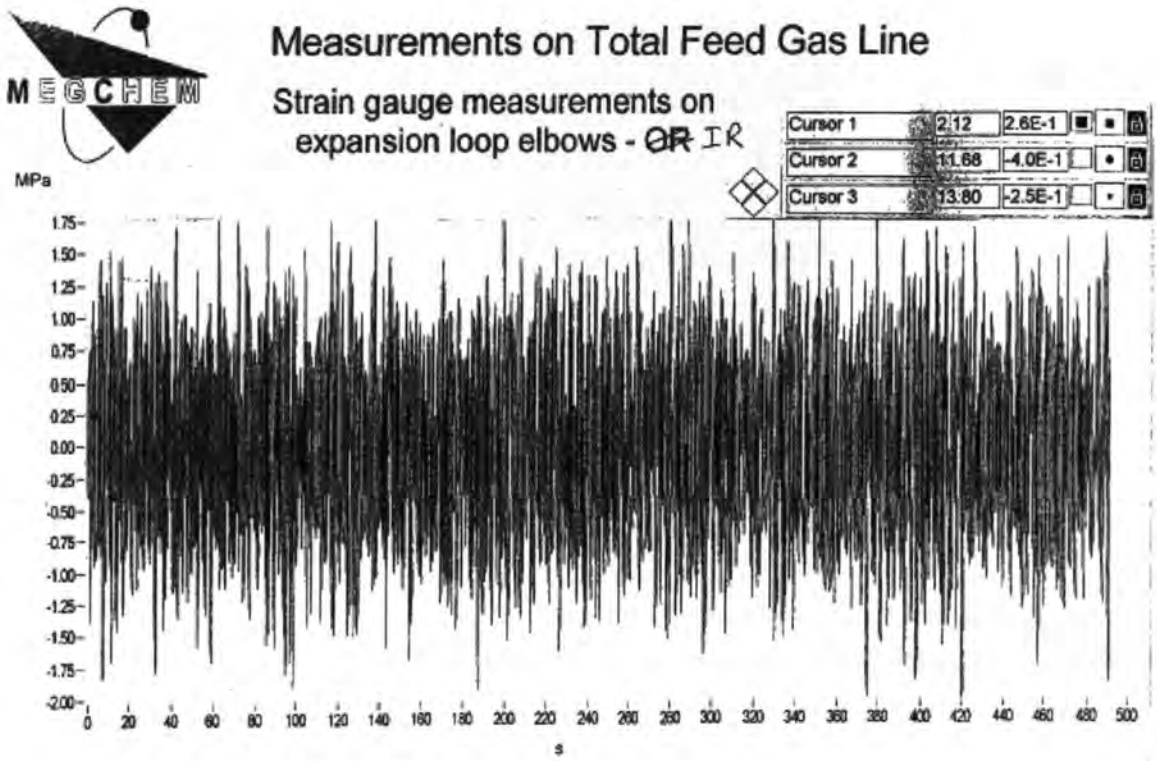

APPENDIX B. – Lean Gas By-Product water Magnetic Particle Test results

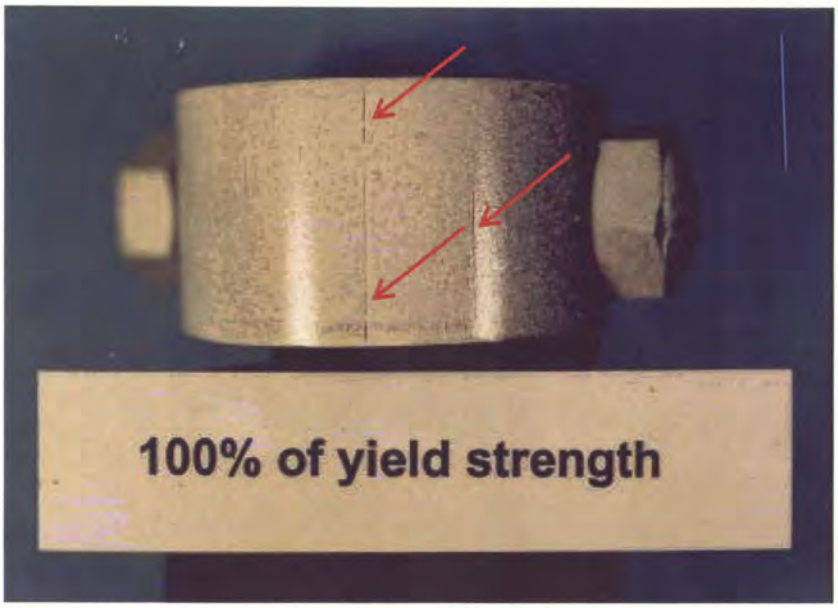

Figure B-1. Magnetic particle test on the specimen stressed to 100% of the yield strength exposed to leaner gas by-product water for 1,000 hours, showing surface cracks as indicated by arrows.

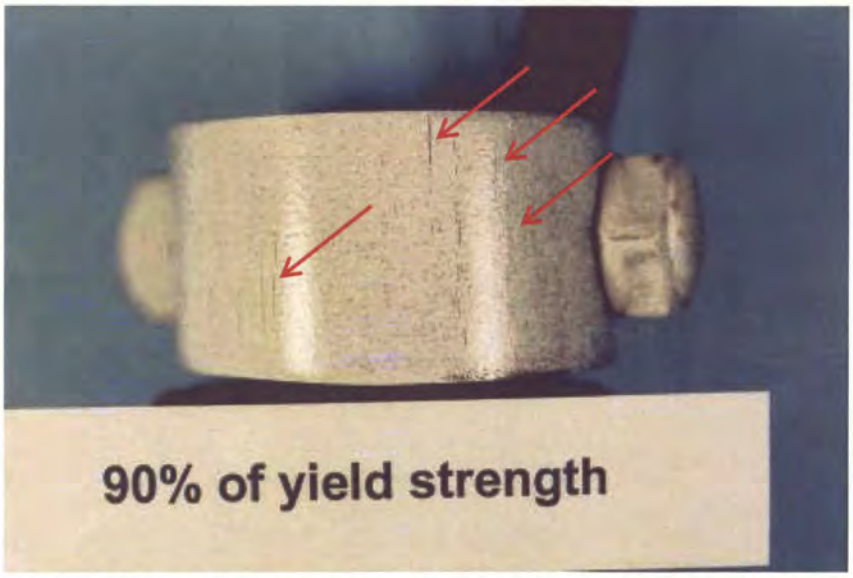

Figure B-2. Magnetic particle test on the specimen stressed to 90% of the yield strength exposed to leaner gas by-product water for 1,000 hours, showing surface cracks as indicated by an arrow.

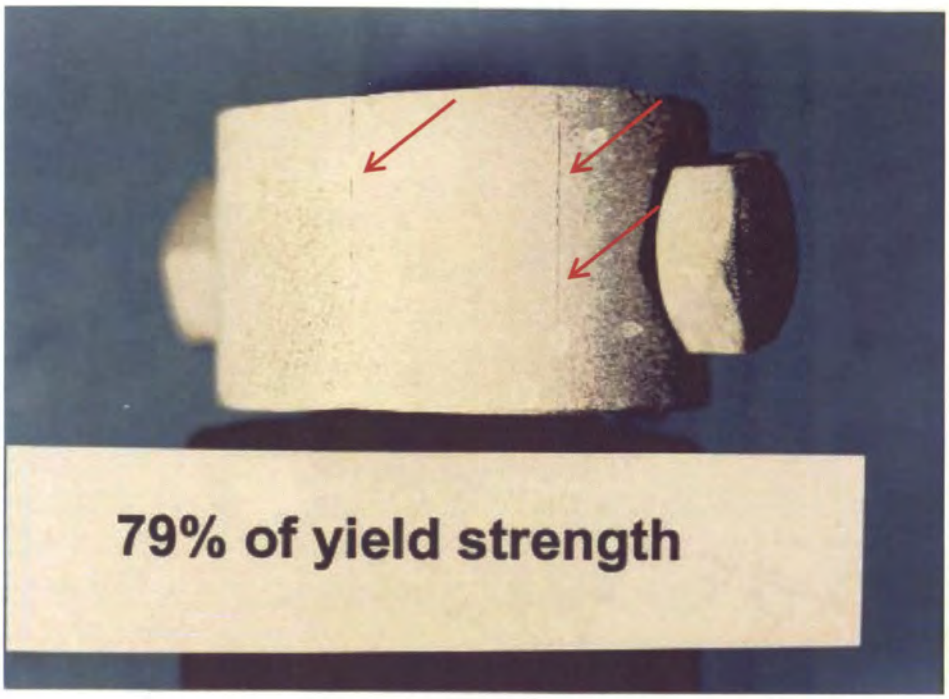

Figure B-3. Magnetic particle test on the specimen stressed to 79% of the yield strength exposed to leaner gas by-product water for 1,000 hours, showing surface cracks.

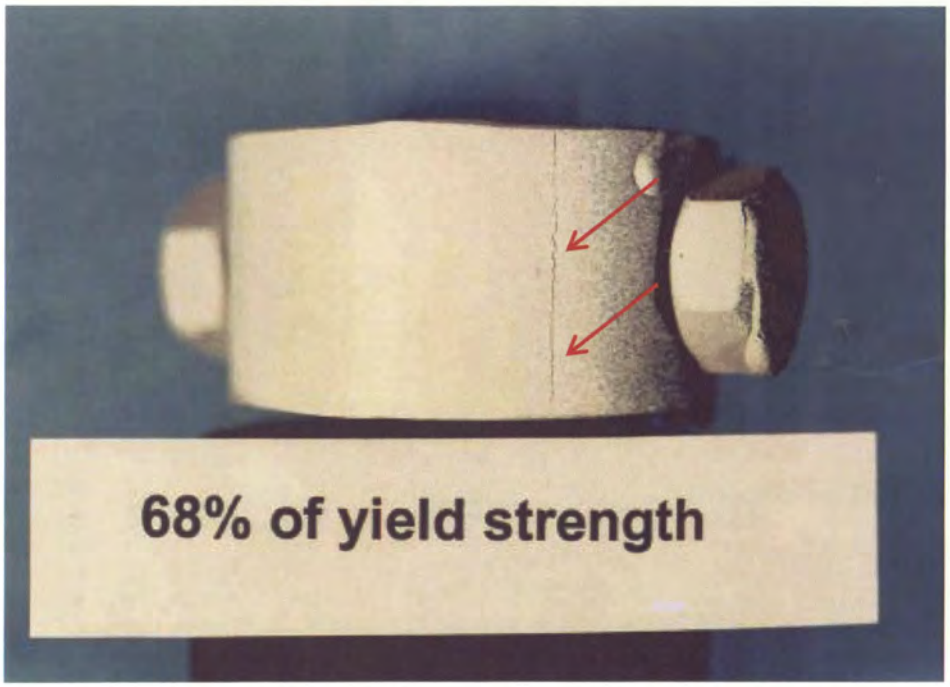

Figure B-4. Magnetic particle test on the specimen stressed to 68% of the yield strength exposed to leaner gas by-product water for 1,000 hours, showing surface cracks.

Figure B-5. Magnetic particle test on the specimen stressed to 56% of the yield strength exposed to leaner gas by-product water for 1,000 hours, showing surface cracks.

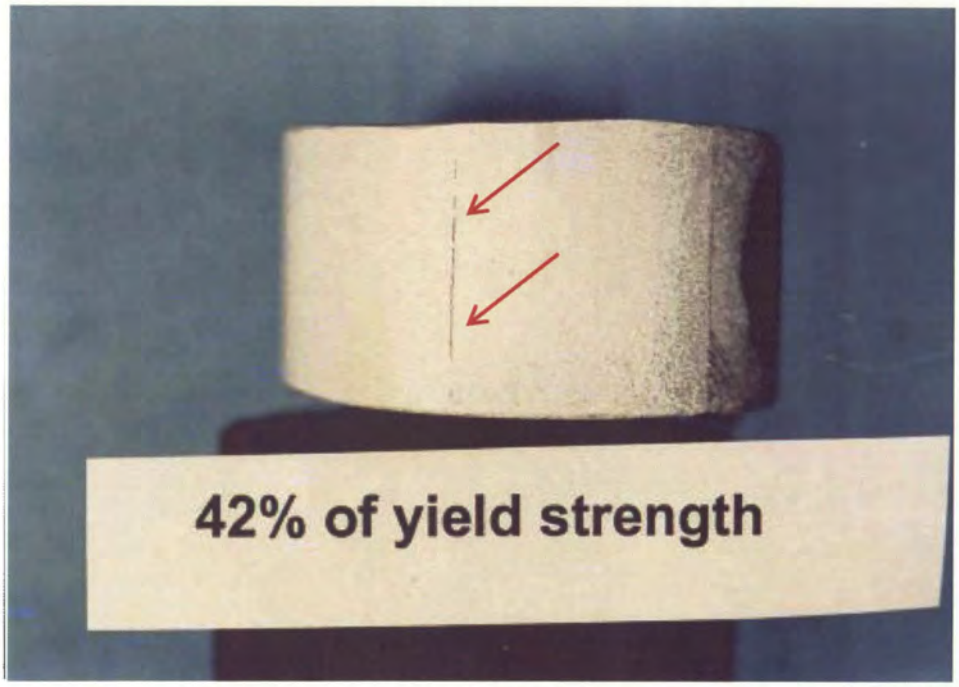

Figure B-6. Magnetic particle test on the specimen stressed to 42% of the yield strength exposed to leaner gas by-product water for 1,000 hours, showing significant surface cracks.

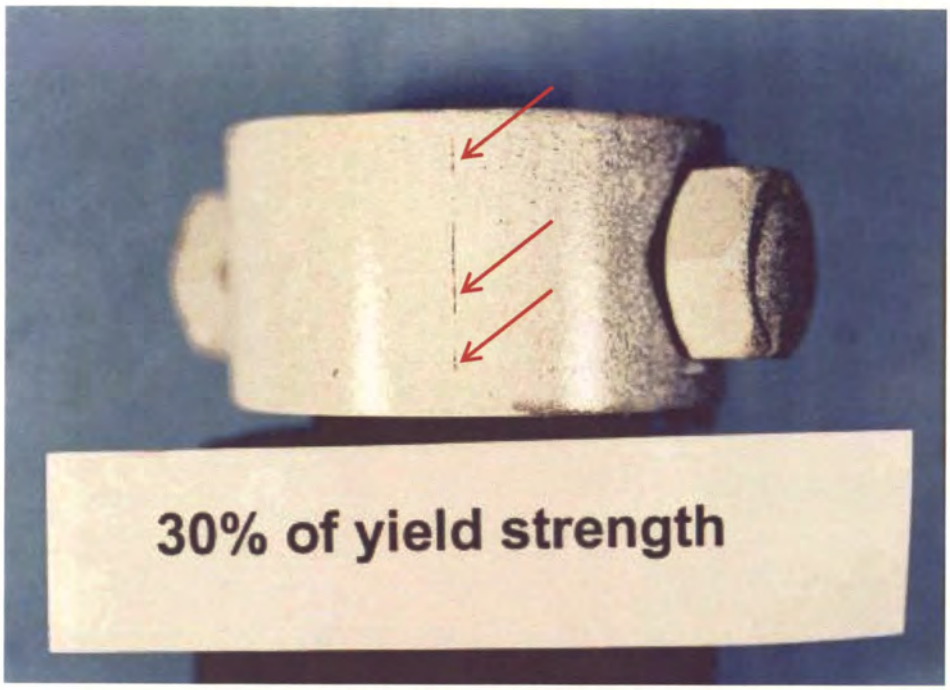

Figure B-7. Magnetic particle test on the specimen stressed to 30% of the yield strength exposed to leaner gas by-product water for 1,000 hours, showing surface cracks.

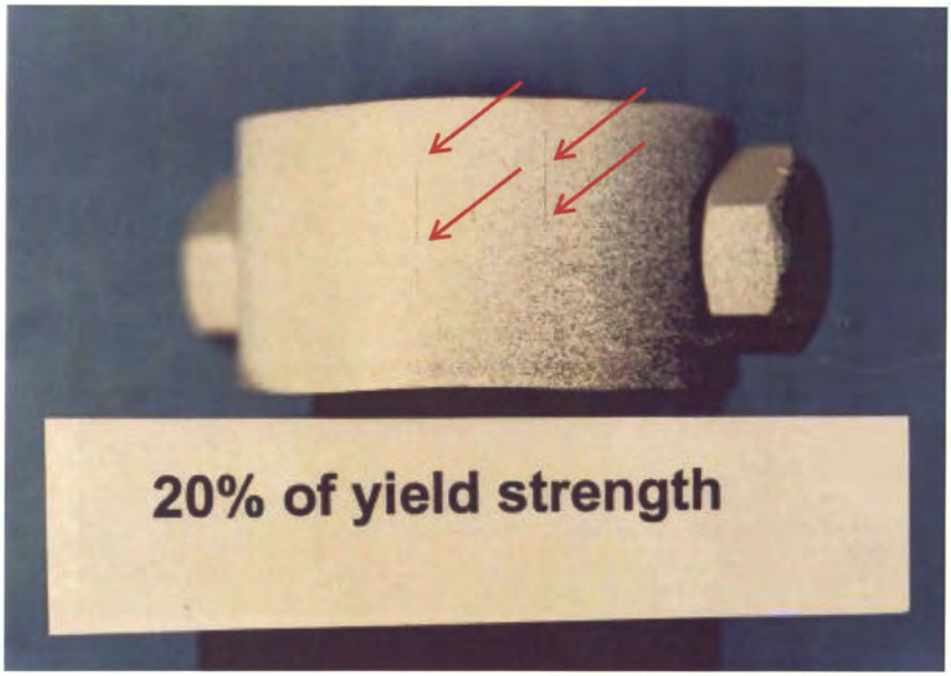

Figure B-8. Magnetic particle test on the specimen stressed to 20% of the yield strength exposed to leaner gas by-product water for 1,000 hours, showing surface cracks.

APPENDIX C.– Lean Gas By-Product water Magnetic Particle Results

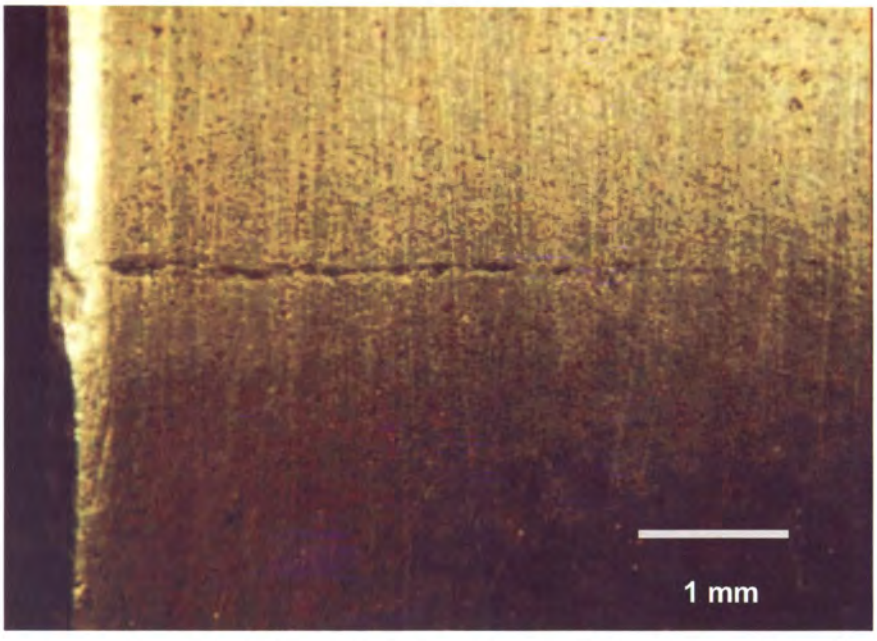

Figure C-1. Crack found on the specimen stressed to 30% of the yield strength.

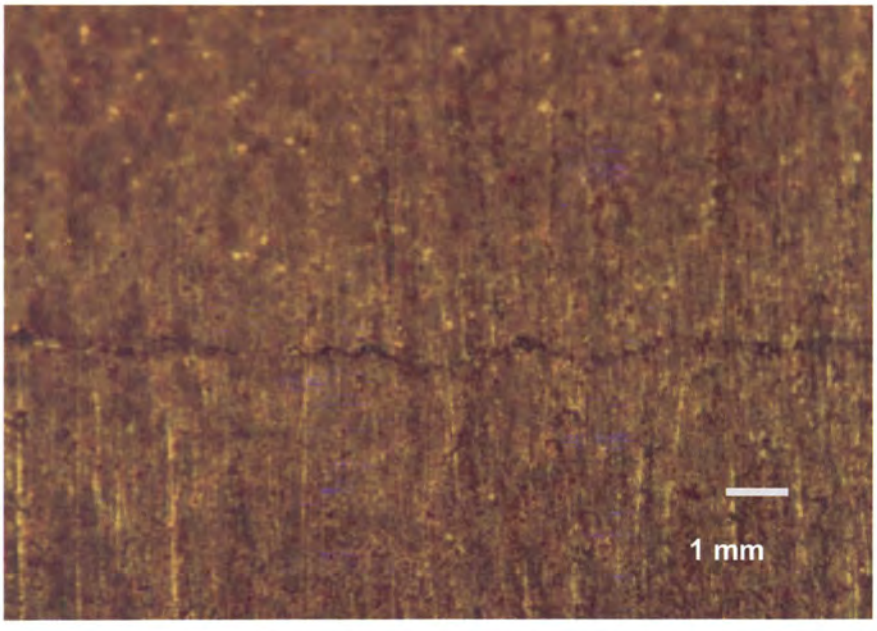

Figure C-2. Crack found on the specimen stressed to 42% of the yield strength.

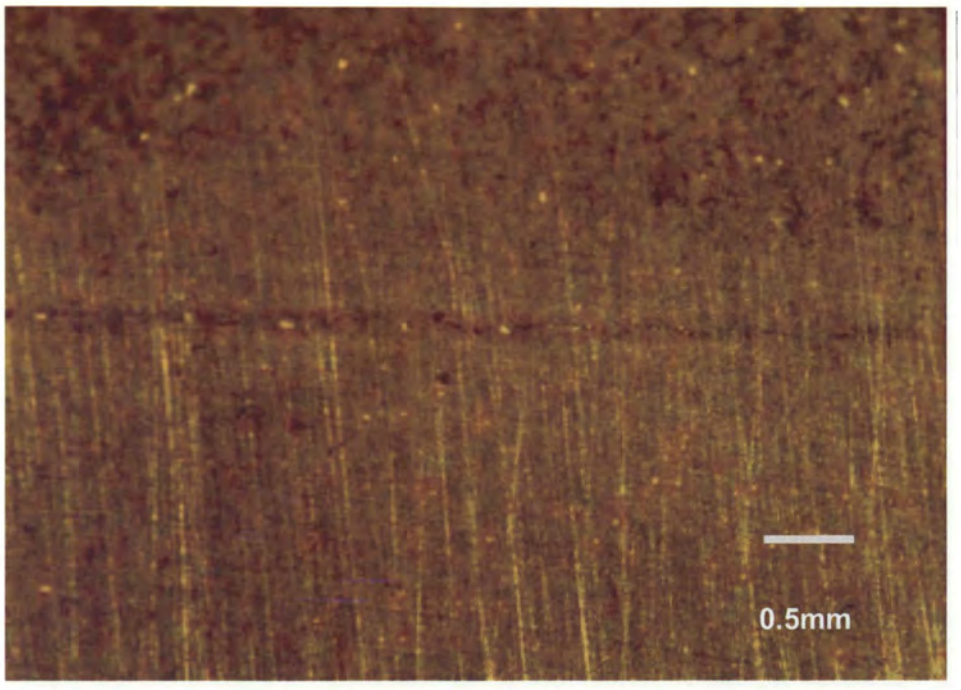

Figure C-3. Crack found on the specimen stressed to 56% of the yield strength.

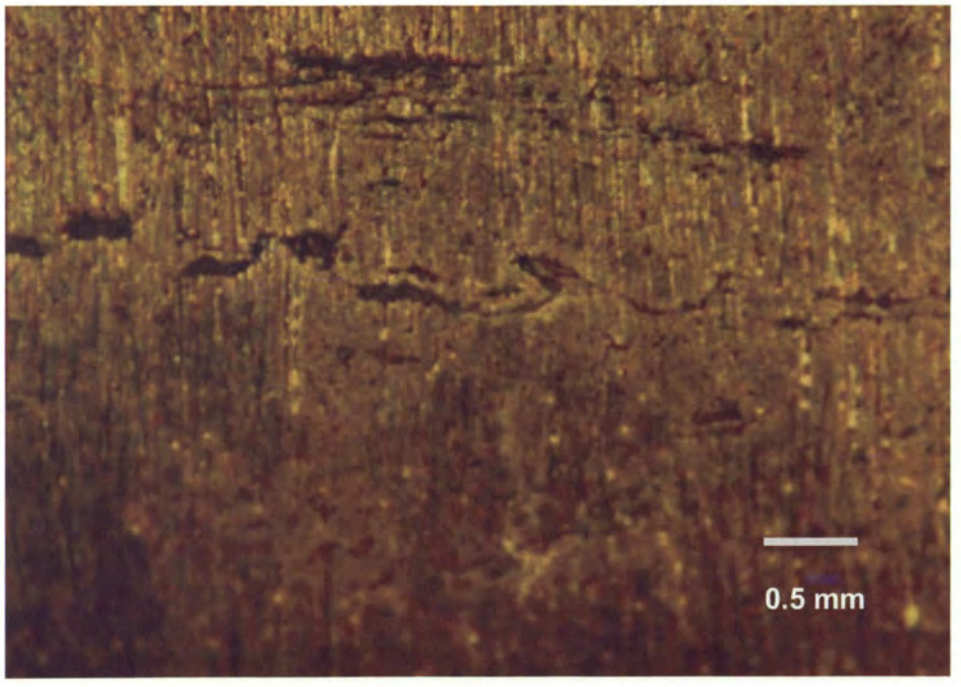

Figure C-4 . Crack found on the specimen stressed to 68% of the yield strength.

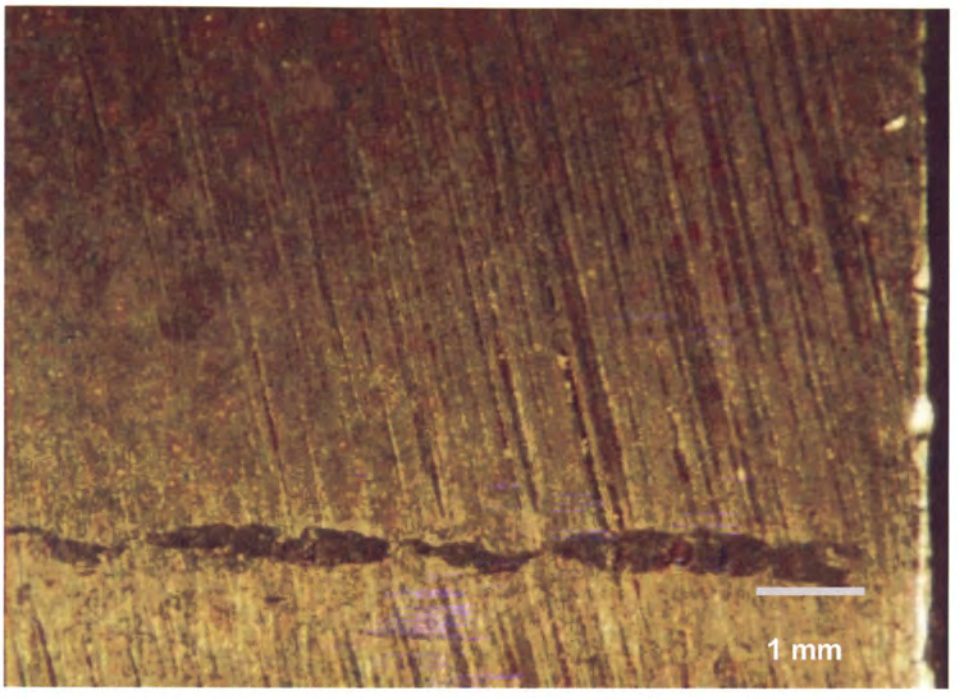

Figure C-5. Crack found on the specimen stressed to 79% of the yield strength.

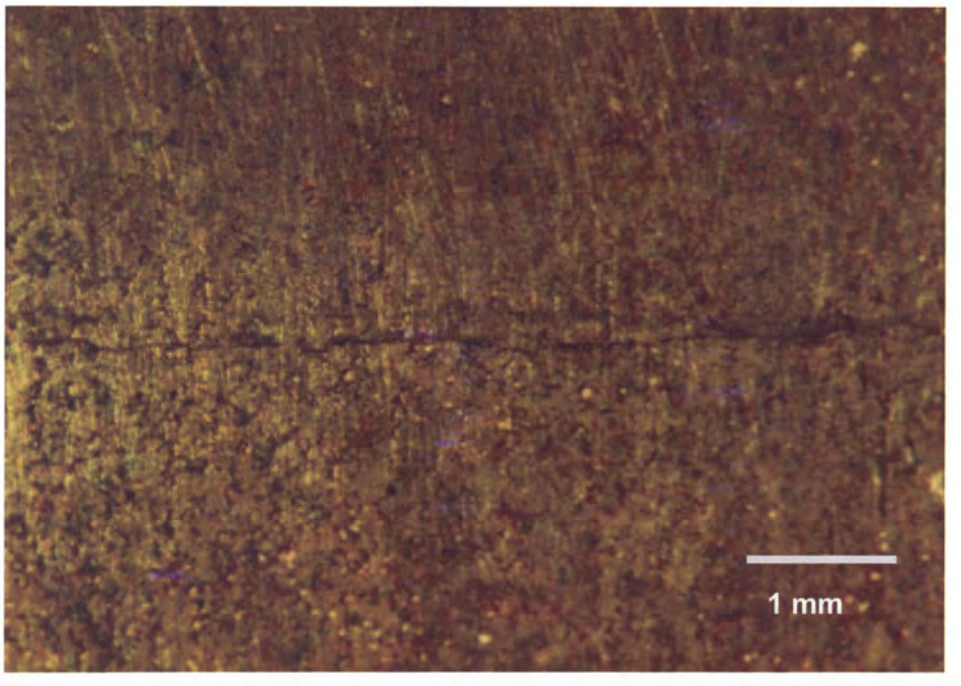

Figure C-6. Crack found on the specimen stressed to 100% of the yield strength.

APPENDIX D.- Rich Gas By-Product Water Stereo Photographs

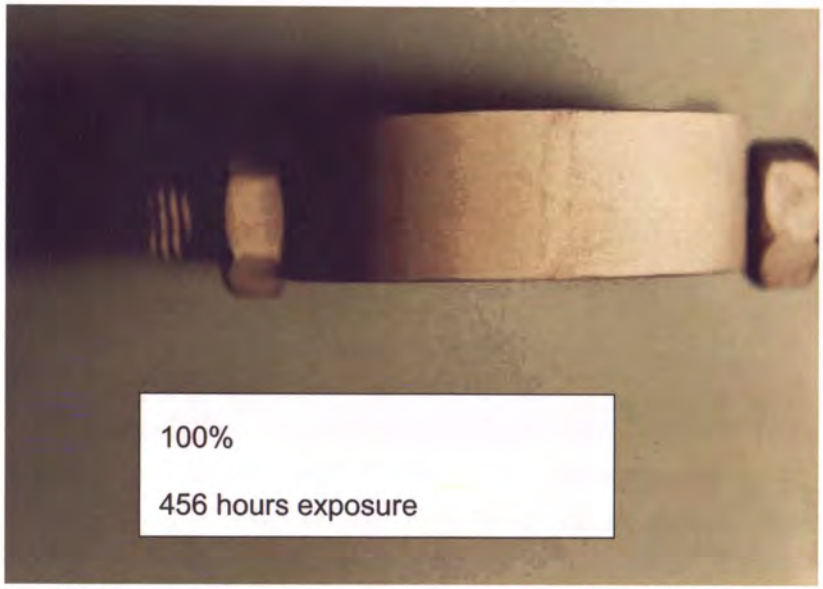

Figure D-1. Magnetic particle test on the specimen stressed to 100% of the yield strength exposed to rich gas by-product water for 456 hours, showing slight evidence of cracks.

Figure D-2. Magnetic particle test on the specimen stressed to 90% of the yield strength exposed to rich gas by-product water for 456 hours, showing slight evidence of cracking.

Figure D-3. Magnetic particle test on the specimen stressed to 80% of the yield strength exposed to richer gas by-product water for 456 hours, showing no sign of cracks.

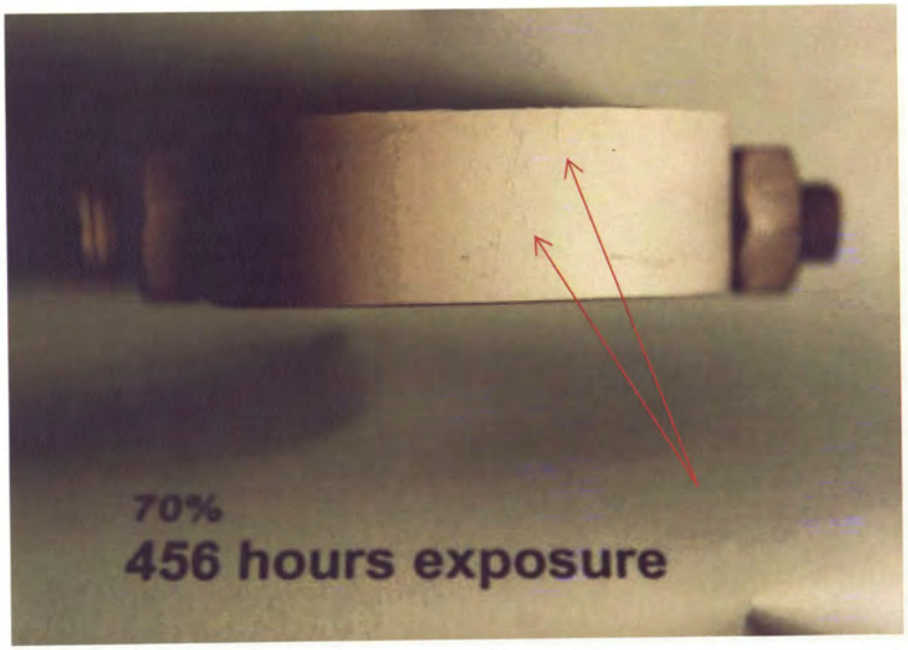

Figure D-4. Magnetic particle test on the specimen stressed to 70% of the yield strength exposed to richer gas by-product water for 456 hours, showing surface cracks.

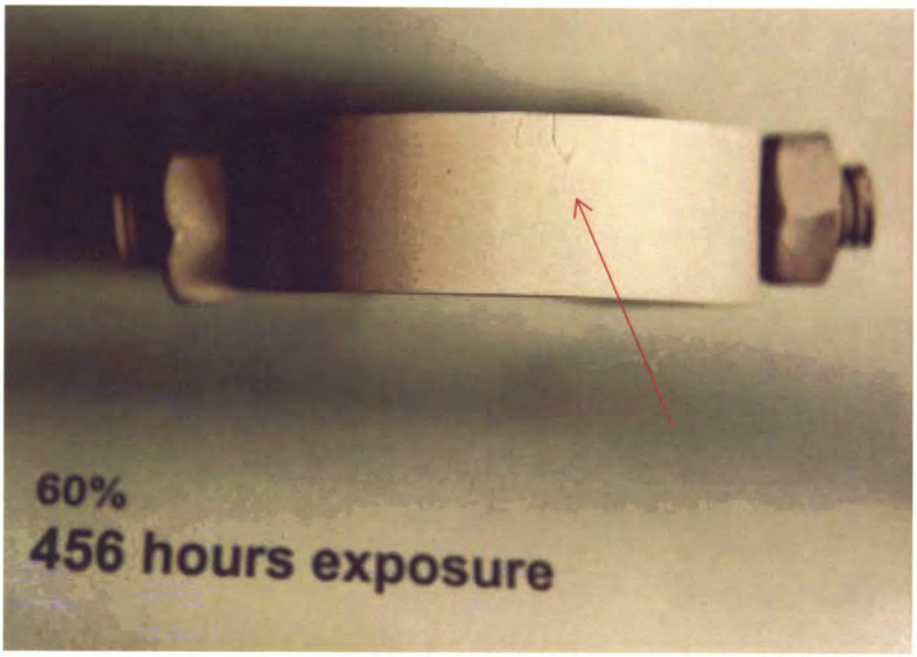

Figure D-5. Magnetic particle test on the specimen stressed to 60% of the yield strength exposed to richer gas by-product water for 456 hours, showing surface cracks.

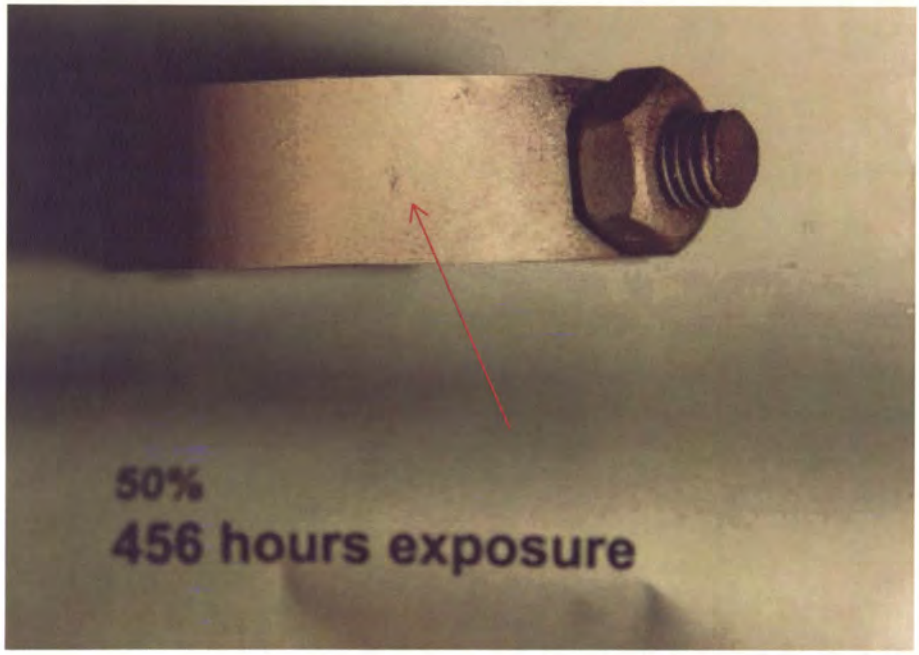

Figure D-6. Magnetic particle test on the specimen stressed to 50% of the yield strength exposed to richer gas by-product water for 456 hours, showing slight surface cracks.

Figure D-7. Magnetic particle test on the specimen stressed to 40% of the yield strength exposed to richer gas by-product water for 456 hours, showing slight surface cracks.

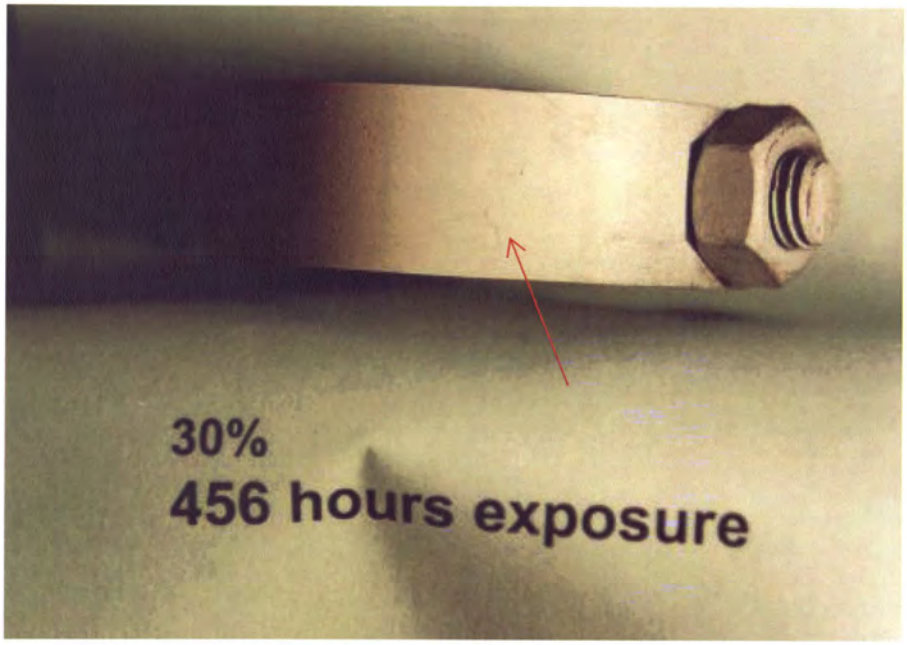

Figure D-8. Magnetic particle test on the specimen stressed to 30% of the yield strength exposed to richer gas by-product water for 456 hours, showing slight surface cracks.

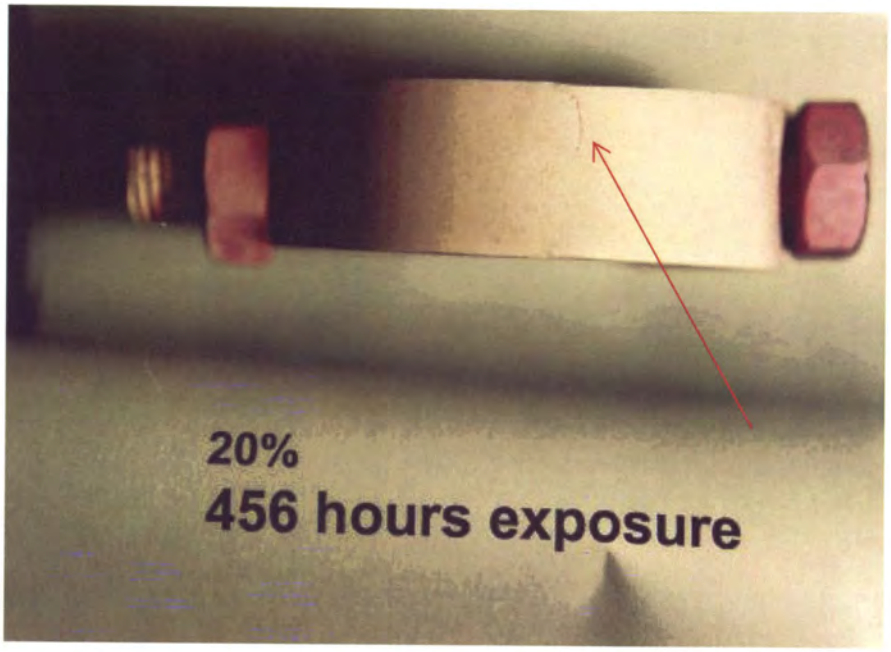

Figure D-9. Magnetic particle test on the specimen stressed to 20% of the yield strength exposed to richer gas by-product water for 456 hours, showing surface cracks.

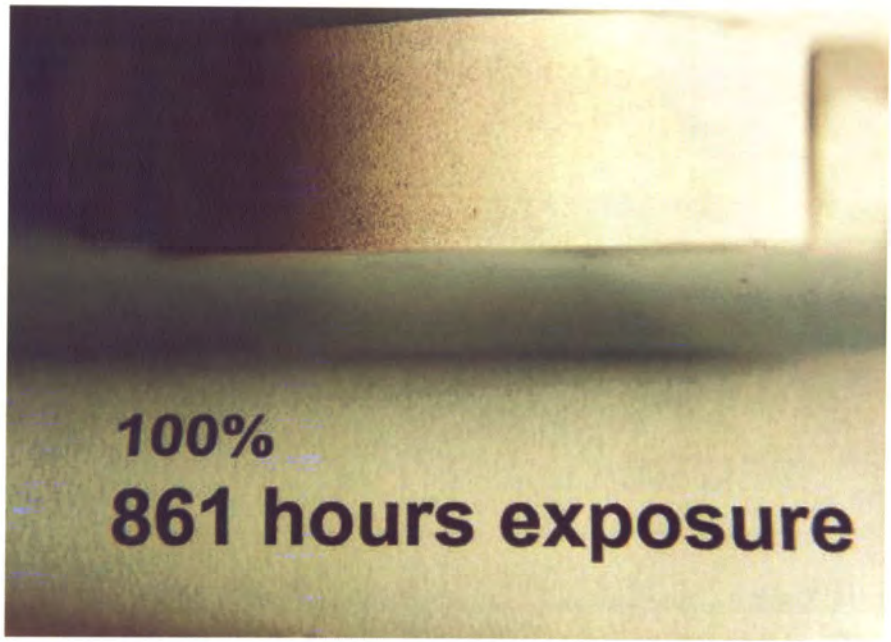

Figure D-10. Magnetic particle test on the specimen stressed to 100% of the yield strength exposed to richer gas by-product water for 861 hours, showing no surface cracks.

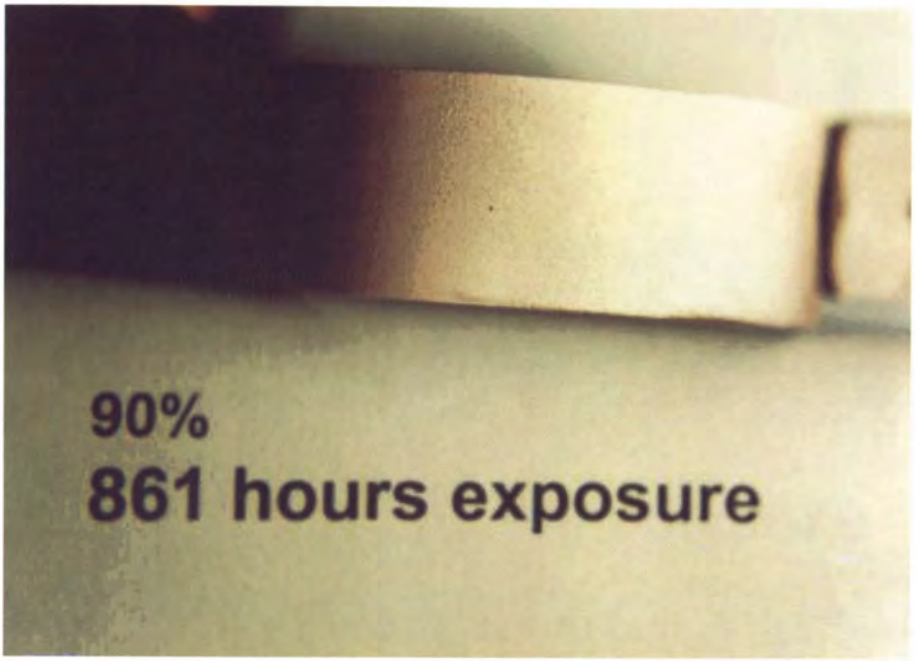

Figure D-11. Magnetic particle test on the specimen stressed to 90% of the yield strength exposed to richer gas by-product water for 861 hours, showing no surface cracks.

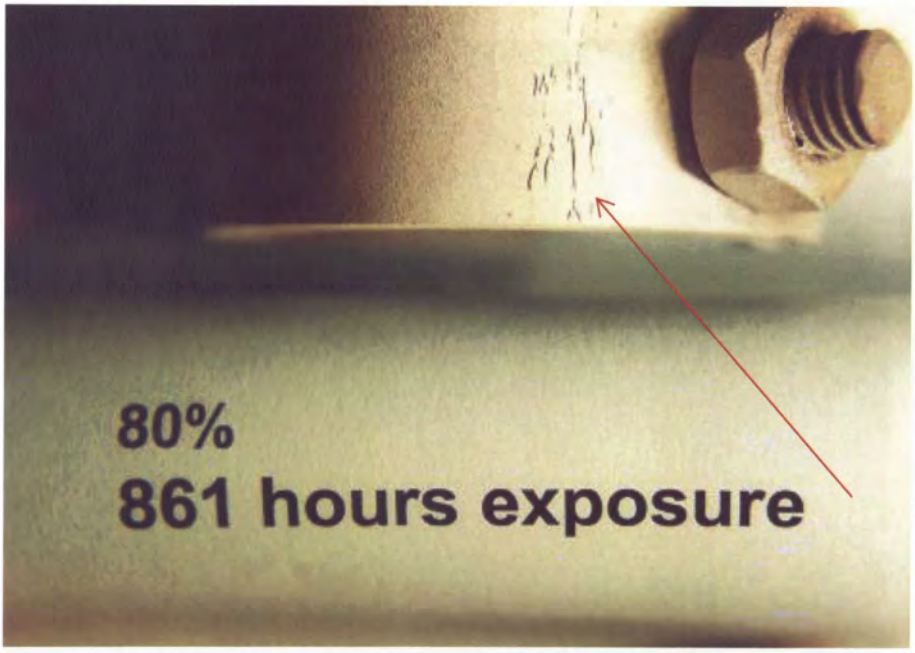

Figure D-12. Magnetic particle test on the specimen stressed to 80% of the yield strength exposed to richer gas by-product water for 861 hours, showing significant surface cracks.

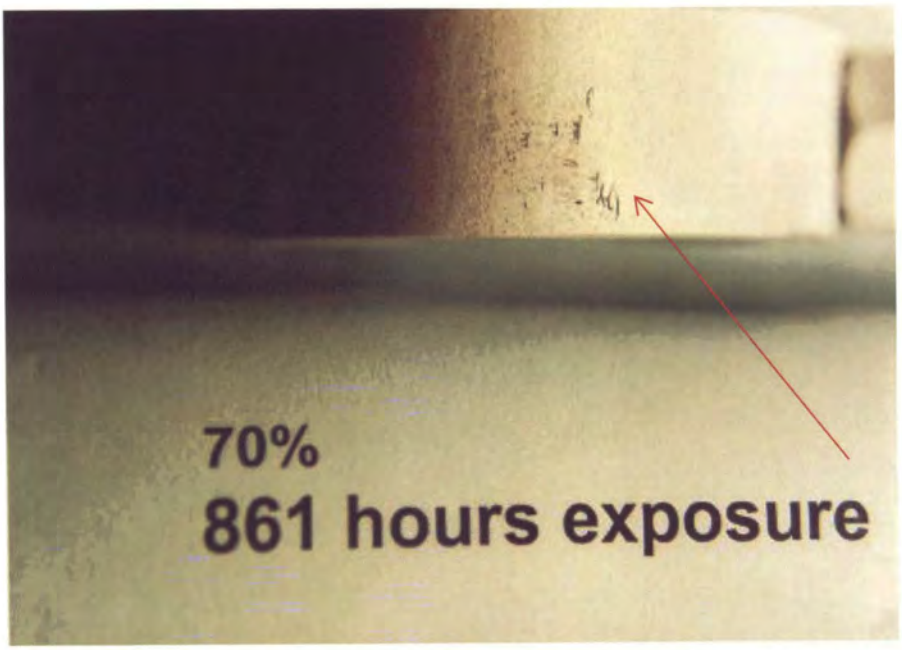

Figure D-13. Magnetic particle test on the specimen stressed to 70% of the yield strength exposed to richer gas by-product water for 861 hours, showing surface cracks.

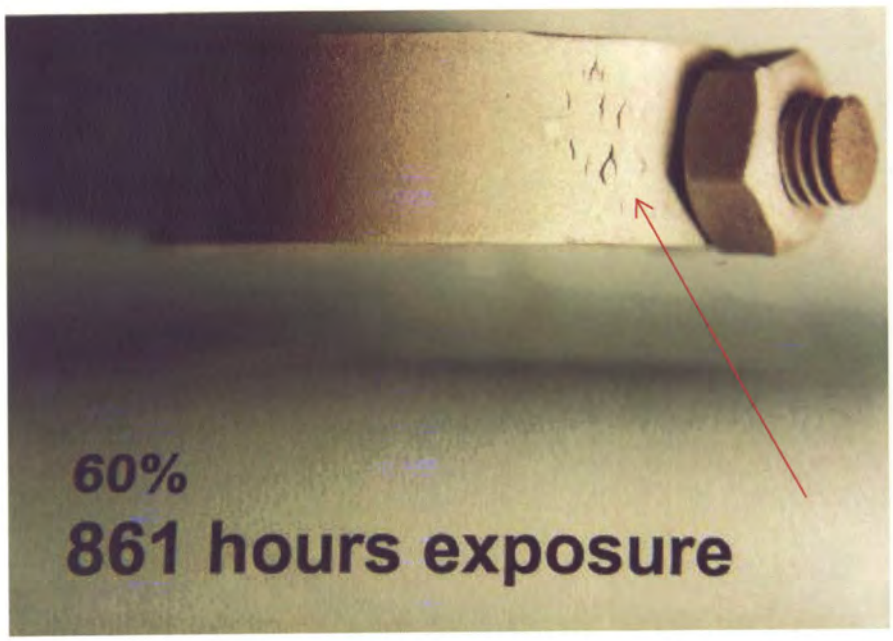

Figure D-14. Magnetic particle test on the specimen stressed to 60% of the yield strength exposed to richer gas by-product water for 861 hours, showing significant surface cracks.

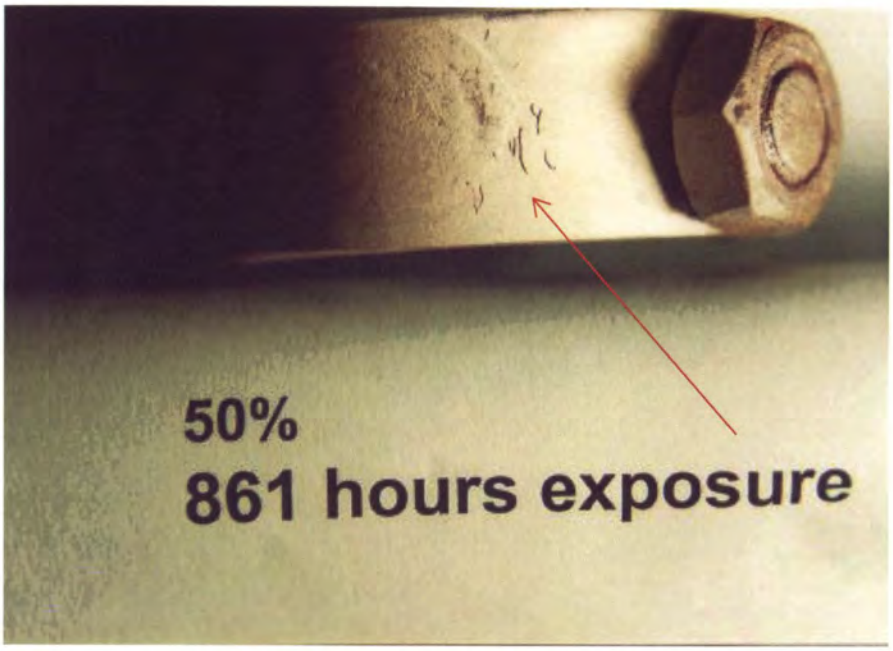

Figure D-15. Magnetic particle test on the specimen stressed to 50% of the yield strength exposed to richer gas by-product water for 861 hours, showing significant surface cracks.

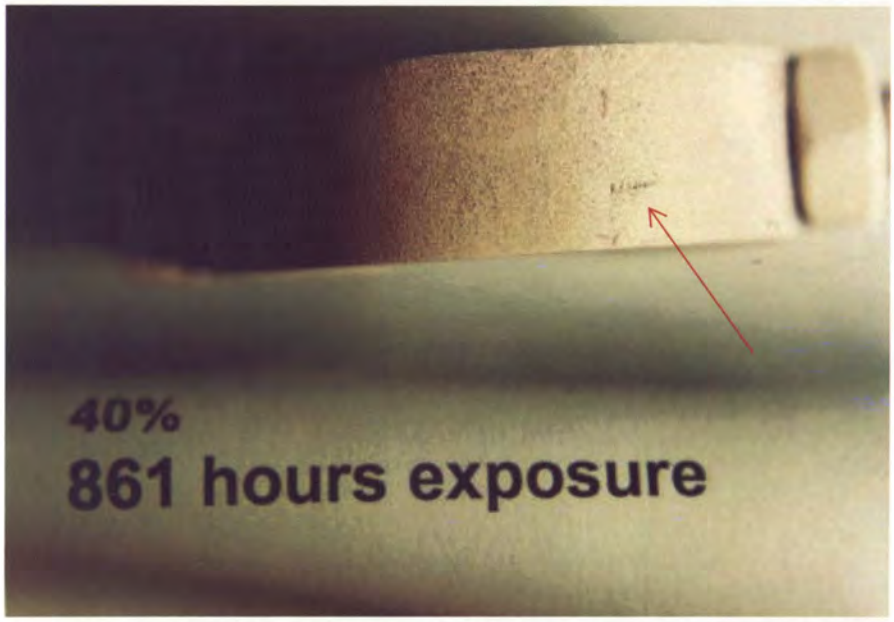

Figure D-16. Magnetic particle test on the specimen stressed to 40% of the yield strength exposed to richer gas by-product water for 861 hours, showing slight surface cracks.

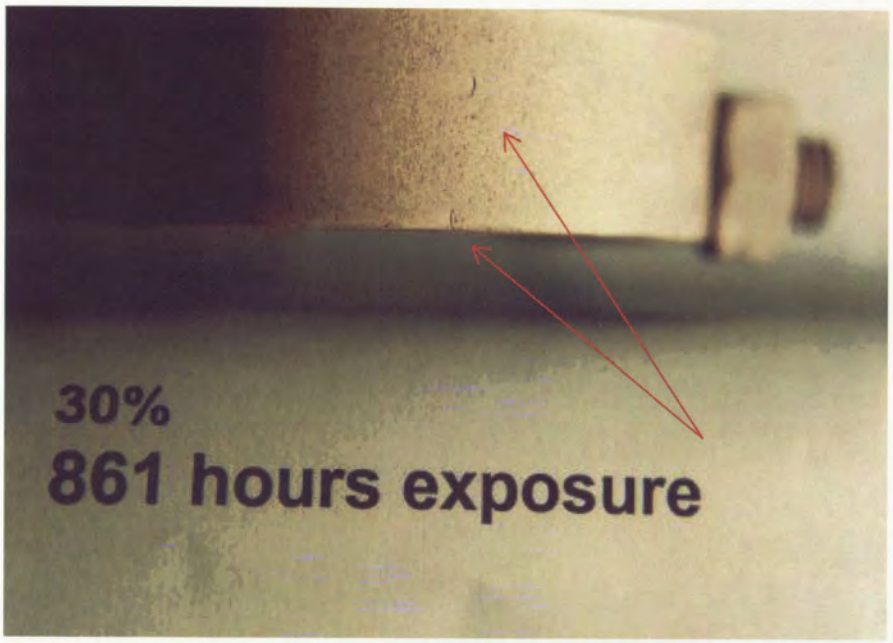

Figure D-17. Magnetic particle test on the specimen stressed to 30% of the yield strength exposed to richer gas by-product water for 861 hours, showing surface cracks.

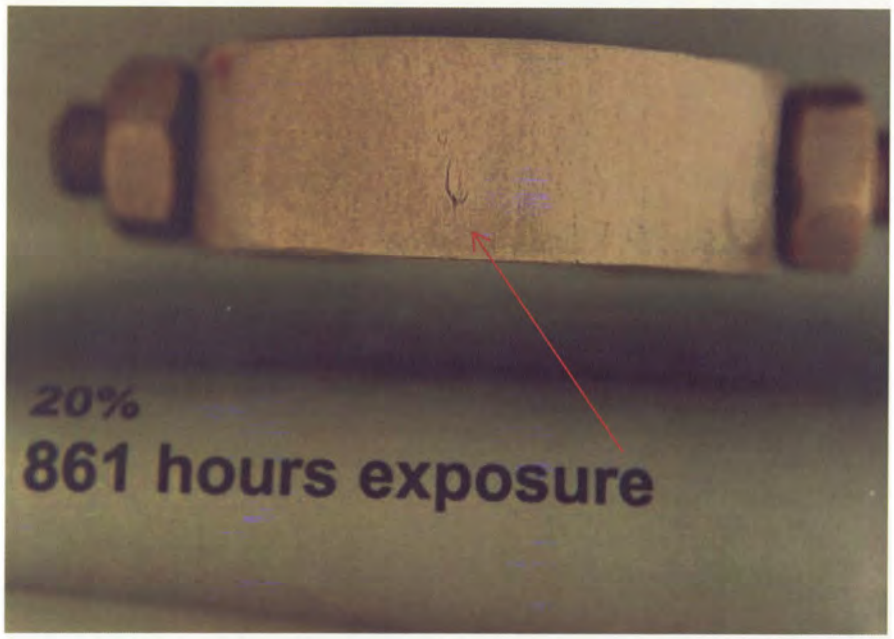

Figure D-18. Magnetic particle test on the specimen stressed to 20% of the yield strength exposed to richer gas by-product water for 861 hours, showing surface cracks.

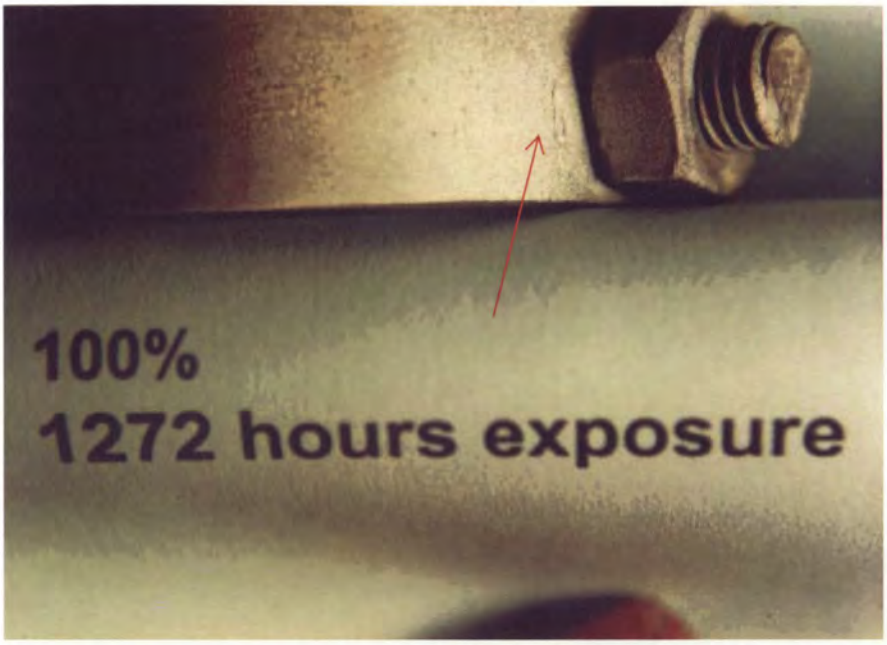

Figure D-19. Magnetic particle test on the specimen stressed to 100% of the yield strength exposed to richer gas by-product water for 1,272 hours, showing surface cracks.

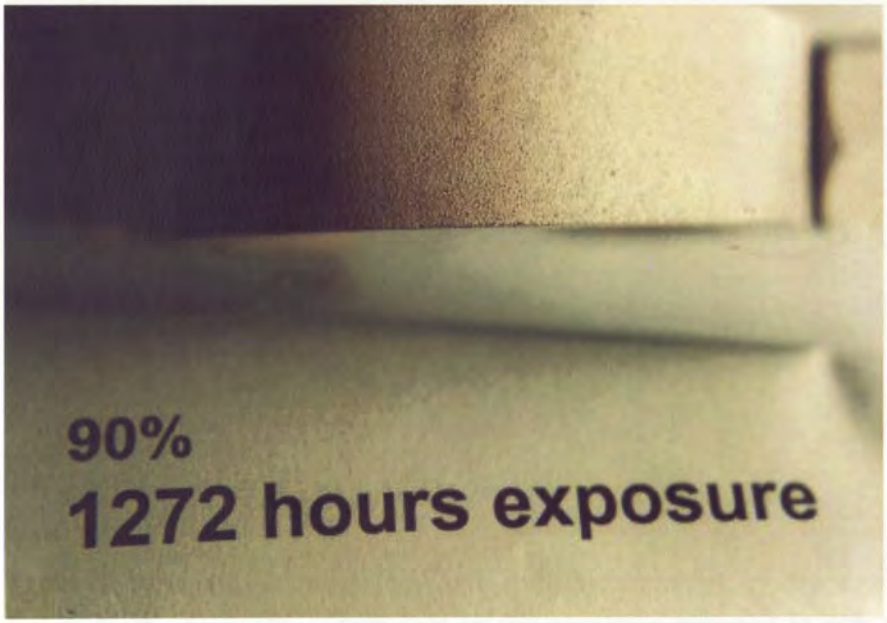

Figure D-20. Magnetic particle test on the specimen stressed to 90% of the yield strength exposed to richer gas by-product water for 1,272 hours, showing no surface cracks.

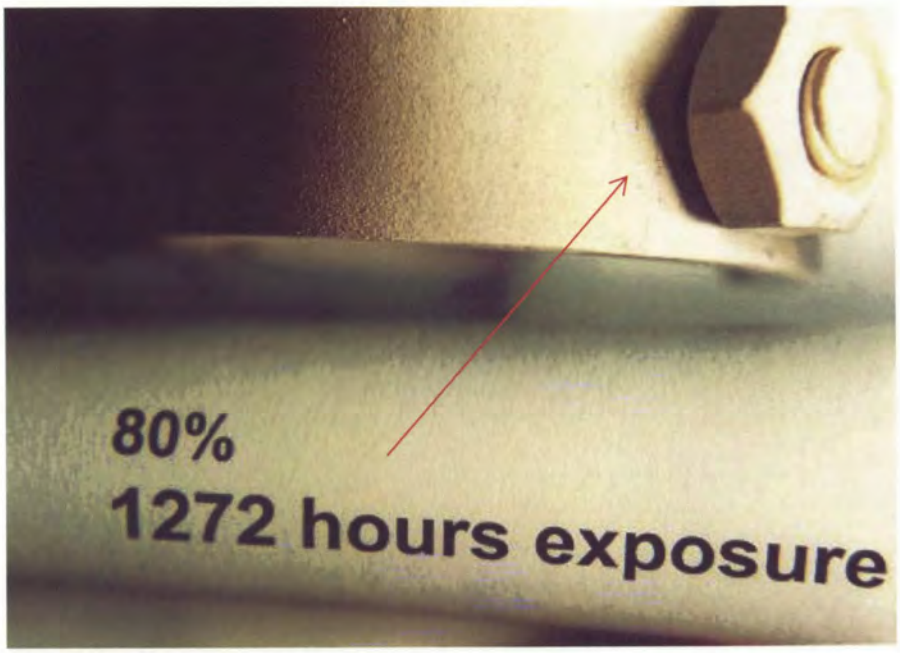

Figure D-21. Magnetic particle test on the specimen stressed to 80% of the yield strength exposed to richer gas by-product water for 1,272 hours, showing slight surface cracks.

Figure D-22. Magnetic particle test on the specimen stressed to 70% of the yield strength exposed to richer gas by-product water for 1,272 hours, showing no surface cracks.

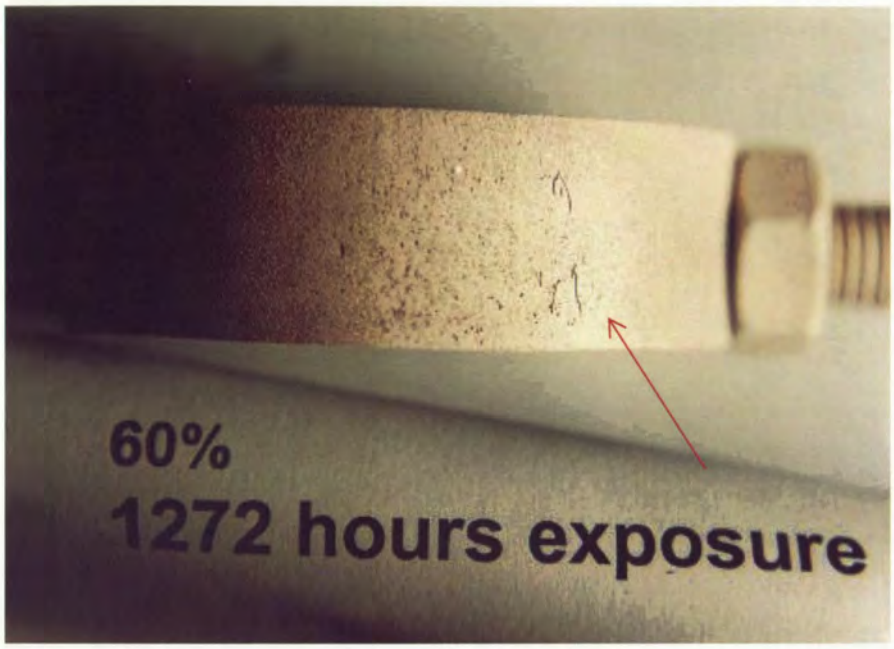

Figure D-23. Magnetic particle test on the specimen stressed to 60% of the yield strength exposed to richer gas by-product water for 1,272 hours, showing surface cracks.

Figure D-24. Magnetic particle test on the specimen stressed to 50% of the yield strength exposed to richer gas by-product water for 1,272 hours, showing surface cracks.

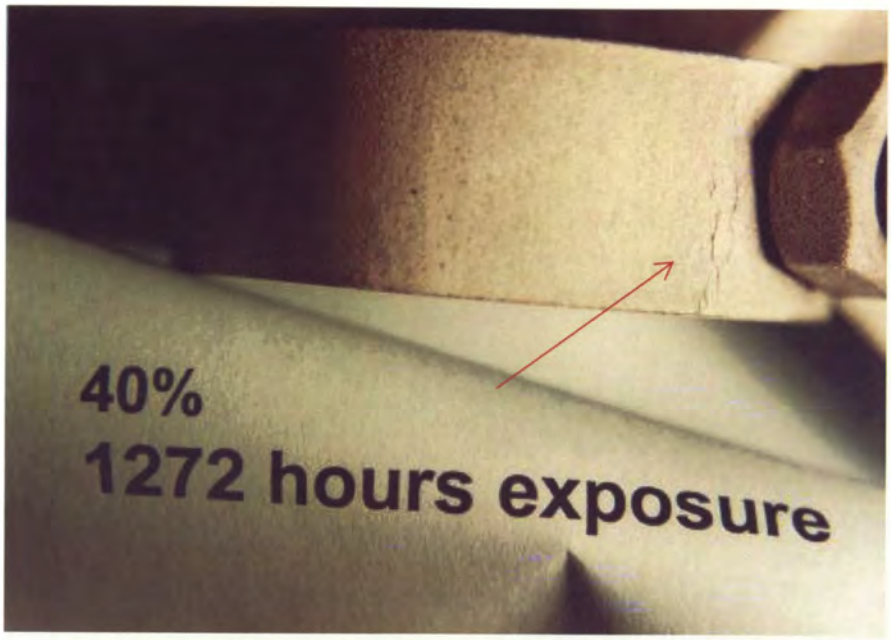

Figure D-25. Magnetic particle test on the specimen stressed to 40% of the yield strength exposed to richer gas by-product water for 1,272 hours, showing surface cracks.

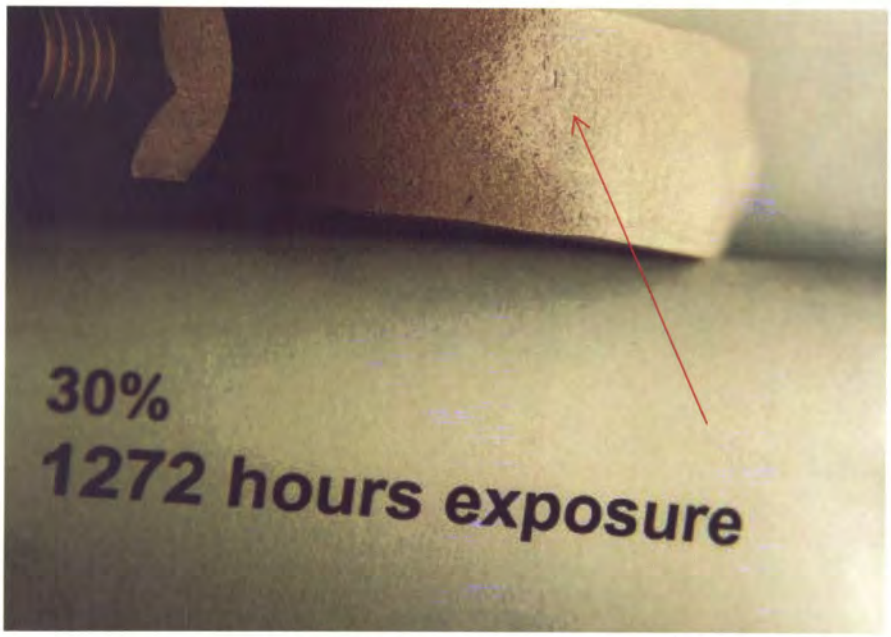

Figure D-26. Magnetic particle test on the specimen stressed to 30% of the yield strength exposed to richer gas by-product water for 1,272 hours, showing surface cracks.

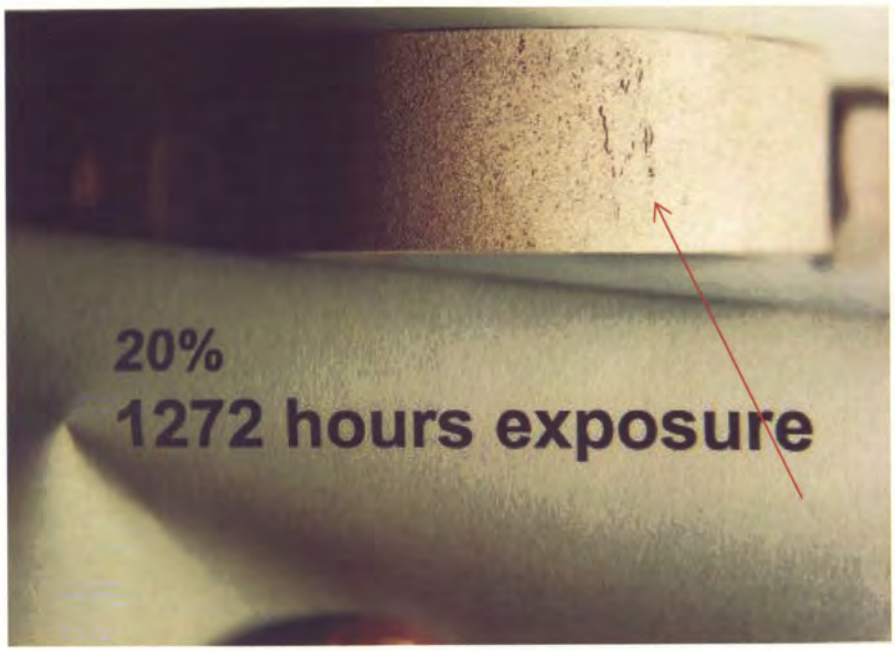

Figure D-27. Magnetic particle test on the specimen stressed to 20% of the yield strength exposed to richer gas by-product water for 1,272 hours, showing surface cracks.